

**University of Strathclyde,
Department of Pure and Applied Chemistry**

Development of Colorimetric Indicators Based on Methylene Blue.

by David Hazafy.

A thesis presented in part fulfilment of the requirements for the degree of Doctor of
Philosophy.

2012

This thesis is the result of the author's original research. It has been composed by the author and has not been previously submitted for examination which has led to the award of a degree.

The copyright of this thesis belongs to the author under the terms of the United Kingdom Copyright Acts as qualified by University of Strathclyde Regulation 3.50. Due acknowledgement must always be made of the use of any material contained in, or derived from, this thesis.'

Signed:

Date:

Acknowledgements

Thanks go to the EPSRC for funding this research and to my supervisor, Prof. Andrew Mills, who took a chance on a wide-eyed summer student from the Czech Republic. To the other members of the Mills group, past and present, thanks for helping me to adjust to and appreciate life at Strathclyde and in Scotland. In addition I would like to thank the technical staff at Strathclyde, some of whom have gone above and beyond the call of duty, thank you.

Special thanks go to my family for their support and in particular to my wife for her patience, self-sacrifice and support of me in the pursuit of my studies.

Some of this work would not have been made remotely possible without the much appreciated effort and expertise of a few individuals, namely John Parkinson (NMR), Tell Tuttle (molecular modelling) and Mike Hutchings (dye chemistry).

Abstract

This study largely focuses on the development of an oxygen indicating label for possible use in modified atmosphere packaging. The work presented here builds on a system developed by Mills *et al.*, *i.e.* a UVA-light activated reversible oxygen indicator ink comprised of a nanoparticulate semiconducting photocatalyst (usually TiO₂), redox dye (usually methylene blue), sacrificial electron donor and an encapsulating polymer. This ink could be cast as a thin film activated by UV light which, upon its absorption by the photocatalyst, creates an electron-hole pair. The photogenerated holes oxidise the concomitant sacrificial electron donor while the photogenerated electrons reduce the redox dye. This results in a dramatic colour change (usually blue to colourless). A photobleached film thus remains colourless in the absence of oxygen but quickly regains its original blue colour if oxygen is reintroduced. However, this ink is water-soluble and not suitable for printing on common packaging materials; this problem is addressed in Chapters 3 and 5 where solvent-based alternative O₂-sensitive inks are described. The development of a more photo-stable ink, activated by UVB rather than UVA light, is the subject of Chapter 4.

Interesting observations made while working on the above indicators lead to development of a series of humidity and temperature indicators based on phenothiazine dyes (Chapter 6). Methylene Blue and urea within a supporting polymer makes an ink which casts as a pink opaque film which turns into transparent blue film after reaching a humidity threshold (>80% RH). In addition, a combination of a polymer (hydroxypropyl cellulose) and a phenothiazine dye cast as a film was found to change colour upon heating, which could then be reversed by exposing the film to a humid air stream. Potential uses of such indicators are discussed.

Chapter 7 reports on the red coloured forms of Methylene Blue observed upon treatment with alkali and helps correct the literature associated with this effect.

Publications resulting from this work are attached at the end of the thesis.

Abbreviations List

A Absorbance

AH Absolute humidity

Asc Ascorbic acid

AzA, AzB, AzC Azure A, Azure B, Azure C; demethylated analogues of Methylene Blue.

c concentration

CA Contact angle

D_{ox}, D_{red} Oxidised and reduced form of a dye

ϵ, α Extinction coefficient

E_{bg} Energy band gap between the conduction and the valence band in a semiconducting material

EPR Electron paramagnetic resonance

E_T Energy of transmission, measure of

(Glu-H) GH Protonated glucose

HEC Hydroxyethyl cellulose.

HPC Hydroxypropyl cellulose.

I Light intensity

K_D Dimmerisation equilibrium constant

LMB Leuco methylene Blue, reduced form of this dye

MAP Modified atmosphere packaging.

MB Methylene Blue

MB-AQ Free Methylene Blue, aqueous soluble dye

MB-DS Methylene Blue ion-paired with dodecyl sulfate

MB-OH N-hydroxy adduct of Methylene Blue

MB-SPS Methylene Blue ion-paired with sulfonated polystyrene

MVB Methylene Violet (Bernthsen), product of MB oxidation

NBO Natural bond orbitals

NMR Nuclear magnetic resonance

P25 Commercial TiO₂ photocatalyst.

PCM Polarisable continuum model

PE Polyethylene

PET Polyether terephthalate

PP Polypropylene

PVP Polyvinyl pyrrolidone

RH Relative humidity.

T Transmittance

TEM Transmission electron microscopy

TD-DFT Time dependant density functional theory

TH Thionine, demethylated form of Methylene Blue

TLC Thin layer chromatography

UVA (UVB, UVC) Ultraviolet electromagnetic radiation of wavelength: 200-270 nm (270-320 nm, 320-400) respectively.

WW Warm white light fluorescent tube

XRD X-Ray diffraction

Contents

Acknowledgements	i
Abstract	ii
Contents	v
List of Tables	viii
List of Figures	ix

CHAPTER 1

INTRODUCTION	1
1.1 Modified Atmosphere Packaging and Oxygen indicators	2
1.1.1 Intelligent Packaging	5
1.2 Methylene Blue	6
1.2.1 The Redox Chemistry of Methylene Blue.....	6
1.2.2 Colour Effects from Dye-Dye Interactions and Humidity Indicator Based on MB.	8
1.3 Colorimetric Redox Dye-Based O₂ Indicators	12
1.4 Semiconductor Photocatalysis	15
1.4.1 Titanium Dioxide as a Photocatalyst.....	19
1.5 UV-Light-Activated Colorimetric Redox Dye-Based Indicators	21
1.5.1 Colorimetric Oxygen Indicators for MAP: Solvent-based Demand	24
1.6 Aims and Objectives	25
1.7 References	26

CHAPTER 2

EXPERIMENTAL	28
2.1 General Preparation of Oxygen Indicator	29
2.2 Photocatalyst Characterisation	30
2.3 Polymer and Dye Characterization	32
2.4 Light Sources and Spectrophotometry.	37
2.5 Other Methods	43
2.6 References	45

CHAPTER 3

FIRST GENERATION OF SOLVENT-BASED MB OXYGEN FILM INDICATOR	47
3.1 Introduction.....	48
3.2 Experimental	48
3.2.1 Materials and Chemicals	48
3.2.2 Preparation of Methylene Blue Ion-paired with dodecyl sulfate.....	48
3.2.3 Ink and Film Preparation	49
3.2.4 Irradiation and Colour Change Measurements	50
3.2.5 Contact Angle Measurement	51
3.3 Results and discussion	51
3.3.1 The Photobleaching Process (Step 1)	53
3.3.2 The ‘Dark’ Recovery Process (Step 2)	58
3.3.3 Contact Angle Measurements.....	60
3.4 Conclusion	61
3.5 References.....	62

CHAPTER 4

NANOCRYSTALLINE SnO₂-BASED, UVB-ACTIVATED, COLORIMETRIC OXYGEN INDICATOR.....	63
4.1 Introduction.....	64
4.2 Experimental	64
4.2.1 Materials and Chemicals	64
4.2.2 Ink and film preparation	65
4.2.3 Irradiation and colour measurement	66
4.3 Results and Discussion.....	69
4.3.1 Diffuse Reflectance Spectra of SnO ₂ and P25 TiO ₂	69
4.3.2 The UVB Activation and Recovery of a Typical nSnO ₂ Film	70
4.3.3 UV sensitivity of nSnO ₂ and P25 TiO ₂ based films (step 1)	72
4.3.4 Photobleaching (Step 1) as a Function of Irradiance.....	76
4.3.5 The Dark O ₂ Response (Step 2).....	77
4.4 Conclusion	78
4.5 References.....	79

CHAPTER 5

SECOND GENERATION OF SOLVENT-BASED OXYGEN INDICATORS 80

5.1	Introduction.....	81
5.2	Experimental	81
	5.2.1 Dye-Ion pair Preparation and Ink Formulation	81
5.3	Results and Discussion.....	83
	5.3.1 Photo-Activation Step (Step 1).....	83
	5.3.2 Dark Recovery Step (step 2).....	89
	5.3.3 O ₂ Inks in an Aqueous Media.....	93
	5.3.4 O ₂ Inks in a Freezer	95
	5.3.5 O ₂ Inks Detect H ₂ O ₂	97
5.4	Conclusion	98
5.5	References.....	99

CHAPTER 6

TEMPERATURE ACTIVATED HUMIDITY SENSORS 100

6.1	Introduction.....	101
6.2	Experimental	103
	6.2.1 Preparation of Inks	103
	6.2.2 Measuring Relative Humidity	104
	6.2.3 High Temperature UV/Vis on MB/HPC humidity indicator inks .	105
	6.2.4 UV/Vis Spectra Recording of the MB/HPC Humidity Indicator Films 105	
6.3	RESULTS AND DISCUSSION	106
	6.3.1 Methylene Blue/Urea System.....	106
	6.3.2 HPC and HEC films of Methylene Blue.....	109
	6.3.3 Methylene Blue in HPC.....	113
	6.3.4 MB / HPC humidity sensor	116
6.4	Conclusions.....	119
6.5	References.....	120

CHAPTER 7

**EFFECT OF ALKALI ON METHYLENE BLUE AND OTHER THIAZINE
DYES 122**

7.1	Introduction.....	123
7.2	Experimental	125

7.2.1	Materials and Chemicals	125
7.2.2	Spectrophotometric Measurements	125
7.2.3	Mass Spectrum Analysis	125
7.2.4	Computational Methods	126
7.2.5	NMR measurements	126
7.3	Results and discussion	126
7.3.1	MB Initial Experiments: Formation of Red MB.....	126
7.3.2	Properties of “Red Methylene Blue”	129
7.3.3	The Nature of Heterocyclic Nitrogen in MB and Analogous Dyes.....	130
7.3.4	Other Thiazines	134
7.4	Conclusions.....	137
7.5	References.....	139

CHAPTER 8

SUMMARY	141
8.1 Development of Colorimetric Indicators Based on Methylene Blue. ...	142
8.2 The Chemistry of Methylene Blue and Other Thiazine Dyes	144
8.3 Further work.....	145

LIST OF TABLES

Table 1.1 Typical refrigerated shelf-lives of food that have been stored in both a non-MAPed and MAPed environment.....	2
Table 1.2 Selected examples of MAP systems.....	3
Table 2.1 Specifications of the K bars used.	30
Table 3.1 (a) and (b) show contact angles measured on hydrophobic surface and hydrophilic surface for blank polymer solutions and inks respectively.....	61
Table 4.1 UV/Visible irradiance levels used in this work with the UVB, UVA and WW lamps.....	68
Table 4.2 UV/Visible irradiance levels used in this work with the UVB, UVA and WW lamps.....	70
Table 7.2 Composition of commercial samples of thiazine dyes used in this study, determined by HPLC.....	135

LIST OF FIGURES

Figure 1.1 Typical oxygen scavenger sachet in a food package; in this case, ham sold by Marks & Spencer, UK. (left), the oxygen scavenger inside the sachet (right).	4
Figure 1.2 The oxidised and reduced forms of methylene blue.....	7
Figure 1.3 The ‘blue bottle’ experiment.....	7
Figure 1.4 UV/Vis spectra of <i>leuco</i> -Methylene Blue (LMB) being re-oxidised to MB^+ and LMB. $[MB^+]_0$ and $[LMB]_0 = 10^{-5}$ M.	8
Figure 1.5 Ideal relative humidity for a range of products.....	9
Figure 1.6 An example of a cobalt free humidity indicating card.....	10
Figure 1.7 Schematic diagram of the relationship between relative orientation of chromophores and spectral shifts based upon molecular exciton theory.....	12
Figure 1.8 Two redox forms of the usually employed redox indicator dye, methylene blue. The reduced, colourless, leuco-methylene blue (LMB) undergoes rapid oxidation in the presence of oxygen to its blue form (MB^+).	13
Figure 1.9 A schematic picture of Ageless Eye TM oxygen indicator showing all redox processes involved.	14
Figure 1.10 Illustrations of Ageless Eye TM showing its colour changes in the absence and presence of oxygen.	15
Figure 1.11 Change in the electronic structure of a semiconductor compound as the number N of monomeric units present increases from unity to clusters of more than 2000.....	17
Figure 1.12 Illustration of the major processes occurring on a semiconductor particle following electronic excitation.....	18
Figure 1.13 Crystal structures of titanium oxide and TEM micrograph of P25 (x40000).....	19
Figure 1.14 Valence and conductance band positions for various semiconductors, and useful, relevant redox couples at pH 0.	20
Figure 1.15 Suggested models of P25 activity explaining the roles of the anatase and rutile phase respectively	21
Figure 1.16 Schematic illustration of the key processes involved in the UV-activation and subsequent response towards oxygen of a $TiO_2/MB/glycerol/HEC$	

visual oxygen indicator.... leading to recovery of initial colour, by the ambient oxygen.....	22
Figure 1.17 Photoactivation of a typical water-based, UV-activated, colorimetric oxygen indicator.....	23
Figure 1.18 Change in the normalized absorbance (measured at 610 nm) of a typical UV-activated, colorimetric oxygen indicator film as a function of time under an ambient atmosphere with different levels of O ₂ present.....	24
Figure 2.1 Apparatus for UV irradiation; A – 8W (with 2 × UVA); B – 6W (with 2 × UVC); C – 4W (with 2 ×UVC); D – PVP UV meter with detector.....	37
Figure 2.2 An illustration of a beam of light passing through a dilute solution.....	39
Figure 2.3 Showing a schematic diagram of the Perkin-Elmer LS-50B Luminescence Spectrophotometer.....	42
Figure 2.4 A diagram of interfacial energies acting on a sessile drop resting on a surface.....	43
Figure 2.5 A photograph of the (First Ten Angstroms 200) contact angle instrument used to measure contact angles.....	44
Figure 3.1 Methylene blue-dodecylsulphate ion pair.....	49
Figure 3.2(a) Typical diffuse reflectance spectrum of TiO ₂ /MB-DS/glycerol/zein oxygen indicator, before and after UVA light irradiation (provided by two 8 W blacklight blue tubes), typically for 5 s.....	52
Figure 3.2(b) Photographs of a typical oxygen indicator ink printed as the letters ‘TiO ₂ ’ on plastic.....	53
Figure 3.3 Schematic illustration of the key processes involved in the UV-activation and subsequent response towards oxygen of a TiO ₂ /MB/glycerol/HEC visual oxygen indicator.... leading to recovery of initial colour, by the ambient oxygen.....	54
Figure 3.4 Plots of FR as a function of irradiation time profiles for the photobleaching of P25 and TiO ₂ nano-rutile films in N ₂ using different light sources conditions.....	55
Figure 3.5 TEMs pictures of Degussa P25 TiO ₂ (A) and nano-rutile TiO ₂ (B) revealing very different morphologies that may be responsible for the different photoactivities.....	56
Figure 3.6 Plots of normalised initial rate (= $R_i = (dFR/dt)_{t=0} / FR_{t=0}$) vs. incident UVA light irradiance, I.....	57

Figure 3.7 Dark recovery in the diffuse reflectance spectrum of a nano-rutile TiO ₂ /MB-DS/glycerol/zein oxygen indicator film after a initial 5 s irradiation with UVA light ($I = 10 \text{ mWcm}^{-2}$).	58
Figure 3.8 Initial recovery rates for Degussa P25 (○) and nano-rutile TiO ₂ (●) films plotted as a function of the ambient %O ₂ in the gas cell.	59
Figure 3.9 Variation in FR as a function of time recorded for a typical TiO ₂ /MB-DS film subjected to repeated UVA irradiation ($I = 10 \text{ mWcm}^{-2}$) and dark recovery in O ₂ (6 cycles).	60
Figure 4.1(a) Powder XRD spectrum of <i>n</i> SnO ₂ . (b) TEM photographs of <i>n</i> SnO ₂ . ..	65
Figure 4.2 A typical methylene blue spectrum in the HEC film (--, $\lambda_{\text{max}} = 605 \text{ nm}$) and a spectrum of 10 ⁻⁵ M water solution of methylene blue (—, $\lambda_{\text{max}} = 665 \text{ nm}$).	66
Figure 4.3 Schematic illustration of the key processes involved in the UV-activation and subsequent response towards oxygen of a TiO ₂ /MB/glycerol/HEC visual oxygen indicator.... leading to recovery of initial colour, by the ambient oxygen.	67
Figure 4.4 Normalised relative intensity emission spectra of the lamps used in this work; 20 W UVB narrow band lamp (—), 8 W BLB UVA (—) and 8 W warm-white fluorescent tubes (--).	68
Figure 4.5 Reflectance spectra of <i>n</i> SnO ₂ (—) nanopowder (—) and P25 titania.	69
Figure 4.5 (a) Photographs of typical <i>n</i> SnO ₂ oxygen indicating film on glass cover slip (25 mm diameter) before and after 10 min of UVB irradiation (in N ₂). The last picture shows the UV activated film after 15 min in air, by which time it has fully recovered its original colour. (b) UV/vis absorption spectra of a typical <i>n</i> SnO ₂ (100/100/5/100 pphr) indicator film photobleaching as a function of irradiation time (1 min intervals) in the photobleaching step (spectra taken from top to bottom). (c) UV/vis spectra of the P25-based film (100/100/5/100 pphr) using the 2x8 W warm-white fluorescent tubes (UVA $I = 0.04 \text{ mWcm}^{-2}$, $E_v = 7000 \text{ lx}$) under nitrogen atmosphere, spectra were recorded every minute (total of 10 mins).	72
Figure 4.7 (a)-(d) Photobleaching of typical O ₂ indicator films with: (i) <i>n</i> SnO ₂ , composition: 100/100/5/100 (●), (ii) P25 TiO ₂ , composition: 100/100/5/100 (▲), (iii) P25 TiO ₂ , composition: 100/100/5/20 (■) and (iv) ‘no photocatalyst’ (○).	76
Figure 4.8 The plot of the absorbance of a typical <i>n</i> SnO ₂ /MB film at $\lambda_{\text{max}} 605 \text{ nm}$ versus irradiation time profiles using UVB light (TL01 2x20W) at different irradiances	77
Figure 4.9 Recovery of a typical <i>n</i> SnO ₂ film when UV activated (in N ₂) and then exposed to different O ₂ levels (from right to left: 1.3, 2.6, 5.3, 10.5, 21 %O ₂). The inserted diagram shows a subsequent plot of the data in the form of: t_{50} (▲) and $1/t_{50}$ (■) (gradient of the slope = 0.35) as a function of %O ₂	78
Figure 5.1 The reaction scheme of the sulfonation of polystyrene.	81

Figure 5.2 Plot of UV/Vis spectra of a typical MB/SPS/TiO ₂ /glycerol oxygen-indicating film before and during the UVA light activation (60 sec of UVA/7 mWcm ⁻²) step (step (1), Figure 5.4).....	83
Figure 5.3 Photographs of this film before (left) and after the pulse of UVA light.	84
Figure 5.4 Schematic illustration of the key processes involved in the UV-activation and subsequent response towards oxygen of a TiO ₂ /MB/glycerol/HEC visual oxygen indicator.... leading to recovery of initial colour, by the ambient oxygen.	85
Figure 5.5 Absorbance vs. time profiles for a typical O ₂ indicator film photobleaching as a function of different UVA irradiances.	86
Figure 5.6 Relative change in absorbance, ΔAbs, vs. time of UVA photobleaching of a MB/SPS/TiO ₂ /glycerol film as a function of TiO ₂ concentration in the film.....	87
Figure 5.7. Plot of ΔAbs vs. the time of irradiation for a typical O ₂ indicator film containing different pphr of MB.	89
Figure 5.8 A comparison of the recovery (step (2), Figure 1.5) kinetics exhibited by two different MB-based oxygen indicators, namely, an aqueous-based P25 (●) and the novel acetone-based nanorutile; which recovers in ca. 24 hours (▲) as shown in the inserted plot.	90
Figure 5.9 Plot of the relative absorbance of a typical, photobleached indicator vs. time of recovery, in air at 20 °C, as a function of relative humidity (RH).	91
Figure 5.10 Plot of initial rate of recovery of a typical photobleached film vs. concentration of oxygen in 100% RH blends of oxygen and nitrogen gas.....	93
Figure 5.11 The first picture (Dry) shows two films cast to test for leaching in still water; on the left is a typical water-based ink of 100/100/5/20 in HEC and on the right is the solvent-based ink of 100/100/1/40 in PS-SO ₃	94
Figure 5.11 Showing the recovery of a typical solvent-based indicator ink film under still water.....	95
Figure 5.13(a) Shows the response of 7 samples to freezing conditions (-18 °C). Each sample was removed from the freezer on successive days over seven days. So, for example, ‘Sample 3’ was removed from the freezer on day 3 (‘3d’, horizontal axis) and its response monitored over the remaining 4 days. (b) Shows the response of two control samples, one in a freezer and the other at room temperature.	96
Figure 5.14(a) SO ₃ -Ps based indicator recovery in H ₂ O ₂ vapours in comparison to Lissamine Green (time of H ₂ O ₂ vapour exposure, 6% H ₂ O ₂ at RT).....	97
Figure 5.14(b) Shows that the same MB/SPS/TiO ₂ /glycerol oxygen-indicating ink film (also shown in Figure 5.14(a)) can be reactivated with UVA light and re-used, whereas the Lissamine Green film can not.	98

Figure 6.1 - Absorption spectra of MB (0.0215 mol kg ⁻¹) in PVP film at 0 and 88% relative humidity (from Otsuki ²⁶) spectra indicated ‘first’ ‘second’ etc. are from repeat exposures to different humidities	102
Figure 6.2 (a) Experimental set up for measuring relative humidity (RH). Description is given in the text above.	105
Figure 6.3 The set up used for recording the UV/vis spectra at different temperatures. Sample is fitted in the furnace and connected with the source and detector using optical fibres.	106
Figure 6.4 - Photographs of a typical MB/urea/HEC relative-humidity indicator changing colour from pink (left) to blue (right) upon exposure to 100% RH air, from the bottom right.	107
Figure 6.5 Spectral changes of a typical MB/urea/HEC relative-humidity indicator film before (—) and after (■) exposure to 100% RH air.	107
Figure 6.6 - Photographs of a urea/HEC with no dye changing from an opaque film (left) to a clear film (right) upon exposure to 100% RH air.	108
Figure 6.7 Showing the difference in structure between HEC and HPC.	110
Figure 6.8 Photographs of freshly prepared MB/HEC and MB/HPC films (left); same films left to dry at room temperature (centre); and colour change induced by exposing the dried films to humidity(right).	110
Figure 6.9 Showing the colour change of freshly cast Methylene Blue/HPC exposed to a 3 s heat pulse.	111
Figure 6.10 (a) Photographs of freshly prepared MB/HPC (left, pink/purple). Same film thermally activated using a heat gun (middle, blue) and then exposed to 100% humid air (right, pink). (b) A UV/vis spectrum of the three colorations of the MB/HPC film from (a). The freshly prepared film shows lower absorbance ($\lambda_{\max} = 505$ nm, black line) and 20 nm blue shift before the heat/humidity activation ($\lambda_{\max} = 530$ nm, red line). Heat gun activated blue film has much higher absorbance ($\lambda_{\max} = 605$ nm, blue line).	112
Figure 6.11 (a) A 3D waterfall plot showing the effect of a 3.5 second pulse of heat from a heat gun on the spectrum of a freshly cast MB/HPC film. The spectra marked in red are recorded at 0.9, 1.9, 2.9 and 3.9 seconds. (b) A detailed plot of Abs _λ vs. time profiles using data from the 3D plot are shown here as well as the temperature vs. time profile (red line).	114
Figure 6.12 - MB/HPC disc heat gun pulse followed by 100% humid air measured abs at 660 nm.	116

Figure 6.13 Photos of successive humidifying (◆) and heating (Δ) showing the colour of a typical MB/HPC film with dry/heated films on the left and wet films on the right.	117
Figure 6.14(a) The response of a typical MB/HPC film under 70% humid air stream. (b) Absorbance vs time profile shown for $\lambda_{\text{max}} = 660$ nm.	118
Figure 6.15 Initial rate of recovery vs. % relative humidity of MB/HPC films. The inserted plot shows a sorption isotherm as measured by Yakimets.	119
Table 7.1. Summary of structural, spectral and physical characteristics of MB and other relevant thiazine dyes and derivatives.	124
Figure 7.1 (a) - Top: Photographs of a fresh 10^{-4} M MB, 0.1 M NaOH aqueous solution (from left to right): before, directly after and 5h after mixing and shaking with an equal volume of toluene.	128
Figure 7.1 (b) - Visible absorption spectrum (measured in 1 cm cuvette) of the aqueous MB solution (i) before, (ii) directly following, and (iii) 5h after (grey line) mixing and shaking with an equal volume of toluene.	128
Figure 7.2 ^1H NMR spectra of (top to bottom) purchased MVB (Aldrich), red MB* (both recorded in CCl_4 using Bruker Avance-III 600 NMR spectrometer) and methylene blue (Acros) (recorded in D_2O using Bruker Avance/DRX 500 NMR spectrometer).	130
Figure 7.3 Major valence bond resonance structures of MB. Alternative Kekule structures of benzenoid rings and charged-carbon mesomers are not shown.	131
Figure 7.4 NBO charge distribution on the PCM/B3LYP electronic ground state of MB. See Computational Methods for details.	132
Figure 7.5 Photographs of a range of freshly made 10^{-4} M thiazine dye solutions in 0.1 M NaOH (from left to right): before, directly after, and 5h after mixing and shaking with an equal volume of toluene.	136
Figure 7.6 Summary of reactions of MB with alkali.	138

CHAPTER 1

INTRODUCTION

1.1 MODIFIED ATMOSPHERE PACKAGING AND OXYGEN INDICATORS

Developments in food packaging have been driven in recent years by increased demands on, for example, product safety, cost-efficiency and consumer convenience.¹ Oxygen is implicated in the spoilage of food,^{2, 3} since its presence allows innumerable aerobic food-spoiling micro-organisms to grow and multiply. Many preservation processes also attempt to eliminate spoilage by lowering the availability of water to microorganisms and a measure of this is what is known as 'water activity'. This is not the same as moisture content, but instead refers to tendency of water to escape from a food as a vapour. The water activity of a food depends not only on its composition but also on its temperature and is why such organisms are active above the freezing point of food and are most prevalent in foods of high water activity. Thus, keeping food chilled in an ambient atmosphere that is low in oxygen features strongly in most current, popular methods of food packaging and storage.

A common example of the latter is modified atmosphere packaging,^{2, 3} MAP (modified atmosphere packaging), a process in which the atmosphere within the food package is flushed with an inert gas, such as nitrogen or carbon dioxide, reducing the oxygen content to typically 0.5–2%. Unlike nitrogen, carbon dioxide is classified as an active gas in food packaging, since it affects most food-spoiling microbes, reducing significantly their growth, even if some oxygen is present.² Both carbon dioxide and nitrogen slow the rates of respiring foods, such as fruits and vegetables and retard oxygen-based spoilage. As a consequence MAP is very effective at extending the shelf-lives of many foods and is widely used in food packaging. Some typical shelf-lives of MAPed and non-MAPed foods are given in **Table 1.1**.

Table 1.1 Typical refrigerated shelf-lives of food that have been stored in both a non-MAPed and MAPed environment.⁴

Shelf-life Extension with MAP (days of refrigerated shelf-life)		
Product	Non-MAP	MAP
Fresh red meat (high O ₂)	2-3	6-10
Fresh red meat (low O ₂)	2-3	21
Fresh sausage	4-5	15-16
Fresh processed poultry	3-10	12-18
Cooked poultry	5-16	21-30
Cooked/cured meats	1	30-45
Cheese	7	180+
Fresh Pasta	3	60+

The modified atmosphere for a package of food must be optimised for each product as shown in **Table 1.2**. If a package's integrity has been compromised by a pin-hole leak then the concentration of oxygen will increase. However, as aerobic microbial growth takes hold, oxygen in the package will be consumed and carbon dioxide will be evolved.⁵ Thus, it is possible to have a package with a pin-hole leak in which the food is not safe to eat (due to oxygen ingress and subsequent microbial metabolism) but with a package head-space that is mainly carbon dioxide and largely oxygen free.

Table 1.2 Selected examples of MAP systems.⁶

Food application	MAP gas mixture
Raw red meat	80% O ₂ , 30 % CO ₂
Cooked, cured and processed meat products	30% CO ₂ , 70% N ₂
Carbonated soft drinks	50% CO ₂ , 50% N ₂
Fresh whole and prepared fruit and vegetable products	5% O ₂ , 5% CO ₂ , 90% N ₂
Hard cheese	100% CO ₂
Grated and soft cheese	30% CO ₂ , 70% N ₂
Dried food products (coffee, milkpowder etc.)	100% N ₂

After flushing a food package with an inert gas the level of residual oxygen in a package head-space is often still significant (0.5-2%), due to poor gas flushing and the ability of the food to trap air. The level of residual air can also increase with time due to poor sealing and the permeation of oxygen through the package material from the surrounding air.² In order to overcome these problems, and ensure a very low residual level of oxygen over the lifetime of the food package, an oxygen scavenger can be added to the packaging, usually in the form of a sachet or label. Typically, such sachets are used to maintain the level of oxygen in a food package at 0.1% or less. Major manufacturers of oxygen scavengers, with their product name in brackets, include Mitsubishi Gas Chemical Company (AgelessTM), Toppan Printing Company (FreshliserTM) and multisorb Technologies (Fresh MaxTM).⁷

The active ingredient in most oxygen scavenger sachets or labels for the food industry is ferrous oxide, FeO.^{3, 8} The sachets or labels are clearly labelled 'Do Not Consume', although the amount of FeO used is, typically, < 200 times that of a lethal dose for an adult. In order to avoid the possible ingestion of the contents of an oxygen scavenger, which can be mistaken as a condiment despite its 'Do Not Consume' warning, such sachets are often placed under the peel-back lids of the packages. **Figure 1.1** illustrates a typical oxygen scavenger sachet concealed in a food package from a UK supermarket.



Figure 1.1 Typical oxygen scavenger sachet in a food package; in this case, ham sold by Marks & Spencer, UK. (left), the oxygen scavenger inside the sachet (right).⁹

A major problem with MAP and/or oxygen scavengers is that a leaking package, or one with significant oxygen content, is not easily identified. An oxygen indicator would therefore act as a leak and tamper detector providing a simple and effective method of quality assurance for the packager. This technology would also reassure the consumer about the freshness of product inside. Moreover this technology would target only compromised packages rather than the wasteful methods currently in use in which a random package is selected per several hundred and is tested using time consuming and expensive methods (e.g. FTIR or GC) performed by a trained technician. If the sample package is found to be compromised then the whole batch is either reprocessed or scrapped. This is clearly not ideal, economically or ecologically, and with the increasing demand for MAP and oxygen scavenged packages the need for an oxygen indicator which is inexpensive, reliable and easy to read is clear.⁷

The most easily used oxygen indicators would be based on a colour change, rather than, a change in fluorescence, since the human eye, rather than an expensive piece of equipment, such as fluorimeter, could be used to rapidly monitor the state of indicator.

1.1.1 Intelligent Packaging

By definition, intelligent packaging monitors and provides the consumer with information about the quality of the packed food. Intelligent packaging also gives information on product quality directly (freshness indicators), the package, its head-space gases (leakage/gas indicators) and the storage conditions of the package (time-temperature indicators). These emerging systems, attached as labels or incorporated into food packaging material, have been seen as potential new technologies offering enhanced possibilities to monitor the product quality trace the critical points and provide more complex information throughout the supply chain. A more effective package/product quality control system facilitates a more efficient production. Higher package and food quality results in fewer complaints and returns from retailers consumers, and so cost-savings and better branding and image for the manufacturer. Also, more product information can be delivered to consumers. The

development of new intelligent systems for food packaging has been one of the focuses of food packaging research since the early 1990s. Clearly, a key MAP package indicator is one based on O₂ detection. Thus, in following text the most important O₂-sensitive colorimetric indicators for potential use in MAP will be described.

1.2 METHYLENE BLUE

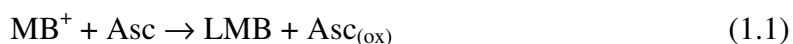
Thiazine dyes are among the earliest of synthetic dyes. Methylene blue (MB⁺) is a classical thiazine dye that was originally synthesized by Heinrich Caro¹⁰ and which has been commercially available since its first production by BASF in 1876¹⁰. During this time it has found numerous and widespread uses^{11, 12} and these include; as a dye for temporary hair colorants, leather and cellulosic fibres; a redox indicator; an ISO test pollutant in semiconductor photocatalysis; a photosensitizer for singlet oxygen generation; an antioxidant and antiseptic; a stain for fixed and living tissues; a diagnostic agent in renal function tests; an antidote to cyanide poisoning; and as a treatment for malaria. Under the name of “rember” it has recently been reported to be effective in arresting the progress of Alzheimer’s disease.^{13, 14}

Methylene blue is stable, cheap, reactive and highly coloured cationic dye usually available in a form of dark green crystals as a chloride salt hydrate. MB⁺ is water soluble (35.5 g L⁻¹), but it dissolves in other protic solvents such as ethanol (14.8 g L⁻¹) and acetone (5 g L⁻¹) to certain degree as well. The few solvents that MB⁺ is not capable of staining are diethyl ether and toluene.

1.2.1 The Redox Chemistry of Methylene Blue

The popularity of Methylene Blue stems from its redox chemistry; the redox indicator properties of this couple have been used extensively in chemical analyses. For example it has been used in the quantitative analysis of a large number of mild reducing agents such as glucose (GH) or ascorbic acid (Asc)¹⁵⁻²⁰ and is also used in a test for the freshness of milk which checks for any reducing species present due to bacterial growth²¹. As we shall see, many *oxygen* indicators, including the commercial product Ageless Eye™, also employ the Methylene Blue/*leuco-*

Methylene Blue redox couple as the key indicator system. In such studies the reduction of MB^+ usually involves two rival processes in which the hydrogenation of the molecule to the colourless *leuco*-Methylene Blue (LMB) by the reducing agent (*e.g.* ascorbic acid) competes against the re-oxidation of LMB back to MB^+ by oxygen as shown below (**Figure 1.2**)²²:



The relationship between MB^+ and LMB can be summarised as follows:

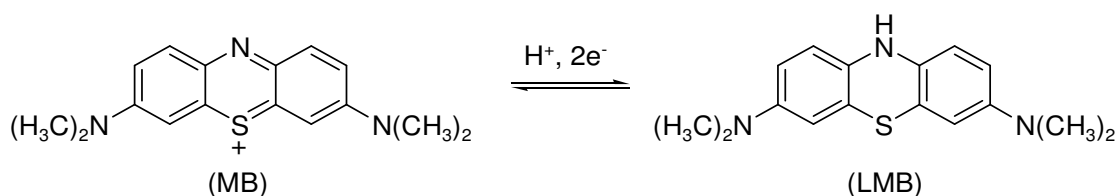


Figure 1.2 The oxidised and reduced forms of Methylene Blue ²².

This is best demonstrated by the famous ‘blue bottle’ experiment²³ (see **Figure 1.3**). The original ‘blue bottle’ experiment comprises the blue-coloured redox indicator dye Methylene Blue, MB, dissolved in an alkaline glucose solution, all sealed in a bottle with a generous headspace, so that when shaken the solution is thoroughly oxygenated. On sitting the solution loses its colour due to the reduction of MB to its reduced form, *leuco*-Methylene Blue (LMB), by the deprotonated glucose present (Glu-H). When shaken, the solution turns blue due to the oxidation of LMB to MB by the dissolved oxygen originating from the headspace.

Figure 1.4 shows a set of absorption spectra taken as LMB is oxidised to MB^+ in air. The spectra revealed wavelengths of absorption of MB^+ at 294 and 665 nm and a wavelength of maximum absorption of LMB at 256 nm. The plot was obtained by reducing $10^{-5} \text{ mol dm}^{-3} \text{ MB}^+$ at pH 2 using a zinc-mercury amalgam to LMB and then remove it and allowing the LMB to air oxidize over time.



Figure 1.3 The ‘blue bottle’ experiment. A stoppered solution of alkaline glucose with MB^+ added loses its colour on standing. After shaking the solution, oxygen is re-introduced into solution and oxidises the colourless LMB back to MB^+ .

After filtration to remove the amalgam a 4 mL extract of this solution was placed into a 1.00 cm quartz cuvette and allowed to react with ambient air and re-oxidise back to MB^+ . The process was monitored in a single beam spectrophotometer and the results clearly show that as the absorption of MB^+ increases that of LMB decreases as the overall re-oxidation process takes place via the reaction described by the equation (1.2) previously.

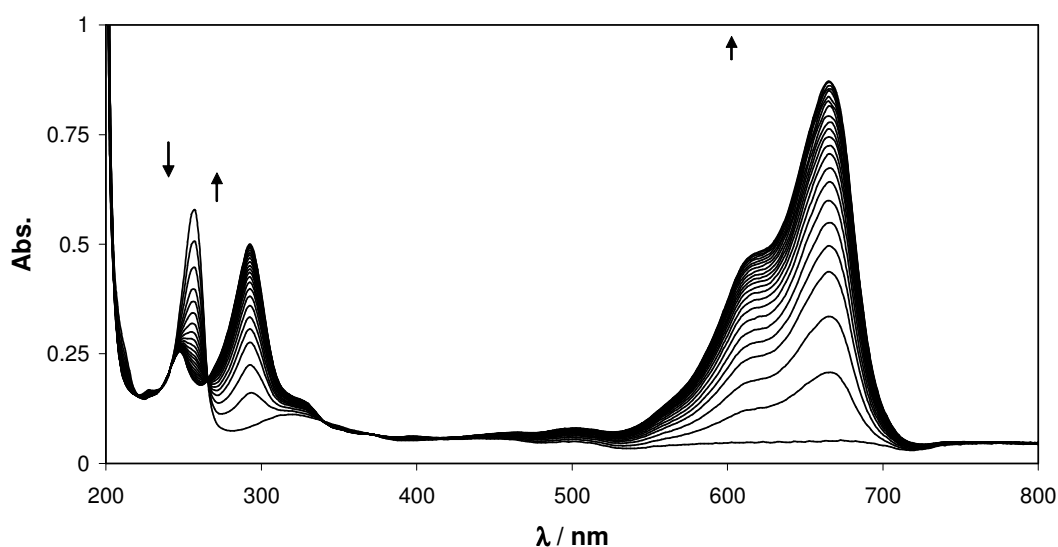


Figure 1.4 UV/Vis spectra of *leuco*-Methylene Blue (LMB) being re-oxidised to MB^+ and LMB. $[\text{MB}^+]_0$ and $[\text{LMB}]_0 = 10^{-5} \text{ M}$.²² The spectrum was recorded every 30 s.

1.2.2 Colour Effects from Dye-Dye Interactions and Humidity Indicator Based on MB.

The shelf-life of many products depends greatly on the level of moisture in a package. Thus, an active moisture regulation system is essential to keep the goods in the optimum, sometimes very narrow range humid environment. Raisins, for example will become hard, beef jerky loses its tasty texture in less than 70% relative humidity. Ready to eat cereals lose the crisp consistency if stored under more humid conditions (see **Figure 1.5**). For some products, like cigars, the ideal %RH provides a thriving environment for moulds and other microorganisms so beside the humidity controlling pouches an oxygen scavenger is also present for an effective mould growth inhibition.

Product	Ideal RH storage value (%)
Fruits and vegetables	>90
Beef jerky	88
Raisin	74-75
Cigars	68-72
Wooden instruments	50
Artwork	50
Coffee beans	30
Dry cereal	30
Electric circuits boards	20

Figure 1.5 Ideal relative humidity for a range of products.¹

Technologies using desiccants such as silica gels, molecular sieves or certain clays are commonly used to maintain low humidity. Wicks or sponges will help to retain higher moisture content. Humidipak is an example of a commercially available moisture regulator which can be tailored to maintain certain %RH. Electronic devices to maintain stable humidity are also available, though, they are rather expensive.

The majority of colorimetric humidity indicators are based on cobalt(II) chloride and historically are tied to military industry to prevent corrosion of metal-based weaponry. However, their usage spread with the development of information technologies which use moist sensitive semiconducting parts. **Figure 1.6** shows an example of a cobalt free humidity indicator.



Figure 1.6 An example of a cobalt free humidity indicating card.²⁴

Otsuki and Adachi *et al.*²⁵ have shown that films of PVP containing Rhodamine 6G or Methylene Blue undergo changes in absorbance when exposed to air streams of varying relative humidity. These changes are ascribed to aggregation of the dyes, with both dyes showing a shoulder in their spectra due to the formation of higher aggregates when exposed to higher relative humidities (ranging from RH of 0% to 88%). The peak ratio of aggregate to monomer also increased with increasing concentration of dye in the film, *i.e.* the higher the dye concentration the more significant the colour change and this was seen as further evidence of dye aggregation as the reason for the colour change of the film on exposure to humid air. More interestingly however the authors used Reichardt's dye and the computed $E_T(30)$, energy of transition, value²⁶ to show that the PVP film polarity increases considerably with increasing relative humidity. They also state, however, that changes in the polarity of the PVP cannot be the only reason for induced dye aggregation. Rather they suggest that the PVP-absorbed water, at high relative humidity, forms clusters in the film which then attract and accumulate the dyes in them causing the formation of the aggregates.

Matsushima *et al.*²⁷ have reported reversible temperature and humidity dependent colour changes in solid thin films of sugar gels (*kappa*-carrageenan) containing flavillium perchlorate. The colour changes, as measured by UV/Visible spectrophotometry, were ascribed to the formation and deformation of extended dye-

aggregates. Absorbance spectra of aqueous alcohol solutions of the flavillium containing sugar gel showed greater colour changes with temperature compared to the dried thin films; extended aggregates were present at low temperature (0 °C) and the monomer at high temperature (50 °C). The thin films however were much less sensitive to temperature with the dye aggregate shoulder dominating even at higher temperature (50 °C). It is also mentioned that although these dye-containing sugar gel films revealed good reversibility toward temperature they showed only moderate reversibility towards humidity. The authors also mention in a footnote that similar humidity- and temperature-sensitive colour changes have been observed in thin films with Methylene Blue and thionine.

The above mentioned observations are based on thiazine dyes ability of forming aggregates with increasing concentration; this is due to their charge and planar shape which allows easy stacking of the monomers on top of each other. The extent of aggregation of MB⁺ is limited to simple dimerization in the concentration range 1×10^{-5} to 1×10^{-3} M ($K_D = 3.97 \times 10^3 \text{ M}^{-1}$) in aqueous solutions²⁸. This results in maximum absorbances in the visible region at 660 and 610 nm for the monomeric and dimeric species respectively²⁹. The higher aggregates are formed in hydrogels or in solid phase³⁰. The hypsochromic shift due to this aggregation of the dye molecules could result in a pink to red coloration.

Exciton theory describes the way in which two chromophores interact on photoexcitation.³¹ A simple explanation of the main effect relies on dipole interactions where energy splitting depends on the relative orientation of the transition dipoles.

When the dipoles are aligned in the same direction (nearest neighbour +ve aligned with +ve and -ve aligned with -ve) they are said to be in phase and the transition is allowed. On the other hand when the dipoles are aligned oppositely the transition is disallowed. There are two ideal cases, when the interacting dyes are fully face-to-face and parallel (**Figure 1.7** left), and when they are 'slipped' with respect to the other, giving a head-to-tail arrangement (as on the right of **Figure 1.7**).

In the first case when the dyes are fully parallel (like charges aligned to each other, +/+ and -/-) the transition dipole combination is destabilising due to the repulsive like/like interaction and is higher in energy than the out of phase combination (two

stabilizing nearest neighbour +ve/-ve adjacencies). In the second case when the dipoles are not fully parallel but instead are ‘slipped’ with respect to the other, to give a head-to-tail arrangement, the stabilizing nearest neighbour +/- interaction of the in-phase combination becomes lower in energy than the out-of-phase. Thus a fully parallel arrangement, will display a hypsochromic or ‘blue’ shift relative to the monomer, while the head-to-tail arrangement, will have a bathochromic or ‘red’ shift. The parallel face-to-face arrangement is known as a H-dimer, or more generally H-aggregate for more extensive combinations (“pile of coins”). The head-to-tail arrangement is known as a J-dimer or J-aggregate.

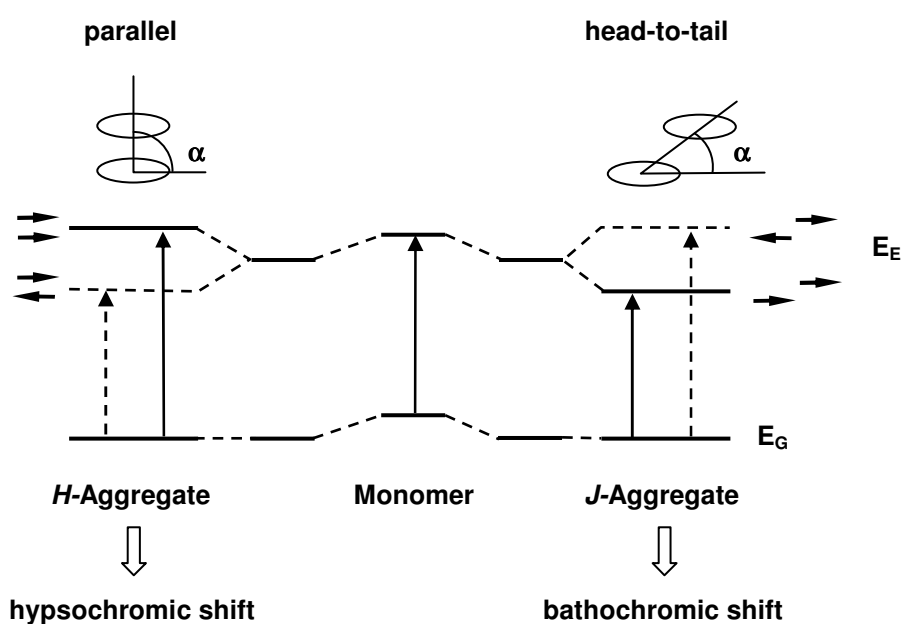


Figure 1.7 Schematic diagram of the relationship between relative orientation of chromophores and spectral shifts based upon molecular exciton theory.³²

The above helps explain the initial observation of reports of MB as a potential humidity indicator.

1.3 COLORIMETRIC REDOX DYE-BASED O₂ INDICATORS

The most commonly used O₂ indicators used in food packaging are colorimetric and use a redox dye.⁵ Such indicators can take several forms, such as a tablet^{33, 34} or a printed layer³⁵⁻³⁷. Alternatively, they can be laminated in a polymer film.³⁸ An

example of this technology is the Ageless Eye™ oxygen indicator. Generally these indicators include a redox indicator, such as Methylene Blue (MB⁺), and a strong reducing agent, such as glucose in an alkaline medium (so as to prevent the dye being oxidised too rapidly by oxygen), see **Figure 1.8**.

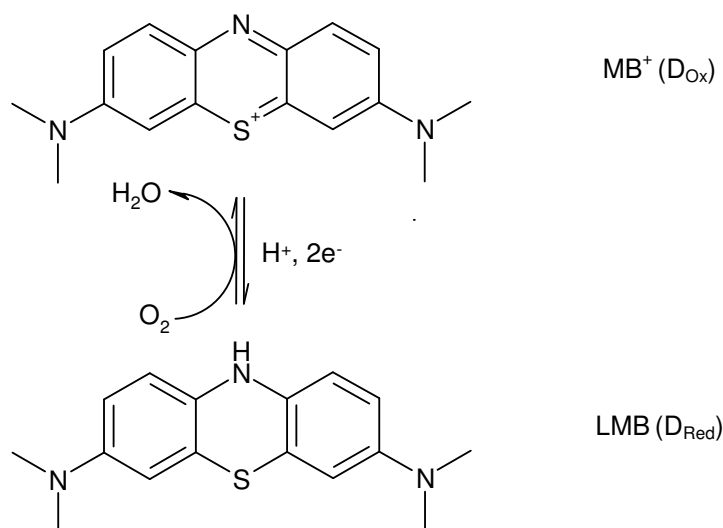


Figure 1.8 Two redox forms of a usually employed redox indicator dye, Methylene Blue. The reduced, colourless, *leuco*-Methylene Blue (LMB) undergoes rapid oxidation in the presence of oxygen to its blue form (MB⁺).

In the absence of oxygen the redox-indicator will exist in its reduced form (which is often colourless, as in the case of *leuco*-Methylene Blue, LMB), D_{Red} due to reduction by the reducing agent present (usually glucose in alkali). Thus, in the absence of a significant level of oxygen (typically <0.1 %) the following bleaching reaction dominates and most of the dye is reduced:



However, in the presence of a significant level of oxygen (typically >0.1 %) the redox-indicator is oxidised to its usually more highly-coloured form, D_{Ox}, and the following oxidation reaction dominates:



In the case of Ageless Eye™, $D_{Ox} = MB^+$, $D_{Red} = LMB$. Glucose is the reductant and gluconic acid is the oxidised form of the reductant, see **Figure 1.9**. Additional components usually employed in commercial forms of this indicator system include a non-redox indicator dye, Acid Red 52, which is added to provide a background pink colour to the indicator^{4, 34} and magnesium hydroxide, to provide an alkaline environment.

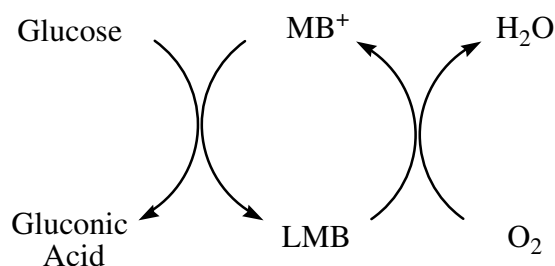


Figure 1.9 A schematic picture of Ageless Eye™ oxygen indicator showing all redox processes involved.

The components are often combined and pressed together to form a pellet or tablet. This is then encapsulated in a clear plastic sachet (to prevent direct contact with food due to the water soluble nature of the components) which is oxygen permeable but ion impermeable. **Figure 1.10** below shows a diagram of Ageless Eye™ and reveals the colour change it undergoes in the absence and presence of oxygen.⁴ Despite the success of such indicators as Ageless Eye™, several issues regarding their production and usage have proved to be problematic. For example, the indicators are relatively expensive to produce ($\gg 1$ cent) and so cannot be used in every oxygen scavenged food package. Furthermore, they require storage under anaerobic conditions due to the consumption of glucose in air and are also usually moisture sensitive, working best under humid conditions. As a consequence, the Ageless Eye™ and other colorimetric redox-indicators have been confined to research or testing of packaging equipment. Issues such as cost, reversibility and storage have, thus far, proved to be major obstacles to their general usage in oxygen scavenged food packages.⁷

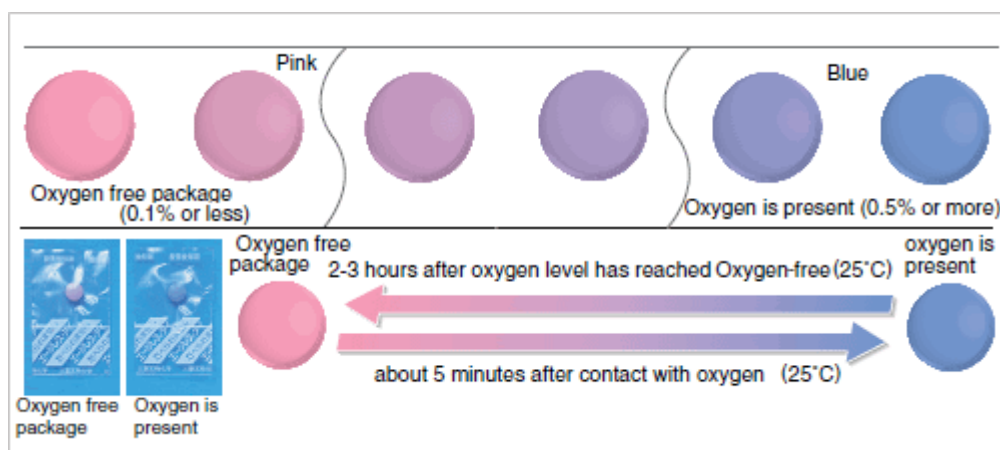


Figure 1.10 Illustrations of Ageless Eye™ showing its colour changes in the absence and presence of oxygen.⁴

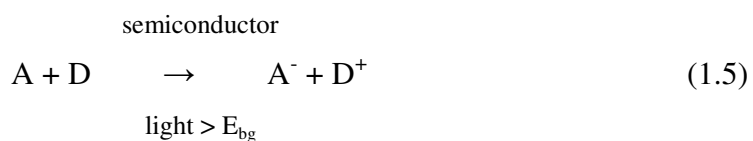
In a recent development our group has created a new range of oxygen, colorimetric indicators³⁹. These indicators are UV-activated and utilize nanoparticulate titania as a semiconductor photosensitizer. Before discussing these indicators it is appropriate to review briefly the basic principles of semiconductor photocatalysis.

1.4 SEMICONDUCTOR PHOTOCATALYSIS

Semiconductor photocatalysis is one of the most active, current areas of interdisciplinary research, attracting efforts from photochemists, photophysicist environmental engineers, and scientists in related fields. The initial driving force for these efforts was the search for alternative energy sources due to the oil crisis in early 1970s and subsequently over 2000 papers have been published in this general area.⁴⁰ A catalyst is a substance that accelerates a reaction without being consumed as a reactant. In redox-induced reactions of organic materials a catalyst involved in such a transformation can itself be organic or inorganic. As long as it does not participate in bonding with the products that are ultimately formed, the chemical nature of the catalyst is immaterial. A thermal catalyst is one that is activated by heat. More precisely, a thermal catalyst is a substance that appears in the rate expressions that describes its reaction without appearing in the stoichiometric equation.⁴¹ A parallel definition of photocatalysis will thus involve a substance whose chemical function is activated by a photon rather than by heat. The photocatalyst is not consumed in a

photochemical reaction, although it will improve the attainable efficiency of a given photo-conversion.⁴² In reality the term "photocatalysis" is in widespread use and is here to stay; it is not meant to, nor should it ever be used to, imply catalysis by light, but rather the "acceleration of a reaction by the presence of a photo-sensitizer". Photosensitization is a process by which a photochemical alteration occurs in one chemical species as a result of the initial absorption of radiation by another chemical species called the photosensitizer.⁴⁰

The overall process of semiconductor-sensitized photoreactions can be summarized as follows



where E_{bg} is the bandgap of the semiconductor (see below). If, in the absence of semiconductor and light of energy greater than or equal to E_{bg} , ΔG° for reaction (1.5) is negative, the semiconductor-sensitized photoreaction is an example of photocatalysis.⁴³ Alternatively, if ΔG° for reaction (1.5) is positive, the semiconductor-sensitized photoreaction is an example of photosynthesis.⁴⁰

As indicated in **Figure 1.11**, for many compounds as the number N of monomeric units in a particle increases, the energy necessary to photo-excite the particle decreases. When $N \gg 2000$, it is possible to end up with a particle which exhibits the band electronic structure of a semiconductor.

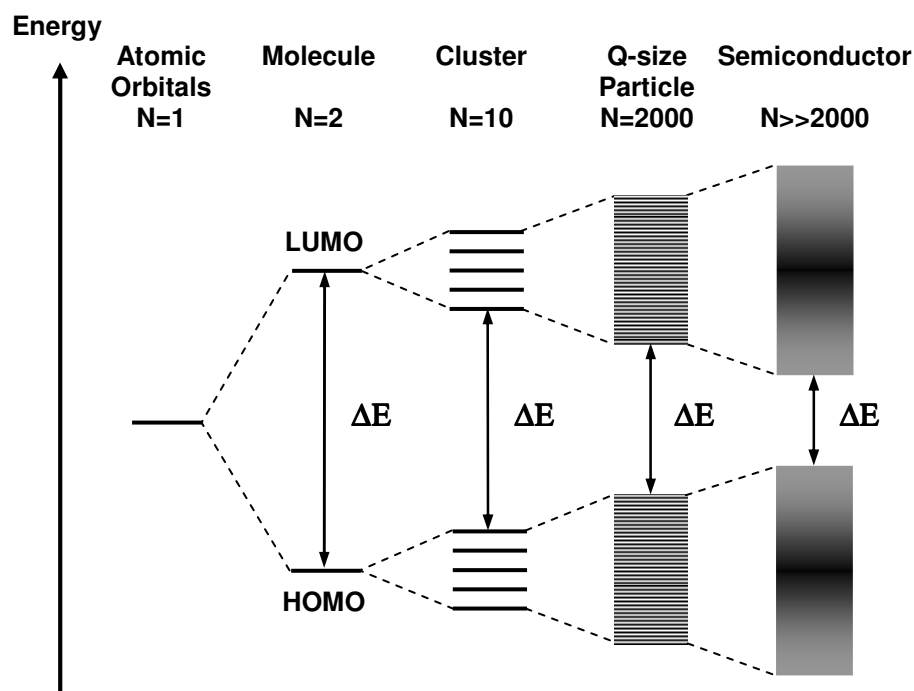


Figure 1.11 Change in the electronic structure of a semiconductor compound as the number N of monomeric units present increases from unity to clusters of more than 2000.⁴⁴

In a semiconductor the highest occupied band (the valence band) and lowest unoccupied energy band (the conductance band) are separated by a bandgap E_{bg} , a region devoid of energy levels in a perfect crystal.

Activation of the semiconductor photocatalyst for reaction (1.5) is achieved through the absorption of a photon of ultra-bandgap energy, which results in the promotion of an electron e^- from the valence band to the conduction band, with the concomitant generation of a hole h^+ in the valence band as illustrated by the diagram in **Figure 1.12**. For a semiconductor photocatalyst to be efficient, the different interfacial electron processes involving e^- and h^+ , i.e. reactions (c) and (d) in **Figure 1.12**, must compete effectively with the major deactivation processes involving $e^- - h^+$ recombination, i.e. reactions (a) and (b) in **Figure 1.12**.

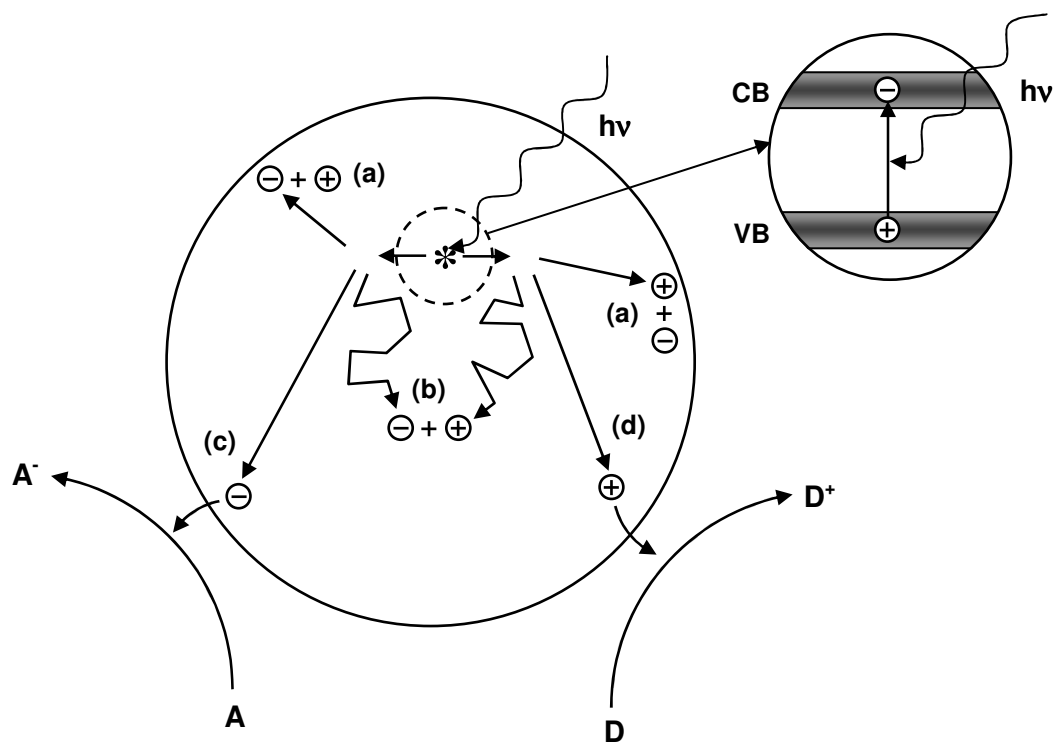


Figure 1.12 Illustration of the major processes occurring on a semiconductor particle following electronic excitation. Electron-hole recombination can occur at the surface (reaction (a)) or in the bulk (reaction (b)) of the semiconductor. At the surface of the particle, photo-generated electrons can reduce an electron acceptor A (reaction (c)) and photo-generated holes can oxidize an electron donor D (reaction (d)). The combination of reactions (c) and (d) represents the semiconductor sensitization of the general redox reaction (1.3) given in the text.⁴⁴

1.4.1 Titanium Dioxide as a Photocatalyst

There are three types of crystal structures in natural titanium oxide: rutile, anatase, and brookite (**Figure 1.13**). All three of these types are expressed using the same chemical formula (TiO_2); however, their crystal structures are different. Titanium oxide absorbs light having an energy level higher than that of the band gap, and causes electrons to jump to the conduction band to create positive holes in the valence band. Despite the fact that the band gap value is 3.0 eV for the rutile type and 3.2 eV for the anatase type, they both absorb high energy, UV or near UV light. Obviously, rutile TiO_2 can absorb some visible (*i.e.* > 400 nm) light.

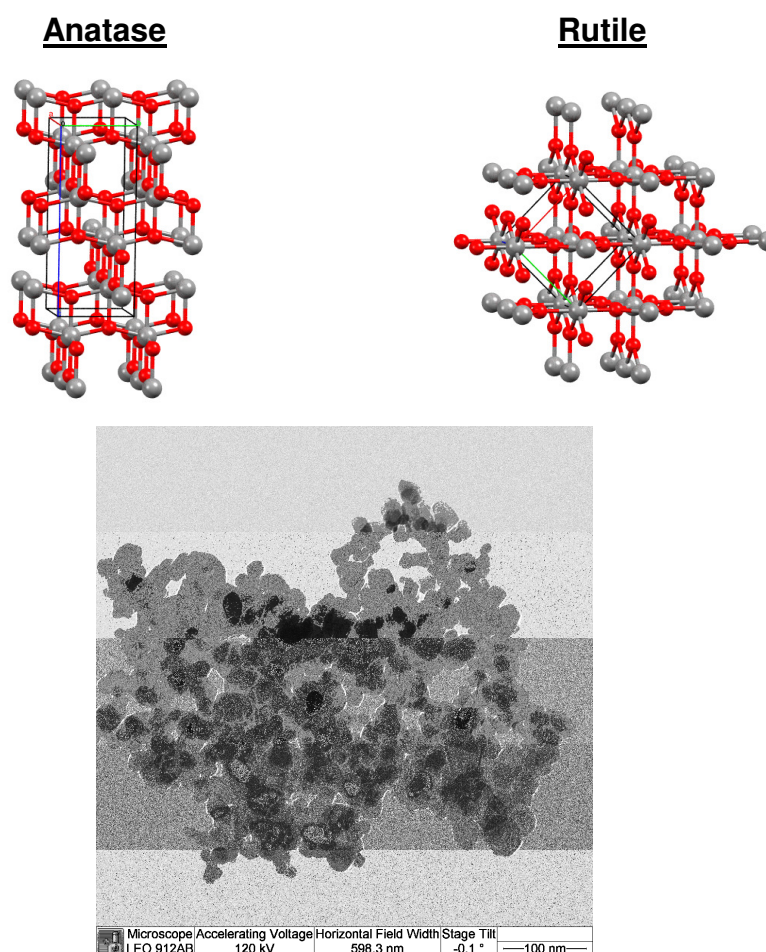


Figure 1.13 Crystal structures of titanium oxide and TEM micrograph of P25 (x40000).

As rutile can absorb light of a wider wavelength range, it seems logical to assume it is more suitable for use as a photocatalyst. However, in reality, anatase TiO_2 exhibits

higher photocatalytic activity. One of the reasons for this is the difference in energy structure between the two types. In both types, the position of the valence band is deep, and the resulting positive holes show sufficient oxidative power. However, the conduction band is positioned near the oxidation-reduction potential of the hydrogen, indicating that both types are relatively weak in terms of reducing power. It is known that the conduction band in anatase TiO_2 is more negative than rutile TiO_2 ; therefore, the reducing power of anatase titanium is stronger than that of its rutile phase (**Figure 1.14**).

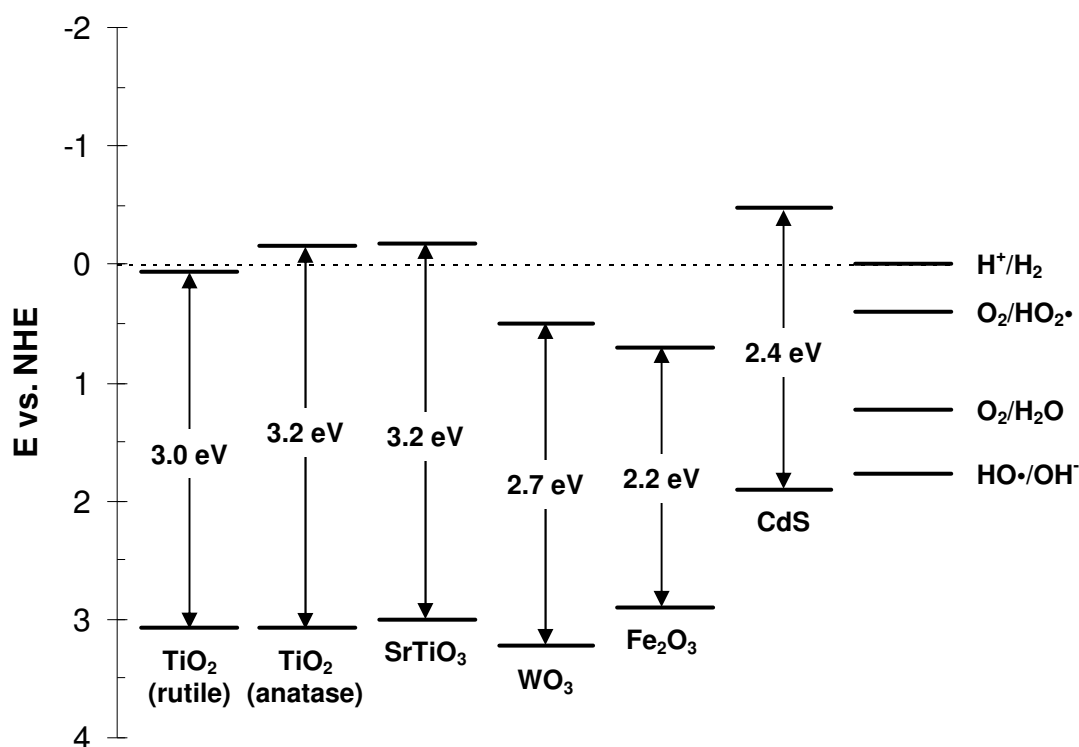


Figure 1.14 Valence and conduction band positions for various semiconductors, and useful, relevant redox couples at pH 0 (diagram from Mills *et. al.*⁴⁰). In order to photo-reduce a chemical species, the conduction band of the semiconductor must be more negative than the reduction potential of the chemical species to be reduced; to photo-oxidize a chemical species, the potential of the valence band of the semiconductor must be more positive than the oxidation potential of the chemical species to be oxidised.

Due to the difference in the position of the conduction band, anatase TiO_2 exhibits higher overall photocatalytic activity than the rutile type. However, some studies⁴⁵ show that a mixture of rutile and anatase, as found in P-25 TiO_2 sold by Degussa, exhibits an enhanced photo-activity compared to the anatase phase itself. It was

shown that the rutile phase both extends the wavelength range of activity of the catalyst and shuttles electrons to anatase away from photogenerated holes on the rutile particles leading to a more active catalyst. Specifically, by using EPR (electron paramagnetic resonance), it was determined that under visible illumination conditions, electron transfer occurs from rutile to anatase (**Figure 1.15**).⁴⁶ This observed electron transfer leads to a more active catalyst by two mechanisms. The lower band gap of rutile allows for greater absorption of solar radiation, and so rutile acts as an antenna for anatase, increasing the spectral range of activity of the catalyst. In addition, this charge transfer also further separates the photo-generated holes and electrons spatially. This increased charge separation, relative to a pure phase material, reduces recombination and increases the efficiency of the catalyst.

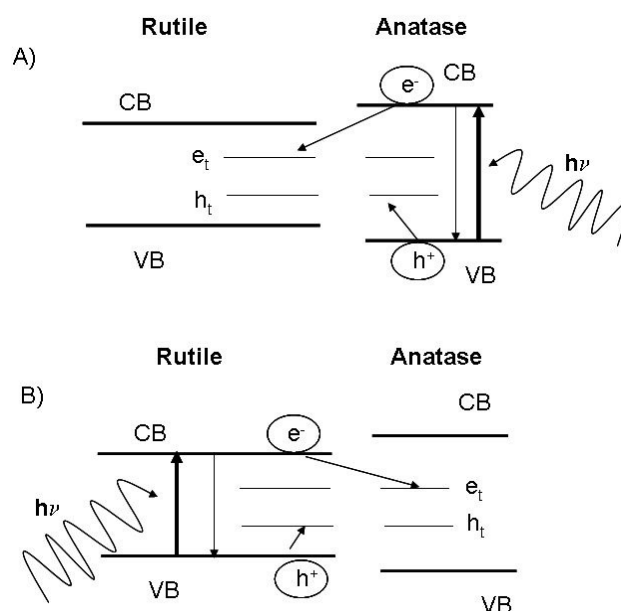


Figure 1.15 (A) Previously speculated model of P25 activity where charge separation occurs on anatase and rutile acts as an electron sink. (B) Proposed model of a rutile antenna and subsequent charge separation.⁴⁶

1.5 UV-LIGHT-ACTIVATED COLORIMETRIC REDOX DYE-BASED INDICATORS

The new oxygen colorimetric indicators recently developed by this group³⁹ are irreversible, reusable, UV light activated and use Methylene Blue as the redox dye indicator. The irreversible nature of the indicator is achieved by using UV light-

activated, nanoparticulate TiO_2 , a semiconducting material with a bandgap of ca. 3.2 eV. The use of nano, rather than micro, particulate crystalline titania is preferred since such material has a much higher specific surface area and as a consequence much less titania is required to make the inks effective for oxygen detection. In addition, nanoparticulate titania (up to 10 nm particle size) can exhibit a much greater photoactivity due to a quantisation effect.⁴⁷ The basic working principles of such an irreversible oxygen indicator are illustrated in **Figure 1.16**.

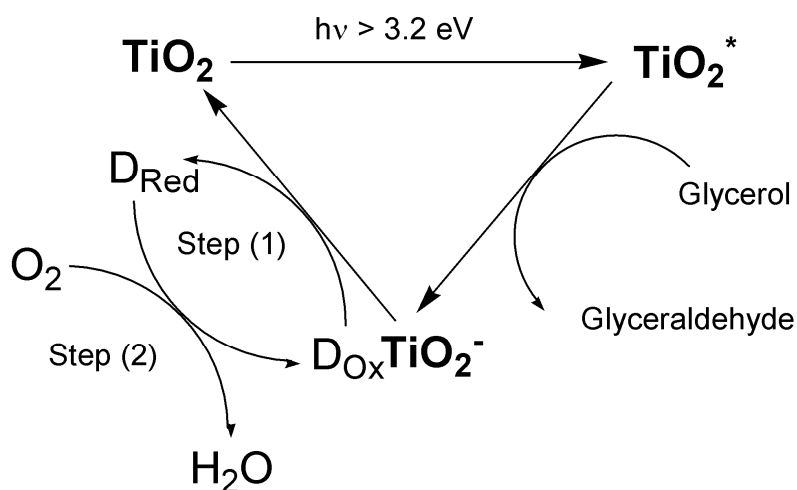


Figure 1.16 Schematic illustration of the key processes involved in the UV-activation and subsequent response towards oxygen of a $\text{TiO}_2/\text{MB}/\text{glycerol}/\text{HEC}$ visual oxygen indicator. Step (1) refers to photo-induced reduction of the redox sensitive dye D_{Ox} (MB) to its reduced form, D_{Red} , colourless LMB, whereas step (2) illustrates the ‘dark’ back re-oxidation of the dye, leading to recovery of initial colour, by the ambient oxygen.

Thus, upon irradiation with UVA light, ultra-bandgap illumination of the TiO_2 semiconductor photosensitizer particles create electron-hole pairs (TiO_2^* (e^- , h^+)). The photogenerated holes, h^+ , oxidise the mild sacrificial electron donor (SED), glycerol to glyceraldehyde. The remaining photogenerated electrons, *i.e.* TiO_2^- in **Figure 1.16**, reduce the redox-sensitive dye, D_{Ox} (in this work D_{Ox} = Methylene Blue, MB), to a reduced form, D_{Red} (*leuco*-Methylene Blue, LMB) that has a different colour to D_{Ox} . The above key components are encapsulated in a polymer, usually hydroxyethyl cellulose (HEC), to create an O_2 sensitive, UV-activated film, but all are readily dissolved or dispersed in water to create an intelligent, water-based ink for oxygen³⁹. **Figure 1.17** shows results of UVA light exposure of such water-

based oxygen indicator, where the blue coloured film loses its colour via processes explained in Step (1) in **Figure 1.16**. The film is fully bleached, *i.e.* colourless in *ca.* 3 minutes.

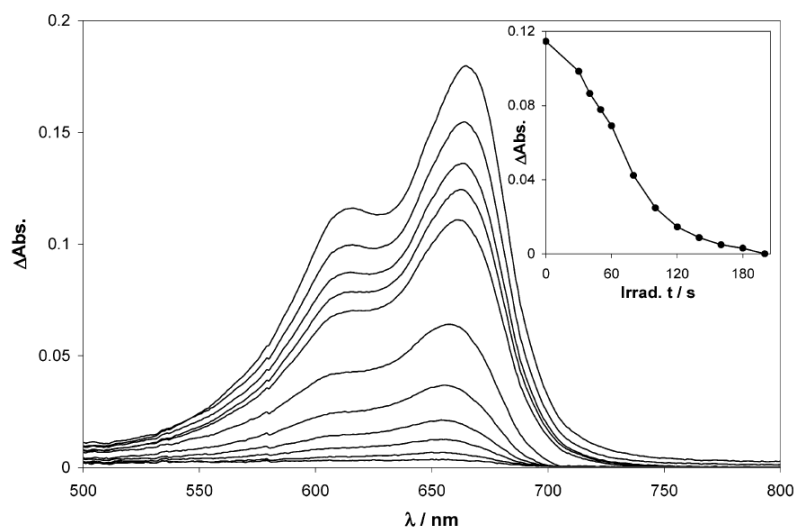


Figure 1.17 Recorded change ΔAbs in the visible absorbance spectrum of an indicator film upon exposure to UVA light (intensity 4 mWcm^{-2}) as a function of irradiation time. The change in absorbance ΔAbs at any wavelength was taken as the actual absorbance of the film minus the absorption of a fully bleached film (*i.e.*, one irradiated for *ca.* 200 s). The ΔAbs vs wavelength absorption spectra illustrated correspond to the following irradiation times (from top to bottom): 0, 30, 40, 50, 60, 80, 100, 120, 140, 160, and 180 s, respectively. The insert diagram illustrates the change in absorbance of the indicator film at 610 nm as a function of irradiation time, derived using data from the main diagram.

The redox dye, Methylene Blue, will remain in its reduced form in an oxygen free atmosphere. The recovery step, Step (2) in **Figure 1.16** will drive the oxidation of reduced *leuco*-Methylene Blue if oxygen is present. The rate of the recovery depends on the oxygen concentration and **Figure 1.18** illustrates that dependence. The oxygen indicator regain its original blue colour within an hour if let in ambient air atmosphere (21 % O_2).

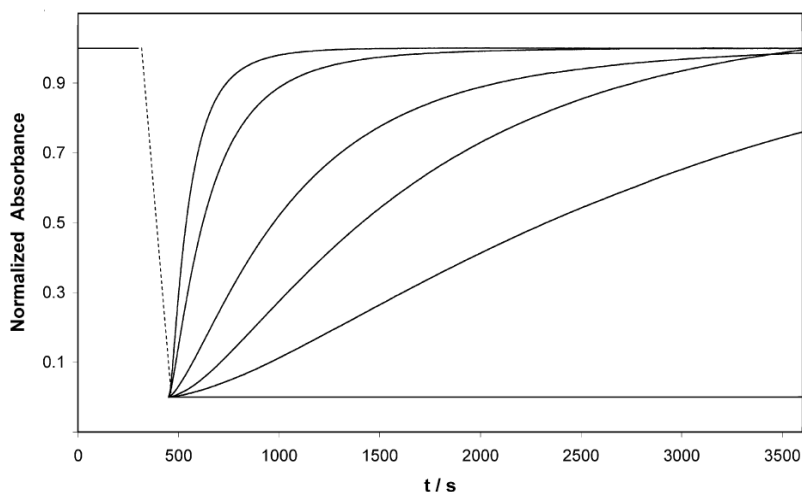


Figure 1.18 Change in the normalized absorbance (measured at 610 nm) of a typical UV-activated, colorimetric oxygen indicator film as a function of time under an ambient atmosphere with different levels of O₂ present. Each film was UV-irradiated for 2.5 min (100W BLB) (broken line) under aerobic conditions before being exposed to a range of different oxygen levels. The %O₂ levels used to generate different profiles were as follows: 100 (fastest recovery), 60, 21, 10, 5, and 0 (slowest, *i.e.* no recovery) % oxygen.

It should be noted, that the fluorescent light tubes commonly used in food cabinets in food supply chains do have a UVA light spike in the emission spectra and therefore are theoretically capable of reactivating the indicator via step 1 in **Figure 1.16**. This problem could be solved by either using a UV-light screening film or by employing a nanoparticulate semiconductor with a larger band-gap than TiO₂ and therefore light of higher energy, that is not present in the fluorescent light tubes, is needed in order to activate the indicator. This possibility is explored in Chapter 4.

In this work the preparations and characterisations of various novel colorimetric, UV-activated *solvent-based* intelligent inks for oxygen detection based on the above process are described.

1.5.1 Colorimetric Oxygen Indicators for MAP: Solvent-based Demand

The issues with other indicators such as the aforementioned Ageless Eye™ mean that a simpler solution would be required. An ideal oxygen indicator should be colorimetric (rendering it detectable by eye), non-toxic and have non-water soluble

components, which preferably have food contact approval, since this offers the possibility of placing the indicator inside the food package.⁷ It should also have an irreversible response towards oxygen because a reversible indicator might give a false-negative reading. For example if a package suffered a very minor break in its integrity and the level of microbe metabolism inside the package rose to such a level that the small rate of oxygen ingress was matched by the rate of microbe respiration so that the atmosphere in the package will be largely carbon dioxide.

An intelligent ink such as the one developed by Lee *et. al.*³⁹ would seem to fulfil this requirement, as it is cheap both to produce and print on food packaging using existing printing and packaging technology. However, the major drawback of water-based indicator inks is the hydrophilic, water-soluble nature of the ink, which limits its applications, especially in food packaging, since it is difficult to print on the mostly hydrophobic plastics used in packaging, such as polypropylene (PP), polyethylene terephthalate (PET), polyethylene (PE) etc. Another obvious requirement is that the indicator film, in the typically humid environment inside a package (it will be printed on the inside of the package), may become solubilised thereby destroying its functionality and possibly contaminating the food.

This problem could be addressed by an oxygen-permeable barrier layer which would protect the film but possibly alter the response and add to the cost. So the demand for a UV-activated solvent-based intelligent ink for oxygen which readily wets and prints onto plastics is clear.

1.6 AIMS AND OBJECTIVES

The main aim of this project was to produce an oxygen indicator based on the UV light activated, irreversible indicator ink developed by Mills *et al.* which is solvent-based and suitable for printing on the plastics commonly used in food packaging.

A subsequent aim was to investigate the potential use of Methylene Blue as a humidity indicator for possible use in packaging.

1.7 REFERENCES

1. J. Kerry and P. Butler, *Smart Packaging Technologies for Fast Moving Consumer Goods*, John Wiley & Sons Ltd., Chichester, 2008.
2. A. L. Brody, B. R. Strupinsky and L. R. Kline, *Active Packaging for Food Applications*, Technomic Publishing Co, Lancaster, 2001.
3. M. L. Rooney, *Active Food Packaging*, Blackie, London, 1995.
4. <http://www.cptplastics.com/aboutMAP.html>, Accessed April, 2011.
5. R. Anhvenian and E. Hurme, *Food Addit. Contaminants*, 1997, **14**, 753.
6. <http://www.modifiedatmospherepackaging.com>, Accessed June, 2011.
7. A. Mills, *Chem. Soc. Rev.*, 2005, **34**, 1003-1011.
8. M. Smolander, *Trends in Food Sci. Technol.*, 1997, **8**, 101.
9. www.keepsafe.ca/AgelsFood.htm (accessed April 2011).
10. A. S. Travis, *The Rainbow Makers*, Associated University Presses, London, 1993.
11. http://en.wikipedia.org/wiki/Methylene_blue, Accessed August 2010.
12. *The Merck Index*, 11th edn., Merck & Co., Inc., Rahway, 1989.
13. A. D. Murray, R. T. Stuff, T. S. Ahearn, P. Bentham, K. M. Seng and C. Wischik, *Alzheimer's and Dementia*, 2008, **4**, T786-T787.
14. *U.S. patent 2006/0287523 A1 published Dec 21st 2006 Pat.*, US 2006/0287523 A1, 2006.
15. V. R. White and J. M. Fitzgerald, *Anal. Chem.*, 1972, **44**, 1267.
16. V. R. White and J. M. Fitzgerald, *Anal. Chem.*, 1975, **47**, 903-908.
17. A. Sanz-Martínez, A. Ríos and M. Valcárcel, *Analyst*, 1992, **117**, 1761-1765.
18. A. G. Cook, R. M. Tolliver and J. E. Williams, *J. Chem. Ed.*, 1994, **71**, 160.
19. L. E. León, *Talanta*, 1996, **43**, 1275-1279.
20. J. A. Cooper, K. E. Woodhouse, A. M. Chippindale and R. G. Compton, 1999, **11**, 1259-1265.
21. S. B. Thomas and B. F. Thomas, *Dairy Ind. Int.*, 1973, **38**, 360-362.
22. S. K. Lee and A. Mills, *ChemCom*, 2003, 2366-2367.
23. A. Mills, K. Lawrie and M. McFarlane, *Photochem. Photobiol. Sci.*, 2009, **8**, 421-425.
24. http://en.wikipedia.org/wiki/Humidity_indicator_card, Accessed June 2011.
25. S. Otsuki and K. Adachi, *Polym. J.*, 1995, **27**, 655-658.
26. C. Reichardt, *Solvents and Solvent Effects in Organic Chemistry*, 3rd edn., WILEY-VCH Verlag GmbH & Co., Weinheim, 2003.
27. R. Matsushima, A. Ogiue and Y. Kohno, *Chem. Lett.*, 2002, 436-437.
28. W. Spencer and J. R. Sutter, *J. Phys. Chem.*, 1979, **83**, 1573-1576.
29. R. B. McKay, *Trans. Faraday Soc.*, 1965, **61**, 1787-1799.
30. S. M. Ohline, S. Lee, S. Williams and C. Chang, *Chem. Phys. Lett.*, 2001, **346**, 9-15.
31. M. Kasha, H. R. Rawls and M. A. El-Bayoumi, *Pure Appl. Chem.*, 1965, **11**, 371-392.
32. P. Bamfield and M. G. Hutchings, *Chromic Phenomena*, The Royal Society of Chemistry, Cambridge, 2010.
33. *Japan Pat.*, 62 259059, 1987.
34. *US Pat.*, 4 169 811, 1979.
35. *UK Pat.*, UK Patent 2 298 273, 1996.

36. *US Pat.*, 2 298 273, 1992.
37. *US Pat.*, 4 349 509, 1982.
38. *Japan Pat.*, JP Patent 62 183834, 1987.
39. S. Lee, A. Mills and A. Lepre, *Chem. Comm.*, 2004, 1912-1913.
40. A. Mills and S. Le Hunte, *J. Photochem. Photobiol. A: Chem.*, 1997, **108**, 1.
41. G. Wubbels, *Acc. Chem. Res.*, 1983, **16**, 285.
42. M. A. Fox, in *Photocatalysis: Fundamentals and Applications*, eds. N. Serpone and E. Pelizzetti, John Wiley & Sons, New York, Editon edn., 1989, pp. 603–637.
43. A. J. Bard, *Science* 1980, **207**, 139-144
44. M. R. Hoffmann, S. T. Martin, W. Choi and D. W. Bahnemann, *Chem. Rev.*, 1995, **95**, 69-96.
45. T. Ohno, K. Tokieda, S. Higashida and M. Matsumura, *Appl. Catal. A.*, 2003, **244**, 383-391.
46. K. A. Gray, D. C. Hurum and A. G. Agrios, *J. Phys. Chem. B.*, 2003, **107**, 4545-4549.
47. C. Kormann, D. W. Bahnemann and M. R. Hoffmann, *J. Phys. Chem.*, 1988, **92**.

CHAPTER 2

EXPERIMENTAL

2.1 GENERAL PREPARATION OF OXYGEN INDICATOR

Ink and Film Preparation¹

A typical ink used in this work comprised: a redox-sensitive dye Methylene Blue (MB), a TiO₂ photocatalyst, a sacrificial electron donor (SED), and a polymer to encapsulate the components together onto a substrate. The formulation for a standard water-based colorimetric oxygen indicator consisted of 2 g of a 5 % (w/v) hydroxyethyl cellulose polymer-water solution (*i.e.* 100 parts per hundred resin \equiv 100 mg of HEC, pphr) into which 5 mg MB (*i.e.* 5 pphr), 20 mg TiO₂ (*i.e.* 20 pphr) and 100 mg glycerol (*i.e.* 100 pphr) were added. The resulting blue ink was stirred for about 30 minutes, followed by 30 minutes of sonication in an ultrasonic bath. Sonification helped to dissolve all of the components and disperse the TiO₂ powder particles as well as remove any air bubbles that may have been present after stirring.

Note: This formulation is for a well described water-based ink which served as a standard for comparison in trying to achieve a solvent based system with the same or similar performance characteristics. Experimental details of these new systems can be found at the beginning of each chapter.

Depending on the substrate films were either cast using a K bar (on polymer sheets) or using a spin coater (glass or quartz cover slip).

Wired K bars are produced by winding precision drawn stainless steel wire onto a stainless steel rod resulting in a pattern of identically shaped grooves. These grooves precisely control the wet film thickness. Close wound bars will produce coating thicknesses from 4 to 120 μ m. The specifications of the K bars available are shown in **Table 2.1**.


Table 2.1 Specifications of the K bars used.²

BAR No.	Colour Code	Wire Diameter (mm)	Wet Deposit Film (μm)
0	White	0.05	4
1	Yellow	0.08	6
2	Red	0.15	12
3	Green	0.31	24
4	Black	0.51	40
5	Horn	0.64	50
6	Orange	0.76	60
7	Brown	1.00	80
8	Blue	1.27	100
9	Tan	1.50	120

2.2 PHOTOCATALYST CHARACTERISATION

The experimental conditions used for each technique are given after a brief description of the principle of operation of each instrument and technique.

*Powder X-ray Diffraction*³

Powder X-ray Diffraction	
Siemens D5000 Powder X-ray Diffractometer Range: 2θ , $5^\circ - 30^\circ$ Wavelength: Cu $K\alpha$, 1.5406 \AA	

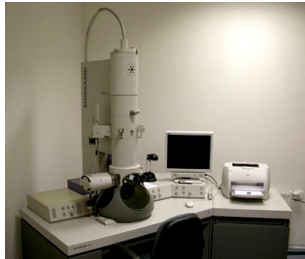
In common with other types of electromagnetic radiation, interaction between the electric vector of x-radiation and the electrons of matter through which it passes results in scattering. When the x-rays are scattered by the ordered environment in a crystal, interference (both constructive and destructive) takes place among the scattered x-rays because the distances between the scattering centres are of the same order of magnitude as the wavelength of the radiation. Diffraction is the result.

When an x-ray beam strikes a crystal surface at some angle θ , a portion is scattered by the layer of atoms at the surface. The unscattered portion of the beam penetrates to the second layer of atoms where again a fraction is scattered, and the remainder passes onto the third layer. The cumulative effect of this scattering from the regularly

spaced centres of the crystal is diffraction of the beam in much the same way as visible radiation is diffracted from a reflection grating. The requirements for the x-ray diffraction are: (1) the spacing between the layers must be roughly the same wavelength of the radiation and (2) the scattering centres must be spatially distributed in a highly regular way.

The photocatalytic powders used in this work were characterized using powder x-ray diffraction to confirm their crystallinity and phase purity.

*Transmission Electron Microscopy*⁴


Transmission Electron Microscopy	
FEI Morgagni 268(D) Transmission Electron Microscope.	

The transmission electron microscope (TEM) operates on the same basic principles as the light microscope but uses electrons instead of light. What you can see with a light microscope is limited by the wavelength of light. TEMs use electrons as a “light source” and their much lower wavelength make it possible to get a resolution a thousand times better than with a light microscope. You can see objects to the order of a few angstroms (10^{-10} m). For example, you can study small details in materials down to near atomic levels. The possibility for high magnifications has made the TEM a valuable tool in both medical, biological and materials research.

The samples for TEM were measured at Glasgow University by Dr. L. Tetley. Specimens were dispersed in water dropped onto carbon-backed, Formvar-coated 300 mesh grids and allowed to dry. The instrument used was a zero loss energy-filtered transmission electron microscope. Images were digitally recorded using a Zeiss 912 EFTEM operating at 120kV and a 14 bit Proscan Sharp Eye 2K slow scan CCD camera via iTEM PC software (Olympus SIS).

In this work the photocatalytic powders were characterized using TEM to explore the particle size and shape.

Surface Area Determination by Nitrogen Adsorption (BET)⁵

BET Surface Area	
Micromeritics ASAP 2010 Analyser Gas: Nitrogen Temperature: 66K	

BET surface area measurements were obtained using nitrogen adsorption and a Micromeritics ASAP 2010 Analyser. The surface area of the photocatalytic nanopowders were determined using the well known Brunauer Emmett Teller equation which is based on the theory that the first layer is physisorption and subsequent layers behave as a liquid, so that the latent heat of condensation controls desorption.

2.3 POLYMER AND DYE CHARACTERIZATION

Differential Scanning Calorimetry⁶


DSC	
TA Instruments Q1000	

Differential scanning calorimetry (DSC) or Differential Thermal Analysis is a method which measures the difference in temperature between a sample and reference as a function of temperature. Both the sample and reference are subjected

to the same controlled temperature program such that the sample holder temperature increases linearly as a function of time. The difference in temperature ΔT between the sample temperature (T_s) and the reference temperature (T_r), $\Delta T = T_s - T_r$ is then monitored and plotted against sample temperature to give a differential thermogram. Using this technique it is possible to observe changes in the sample such as melting, glass transition and crystallization.

In this work this technique was used to determine purity and melting temperatures of different polymers.

Elemental Microanalysis

Elemental Microanalysis	
2400 Series II CHNS/O System	

CHN Analysis is a form of elemental analysis concerned with determination of only Carbon (C), Hydrogen (H) and Nitrogen (N) in a sample. The common technology behind the CHN analysis is combustion method where the specimen is first fully combusted and then the products are analyzed. The full combustion is usually achieved by providing an excess of oxygen during the combustion process. The products of combustion are separated on a packed chromatographic column. The column converts the products into combination of NO_2 , CO_2 , SO_2 and H_2O . These simple compounds are then measured using a TCD (thermal conductivity) detector.

In Chapter 5 CHN analysis was used to assess the degree of sulfonation of the synthesized, partially sulfonated polystyrene.

*TLC, HPLC*³

Thin layer chromatography (TLC) is a chromatography technique used to separate mixtures. The process is similar to paper chromatography with the advantage of faster runs, better separations, and the choice of different stationary phases. Thin layer chromatography is performed on a sheet of glass, plastic, or aluminium foil, which is coated with a thin layer of adsorbent material, usually silica gel, aluminium oxide, or cellulose (blotter paper). Because of its simplicity and speed TLC is often used for monitoring chemical reactions and for the qualitative analysis of reaction products.

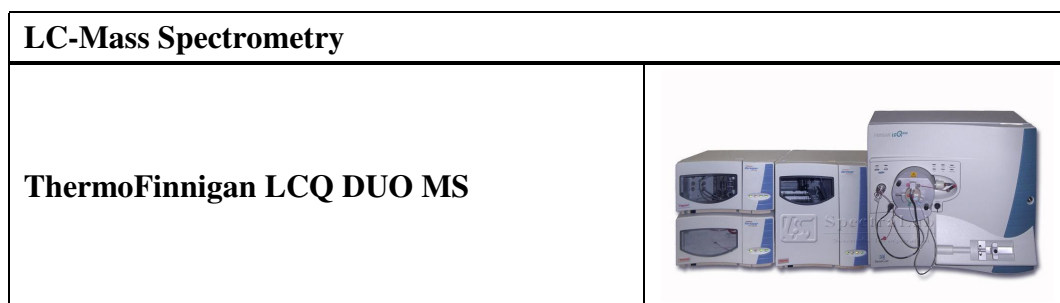
A small spot of solution containing the sample is applied to a plate, about 1.5 centimeters from the bottom edge and allowed to completely evaporate off. A small amount of an appropriate solvent (elutant) is then poured into a glass beaker to a depth of less than 1 centimeter. The container is closed with a cover glass or any other lid and is left for a few minutes to let the solvent vapours ascend the filter paper and saturate the air in the chamber. The TLC plate is then placed in the chamber so that the spot(s) of the sample do not touch the surface of the elutant in the chamber, and the lid is closed. The solvent moves up the plate by capillary action, meets the sample mixture and carries it up the plate (elutes the sample). When the solvent front reaches just below the top the TLC plate should be removed and dried.

Different compounds in the sample mixture travel at different rates due to the differences in their attraction to the stationary phase, and because of differences in solubility in the solvent. By changing the solvent, or perhaps using a mixture, the separation of components (measured by the R_f value) can be adjusted. Also, the separation achieved with a TLC plate can be used to estimate the separation of a flash chromatography column. Detection of the spots is easier when the analyte is coloured. As the chemicals being separated may be colourless, several methods exist to visualize the spots. The most common uses a small amount of a fluorescent compound, usually manganese-activated zinc silicate, is added to the adsorbent that allows the visualization of spots under a blacklight (UVA). The adsorbent layer will thus fluoresce light-green by itself, but spots of analyte quench this fluorescence.

The plates used in this work was Sigma-Aldrich® TLC plates silica gel matrix, pore size 60 Å, layer thickness 250 µm, particle size 17 µm.

High performance liquid chromatography (HPLC) has several advantages over TLC; it has lower detection limits, better reproducibility and provides quantitative analytical data. HPLC typically utilizes different types of stationary phases, a pump that moves the mobile phase(s) and analyte through the column, and a detector that provides a characteristic retention time for the analyte. The detector may also provide other characteristic information (i.e. UV/Vis spectroscopic data for analyte if so equipped). Analyte retention time varies depending on the strength of its interactions with the stationary phase, the ratio/composition of solvent(s) used, and the flow rate of the mobile phase. With HPLC, a pump (rather than gravity) provides the higher pressure required to propel the mobile phase and analyte through the densely packed column. The increased density arises from smaller particle sizes. This allows for a better separation on columns of shorter length when compared to ordinary column chromatography.


LC-MS⁷



Two different mass spectrometers were used in this work. The majority of the experiments were run on an ESI-MS (ThermoFinnigan LCQ DUO MS) using either the direct injection port or via an HPLC system (i.e. LC-MS). In the latter the HPLC column was a Phenomenex Gemini, C18, 5 µm, 50 x 2.0 mm. A graded mobile phase was used comprising initially 0.1% formic acid in water, becoming 0.1% formic acid in acetonitrile, over 15 min at 150 µl/min flow rate. An LDI-MS

(Shimadzu, AXIM-CFR) was also used to record the spectra of the thiazine dyes as well as the MB base hydrolysis products in Chapter 7.

*NMR Spectroscopy*⁷

NMR	
Bruker Avance/DRX 500 NMR spectrometer	

Nuclear magnetic resonance spectroscopy, most commonly known as NMR spectroscopy, is a technique that exploits the magnetic properties of certain nuclei. The most important applications for the organic chemist are proton NMR and carbon-13 NMR spectroscopy. When placed in a magnetic field, NMR active nuclei (such as ^1H or ^{13}C) absorb at a frequency characteristic of the isotope. The resonant frequency, energy of the absorption and the intensity of the signal are proportional to the strength of the magnetic field.

Depending on the local chemical environment, different protons in a molecule resonate at slightly different frequencies. Since both this frequency shift and the fundamental resonant frequency are directly proportional to the strength of the magnetic field, the shift is converted into a field-independent dimensionless value known as the chemical shift. The chemical shift is reported as a relative measure from some reference resonance frequency. (For the nuclei ^1H , ^{13}C , and ^{29}Si , TMS (tetramethylsilane) is commonly used as a reference.) This difference between the frequency of the signal and the frequency of the reference is divided by frequency of the reference signal to give the chemical shift. By understanding different chemical environments, the chemical shift can be used to obtain some structural information about the molecule in a sample. The NMR instruments used in this work were Bruker AVANCE-III and Avance/DRX NMR spectrometers operating at 600.13 and 500.13 MHz.

2.4 LIGHT SOURCES AND SPECTROPHOTOMETRY.

Light sources

Throughout this work UV irradiation was carried out with one of three forms of UV source: hand-held two-tube sources with 2×8W (**Figure 2.1 A**), 2×6W (**Figure 2.1 B**), or 2×4W (**Figure 2.1 C**) bulbs fitted. The two-tubes were fitted with UVA (BLB bulbs, 365 nm), UVB (312 nm), UVC (mercury discharge bulbs, 254 nm) or warm-white (WW) visible light fluorescent bulbs, the irradiation source and typical intensity value are quoted for each experiment, or at the beginning of the relevant section. Intensities were measured using a PVP ultraviolet radiation detector, supplied with UVA, UVB or UVC attachments (**Figure 2.1 D**).

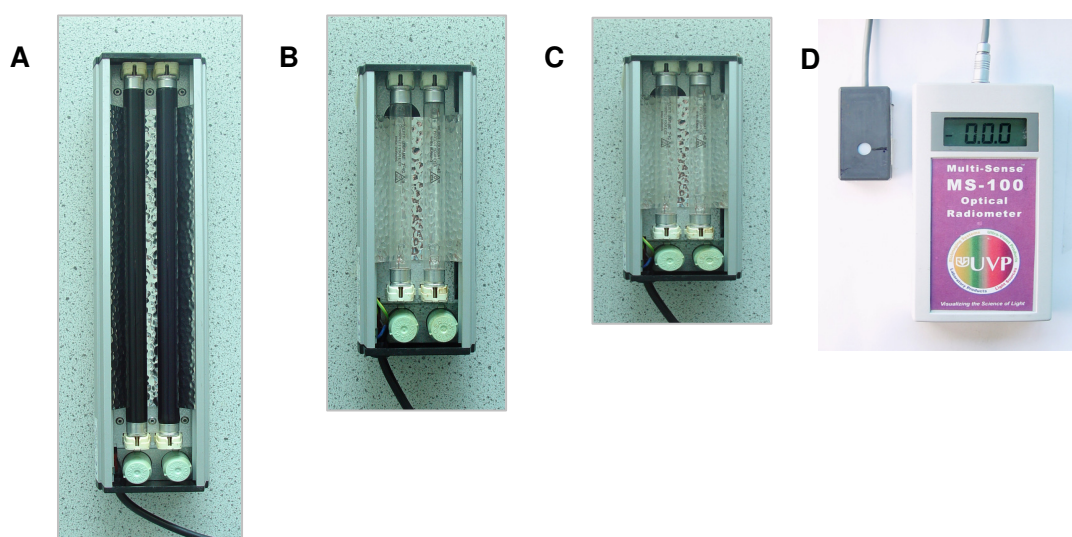

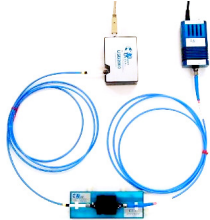


Figure 2.1 Apparatus for UV irradiation; A – 8W (with 2 × UVA); B – 6W (with 2 × UVC); C – 4W (with 2 × UVC); D – PVP UV meter with detector.

UV/Visible Spectroscopy	
Varian Cary 50 UV/Visible Spectrophotometer	
UV/Visible Spectroscopy at High Temperatures	
Ocean Optics USB2000 Spectrometer System USB2000 detector, LS-1 tungsten-halogen light source through a CUV temperature-controlled sample holder	

A molecule is usually coloured because it undergoes an electronic transition brought about by absorption of light in the visible region of the spectrum. The intensity of light absorption at a particular wavelength of a molecule in solution can be determined by passing a monochromatic beam of light through a known thickness (l) and concentration (c or α) of a solution and measuring the intensity of the transmitted light (I) relative to the intensity of the incident light (I_0).

These factors are related by the Beer-Lambert law which states that the Transmittance T , the ratio of the incident intensity (I_0) to the transmitted intensity (I), is proportional to the pathlength (l) and the concentration of the absorbing species (c) and is given by:

$$\log T = -\epsilon cl \quad T = \frac{I}{I_0} \quad (2.1)$$

The coefficient ϵ is known as the molar absorption coefficient of the absorbing species and its units are those of $1/(\text{concentration} \times \text{pathlength})$ and is usually reported in litres per mole per centimetre ($\text{L mol}^{-1} \text{cm}^{-1}$ or $\text{dm}^3 \text{mol}^{-1} \text{cm}^{-1}$).

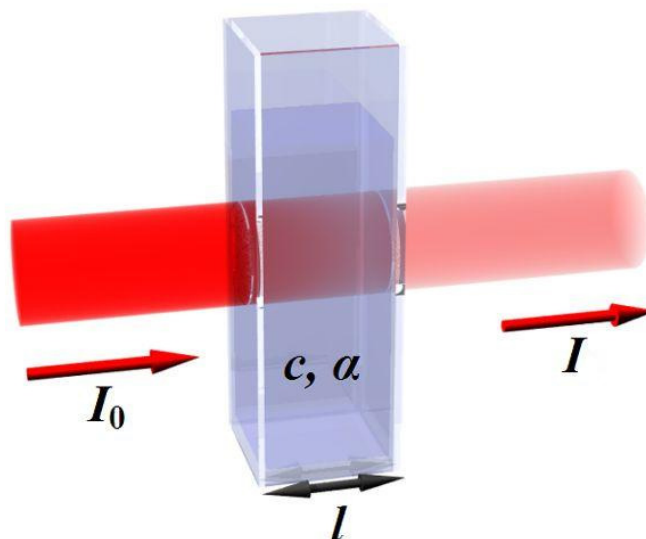


Figure 2.2 An illustration of a beam of light passing through a dilute solution.

In a double-beam UV/Vis. spectrophotometer a beam of monochromatic light from a diffraction monochromator is split into two parallel beams. Each of these beams passes through a cell; one cell containing the dissolved sample (giving I) and the other the solvent alone (giving I_0). The Transmittance (T) is given by the ratio of the intensities passing through each.

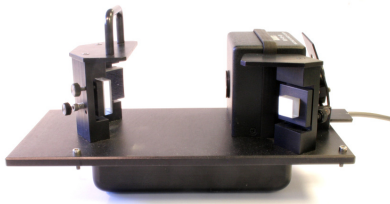
The Beer-Lambert law can also be written as:

$$I = I_0 \times 10^{-\epsilon cl} \quad (2.2)$$

showing that Transmittance decreases exponentially with an increase in pathlength and/or concentration. A more convenient measure of the intensity of light absorbed by a solution is the Absorbance (A), a dimensionless product, which is defined by:

$$A = \epsilon cl = -\log T \quad (2.3)$$

At low concentrations a plot of Absorbance vs. concentration gives a straight line, the gradient of which is the molar absorption coefficient.

Diffuse Reflectance Spectroscopy	
Perkin-Elmer Lambda 35 Labsphere RSA-PE-20 Reflectance Accessory	

Absorbance measurements of solutions under ideal conditions are relatively straightforward. Measurement of solid or opaque samples, however, presents much more of a challenge and is made by the use of Diffuse Reflectance Spectroscopy. Many substances, in particular powders and rough surface solids, exhibit diffuse reflection, *i.e.* incident light is scattered in all directions as opposed to specular (mirror-like) reflection where the angle of incidence equals the angle of reflection. The technique of diffuse reflectance spectroscopy is generally based on integrating sphere technology whereby light reflected from the sample is collected by a small sphere. The interior surface of the sphere is coated with a highly efficient reflective, white coating.

In practice, diffuse reflectance spectra are complex and are strongly dependent upon the conditions under which they are obtained. These spectra can exhibit both absorbance and reflectance features due to contributions from transmission, internal and specular reflectance components as well as scattering phenomena in the collected radiation. Diffuse reflectance spectra are further complicated by sample preparation, particle size, sample concentration and optical geometry effects, to name a few.

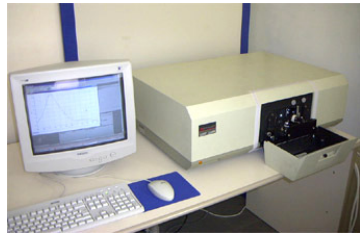
In principle, any photon hitting the inner surface of the sphere will reflect and "bounce around" until it exits the sphere and encounters the photomultiplier tube (PMT), at which point it becomes part of the measurement. That is, with a perfect sphere having a perfect reflective surface, all photons will eventually reach the photodetector, perhaps after hundreds or thousands of "bounces" off of the inside surface of the sphere; thus, there will be no apparent losses due to scatter by the sample. The instrument is zeroed using a standard of Spectralon® produced by Labsphere which is a thermoplastic resin which has a very high reflectance.

The data produced by this technique can be either % reflectance or a computed function (analogous to absorbance) called the Kubelka-Munk function vs. wavelength. . Kubelka-Munk theory for the diffuse reflectance of dyes adsorbed on powdered samples shows that the Kubelka-Munk function (FR), at any wavelength where the dye absorbs, varies linearly with concentration, C ,^{8,9} *i.e.*

$$FR = \frac{(1 - R'_{\infty})^2}{2R'_{\infty}} = \alpha bc \quad (2.4)$$

where α is the molar absorptivity of the dye at that wavelength, c is its concentration and b is a constant. It follows that in this work the reflectance data can be used to generate the associated FR value at the wavelength of maximum absorption, λ_{max} , which in turn is related to the concentration of the oxidised dye, MB, in the film.

*Fluorescence Measurement*⁷

Fluorescence Spectroscopy	
<p>Perkin-Elmer LS50-B Luminescence Spectrophotometer</p>	

Unlike transmission spectroscopy, in fluorescence measurement the sample is observed perpendicularly to the incident excitation beam. In modern equipment, monochromators are placed both in the path of the excitation beam and the observation beam. Since no direct comparative measurement is possible in fluorescence, the intensity of the excitation light beam is usually controlled at least by a beam splitter and a reference photomultiplier tube. The basic layout and beam path in the P-E LS-50B luminescence spectrophotometer is shown in **Figure 2.3**.

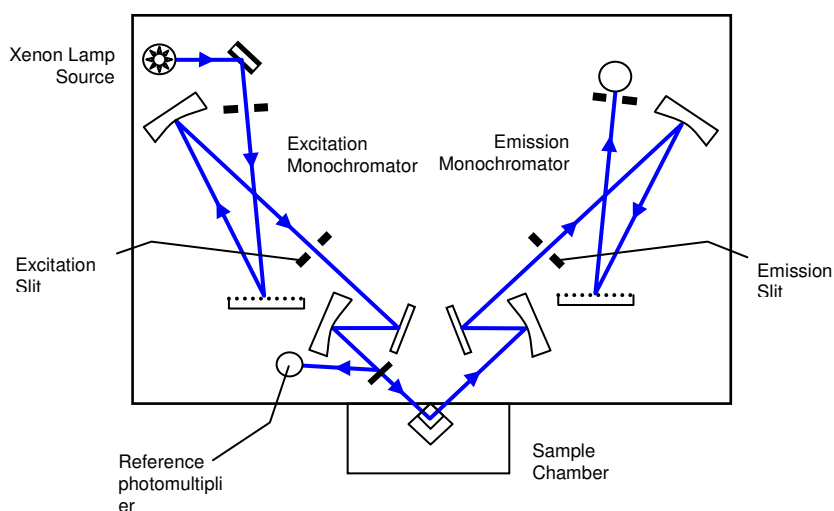


Figure 2.3 Showing a schematic diagram of the Perkin-Elmer LS-50B Luminescence Spectrophotometer.

To measure a fluorescence spectrum, the wavelength of the excitation beam is kept constant and the wavelength of the observation monochromator is varied. For observation of fluorescence excitation spectra, the monochromator at the observation end is adjusted to a wavelength of highest possible fluorescence intensity, and the wavelength of the monochromator on the excitation side is varied. Hence, for these spectra, a shape analogous to an absorption spectrum is obtained.

In a fluorescence spectrophotometer the measurement is not a transmitted beam but rather the incident beam is used to excite the sample and the fluorescence is observed at a 90° angle. The equivalent of the Beer-Lambert law for fluorescence is given by:

$$F = \phi I_0 (1 - 10^{-\epsilon c l}) \quad (2.5)$$

Where the quantum efficiency (ϕ) is the percentage of molecules in an excited electronic state which decay to ground state by fluorescent emission. This value is always less than or equal to one and is characteristic of the molecular structure. It is found that for dilute concentrations, where $A = \epsilon [c] l < 0.05$, the equation reduces to the following:

$$F = k \phi I_0 \epsilon c l \quad (2.6)$$

Where k is the instrument factor.

2.5 OTHER METHODS

Contact Angle Measurement^{5, 10}

The term 'hydrophilic' is generally accepted as meaning 'water liking'. IUPAC define it as "The capacity of a molecular entity or of a substituent to interact with polar solvents, in particular with water, or with other polar groups." So a hydrophilic surface might be described as 'water liking' and one in which the contact angle with a polar solvent (such as water) is small. Conversely, a hydrophobic surface is one which appears to be repelled by water (a high contact angle); in reality it is the water molecules strongly interacting with each other that keep them from interacting with a much less polar surface.

Evaluation of hydrophilicity is invariably by the sessile drop method – a water droplet is deposited onto the horizontal subject surface and the angle between the droplet and the substrate is measured, termed the contact angle (CA, also referred to as θ in literature). Contact angle is specific to liquid and solid, and with a known liquid, such as water, contact angle is a simple, low-tech, method of surface analysis for solids. The minimum surface energy for a liquid is achieved for a droplet, free of external forces, as a perfect sphere. Water has high surface energy, consisting of polar bonds exerting hydrogen bonding forces. When in contact with a solid a water droplet will minimise its surface energy, and therefore its shape, dependant upon the combination of energies of three interfaces: solid-liquid (γ_{SL}), solid-gas (γ_{SG}) and liquid-gas (γ_{LG}), **Figure 2.4**.

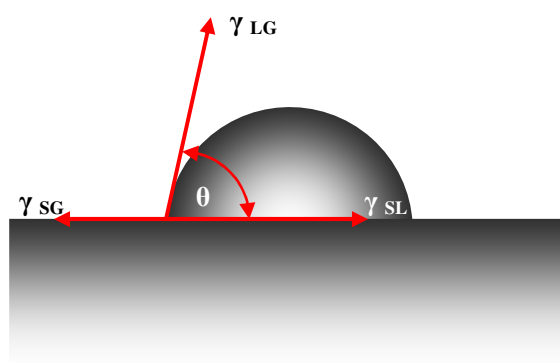


Figure 2.4 A diagram of interfacial energies acting on a sessile drop resting on a surface.

A liquid on a surface will reach equilibrium when the forces acting on it are balanced and the surface tension is at a minimum. The forces at equilibrium are described by Young's equation; equation 2.7.

$$\gamma_{LG} \cos\theta = \gamma_{SG} - \gamma_{SL} \quad (2.7)$$

The balance of forces acting upon the point where the droplet meets the surface and the gas-phase causes the droplet to stop advancing across the surface. The wetting ability of a liquid is a function of the surface energies of these three interfaces.

Contact angle measurements were taken using FTA (First Ten Angstroms) 200 contact angle instrument, supplied by Camtel. The apparatus is shown in **Figure 2.5**.

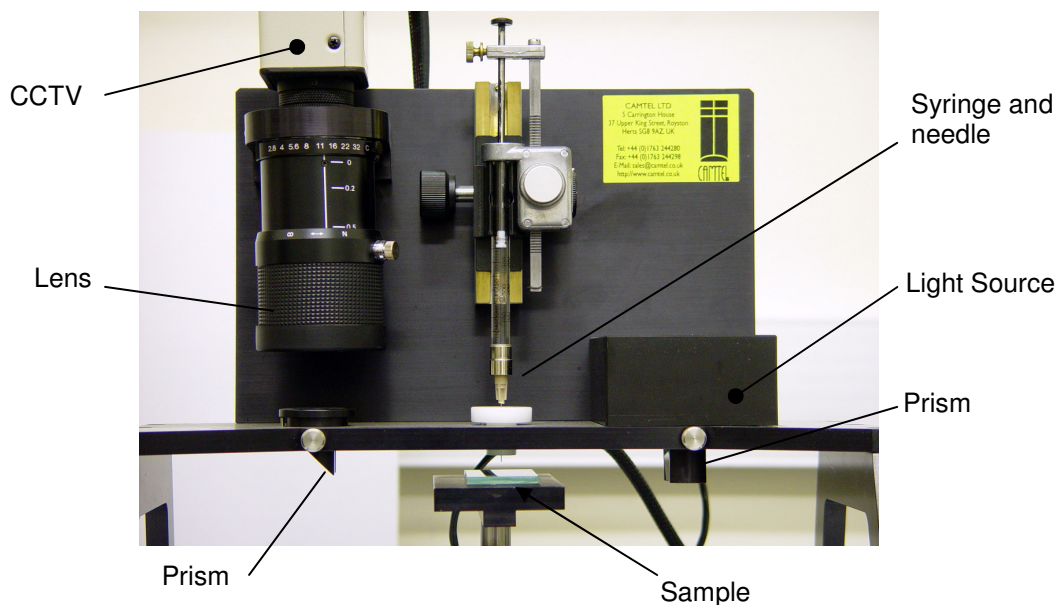


Figure 2.5 A photograph of the (First Ten Angstroms 200) contact angle instrument used to measure contact angles.

Relative Humidity

Relative humidity is defined as the ratio of the partial pressure of water vapour in a gaseous mixture of air and water vapour to the saturated vapour pressure of water at a given temperature. Relative humidity is expressed as a percentage and is calculated in the following manner:

$$RH = \frac{p(H_2O)}{p^*(H_2O)} \times 100\% \quad (2.8)$$

Where $\rho(\text{H}_2\text{O})$ is the partial pressure of water vapour in the gas mixture; $\rho^*(\text{H}_2\text{O})$ is the saturation vapour pressure of water at the temperature of the gas mixture; and RH is the relative humidity of the gas mixture being considered.

A gas in this context is referred to as saturated when the vapour pressure of water in the air is at the equilibrium vapour pressure for water vapour at the temperature of the gas and water vapour mixture; liquid water (and ice, at the appropriate temperature) will fail to lose mass through evaporation when exposed to saturated air. It may also correspond to the possibility of dew or fog forming, within a space that lacks temperature differences among its portions, for instance in response to decreasing temperature. Fog consists of very minute droplets of liquid, primarily held aloft by isostatic motion (in other words, the droplets fall through the air at terminal velocity, but as they are very small, this terminal velocity is very small too, so it doesn't look to us like they are falling and they seem to be being held aloft).

Absolute humidity is the quantity of water in a particular volume of air. The most common units are grams per cubic meter, although any mass unit and any volume unit could be used. If all the water in one cubic meter of air were condensed into a container, the container could be weighed to determine absolute humidity. The amount of vapour in that cube of air is the absolute humidity of that cubic meter of air. More technically: the mass of water vapour m_w , per cubic meter of air, V_a .

$$AH = \frac{m_w}{V_a} \quad (2.9)$$

Absolute humidity ranges from 0 gram per cubic meter in dry air to 30 grams per cubic meter when the vapour is saturated at 30 °C.

A typical digital humidity meter such as the Hanna HI-9564 used in this work uses a resistive humidity sensor where the change in electrical resistance of a material due to humidity is measured.

2.6 REFERENCES

1. S. Lee, A. Mills and A. Lepre, *Chem. Comm.*, 2004, 1912-1913.
2. <http://www.rkprint.com/pdfs/khandcoater.pdf>, Accessed April, 2011.

3. D. A. Skoog, F. J. Holler and S. R. Crouch, *Principals of Instrumental Analysis*, 6th edn., Brooks Cole, Belmont, 2007.
4. D. B. Williams and C. B. Carter, *Transition Electron Microscopy: A Textbook for Material Science*, Springer, New York, 2009.
5. A. W. Adamson and A. P. Gast, *Physical Chemistry of Surfaces*, Sixth edn., John Wiley & Sons, 1997.
6. T. Hatakeyama and F. X. Quinn, *Thermal Analysis Fundamentals and Applications to Polymer Science*, Wiley & Sons, Chichester, 1999.
7. J. M. Hollas, *Modern Spectroscopy*, 4th edn., John Wiley & Sons, Chichester, 2004.
8. M. P. Fuller and P. R. Griffiths, *Anal. Chem.*, 1978, **50**, 1906-1910.
9. P. Kortum, W. Braun and G. Herzog, *Angew. Chem. , Int. Ed. Engl.*, 1963, **2**, 333-341.
10. D. J. Shaw, *Introduction to Colloid and Surface Chemistry*, Fourth edn., Butterworth Heinemann, 1991.

CHAPTER 3

**FIRST GENERATION OF SOLVENT-BASED
MB OXYGEN FILM INDICATOR**

3.1 INTRODUCTION

In this chapter the first example of a solvent-based oxygen indicator is described. Although the solvent used to prepare this oxygen indicating film is partially aqueous, the ink is printable on plastics, polymers like polyethylene (PE) or polypropylene (PP) commonly used in food packaging, and shows increased lipophilicity. Methylene Blue (MB) ion-paired with sodium dodecyl sulfate (DS) was the redox dye used in the ink. The resulting couple (MB-DS) is electro neutral, *i.e.* the cationic dye forms an ionic bond with the dodecyl sulfate anion. The depletion of charged species and the lipophilic C₁₂ (dodecyl) alkyl chain will render the dye overall more soluble in less polar solvents like ethanol, acetone or acetonitrile.

3.2 EXPERIMENTAL

3.2.1 Materials and Chemicals

The semiconductor photocatalysts employed to make the inks were: P25 TiO₂, a mixture of the two TiO₂ crystalline phases, rutile (20 %) and anatase (80 %) (Evonik) and nanopowder rutile TiO₂ from Sigma-Aldrich. Unless stated otherwise all other chemicals were from Sigma-Aldrich, with the exception of the ethanol-soluble polymer zein purchased from Fluka. The zein polymer solution was prepared by adding 10 g of zein to a solution of 36 g of ethanol and 4 g of water. The final solvent-based ink was printed on 40 µm thick PET foil provided by Crown Holdings Inc.. Other hydrophobic polymer substrates, such as nylon, and PP appeared equally effective.

3.2.2 Preparation of Methylene Blue Ion-paired with dodecyl sulfate

Methylene Blue (MB), a cationic thiazine redox dye, is very water-soluble and in order to render it solvent-soluble and water insoluble, its water-soluble cationic form was ion-paired with a solvent-soluble anion, dodecyl sulfate (DS). The product, MB-

DS is water-insoluble, but solvent-soluble. To make MB-DS, 3.74 g, (0.01 mol) of MB were dissolved in 200 mL of water and a solution of 2.88 g (0.01 mol) of sodium dodecyl sulfate (SDS) in 150 mL of water added. The mixture was stirred for 12 hours, and then chilled to 4°C for 2 hours. The resulting dark blue precipitate was filtered, using a glass frit, washed with water and dried overnight in an oven to give 3.9 g of the desired product, MB-DS (see **Figure 3.1**).

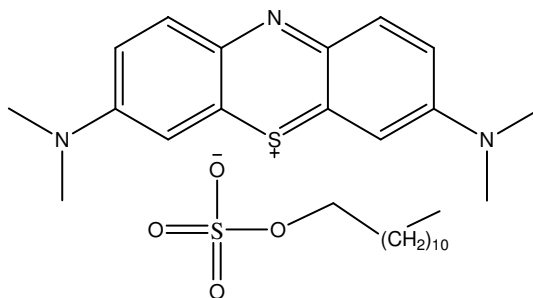


Figure 3.1 Methylene Blue-dodecylsulfate ion pair.

3.2.3 Ink and Film Preparation

Preparation of Water-Soluble Methylene Blue (MB) Based Films

Aqueous-based oxygen indicating films and their properties are described in detail in preceding work published by Mills *et al.*¹ In this work the typical water-based indicator is used as a standard to which the newly formulated inks were compared. The aqueous film preparation is described in section 2.1.

Preparation of Solvent-Soluble Methylene Blue (MB) Based Films

The solvent-based oxygen ink was prepared by combining 3 g of the zein solution with 600 mg of glycerol, 600 mg of TiO₂ photocatalyst and 15 mg of the MB-DS dye. The resulting mixture was stirred for 30 minutes, followed by 30 minutes sonication to ensure all the photocatalyst particles were well dispersed and the MB-DS, glycerol and zein dissolved. The resulting dark blue ink was then cast onto a PET plastic foil using a drawdown technique (K-bar No. 2) to produce a film with an average thickness of ca. 5 μm. The film was dried in air at ambient temperature and stored in the dark.

3.2.4 Irradiation and Colour Change Measurements

In order to make useful absorbance measurements using diffuse reflectance the MB-DS ink-coated plastic foil, which was highly coloured but also opaque, was cut to fit in a brass gas cell that could be used to maintain the sample in different controlled gaseous atmospheres (e.g. N₂ or O₂ or mixture there of). In most of the initial work the variation in the diffuse reflectance parameter, FR, was monitored as a function of irradiation time under either aerobic or anaerobic conditions. In a later study of the rate of colour recovery (after photobleaching) as a function of %O₂, the MB-DS film was first irradiated, *i.e.* photobleached, outside the gas cell using 2x8 W BLB UVA tubes (Philips F8/T5/BLB in a Vilber-Lourmat, model no. VL-208 irradiation unit, irradiance = 10 mW cm⁻²), then placed in the gas cell in a gaseous environment of known %O₂, produced using a calibrated gas blender, flowing at 300 mL min⁻¹, and its spectrum recorded using a Perkin Elmer Lambda 20 spectrophotometer as a function of time using a diffuse reflectance attachment (Labsphere RSA-PE-20).

In all diffuse reflectance work, the data obtained were reported as the percent reflectance relative to a white standard reflectance plate, R'_∞;

$$R'_{\infty} = \frac{R'_{\infty}(\text{sample})}{R'_{\infty}(\text{std.})} \times 100 \quad (3.1)$$

where the standard is a non-absorbing material (Spectralon) that optimally diffuses light. Kubelka-Munk theory for the diffuse reflectance of dyes adsorbed on powdered samples shows that the Kubelka-Munk function (FR), at any wavelength where the dye absorbs, varies linearly with concentration, C,^{2,3} *i.e.*

$$FR = \frac{(1 - R'_{\infty})^2}{2R'_{\infty}} = \alpha bc \quad (3.2)$$

where α is the molar absorptivity of the dye at that wavelength, c is its concentration and b is a constant. It follows that in this work the reflectance data can be used to generate the associated FR value at the wavelength of maximum

absorption, λ_{max} , which in turn is related to the concentration of the oxidised dye, MB, in the film. The variation in the batch-to-batch reproducibility of these films for both the photobleaching, and more crucially, the dark colour recovery step was better than 10%, which is acceptable for qualitative or semi-qualitative analysis of oxygen levels.

3.2.5 Contact Angle Measurement

The contact angle of the MB-DS ink and of the standard aqueous ink was measured to assess its affinity to various substrates *i.e.* how well the ink might wet a hydrophobic polymer plastic sheet. Two substrates, borosilicate glass and scotch tape, were chosen to represent hydrophilic and hydrophobic surfaces respectively.

3.3 RESULTS AND DISCUSSION

Using a typical MB-DS ink to create a film on PET, nanopowder TiO_2 was used as the semiconductor, and the diffuse reflectance spectra of the highly coloured film recorded before and after exposure to 5 s of UVA light ($I = 10 \text{ mW cm}^{-2}$), the results of which are illustrated in **Figure 3.2(a)**. From these results it is clear that the initially highly coloured MB-DS film is photobleached rapidly (*i.e.* within 5 s) by the UV light. In the absence of any of the ingredients (*i.e.* TiO_2 or glycerol) this photobleaching process does not occur; nor is it effected using visible, rather than UV light.

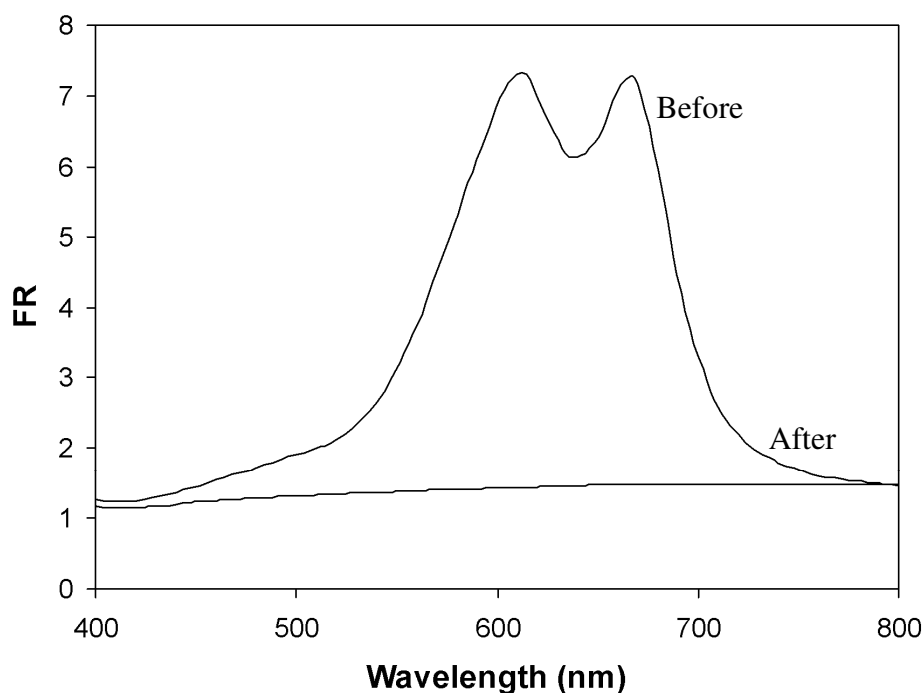


Figure 3.2(a) Typical diffuse reflectance spectrum of $\text{TiO}_2/\text{MB-DS}/\text{glycerol}/\text{zein}$ oxygen indicator, before and after UVA light irradiation (provided by two 8 W blacklight blue tubes), typically for 5 s. The absence of a peak in the latter spectrum indicates that all dye has been reduced to its colourless, LMB form ($I = 10 \text{ mW cm}^{-2}$). FR is the Kubelka-Munk function (See Equation 3.2).

Figure 3.2(b) contains photographs of a typical ink cast onto a film of PET through a metal template, with the letters ‘ TiO_2 ’ cut through it. The product was a PET film with the image ‘ TiO_2 ’ in blue ink printed on its surface. As illustrated by the results in **Figure 3.2(b)**, this image was photobleached upon UV irradiation (30 s, $I = 10 \text{ mW cm}^{-2}$) in air (*i.e.* step (1) in **Figure 3.3**), but subsequently regained its original blue colour in the absence of UV irradiation after 60 min, due to LMB’s reoxidation, *i.e.* via step (2) in **Figure 3.3**.

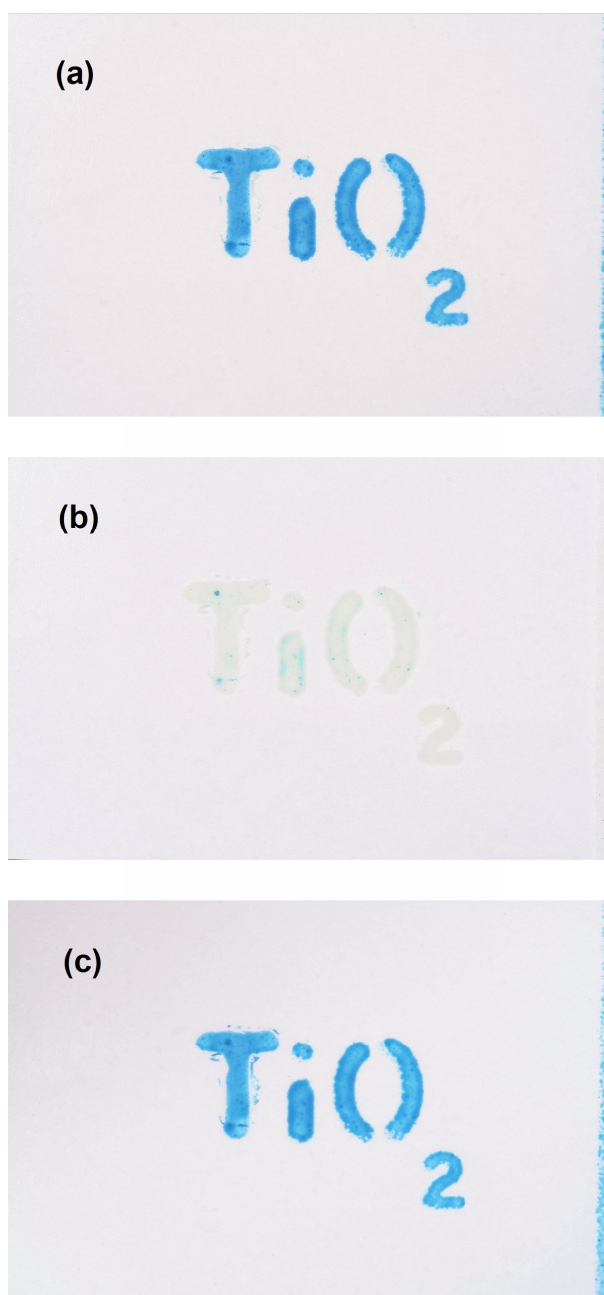


Figure 3.2(b) Photographs of a typical oxygen indicator ink printed as the letters 'TiO₂' on plastic. The photographs are for a nano-rutile TiO₂/MB-SD/glycerol/zein film (a) before, (b) after 30 seconds exposure to UVA light ($I = 10 \text{ mW cm}^{-2}$), and (c) 1 h after (b) and storage in the dark in air.

3.3.1 The Photobleaching Process (Step 1)

An important feature of the MB-SD ink is that it is activated, *i.e.* rendered oxygen-sensitive, by converting MB to LMB using UV light, *i.e.* light not absorbed by the

dye, which has an absorption window in the 330 - 400 nm region, but rather by the semiconductor photocatalyst, TiO₂. Evidence that the TiO₂ and not the dye, is the light-absorbing species responsible for the photobleaching process is provided by the observation that visible light (*i.e.* $\lambda > 400$ nm) is not able to photobleach the ink. However, most visible fluorescent lights, such as the ‘cool white’ light fluorescent tubes used in food cabinets, have a UVA spike in their emission profiles at 365 nm. At a normal distance (*i.e.* > 10 cm) this ‘spike’ is not usually sufficient in intensity (< 0.01 mW cm⁻²) to photobleach a typical MB-DS ink film in air, because the rate of photobleaching, *i.e.* step (1) in **Figure 3.3**, is then very low, compared to that of step (2) in **Figure 3.3**, the LMB reoxidation, colour-recovery step. However, in the absence of oxygen, *i.e.* in nitrogen, 2×8 W ‘cool white’ fluorescent tubes (HYBEC F8/T5/CW in a Vilber-Lourmat, model no. VL-208 irradiation unit), when placed close up (< 1 cm) to a MB-DS film, are able to photobleach the MB to LMB, albeit very slowly, via step (1), since the colour recovery step (2), is absent and the UVA irradiance significant, *i.e.* typically > 0.01 mW cm⁻².

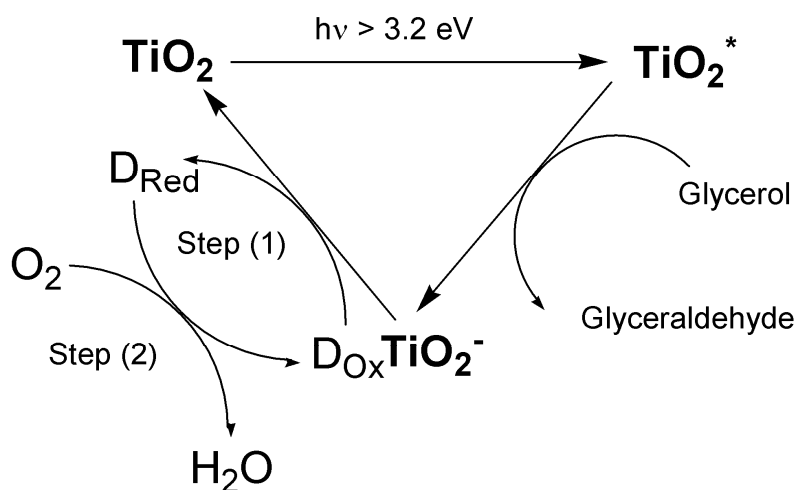


Figure 3.3 Schematic illustration of the key processes involved in the UV-activation and subsequent response towards oxygen of a TiO₂/MB/glycerol/HEC visual oxygen indicator. Step (1) refers to photo-induced reduction of the redox sensitive dye D_{Ox} (MB) to its reduced form, D_{Red}, colourless LMB, whereas step (2) illustrates the ‘dark’ back re-oxidation of the dye, leading to recovery of initial colour, by the ambient oxygen.

This photobleaching (activation) by the UVA light component in a white fluorescent tube, in the absence of O₂, is undesirable if these indicators are to be

incorporated in food packages, as such lamps are used in food cabinets and could lead to the reactivation of the O₂-indicator (*i.e.* photobleaching) if the package's integrity has been compromised (*i.e.* a false-negative result). However, the UVA absorptivity of TiO₂ depends upon many factors, including particle size and morphology, since both can produce a change in the bandgap of the semiconductor and absorptivity. An illustration of this feature was provided by a series of irradiations, using either two 8 W BLB, *i.e.* UVA ($I = 3 \text{ mW cm}^{-2}$), or two 8 W 'cool white' light fluorescent tubes ($I = 0.05 \text{ mW cm}^{-2}$), on two otherwise identical ink films, containing either nanoparticulate rutile, or Degussa P25 TiO₂ (titania).

The values of the Kubelka-Munk function of these films, *i.e.* FR, were measured at λ_{max} (= 665 nm) for MB in the dried ink as a function of irradiation time and the results are illustrated in **Figure 3.4**.

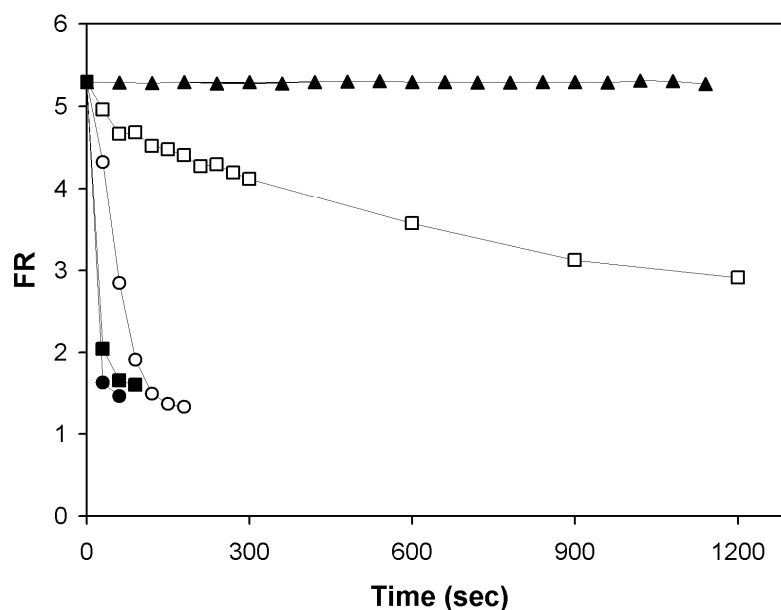


Figure 3.4 Plots of FR as a function of irradiation time profiles for the photobleaching of P25 and TiO₂ nano-rutile films in N₂ using different light sources conditions. The top straight line refers to P25 and nano-rutile films in the dark (▲). In contrast, the Degussa P25 film irradiated using two 8 W 'cool white' lights (○) is bleached rapidly, whereas the nano-rutile TiO₂ is not (□). When irradiated with two 8 W blacklight blue (BLB) lamps, *i.e.* the usual UVA source used in this work, nano-rutile TiO₂ (■) and P25 (●) were both bleached rapidly. The irradiance of the incident UVA light was 3 mW cm^{-2} , when using the $2 \times 8 \text{ W}$ UVA BLB lamps, and 0.05 mW cm^{-2} , when using $2 \times 8 \text{ W}$ 'cool white' fluorescent lights. The maximum error was less than 10%.

These show that whereas both films are photobleached at a similar rate using UVA light from a blacklight blue UVA lamp, the rate is slower when a ‘cool white’ lamp placed very close to the films, is used as a source of UVA, especially for the nanoparticulate rutile films. **Figure 3.5** illustrates TEMs of both the P25 TiO₂ and nanoparticulate rutile TiO₂ and reveal some striking differences, including that P25 TiO₂ comprises primary particles ca. 30 nm diameter, aggregated together to form larger (up to 0.1 μm) particles, whereas the nano rutile powder comprises thin needle-like particles (ca. 15 nm x 70 nm) that are less aggregated.

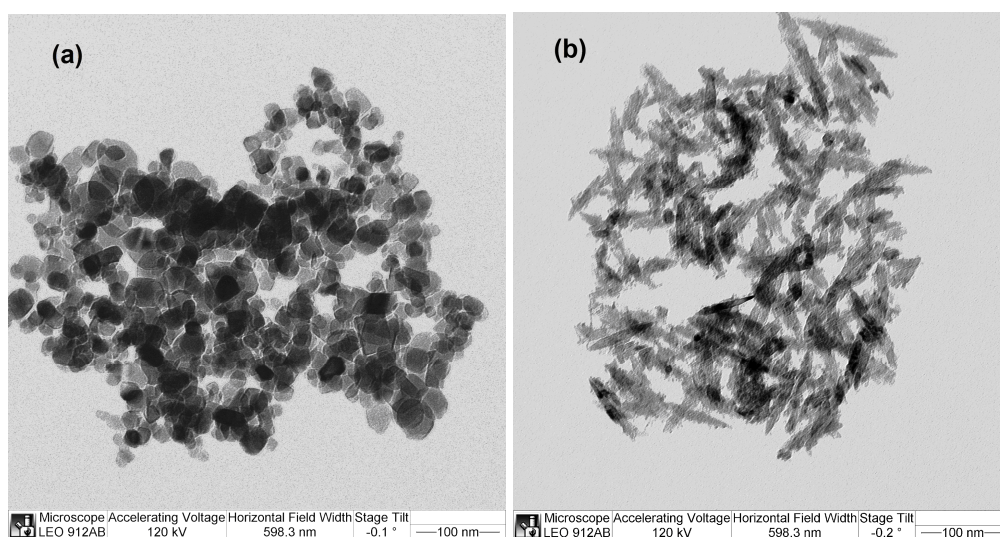


Figure 3.5 TEMs pictures of Degussa P25 TiO₂ (A) and nano-rutile TiO₂ (B) revealing very different morphologies that may be responsible for the different photoactivities. P25 particles appear aggregated together, forming large clusters; a fact reflected by the smaller surface area for P25 (50 m² g⁻¹) compared to that of nano-rutile TiO₂ (120 m² g⁻¹).

The latter particles appear to absorb the light associated with the UVA ‘spike’ in the cool-white lamps much less than those in P25 TiO₂, possibly due to a slightly lower bandgap arising from a quantisation effect.⁴ Whatever the cause, it is promising to note that these nano-rutile, MB-DS films are not very sensitive to the UVA component in visible fluorescent lamps even when the latter are placed very close (< 1 cm).

The kinetics of the photo-reduction of MB to LMB, *i.e.* step 1, is obviously UV irradiance dependant and an investigation of this feature, using a typical nano-rutile ink, generated the plot of normalised initial rate, R_i , [where initial rate = $r_i = (dFR/dt)_{t=0}$ and $R_i = r_i / FR_{t=0}$] versus the incident UVA irradiance, illustrated in **Figure 3.6**. The plot is typical of many photocatalytic systems⁵, in which, at low irradiances, the initial rate is usually found to be either, proportional to the irradiance, I , (indicating that electron-hole recombination is not significant) or, proportional to $I^{1/2}$ at high irradiances (indicating that recombination is the predominant fate of photogenerated electron-hole pairs).

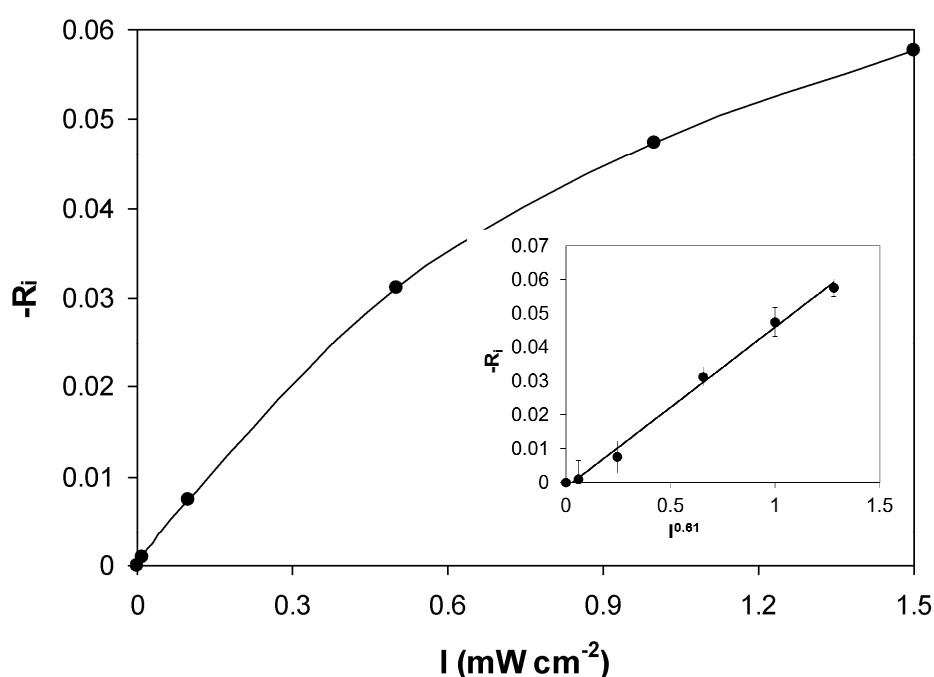


Figure 3.6 Plots of normalised initial rate ($= R_i = (dFR/dt)_{t=0} / FR_{t=0}$) vs. incident UVA light irradiance, I . The insert diagram shows the initial rate data vs. I^Θ , where $\Theta = 0.61$. This value for Θ indicates the electron-hole recombination is significant in these films. The maximum error was less than 10%.

Often, at intermediate irradiances, the initial rate is found to be proportional to I^Θ , where $0.5 < \Theta < 1$, and the results of this work is an example of such a case, with $\Theta = 0.61$, as indicated by the insert plot in **Figure 3.6**, of the data in **Figure 3.6**. The low, near 0.5 value, of Θ , indicates that electron-hole recombination is very significant in these films.

3.3.2 The ‘Dark’ Recovery Process (Step 2)

Once photobleached using UVA light, the solvent-based ink films are very stable in the absence of O₂, remaining colourless for over 12 months, but able to regain their original colour by reacting with ambient oxygen, as illustrated by the photographs in **Figure 3.3(b)**. **Figure 3.7** illustrates the typical ‘dark’ recovery in the diffuse reflectance spectrum of a UV-bleached, nano-rutile, MB-DS ink in air and reveals that its final spectral features are very close to its original.

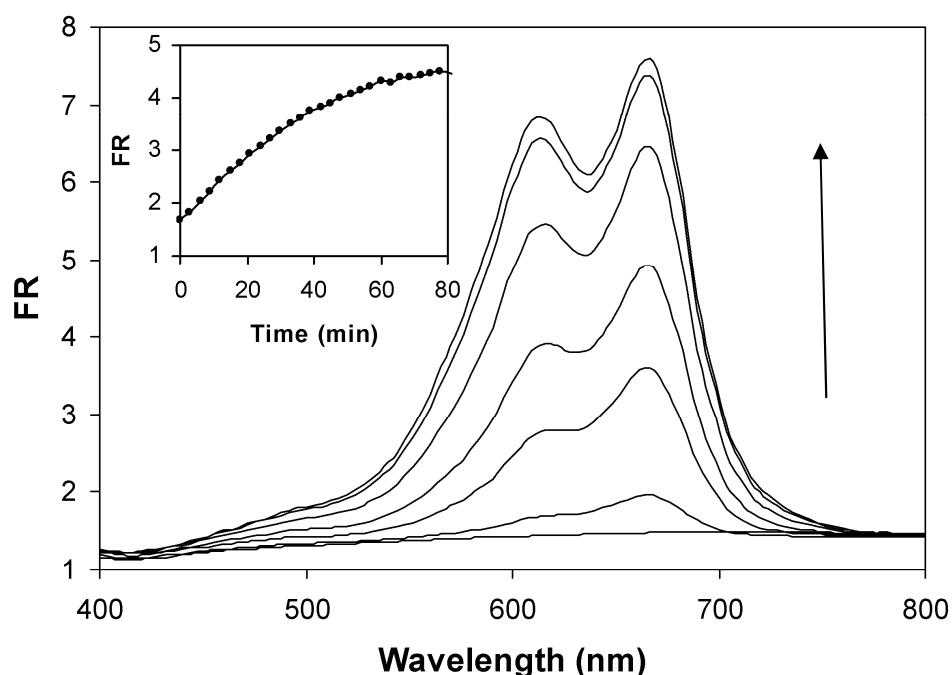


Figure 3.7 Dark recovery in the diffuse reflectance spectrum of a nano-rutile TiO₂/MB-DS/glycerol/zein oxygen indicator film after a initial 5 s irradiation with UVA light ($I = 10 \text{ mW cm}^{-2}$). These spectra were recorded in flow of oxygen (300 mL min^{-1}) every 3 min until the recovery was complete. Inserted plot shows the variation in FR at λ_{max} for the dark recovery of a photobleached nano-rutile TiO₂ (○) film in air (300 mL min^{-1}).

In a separate study, the variation of the initial rate of this recovery, R_i , was studied as a function of the %O₂ in the gas phase, using the nano-rutile ink and the results are illustrated in **Figure 3.8**. These results show that although, curiously, the ‘dark’ recovery of colour of a photobleached film is slower for a P25/MB-DS film than nano-rutile film, in both cases the initial rate is directly

proportional to % O₂ and so can be used to provide a quantitative measure of the % O₂ in the ambient gas phase. The direct relationship between R_i and %O₂ is not unexpected given the dark reaction responsible is step (2) in **Figure 3.3**, *i.e.* the reaction of photogenerated LMB with O₂. It is not clear why the photobleached P25 films react more slowly with O₂ than nano-rutile films, although the latter pigment does have a greater surface area (120 m² g⁻¹) than the former (50 m² g⁻¹) and the effect may be simply related to a difference in available surface area.

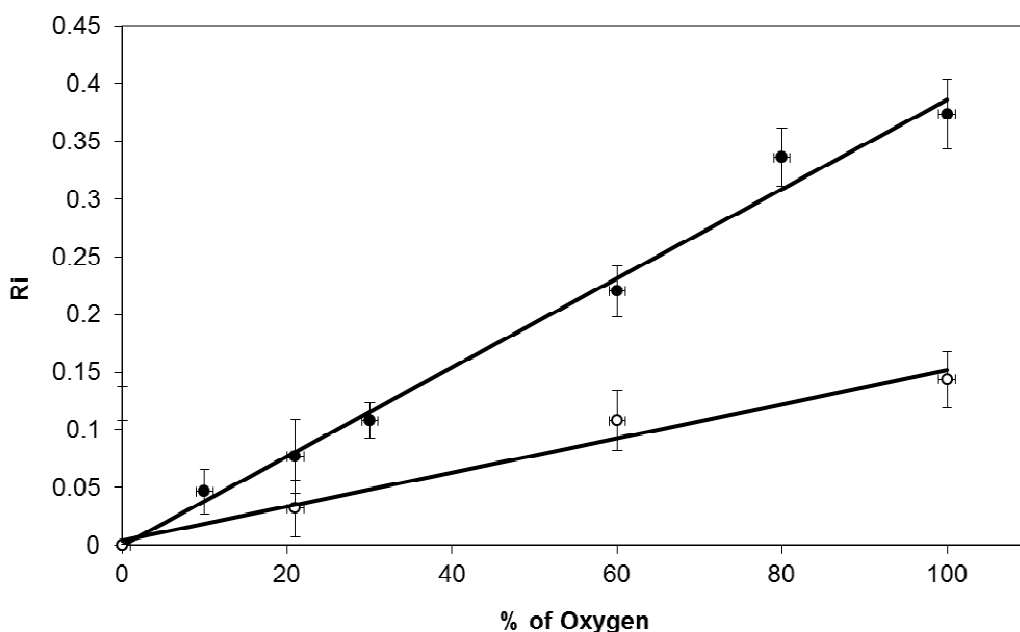


Figure 3.8 Initial recovery rates for Degussa P25 (○) and nano-rutile TiO₂ (●) films plotted as a function of the ambient %O₂ in the gas cell. In this work the films were initially photoreduced with UVA light ($I = 10 \text{ mW cm}^{-2}$ for 5 s).

The above solvent-based, UVA-activated, colorimetric oxygen indicator inks can be re-used a number of times without showing any evidence of deterioration. Thus, a typical nano-rutile TiO₂ MB-DS film was subjected to 6 cycles of a UVA photobleaching (in Ar) step followed by a dark recovery step (in O₂), whilst its FR value at λ_{max} (665 nm) was monitored as a function of time. The results of this work are illustrated in **Figure 3.9** and show that with each irradiation step, the film is photobleached to the same extent in Ar and recovers completely its original colour within ca. 40 min in O₂. These results highlight the reusability of

the ink.

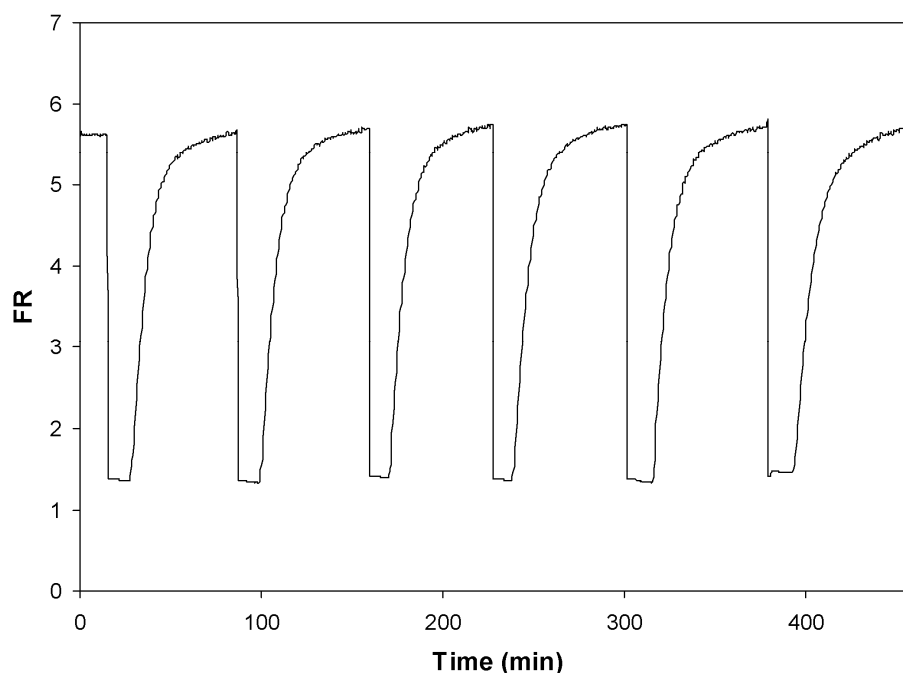


Figure 3.9 Variation in FR as a function of time recorded for a typical TiO₂/MB-DS film subjected to repeated UVA irradiation ($I = 10 \text{ mW cm}^{-2}$) and dark recovery in O₂ (6 cycles). Irradiation with UVA light was for 5 s (in Ar) and followed by 60 min dark recovery in oxygen at flow rate of 300 mL min^{-1} . The maximum error was less than 10%.

3.3.3 Contact Angle Measurements

Contact angles (see **Table 3.1**) recorded by the contact angle instrument showed the increased hydrophobicity of the solvent-based ink with ion-paired MB compared to the water-based standard aqueous ink with non-ion-paired, cationic MB (MB-AQ).

In **Table 3.1 (a)** the transition from hydrophobic scotch tape to hydrophilic glass is most clearly shown by the aqueous HEC solution going from 79.66° to 31.17° . The solvent-based zein solution shows a less marked change, going from 25.84° to 39.47° . In **Table 3.1 (b)**, the inks show very similar behaviour to the polymer solutions, particularly in the case of the aqueous inks which have very similar values to the aqueous polymer solutions. It is interesting to note that on both the Scotch tape and glass the solvent-based ink (consisting of zein polymer solution, MB-DS and

glycerol) shows a contact angle higher than the zein polymer solution alone which is obviously due to the presence of MB-DS and glycerol in the ink. Note also that on going from hydrophobic Scotch tape to hydrophilic glass the increase in contact angle is similar ($\sim 15^\circ$) to the polymer solution alone.

Table 3.1 (a) and **(b)** show contact angles measured on Scotch tape (hydrophobic surface) and Glass (hydrophilic surface) for blank polymer solutions and inks respectively. In **(b)** the abbreviation MB-AQ indicates aqueous inks made with non-ion-paired MB and MB-SB, solvent-based inks made with ion-paired MB.

(a) No MB added		
	Aqueous-based	Solvent-based
Scotch Tape	5 % HEC - 79.66°	20% zein - 25.84°
Glass	5% HEC - 31.17°	20% zein - 39.47°

(b) MB added		
	Aqueous-based	Solvent-based
Scotch Tape	MB-AQ - 83.29°	MB-SB - 59.68°
Glass	MB-AQ - 28.45°	MB-SB - 72.11°

3.4 CONCLUSION

Ion-pairing of MB with dodecyl sulfate (DS), produces a solvent-soluble form of the dye, which can be used to create a solvent-based, UV-activated, oxygen sensitive ink that can be printed on a variety of different hydrophobic polymers, including polyethylene terephthalate (PET). The UV sensitizer in this ink is TiO₂ and P25 TiO₂ based films are bleached quite rapidly under O₂-free conditions by the relatively small amount of UVA light that is present in white fluorescent lights, such as ‘cool white’ tubes. After photobleaching these P25 films are also quite slow to recover their original colour when exposed to air in the dark. In contrast, nano-rutile based films are much less sensitive towards the UV light in white fluorescent tubes, even in the absence of O₂, and, in comparison, rapidly recover their original colour when exposed to air. The initial rate of recovery of the original colour of either P25, or nano-rutile MB-DS, photobleached films, in

the 'dark' step (2) (see **Figure 3.3**), is proportional to the ambient level of oxygen, allowing these indicators to be used for both qualitative and quantitative analysis of the level of ambient oxygen simply by photobleaching with UVA light and monitoring the initial rate of colour recovery. Finally, these films can be re-used a number of times without exhibiting any evidence of photodegradation, brought on by the UVA activation step.

These solvent-based, colorimetric inks for oxygen appear to offer promise as a possible tamper-evident and/or leakage indicators for MAP packaged products.

The main drawbacks of the MB-DS ink identified in this chapter, the fact that it is susceptible to bleaching under most common visible light fluorescent tubes, is addressed by work carried out in Chapter 4. Another drawback, its inability to remain completely insoluble in water, is addressed in Chapter 5.

3.5 REFERENCES

1. S. Lee, A. Mills and A. Lepre, *Chem. Comm.*, 2004, 1912-1913.
2. M. P. Fuller and P. R. Griffiths, *Anal. Chem.*, 1978, **50**, 1906-1910.
3. P. Kortum, W. Braun and G. Herzog, *Angew. Chem. , Int. Ed. Engl.*, 1963, **2**, 333-341.
4. T. Toyoda and I. Tsuboya, *Rev. Sci. Instrum.*, 2003, **74**, 782-784.
5. G. Rothenbergen, J. Moser, M. Graetzel, N. Serpone and D. K. Sharma, *J. Am. Chem. Soc.*, 1985, **107**, 8054-8059.

CHAPTER 4

**NANOCRYSTALLINE SnO₂-BASED, UVB-
ACTIVATED, COLORIMETRIC OXYGEN
INDICATOR**

4.1 INTRODUCTION

To date most work has focussed on the creation and characterisation of HEC/glycerol/MB/TiO₂ colorimetric O₂ indicators.^{1,2} The key condition for this type of indicator is that the incident photons must have energy \geq the band gap of the semiconductor, E_{bg} , to drive the initial light-activation step - step 1 in **Figure 4.3**. In case of TiO₂ this band gap is 3.2 eV, *i.e.* photons of light of wavelength \leq 388 nm are needed to activate a HEC/glycerol/MB/TiO₂ film. These photons fall in the UVA region of the electromagnetic spectrum (320 - 400 nm). Unfortunately, most common visible light fluorescent tubes, such as those used in food cabinet display lighting, have an emission peak in the UVA region (typically at 365 nm), due to an emission line associated with electronically excited mercury vapour, and therefore are capable of activating the HEC/glycerol/MB/TiO₂ indicator. This is an undesirable feature, of the UV-activated colorimetric oxygen indicator, since it allows the indicator to be re-activated in an uncontrolled fashion, by, say, the UVA light component in white light fluorescent tubes, or sunlight. If the above semiconductor-sensitised based indicator technology is to be used in MAP, the ink needs a more controllable route of activation *i.e.* not by light commonly present in room or food cabinet lighting, but rather by, UVB light (240 - 320 nm) which is largely absent from such light sources. In this chapter, a UVB-activated colorimetric oxygen indicator which uses nanoparticulate tin (IV) oxide, $n\text{SnO}_2$, as the semiconductor photosensitizer is described and its response characteristics compared to those of a conventional TiO₂-based, colorimetric oxygen indicator.

4.2 EXPERIMENTAL

4.2.1 Materials and Chemicals

Nanoparticulate tin (IV) dioxide, $n\text{SnO}_2$, was purchased from Aldrich and nanoparticulate titania, P25 TiO₂, was a gift from Degussa (Evonik). XRD analysis of the $n\text{SnO}_2$ revealed a crystalline material, displaying the classic pattern of a rutile crystal structure³, see **Figure 4.1(b)**. The crystalline and nanoparticulate nature of $n\text{SnO}_2$ was also clear from transmission electron micrographs of the powder, a

typical example of which is illustrated in **Figure 4.1(a)**. BET analysis of the powder revealed a specific surface area of $15 \text{ m}^2 \text{ g}^{-1}$, *i.e.* about 30% of that of the P25 TiO_2 . The polymer, HEC (medium viscosity, cellosize-WP 40) was purchased from Fluka. All the other chemicals were obtained from Aldrich and used without further purification.

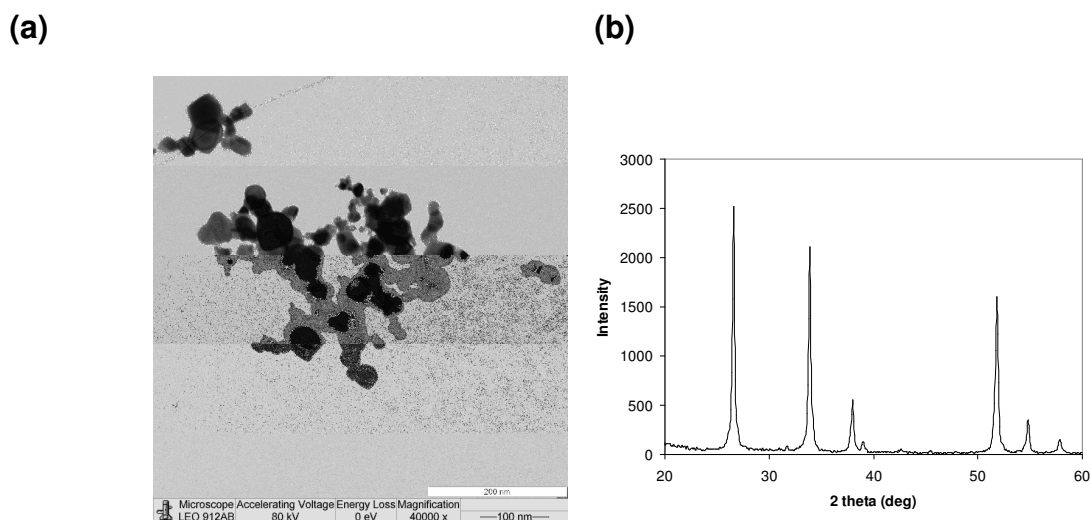


Figure 4.1(a) Powder XRD spectrum of $n\text{SnO}_2$. **(b)** TEM photographs of $n\text{SnO}_2$.

4.2.2 Ink and film preparation

A typical $n\text{SnO}_2$ O_2 -indicator ink was prepared as follows: 2 g of 5 wt.% HEC aqueous solution, 5 mg of redox dye (MB), 100 mg of sacrificial electron donor SED (glycerol) and 100 mg of $n\text{SnO}_2$ were mixed together and stirred for at least 30 minutes, followed by 30 minutes of sonication from an ultrasound bath to ensure thorough mixing and dispersion of the various components. In order to make a typical $n\text{SnO}_2$ film a drop of this blue ink was then placed on the centre of a 25 mm diameter glass cover slip and spun at 3500 rpm for 30 s, to produce a dry film with an average thickness of *ca.* 5 μm . The composition of this typical $n\text{SnO}_2$ film with respect to the other component in the HEC/glycerol/MB/ $n\text{SnO}_2$ film can be summarised as follows: 100/100/5/100 pphr where pphr = parts per hundred resin. Otherwise similar TiO_2 -based inks were also prepared, but with the TiO_2 level at 20 or 100 pphr, to aid comparison

4.2.3 Irradiation and colour measurement

UV/visible absorbance measurements were made with a UV/Vis Cary 300 spectrophotometer and diffuse reflectance spectra of the two different semiconductor powders were measured using a Perkin Elmer Lambda 35 spectrophotometer with a diffuse reflectance attachment (Labsphere RSA-PE-20).

The diffuse reflectance measurements were employed because the high level of light scattering, due to the high catalyst loadings in our samples, did not allow the use of conventional light transmitting spectroscopy. **Figure 4.2** illustrates the increased baseline in a typical HEC/glycerol/MB/ $n\text{SnO}_2$ film (100/100/5/100 pphr) compared to 10^{-5} M aqueous MB solution. **Figure 4.2** demonstrates another noticeable feature: the two spectra have swapped the peak maxima. This is a result of MB monomer (665 nm) - dimer (605 nm) equilibrium being shifted in favour of the dimer in the more compact, solid environment of the film ⁴.

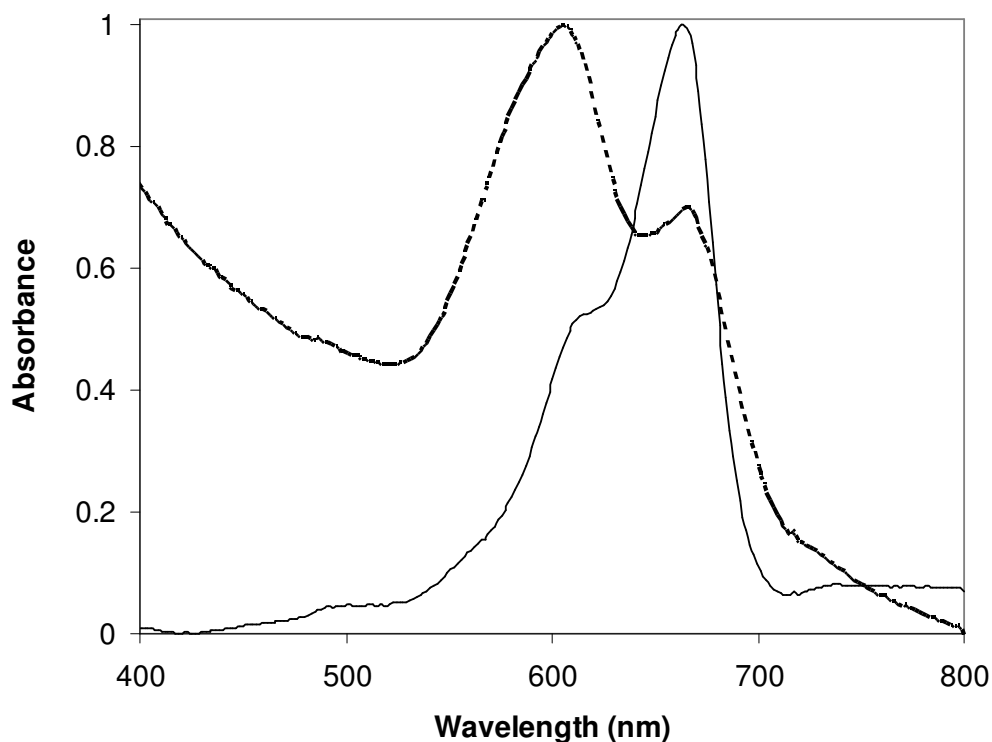


Figure 4.2 A typical Methylene Blue spectrum in the HEC film (--, $\lambda_{\text{max}} = 605$ nm) and a spectrum of 10^{-5} M water solution of Methylene Blue (—, $\lambda_{\text{max}} = 665$ nm). The plot shows different distribution of monomeric (665 nm) and dimeric (605 nm) forms of MB dependency upon the concentration of MB which is higher in the film than in the 10^{-5} M solution.

Unless stated otherwise all irradiations were done in nitrogen, in order to study the UV-activation process, step 1, (**Figure 4.3**) without any interference from the dark recovery step, step 2 (in **Figure 4.3**). In the study of the dark recovery of oxygen response step, step 2, characterisation of the HEC/glycerol/MB/*n*SnO₂ film as a function of %O₂, was carried out using a brass gas cell to maintain the sample in different controlled gaseous atmospheres (*e.g.* N₂ or O₂ or defined mixture of these, all with an overall flow rate of 300 mL min⁻¹).

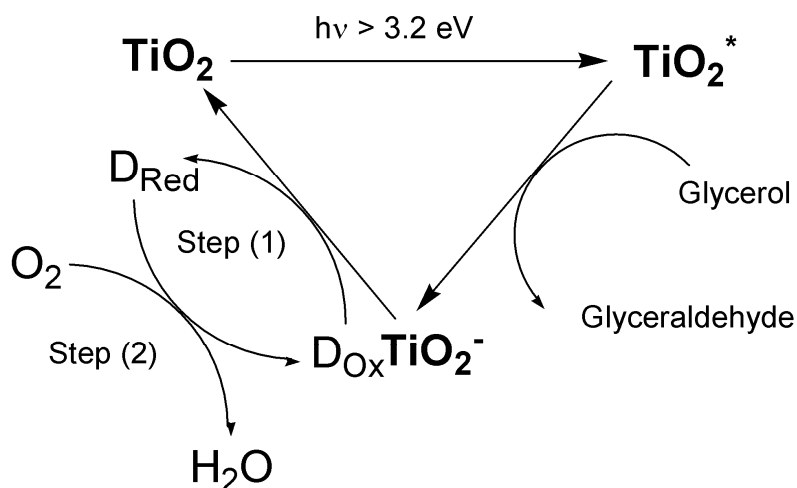


Figure 4.3 Schematic illustration of the key processes involved in the UV-activation and subsequent response towards oxygen of a TiO₂/MB/glycerol/HEC visual oxygen indicator. Step (1) refers to photo-induced reduction of the redox sensitive dye D_{Ox} (MB) to its reduced form, D_{Red}, colourless LMB, whereas step (2) illustrates the ‘dark’ back re-oxidation of the dye, leading to recovery of initial colour, by the ambient oxygen.

Typically three different fluorescent tube light sources were used in this work, namely; (i) 2x20 W Philips TL01 UVB lamps with a narrow emission peak at 315 nm, (ii) 2x8 W Philips F8/T5/BLB UVA tubes with a broad emission peak at 365 nm and finally, (iii) 2x8 W GE T5/F8 warm-white (WW) light fluorescent tubes, frequently used in food cabinet lighting. The emission spectra of these three light sources, *i.e.* UVB (narrow), UVA and WW fluorescent lamps, are illustrated in **Figure 4.4**. The UVA and UVB irradiance levels emitted by these lamps were measured using a UV-meter (UVX digital radiometer, UVP); visible light levels (for the WW lamp) were measured using a LX-101 (Lutron) lux meter. The typical

irradiance levels (and required lamp distances) employed in this work are summarized in **Table 4.1**.

Table 4.1 UV/Visible irradiance levels used in this work with the UVB, UVA and WW lamps

Lamp	UVA int. (mW cm^{-2})	UVB int. (mW cm^{-2})	Illuminance (lux)	Distance (cm)
UVB 2×20W TL01	0.18	1	720	15
UVA 2×8W	1	0.04	120	18
WW 2×8W	0.04	0.01	7000	10

The intensity measurements reported in **Table 4.1** and the plots in **Figure 4.4** reveal that the amount of UVB (due to the 306 and 310 nm Hg vapour emission lines) emitted by the UVA and WW lamps is very small. In contrast, the level of UVA emitted by most white light fluorescent tubes, such as the WW lamps, is not insignificant. The conditions under which the WW lights were used, and their irradiances measured (see **Table 4.1**), are similar to those found in the brightest part (top shelf) in most supermarket food cabinets.

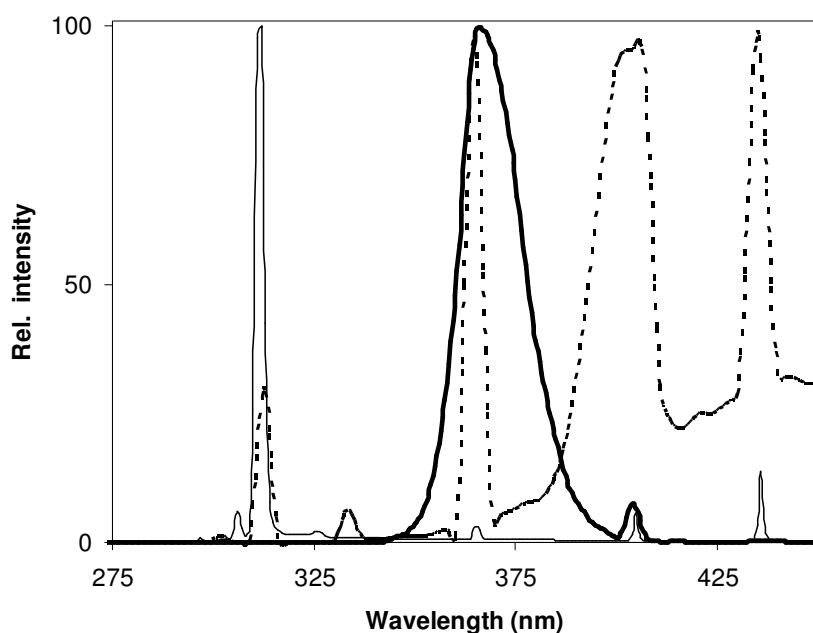


Figure 4.4 Normalised relative intensity emission spectra of the lamps used in this work; 20 W UVB narrow band lamp (—), 8 W BLB UVA (—) and 8 W warm-white fluorescent tubes (--). Note the prevalence of the Hg-vapour emission lines at 365 nm, 310 and 306 nm.

4.3 RESULTS AND DISCUSSION

4.3.1 Diffuse Reflectance Spectra of SnO₂ and P25 TiO₂

The diffuse reflectance spectra of the two nanoparticulate semiconductor powders, *n*SnO₂ and P25 TiO₂ were recorded and are illustrated in **Figure 4.5**. An analysis of this spectral data reveals *n*SnO₂ to have an absorption edge at ca. 344 nm, corresponding to a band gap, of 3.65 eV, whereas P25 TiO₂ begins to absorb at ca. 382 nm, corresponding to a band gap of 3.25 eV^{5,6}. Thus, whereas P25 TiO₂ based indicator will be activated by the UVA emitted by the WW, UVA, as well as the UVB lights used in this work, *n*SnO₂ should be activated by only the UVB light source, since there is very little UVB in the WW and UVA sources used here (**Table 4.1**).

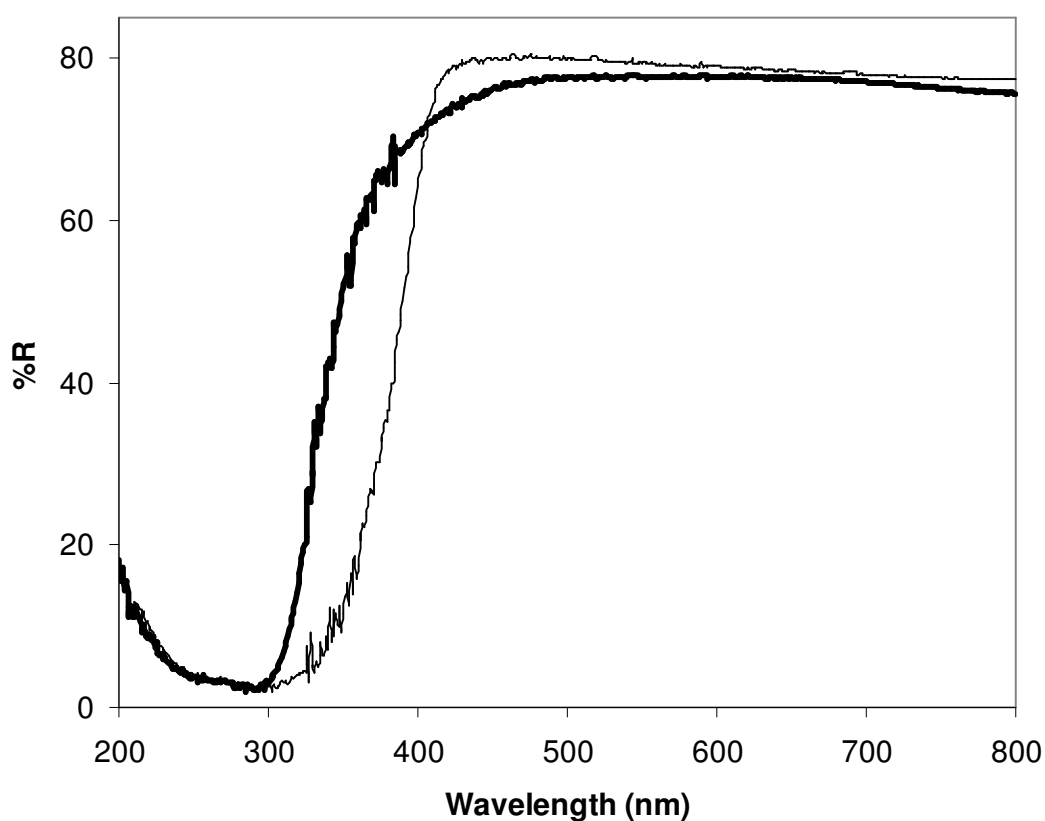


Figure 4.5 Reflectance spectra of *n*SnO₂ (—) nanopowder (—) and P25 titania.

4.3.2 The UVB Activation and Recovery of a Typical $n\text{SnO}_2$ Film

A typical $n\text{SnO}_2$ film was prepared and irradiated with UVB light (1 mW cm^{-2}) in nitrogen. Photographs of the film before and after (10 min) irradiation are shown in **Figure 4.6(a)** and reveal the film to be photobleached, *i.e.* UVB-activated, after this short period of illumination; which corresponds to the activation step, step 1, in **Figure 4.3**. The concomitant change in the UV/visible absorption spectrum of this film is illustrated in **Figure 4.6(b)** and reveals all the MB to be converted to its colourless, reduced form, *leuco*-Methylene Blue, LMB. In this work the change in the absorbance at the absorption maximum for MB, ca. 605 nm, *i.e.* ΔAbs_t , was monitored as a function of irradiation time, t , and usually reported as a relative absorbance change, *i.e.* $rel \Delta Abs$ where $rel \Delta Abs = \Delta Abs_t / \Delta Abs_{t=0}$. Whatever the irradiation source, or semiconductor photosensitizer, with this type of ink film, once UV-activated, *i.e.* photobleached, the indicator dye remains colourless unless, or until, exposed to oxygen, whereupon it regains its original colour as D_{ox} is re-oxidized to D_{red} by O_2 *i.e.* as a result of step 2 in **Figure 4.3**. The last photograph in **Figure 4.6(a)** shows the film regains its original colour when UV activated and then allowed to react with the O_2 in air for 10 min.

In contrast, a film with the same mass of P25 powder as of the $n\text{SnO}_2$ in its formulation (100/100/5/100 pphr) had paler blue and less transparent appearance. This is depicted in **Figure 4.6(c)** by the increased baseline. Also, the P25-based film photobleached fully within 10 minutes of 2x8W warm white fluorescent visible light, *i.e.* under conditions that the $n\text{SnO}_2$ based film shows long-term photostability.



Figure 4.6(a)

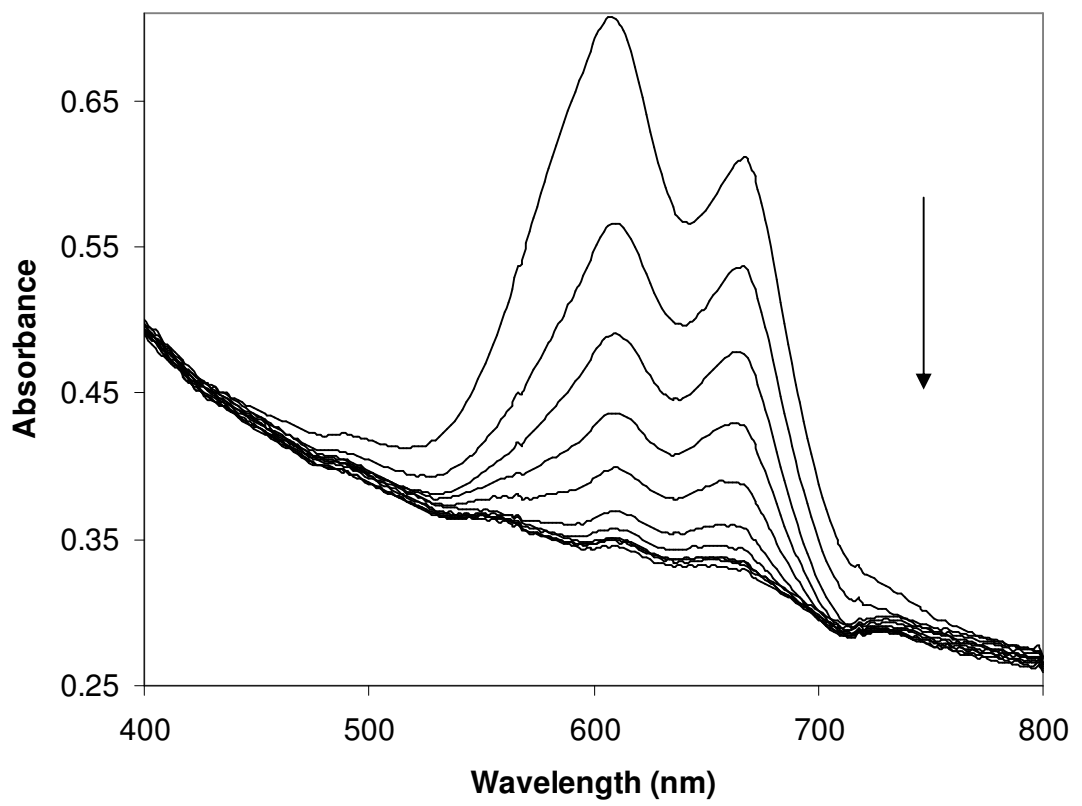


Figure 4.6(b)

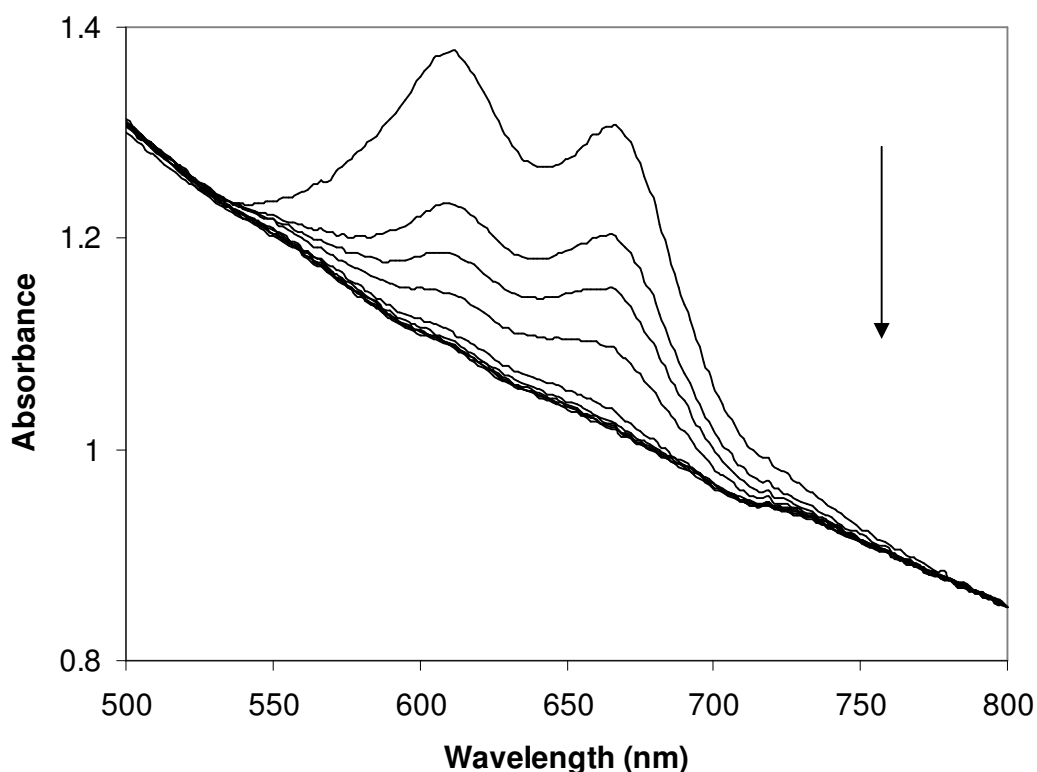


Figure 4.6(c)

Figure 4.6 (a)-(c) (a) Photographs of typical $n\text{SnO}_2$ oxygen indicating film on glass cover slip (25 mm diameter) before and after 10 min of UVB irradiation (in N_2). The last picture shows the UV activated film after 15 min in air, by which time it has fully recovered its original colour. (b) UV/vis absorption spectra of a typical $n\text{SnO}_2$ (100/100/5/100 pphr) indicator film photobleaching as a function of irradiation time (1 min intervals) in the photobleaching step (spectra taken from top to bottom). (c) UV/vis spectra of the P25-based film (100/100/5/100 pphr) using the 2x8 W warm-white fluorescent tubes ($\text{UVA I} = 0.04 \text{ mW cm}^{-2}$, $E_v = 7000 \text{ lx}$) under nitrogen atmosphere, spectra were recorded every minute (total of 10 mins).

4.3.3 UV sensitivity of $n\text{SnO}_2$ and P25 TiO_2 based films (step 1)

Four different HEC/glycerol/MB/semiconductor oxygen-indicator films containing: (i) no photocatalyst, (ii) 100 pphr $n\text{SnO}_2$, (iii) 20 pphr P25 TiO_2 and (iv) 100 pphr P25 TiO_2 were prepared (20 pphr $n\text{SnO}_2$ did not photo-bleach) and irradiated under nitrogen using each of the following three different light sources: (a) warm white (WW) light, (b) UVA and (c) narrow band UVB light at the distances/irradiance levels given in **Table 4.1**; the observed *rel* ΔAbs versus irradiation time profiles arising from this work are illustrated in **Figures 4.7(a) – (c)**, respectively. From the

results in **Figure 4.7(a)** and **(b)** it is clear that both the $n\text{SnO}_2$ and ‘no photocatalyst’ films remained unbleached when exposed to light from either the WW or UVA light source. In contrast, P25 TiO_2 loaded films are readily photobleached/activated by both these light sources and not surprisingly, at a rate that increases markedly with the level of photocatalyst present; *i.e.* the 100 pphr P25 TiO_2 is more readily photobleached than the 20 pphr P25 TiO_2 film. Both the $n\text{SnO}_2$ and P25 TiO_2 films are bleached by UVB light, with only the ‘no photocatalyst’ indicator film remaining unbleached, *i.e.* unactivated, when this light source is used, see **Figure 4.7(c)**. From the results of this work it is clear that when $n\text{SnO}_2$ is used as the photocatalyst in a HEC/glycerol/MB/semiconductor film, the resultant O_2 indicator is not UVA sensitive and, therefore, not readily photobleached by the UVA component of white light fluorescent tubes, such as warm white light. This is not surprising given the band gap of SnO_2 is 3.65 eV (= 340 nm) whereas the UVA Hg vapour emission line present in the UVA and WW light sources is at 365 nm. In contrast, P25 TiO_2 has a band gap of 3.25 eV (= 382 nm) and so is able to absorb these UVA photons much more readily and so all P25-based films are photobleached by the UVA present in the WW and UVA lamps. The use in this work of $n\text{SnO}_2$, rather than TiO_2 , as the semiconductor photosensitizer, in a UV-activated colorimetric indicator, is a major advance as it is a significant barrier to their uncontrolled activation, given the ambient level of UVB in interior room lighting is very small.

Further increase of the energy of the incident UV light into the UVC region ($\lambda \leq 280$ nm) did not speed up the kinetics of the film’s photobleaching substantially. And, as a result of the germicidal UVC light, the Methylene Blue within the film was photobleached permanently. This is demonstrated in **Figure 4.7(d)**.

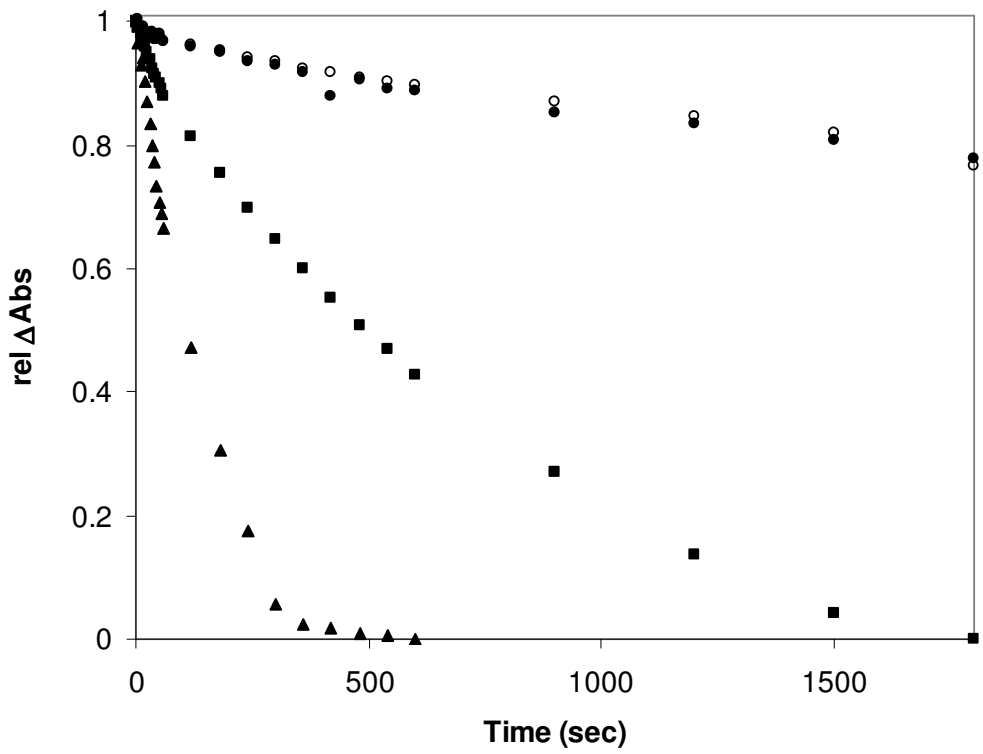


Figure 4.7(a)

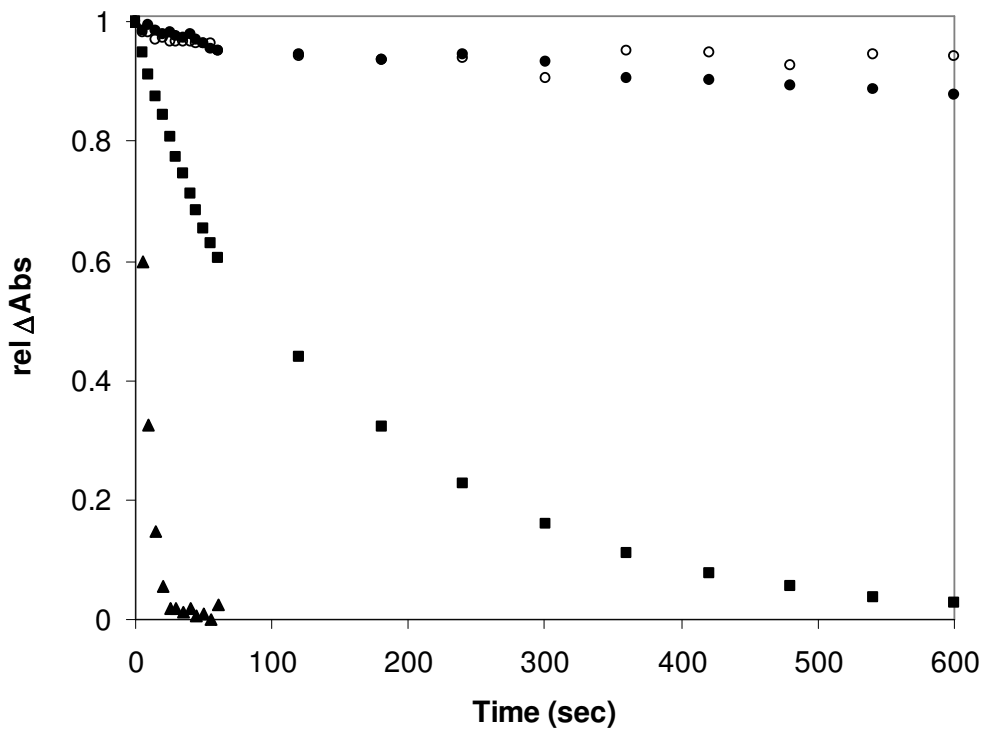


Figure 4.7(b)

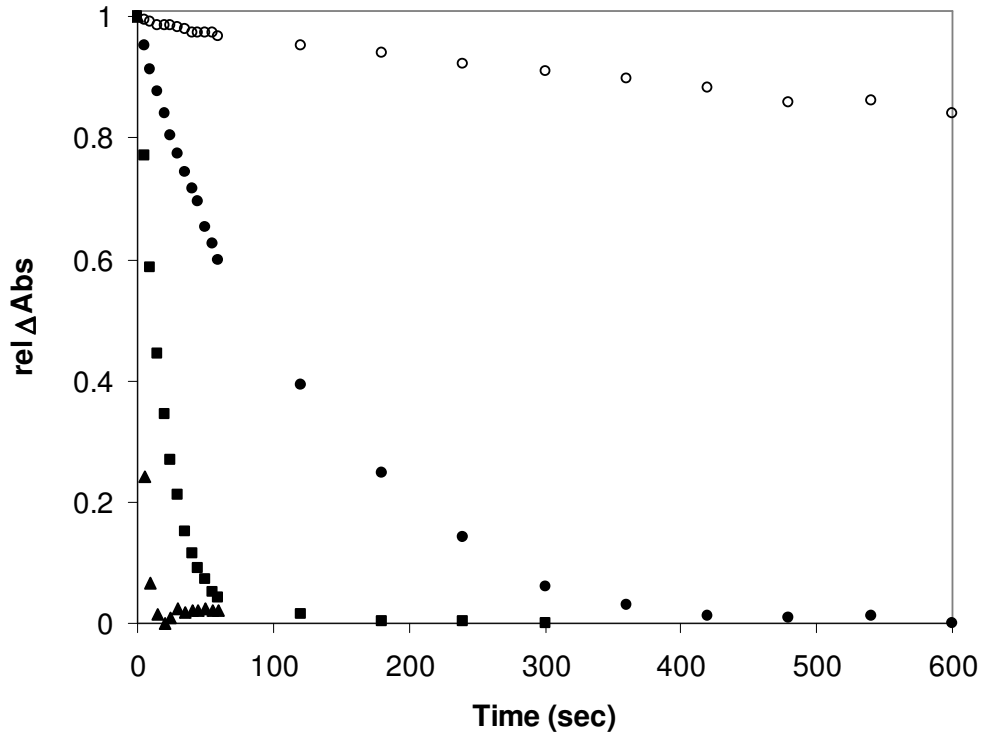


Figure 4.7(c)

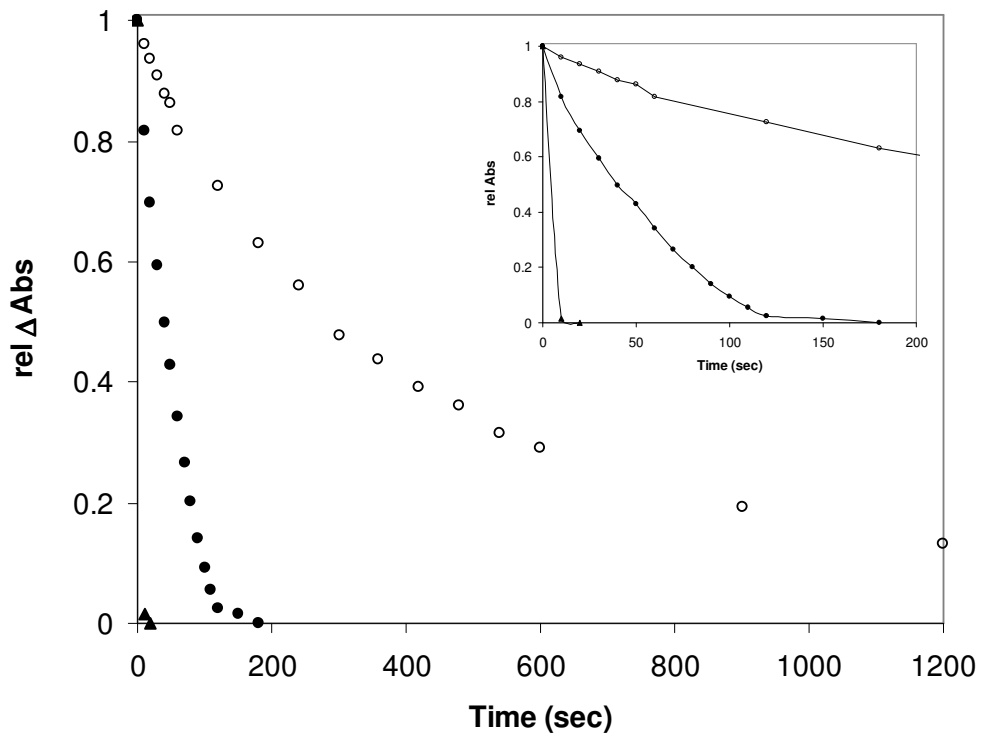


Figure 4.7(d)

Figure 4.7 (a)-(d) Photobleaching of typical O₂ indicator films with: (i) *n*SnO₂, composition: 100/100/5/100 (●), (ii) P25 TiO₂, composition: 100/100/5/100 (▲), (iii) P25 TiO₂, composition: 100/100/5/20 (■) and (iv) ‘no photocatalyst’ (○). The films were irradiated approximately for (a) 1 hour using 2x8 W warm-white fluorescent tubes (UVA I = 0.04 mW cm⁻², E_v = 7000 lx), (b) 10 min using 2x8 W BLB UVA tubes (UVA I = 1.0 mW cm⁻²) and (c) 10 min using 2x20 W TL01 UVB tubes (UVB I = 1.0 mW cm⁻²). (d) The films were irradiated for 20 min using 2x8 W UVC lamp (UVC I = 0.4 mW cm⁻²) under nitrogen atmosphere. Blank film (no semiconductor) is shown for comparison (○). The insert in (d) shows first 3 minutes in detail. All irradiations were carried out under N₂. The maximum error was less than 10%.

4.3.4 Photobleaching (Step 1) as a Function of Irradiance

In order to characterise the HEC/glycerol/MB/*n*SnO₂ O₂ sensitive film in more detail, the photobleaching of a typical *n*SnO₂ film was studied as a function of irradiance, *I*, and the results are illustrated in **Figure 4.8**. The initial rate of photobleaching, *r_i*, appears to be directly related to the incident irradiance, *I*^{0.75}. Such a dependence on irradiance is not unusual in semiconductor photocatalysis, since it is found that *r_i* ∝ *I* at low *I*, due to efficient photochemical reaction at the surface and *r_i* ∝ *I*^{1/2} at high *I*, due to a dominant electron-hole recombination process⁷. Thus, an observed dependence of *r_i* upon *I*^{0.75} signifies a mixed dependency that is expected at the moderate irradiance levels (ca. 1 mW cm⁻²) employed here.

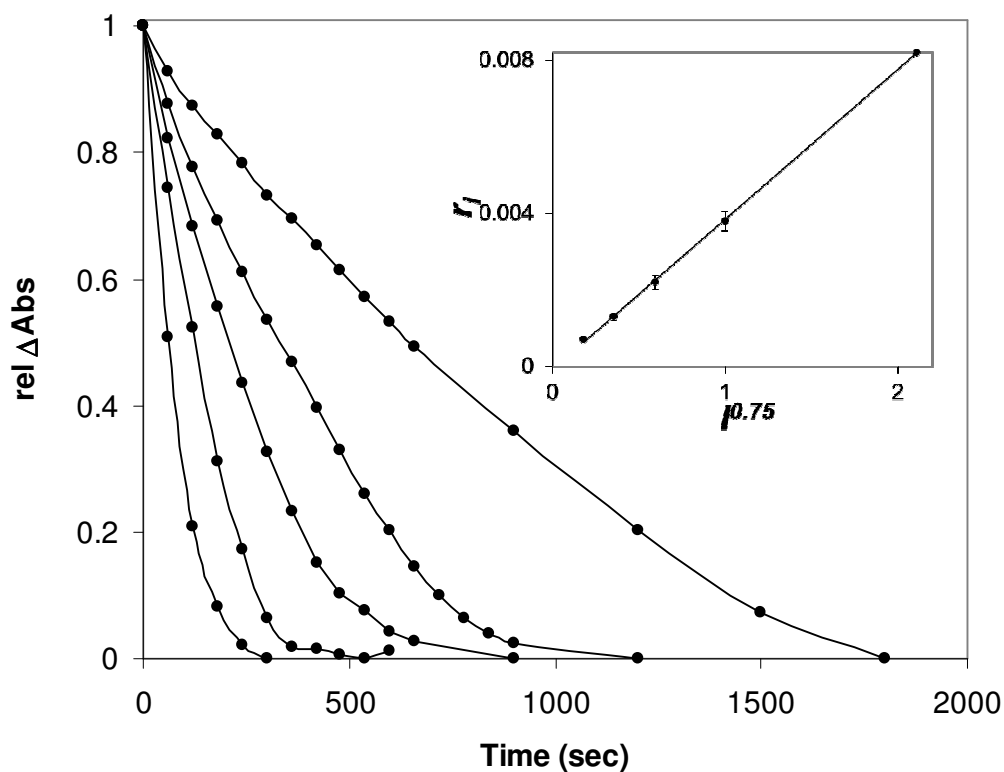


Figure 4.8 The plot of the absorbance of a typical $n\text{SnO}_2/\text{MB}$ film at λ_{max} 605 nm versus irradiation time profiles using UVB light (TL01 2x20W) at different irradiances, I , *i.e.* from left to right: (0.1, 0.25, 0.5, 1.0 and 2.7 mW cm^{-2}). The insert shows a subsequent plot of the data in the main diagram in the form of initial rate, r_i , of photobleaching as a function of $I^{0.75}$. The maximum error was less than 10%.

4.3.5 The Dark O_2 Response (Step 2)

Clearly, a key feature of the HEC/glycerol/MB/ $n\text{SnO}_2$ film is its response to oxygen, *i.e.* step 2 in **Figure 4.3**. The kinetics of this response for a typical UVB-activated (under N_2) $n\text{SnO}_2$ film were recorded as a function of $\% \text{O}_2$ and the results are illustrated in **Figure 4.9**. The kinetics due to the diffusion of oxygen into the heterogeneous medium of the polymer film and subsequent reaction with leuco-MB, are not simple, due to the heterogeneous nature of the polymer film and, therefore, distribution of oxygen solubilities and diffusion coefficients⁸, although a useful, simple measure is the time taken for a film to recover half its final colour, *i.e.* t_{50} , when $\text{rel } \Delta \text{Abs} = 0.5$. Analysis of the recovery data in **Figure 4.9** allows a plot of I/t_{50} versus $\% \text{O}_2$, shown as an insert plot in the figure, which yields a straight line, suggesting that this type of indicator could be used for quantitative analysis of the

ambient oxygen level simply by initially activating with UVB light, and monitoring the time it takes for the film to recover half its original colour. This time, when compared with the data in a calibration graph, such as illustrated in the insert in **Figure 4.9**, would reveal the ambient level of oxygen present.

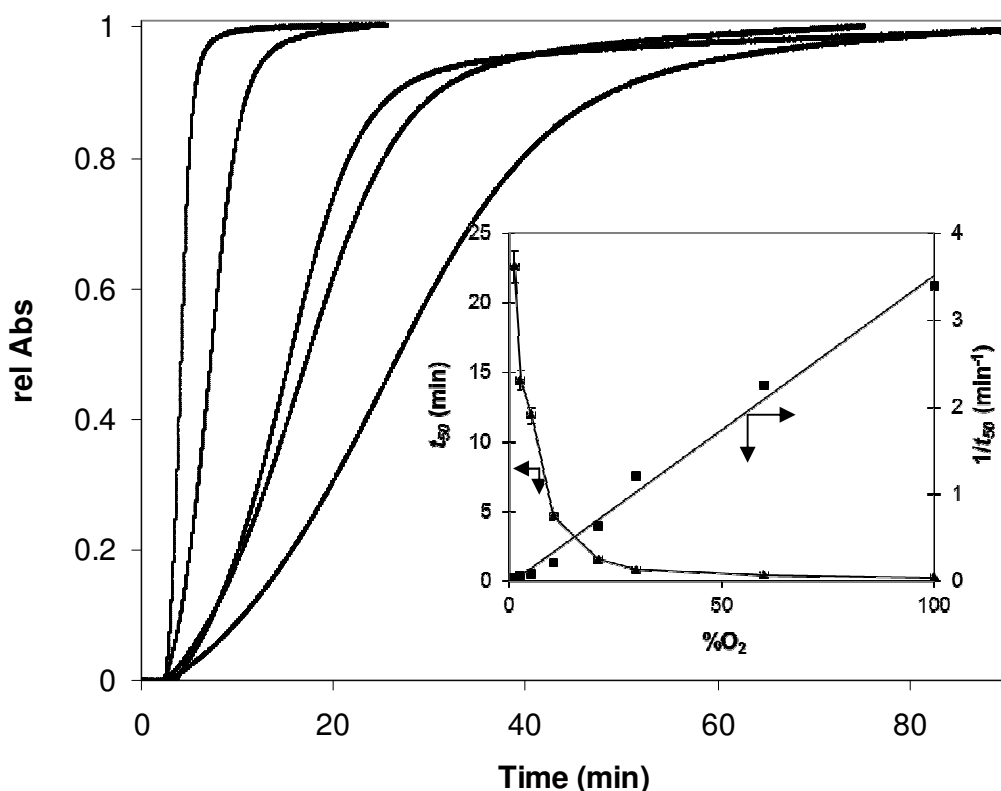


Figure 4.9 Recovery of a typical $n\text{SnO}_2$ film when UV activated (in N_2) and then exposed to different O_2 levels (from right to left: 1.3, 2.6, 5.3, 10.5, 21 % O_2). The inserted diagram shows a subsequent plot of the data in the form of: t_{50} (\blacktriangle) and $1/t_{50}$ (\blacksquare) (gradient of the slope = 0.35) as a function of % O_2 . The $n\text{SnO}_2$ films were bleached in N_2 prior to the exposure to the O_2 -containing atmosphere using 10 min UVB light from 2x6 W broad band lamps, $I = 2.7 \text{ mW cm}^{-2}$). The maximum error was less than 10%.

4.4 CONCLUSION

Nanocrystalline SnO_2 can be used as a photocatalyst in a UV-activated colorimetric oxygen indicator comprising: polymer/ SED/ redox dye/ photocatalyst, where polymer = HEC, donor = glycerol, dye = MB and photocatalyst = $n\text{SnO}_2$. Previous

work had established that P25 TiO₂, although very effective, responds to the UVA component in most fluorescent tubes.

The larger band gap (3.65 eV) of nSnO₂, compared to P25 TiO₂, renders it UVB, but not UVA, sensitive. In particular, nSnO₂ is unable to absorb photons due to the Hg vapour emission line at 365 nm and as a consequence, a HEC/glycerol/MB/nSnO₂ film is not activated (*i.e.* photobleached) by the UVA component in white or UVA fluorescent tubes, but is activated by UVB light.

Other work on the nSnO₂-based O₂-indicator film reveals a fractional power dependence of the kinetics of UV activation on irradiance, *i.e.* $r_i \propto I^{0.75}$, and that the rate of its response towards oxygen, as measured by t_{50} , could be used to assess the ambient level of oxygen. The use of nSnO₂ as a photocatalyst in the UV activated oxygen-sensitive inks opens up many possible avenues of application as it allows the UV-activation step to be much more controllable. In particular, this modified ink has promise as a quality control and tamper-evident indicator in MAP.

The main drawback of this oxygen indicating system in respect to its potential use in MAP food packaging is its water-based nature and the consequential disintegration after it is subjected to the often very moist, environment within such packages. In the next chapter an oxygen indicator that could be printed on plastics and is water stable is introduced.

4.5 REFERENCES

1. S. Lee, A. Mills and A. Lepre, *Chem. Comm.*, 2004, 1912-1913.
2. A. Mills and D. Hazafy, *Analyst*, 2008, **133**, 213-218.
3. B. Grzeta, E. Tkalcec, C. Goebbert, M. Takeda, M. Takahashi, K. Nomura and M. Jaksic, *J. Phys. Chem. Solids*, 2002, **63**, 765-722.
4. H. Nishikiori, S. Nagaya, N. Tanaka, A. Katsuki and T. Fujii, *Bull. Chem. Soc. Jpn.*, 1999, **72**, 915-921.
5. T. Sato, Y. Yamamoto, Y. Fujishiro and S. Uchida, *J. Chem. Soc., Faraday Trans.*, 1996, **92**, 5089-5092.
6. S. Uchida, Y. Yamamoto, Y. Fujishiro, A. Watanabe, O. Ito and T. Sato, *Chem. Soc., Faraday Trans.*, 1997, **93**, 3229-3234.
7. A. Mills, *J. Photoch. Photobio. A*, 1997, **8**, 1-35.
8. A. Mills, *Analyst*, 1999, **124**, 1301-1307.

CHAPTER 5

**SECOND GENERATION OF SOLVENT-
BASED OXYGEN INDICATORS**

5.1 INTRODUCTION

An alternative way to dodecyl sulfate (DS)-MB ion-paired based inks introduced in Chapter 3, and one which might provide more options for the fine tuning of the solubility of the dye-ion pair, is to use an anionic polymer as the counter ion. It was decided that polystyrene sulfonic acid would be a good choice as previous work by others¹⁻³ has shown that hydrophobic polystyrene (PS) can be rendered increasingly soluble in polar solvents by increasing the degree of sulfonation (see **Figure 5.1**).

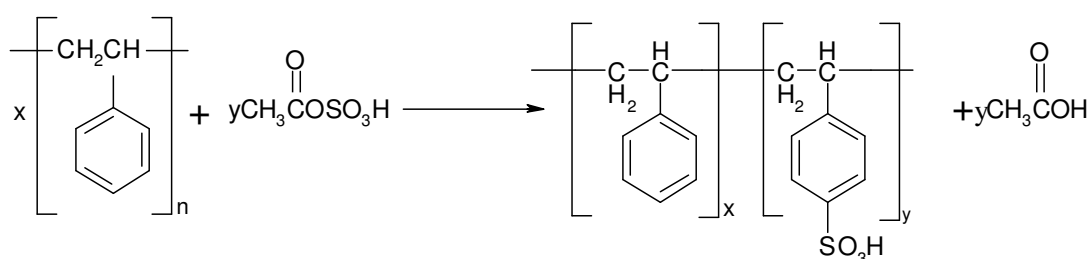


Figure 5.1 The reaction scheme of the sulfonation of polystyrene.

It was hoped that this would provide a way to more finely tune the solubility of the dye-ion pair to meet the requirements of the ideal MAP/O₂ indicator ink. Commercially available styrene sulfonic acids are usually too sulfonated (water soluble) to be of use so samples of sulfonated polystyrene were prepared using a method developed by Makowski⁴.

5.2 EXPERIMENTAL

5.2.1 Dye-Ion pair Preparation and Ink Formulation

Preparation of Sulfonated Polystyrene

In this work an acetone-soluble sample of 10% sulfonated PS was prepared according to an established literature method.^{4, 5} 52 g of polystyrene (average molecular weight 250,000, supplied by Acros Organics) were placed in a 500 mL, 3-necked, round-bottomed flask and dissolved in 245 mL of dichloromethane (DCM) through vigorous stirring. The sulfonating reagent, acetyl sulfate, was prepared separately; 50 mL of DCM was added to 9.5 mL of acetic anhydride in a round-

bottomed flask held in an ice bath under an inert atmosphere of argon. 3.5 mL of 95% sulfuric acid were added dropwise to the DCM/acetic anhydride solution. 35 mL of this sulfonating reagent mixture were removed to the original polystyrene solution and the mixture refluxed at 55°C for 4 hours. 50 mL of ethanol were added to the solution after the reflux and the mixture then poured slowly into 1.75 L of boiling water. As the solution was added, the sulfonated polystyrene precipitates rapidly as a white, fluffy solid. After filtering in air, the precipitate was washed with water several times and dried in an oven at 40°C overnight. Typically the synthesis, as outlined above, yields ca. 50 g of 10% sulfonated PS (SPS) from 52 g of polystyrene (89% isolated yield). The level of sulfonation was characterised using C, H, N, S elemental analysis.

Ink preparation and draw down

0.25 g of the SPS were weighed into a sample vial and dissolved in 2 g of acetone. To this solution were then added 0.25 g of glycerol and, for a standard ink, 0.1 g of nanorutile TiO₂. The solution was stirred until all of the photocatalyst had dispersed throughout the ink, typically 15 min. Once complete, 2.5 mg of Methylene Blue were added and the ink, placed in a stoppered bottle, was stirred for 3 hours to ensure all the Methylene Blue had dissolved. The composition of this typical, acetone-based, oxygen indicating film MB/SPS/TiO₂/glycerol film can be summarised as follows: 1/100/40/100 pphr where pphr = parts per hundred resin (where the resin is the SPS). The resulting blue ink is very stable and can be used for at least 6 months without showing any signs of deterioration.

A doctor-blade technique was used to cast the MB/SPS/TiO₂/glycerol ink onto a plastic film, typically polypropylene (Goodfellow, 75 µm) using a K-bar no. 4 to produce an ink film which was ca. 5-7 µm thick when dry. The resulting blue, dry ink film on the plastic substrate showed good adherence and was stable for more than 6 months under ambient, dark conditions.

5.3 RESULTS AND DISCUSSION

5.3.1 Photo-Activation Step (Step 1)

A typical MB/SPS/TiO₂/glycerol film is first activated, *i.e.* photobleached, by exposing it to ultraviolet light, which took less than 30 s when using a 2 × 8 W UVA lamp (irradiance 4.5 mW cm⁻²). The change in the UV/Vis absorption spectrum of the film as a function of irradiation time was monitored by UV/Vis spectrophotometer and **Figure 5.2** shows the results of this work.

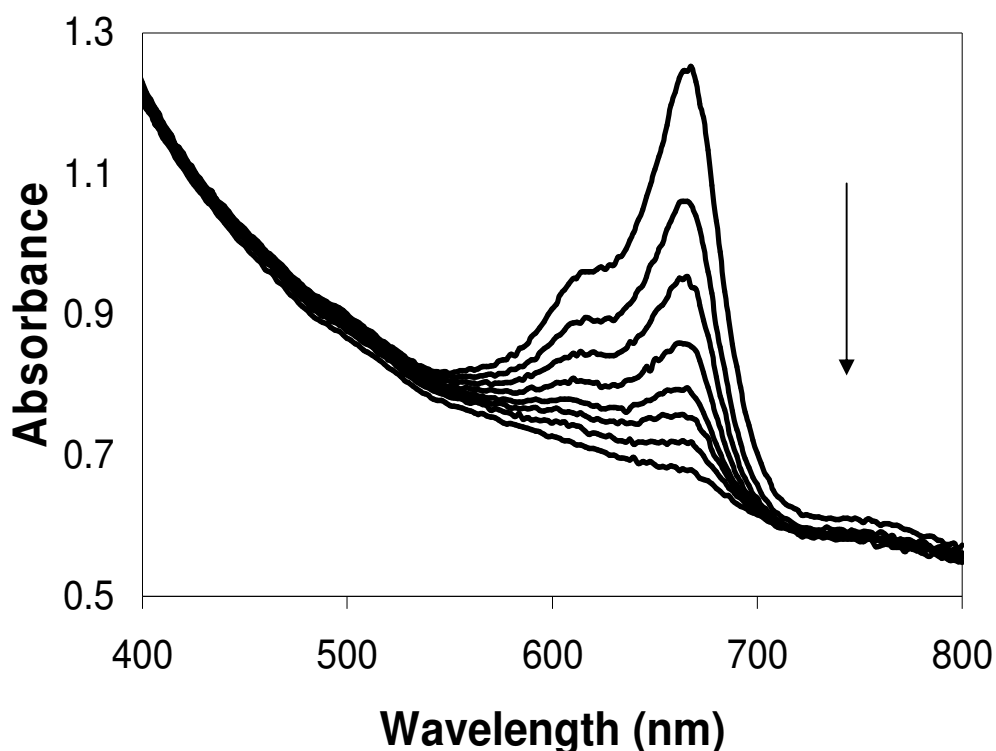


Figure 5.2 Plot of UV/Vis spectra of a typical MB/SPS/TiO₂/glycerol oxygen-indicating film before and during the UVA light activation (60 sec of UVA/7 mW cm⁻²) step (step (1), **Figure 5.4**). The irradiation times are (from top to bottom): 0, 2, 4, 6, 8, 10, 15 and 60 s respectively.

Interestingly, the UV/Vis spectrum of the original, unbleached film resembles that of the monomer of MB, with a maximum absorbance at 665 nm.⁶ In contrast, water-based inks generate films in which the MB appears largely to be in the form of its dimer ($\lambda_{\text{max}} = 605 \text{ nm}$).^{7,8} These observations are consistent with the fact, that MB shows little sign of aggregate formation in non-aqueous solvents.⁹ The photographs in **Figure 5.3** show a typical film before and after UV light activation through a brass

'TiO₂' template. In the absence of UV light, the photobleached areas regained their original blue colouration slowly, but within 24 h upon exposure to air.

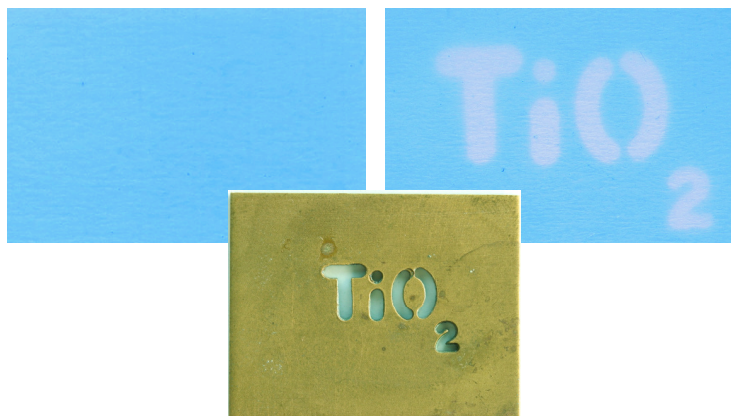


Figure 5.3 - Photographs of this film before (left) and after a brief exposure to UVA light (6.5 mW cm^{-2} for 1 minute).

Note: This very slow recovery is in striking contrast to that exhibited by its water-based counterpart (where $t_{1/2}$ for the dark recovery step is ≤ 5 min). It is not clear why LMB reacts so slowly with O₂ in a hydrophobic polymeric film. However, such a delay is useful as it then makes it possible to use it to indicate how long a package has been open *i.e.* as a 'consume-within' indicator. Such an indicator has some potential in the food packaging industry as greater attention is given to finding ways to minimise food wastage, a particular problem of which is the throwing away of food in opened packages that is still good to eat because of often not necessarily unwarranted concerns regarding freshness. A consume-within indicator would go some way to alleviate these concerns¹⁰ and reduce consumer food waste.

The time needed to fully photobleach a typical MB/SPS/TiO₂/glycerol film was < 1 min, which is ca. 3 times faster than that for a similar, water-based indicator most likely due to the latter's much reduced kinetics for step 2 in **Figure 5.4**; *i.e.* a much reduced O₂-responsivity.

Initial Photobleaching Rate (R_i) vs UVA Light Intensity (I)

The initial rate of photobleaching for a typical film was studied as a function of the incident light irradiance and **Figure 5.5** shows the absorbance at λ_{\max} versus irradiation time profiles for different UVA light irradiance.

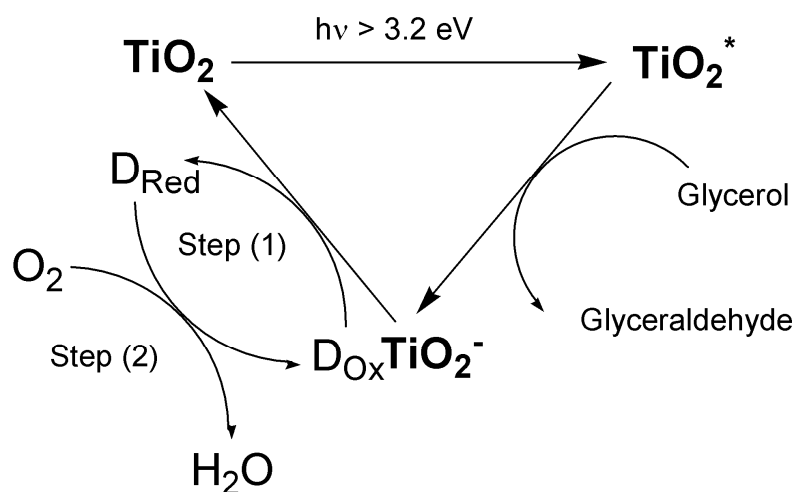


Figure 5.4 Schematic illustration of the key processes involved in the UV-activation and subsequent response towards oxygen of a TiO₂/MB/glycerol/HEC visual oxygen indicator. Step (1) refers to photo-induced reduction of the redox sensitive dye D_{Ox} (MB) to its reduced form, D_{Red}, colourless LMB, whereas step (2) illustrates the ‘dark’ back re-oxidation of the dye, leading to recovery of initial colour, by the ambient oxygen.

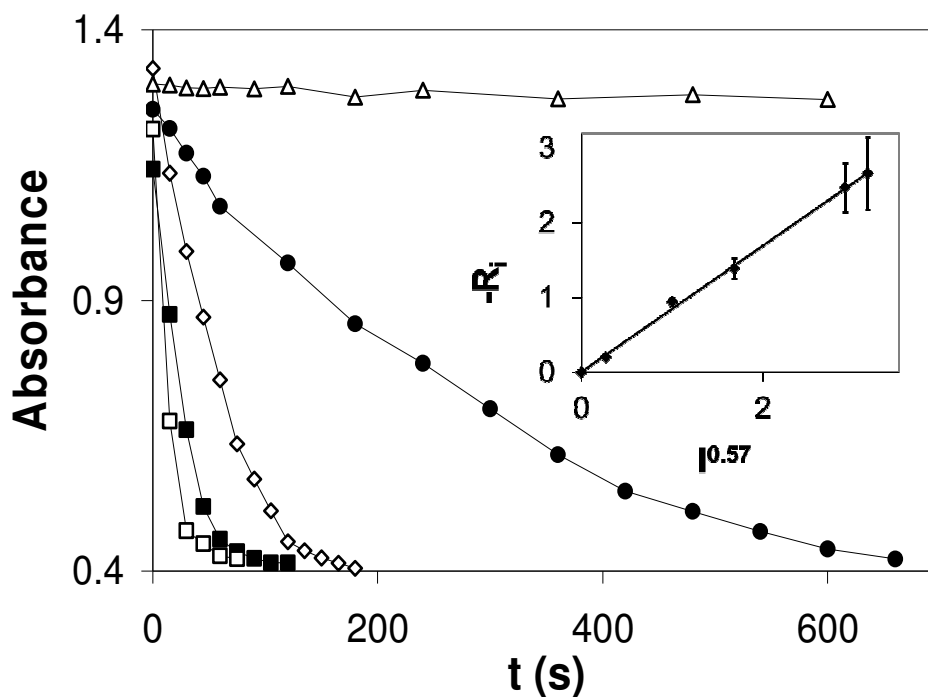


Figure 5.5 Absorbance vs. time profiles for a typical O₂ indicator film photobleaching as a function of different UVA irradiances. The irradiances used were: 0 (Δ), 0.1 (\bullet), 1.0 (\diamond), 2.5 (\blacksquare) and 6.5 (\square) mW cm⁻². The insert shows the relative initial rate dependence on the irradiance.

The plot is typical of many photocatalytic systems, in which, at low irradiances, the initial rate is found to be proportional to the irradiance, I , (indicating that electron-hole recombination is not significant) and, at high irradiancies, proportional to $I^{1/2}$ (indicating that recombination is the predominant fate of photogenerated electron-hole pairs).¹¹ Often,¹² at intermediate irradiancies, the initial rate is found to be proportional to I^Θ , where $0.5 < \Theta < 1$, and the results of this work is an example of such a case, with $\Theta = 0.57$, as indicated by the insert plot of the data in **Figure 5.5**. For a modest irradiance ($I = 6.5$ mW cm⁻²) the quantum efficiency of the photobleaching process was calculated to be 2.9%, based on an initial rate of photobleaching at 665 nm of 4.8 absorbance units/min, an assumed molar absorptivity for MB¹³ of 84,300 M⁻¹ cm⁻¹ and a film thickness of ca. 5.0 μ m.

Initial Photobleaching Rate (R_i) vs Concentration of Photocatalyst [TiO_2]

A study was carried out on the effect of semiconductor photocatalyst concentration in the MB/SPS/ TiO_2 /glycerol indicator on the rate of film photobleaching, using a series of inks prepared with the following TiO_2 contents: 0, 10, 18, 25, 50 and 100% of the typical value used, which was 40 pphr. The results of this work are illustrated in **Figure 5.6** and revealed the initial photobleaching rate to be directly proportional to the amount of TiO_2 , which, again, is quite typical of many photocatalytic systems

14

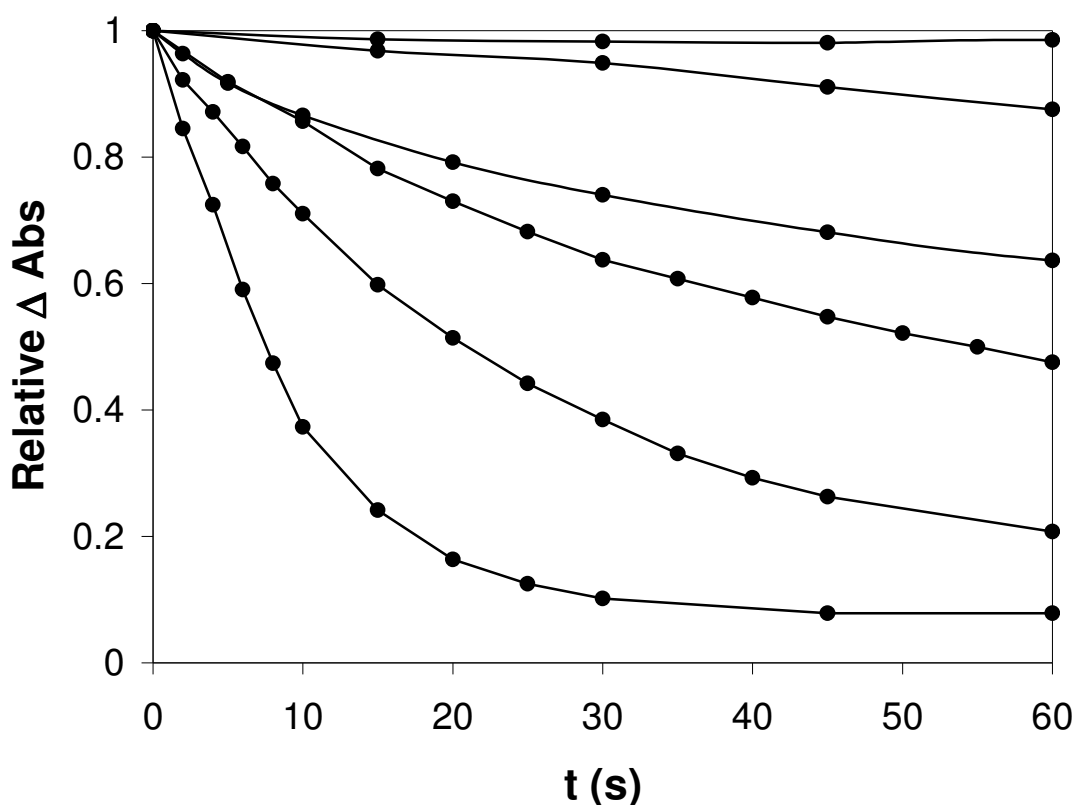


Figure 5.6 Relative change in absorbance, ΔAbs , vs. time of UVA photobleaching of a MB/SPS/ TiO_2 /glycerol film as a function of TiO_2 concentration in the film. The data lines refer to 0, 10, 18, 25, 50 and 100 % (top to bottom) of the typical pphr value of TiO_2 (40 pphr) used in the O_2 indicator formulation. The data in this chart were recorded with maximum error that was less than 10%.

The relative Δ Absorbance was calculated via:

$$rel\Delta Abs = \frac{(Abs_{\lambda_{max}} - Abs_{\lambda_{800nm}})_t}{(Abs_{\lambda_{max}} - Abs_{\lambda_{800nm}})_{t=0}} \quad (5.1)$$

Initial Photobleaching Rate (R_i) vs Concentration of SED [Glycerol]

The effect of the variation of the concentration of the sacrificial electron donor, glycerol, used in the MB/SPS/TiO₂/glycerol was also investigated. From the results of this work it was apparent (from the film's initial absorbance, ΔAbs , at λ_{max} (MB) = 665 nm) that the function of glycerol wasn't just as a source of electrons but also as an aid to dye dissolution; *i.e.* $\Delta Abs_{t=0}$ decreased with decreasing [glycerol] even though the amount of dye used to formulate the ink was the same. Indeed, if no glycerol was used, the film was barely blue and no dye-photobleaching (*i.e.* step 1 in **Figure 5.4**) could be observed! At the high glycerol level (100 pphr) used in this work for a typical MB/SPS/TiO₂/glycerol indicator, most of MB appeared to be dissolved, since further additions of glycerol had no effect on the initial absorbance of the film.

Initial Photobleaching Rate (R_i) vs Concentration of Methylene Blue [MB]

Finally the effect on rate of the concentration of methylene blue, [MB] used in the film formulation on the kinetics of the photobleaching step was also studied and the results are illustrated in **Figure 5.7**. This work shows the usual feature of saturation kinetics, common to studies of photocatalytic systems and referred to as 'Langmuir-Hinshelwood' type kinetics. When applied to this work, the relevant kinetic expression is as follows:

$$r(MB) = k(K[MB]/(1+K[MB])) \quad (5.2)$$

Where, $r(\text{MB})$ is the initial rate of photo-catalysed bleaching of MB by glycerol and k and K are the maximum rate and the ‘apparent’ dark Langmuir adsorption isotherm. Unlike its heterogeneous, dark catalysis counterpart, in most photocatalytic systems, it appears that not only is K not the dark Langmuir adsorption isotherm (which is usually much smaller) but also both k and K are light intensity dependent.

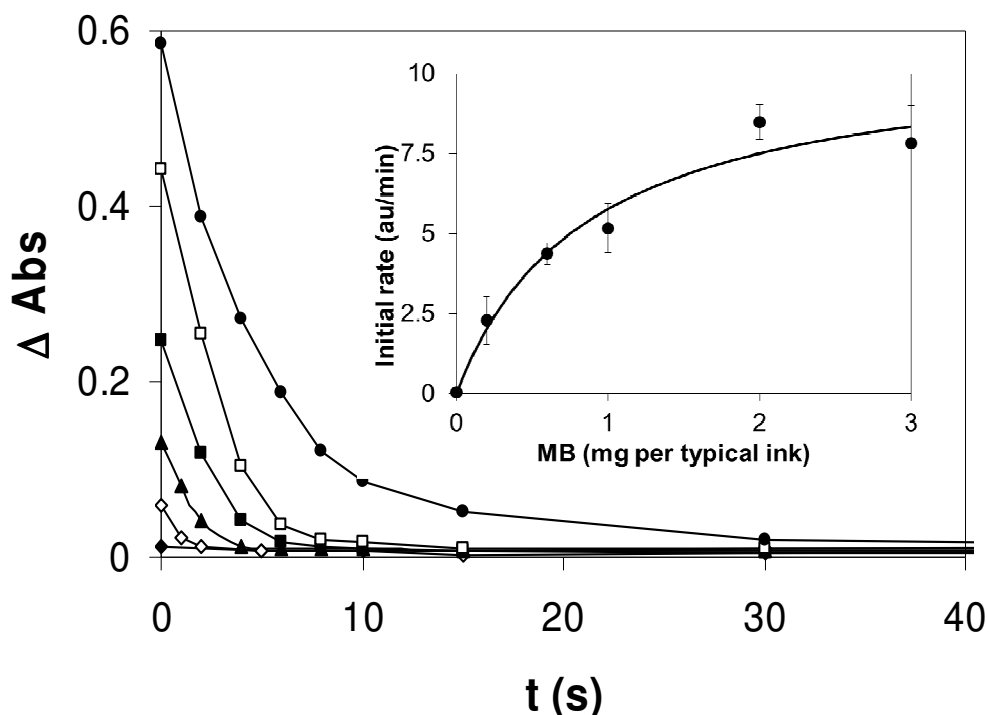


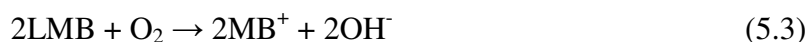
Figure 5.7 Plot of ΔAbs vs. the time of irradiation for a typical O_2 indicator film containing different pphr of MB. The covering range: 0 (\blacklozenge), 0.2 (\diamond), 0.6 (\blacktriangle), 1 (\blacksquare), 2 (\square) and 3 (\bullet) mg of MB. The insert diagram is a subsequent plot of the data in the form of initial rate (r_i) vs. $[\text{MB}]$. The data were obtained with maximum error less than 10%.

Various kinetic models have been promoted (Eley-Rideal) to explain these kinetics features, but the kinetics are complex and the area remains controversial.¹⁵⁻¹⁸ As a consequence, it is appropriate here just to note that, like most photocatalytic systems, the kinetics fit a ‘Langmuir-Hinshelwood’ type expression, eqn (5.2). An analysis of the data illustrated in the insert diagram in **Figure 5.7** revealed values of 6.2 au min^{-1} and 1.4 mg^{-1} for k and K , respectively, for the line of best fit to the data according equation 5.2.

5.3.2 Dark Recovery Step (step 2)

As noted earlier, what is most striking about the MB/SPS/TiO₂/glycerol colorimetric O₂ indicator reported here, is the very slow (ca. 24 h) dark recovery step (step 2 in **Figure 5.4**), which, in contrast, takes only a few minutes in a water-based version of the ink, as illustrated by the recovery data in **Figure 5.8**.

In order to gain a better understanding of the cause of this slow recovery step (step (2)), two 10⁻⁵ M Methylene Blue solutions were prepared using, respectively, water and acetonitrile as a solvent. Both solutions were purged with nitrogen for 10 minutes and zinc amalgam (0.5 g into 100 mL of the MB solution) added to reduce the MB to LMB. After the amalgam was filtered off, the recoveries, due to reaction (equation 5.3), of the original colours of these two solutions were monitored in a spectrophotometer in an open, vigorously-stirred, UV/Vis spectrophotometer cell. The rate of recovery in water was found to be 15 times faster than the one for acetonitrile. This slower recovery in acetonitrile is even more remarkable given that the molar solubility of oxygen is ca. 9 times higher in acetonitrile than in water!¹⁹ The key reaction associated with this dark, recovery-of-colour reaction is as follows:



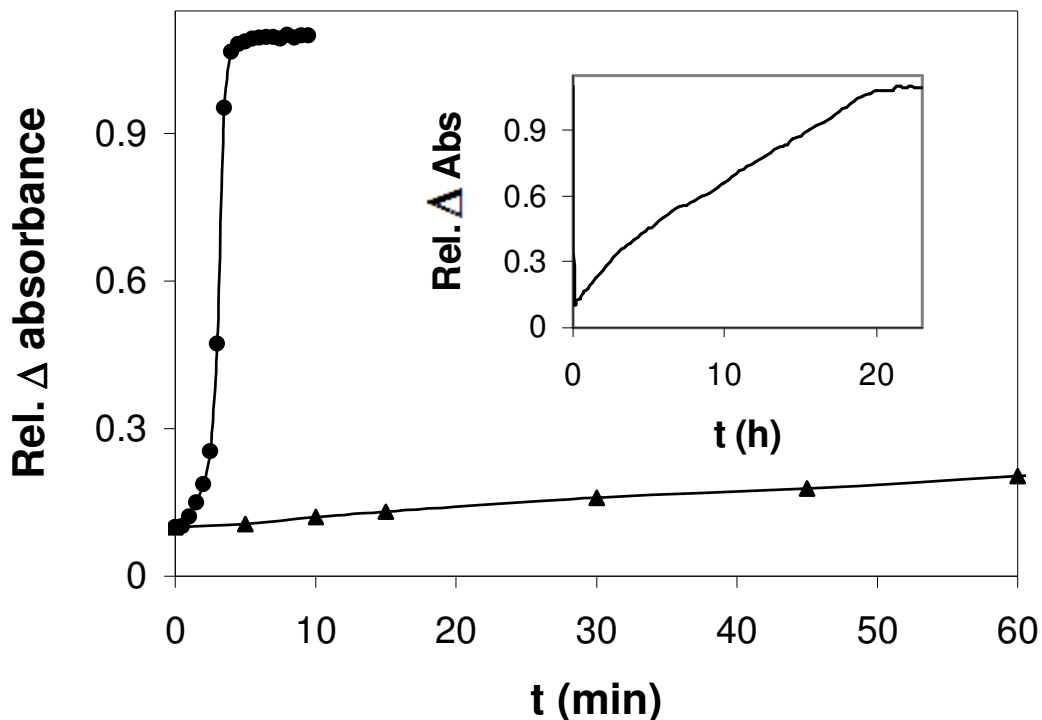


Figure 5.8 A comparison of the recovery (step (2), **Figure 1.5**) kinetics exhibited by two different MB-based oxygen indicators, namely, an aqueous-based P25 (●) and the novel acetone-based nanorutile; which recovers in ca. 24 hours (▲) as shown in the inserted plot. The maximum error in this chart was less than 10%.

Thus, the neutral *leuco*-Methylene Blue is oxidized by oxygen to form the original cationic, oxidised form of the dye, MB^+ and OH^- , both of which are charged species. The results of the above work in films and solutions indicates that the kinetics of reaction (2) are much slower in a less hydrophilic medium (such as that of an ink film or in acetonitrile), rather than in an aqueous solution or a water-based ink film, presumably because the reaction products are much less stable, and so more difficult to form, in such an environment.

This slow recovery feature opens up new potential uses for this indicator, such as the ‘consume-within’ indicator, mentioned earlier, which would be useful to the food industry. It also enhances their potential utilisation in MAP, since there would be less need for maintaining an O_2 free atmosphere during the UV-activation step.

The kinetics of the dark recovery step (2) appear insensitive to variations in [glycerol], $[TiO_2]$ and $[MB]$ as expected given the nature of reaction in equation 5.3.

However, unlike water-based O₂ inks, the recovery of its original blue colour was found to be significantly dependent upon the relative humidity in the ambient gas phase, as illustrated by the results in **Figure 5.9**.

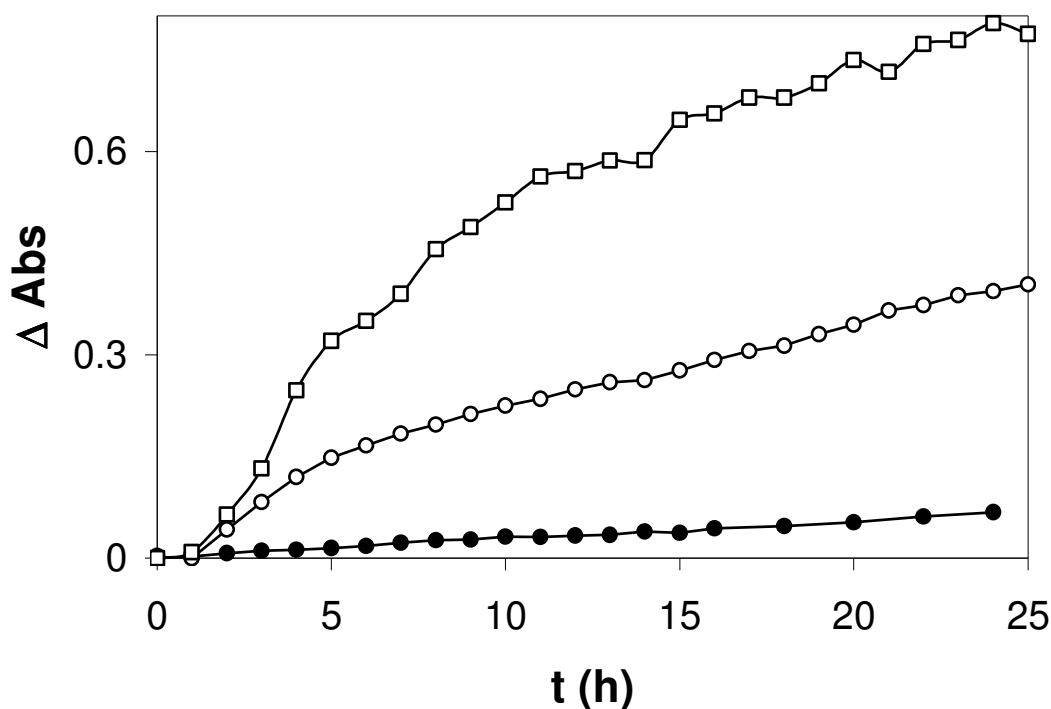


Figure 5.9 Plot of the relative absorbance of a typical, photobleached indicator vs. time of recovery, in air at 20 °C, as a function of relative humidity (RH). In this work the humidity was maintained at: 18, 57 and 96% RH (at 20 °C), respectively (bottom to top). The maximum error in the humidity reading was 10%.

As well as acting as the SED in the film, and helping solubilise the dye, it is believed that glycerol acts as a plasticizer by improving gas-diffusion within the film. Thus, the observed increase in dark step recovery time with decreasing RH is possibly due, in part at least, to the improved plasticizing action of the glycerol due to the latter's hygroscopic nature and tendency to become less viscous, and so, more permeable, with increasing RH. However, the increased level of water in the film, due to an increase in RH, could also be responsible for the observed increase in the kinetics of reaction (Equation 5.2) due to an increase in water content in the encapsulating medium. Interestingly, further work showed that the film exhibited no or little recovery at RH < 20% (over 24 h) at 20°C and this feature opens up the possibility of using the solvent-based indicator as an indirect detector of water vapour for RH values > 20% (at 20°C).

Additional work showed that the rate of the dark film recovery step (in step (2), in **Figure 5.4**) is proportional to the %O₂ in the ambient gas phase. Thus, in a series of experiments, nitrogen and oxygen gas were blended and the resulting mixtures, saturated with water vapour. These were then flowed over a typical, photobleached O₂ indicator and their recoveries monitored spectrophotometrically. A plot of the initial rate of recovery against oxygen concentration revealed a linear dependence as indicated by the results in **Figure 5.10** and suggested by reaction (equation 5.3).

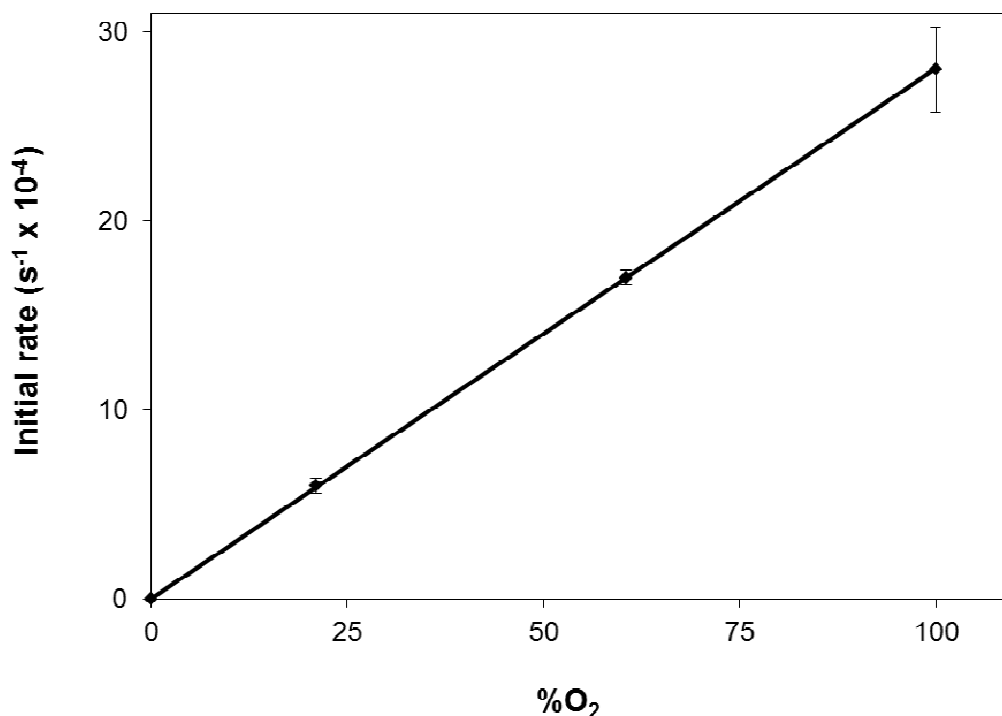


Figure 5.10 Plot of initial rate of recovery of a typical photobleached film vs. concentration of oxygen in 100% RH blends of oxygen and nitrogen gas.

5.3.3 O₂ Inks in an Aqueous Media

A significant advantage of the solvent-based O₂ indicator is its striking stability in water. As shown in **Figure 5.11**, when a *solvent-based* and an *aqueous-based* oxygen indicating film is immersed in water, the dye in the *aqueous-based* indicator leaches out very rapidly, whereas the ion-paired MB in the MB/SPS/TiO₂/glycerol film remains contained in the film indefinitely.

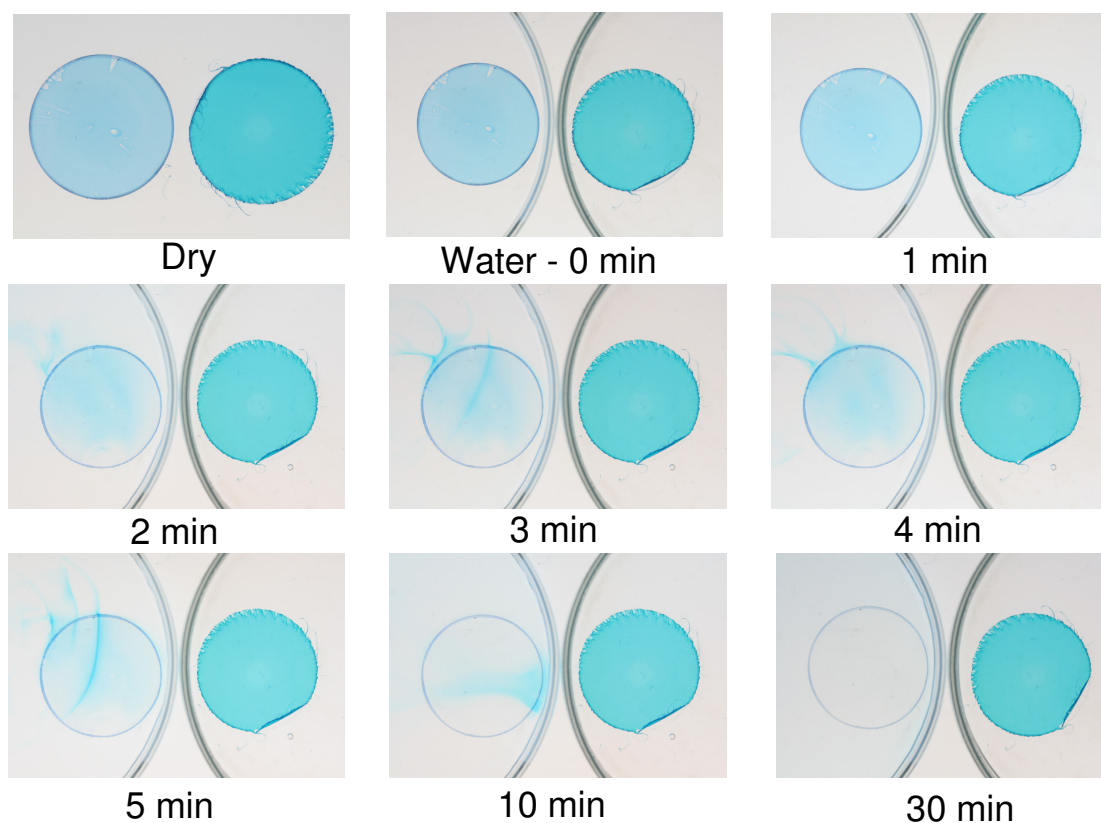


Figure 5.11 The first picture (Dry) shows two films cast to test for leaching in still water; on the left is a typical water-based ink of 100/100/5/20 in HEC and on the right is the solvent-based ink of 100/100/1/40 in SPS. Both films were placed in a petri dish filled with still water and timed. The water-based ink lasts just over minute before significant leaching begins to occur and after 30 minutes the film has all but disappeared. The solvent-based ink on the other hand has remained fast throughout.

The water-proof nature of the solvent-based oxygen indicator was further tested under water. In this experiment, the film was first bleached and then put in a cell filled with water, purged with N_2/O_2 mixtures of different oxygen content, and the recovery monitored with a UV/Vis spectrophotometer. It was found that the recovery in water was about 5 times faster than in 100% RH (at 20°C) ($t_{1/2} = 1.5$ h compared to ca. 8 h) and dependent directly upon the dissolved oxygen concentration. Thus, a final further potential application of this solvent-based O_2 indicator is in the measurement of dissolved levels of oxygen in water. A simple illustration of the film's response to dissolved oxygen is shown in **Figure 5.12**. In this experiment an activated (2 mins of UVA, $I = 7.2 \text{ mW cm}^{-2}$) film of the solvent-based ink was placed in a petri dish filled with still water and timed.

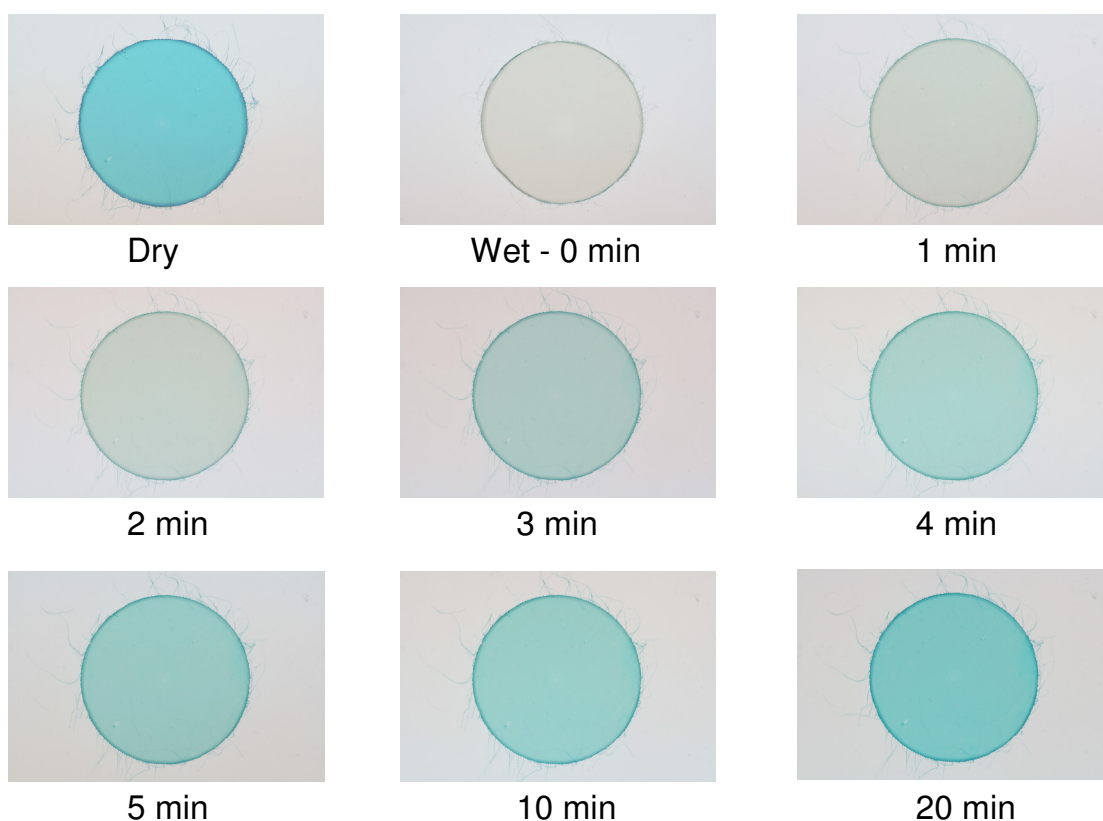


Figure 5.12 Showing the recovery of a typical solvent-based indicator ink film under still water. The first picture (top left) is of a dry film before bleaching (2 mins of UVA, $I = 7.2 \text{ mW cm}^{-2}$) and immersion in the still water (second picture, ‘Wet – 0 min’). The following pictures were taken at the times indicated.

Interestingly, the films were found to photobleach with UVA under water as well. The reliability of the film to photobleaching is reduced however because glycerol, as the only water soluble component of the ink, is able to leach out thereby reducing the ability of the film to photobleach.

5.3.4 O₂ Inks in a Freezer

Another valuable feature of the solvent-based ink is its consistent response regardless of the temperature it has been stored in. This was tested by an experiment in which a solvent-based film was cut into 8 samples which were all bleached (2 mins of UVA, $I = 7.2 \text{ mW cm}^{-2}$) and placed in a freezer (-18 °C). Over seven days, one sample at a time was removed and monitored for colour changes. So, for example, ‘Sample 3’

was removed from the freezer on day 3 ('3d', horizontal axis) and its response monitored over the remaining 4 days.

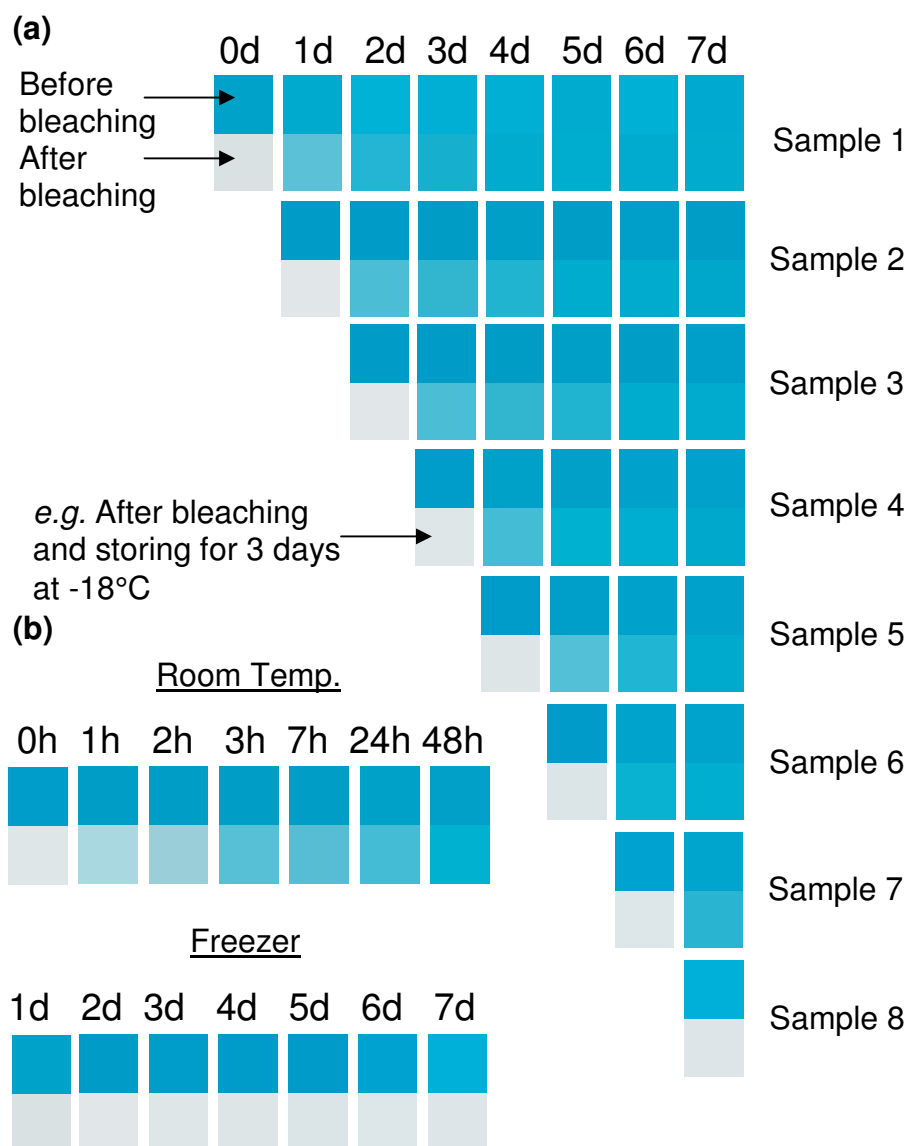


Figure 5.13(a) Shows the response of 7 samples to freezing conditions (-18 °C). Each sample was removed from the freezer on successive days over seven days. So, for example, 'Sample 3' was removed from the freezer on day 3 ('3d', horizontal axis) and its response monitored over the remaining 4 days. **(b)** Shows the response of two control samples, one in a freezer and the other at room temperature.

Some additional work using a TiO₂ catalyst coated with platinum metal particles (precipitation deposition using a platinum colloid according to method by Mills *et al.*²⁰) reduces the response time of the ink to oxygen and is a further way of tuning the film response.

5.3.5 O₂ Inks Detect H₂O₂

A further potential use of these films may be as peroxide/strong oxidiser sensors and pictures of an experiment comparing it with a dye-based optical peroxide sensor are shown in **Figure 5.14(a)** and **(b)**. In this work the response to hydrogen peroxide vapour (6%) of a typical MB/SPS/TiO₂/glycerol oxygen-indicating film was compared to a Lissamine Green (LG)/polyvinyl alcohol (PVA) film²¹.

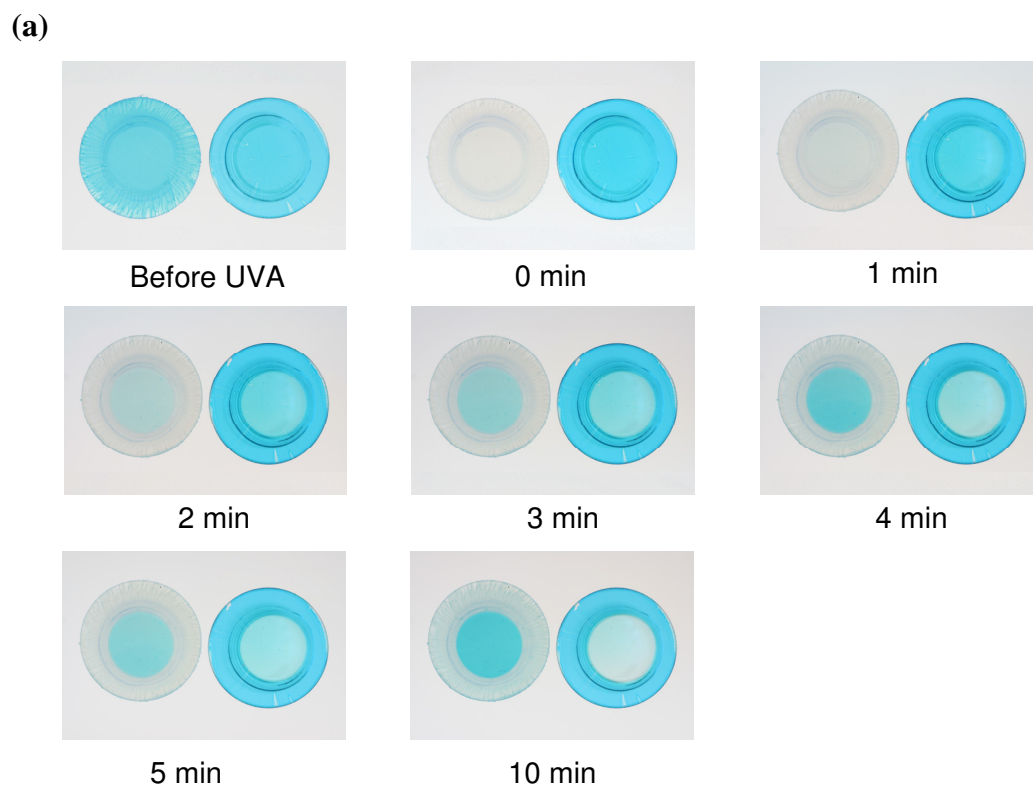


Figure 5.14(a) MB SPS-based indicator (RHS) recovery in H₂O₂ vapours in comparison to Lissamine Green base indicator (LHS) (time of H₂O₂ vapour exposure, 6% H₂O₂ at RT).

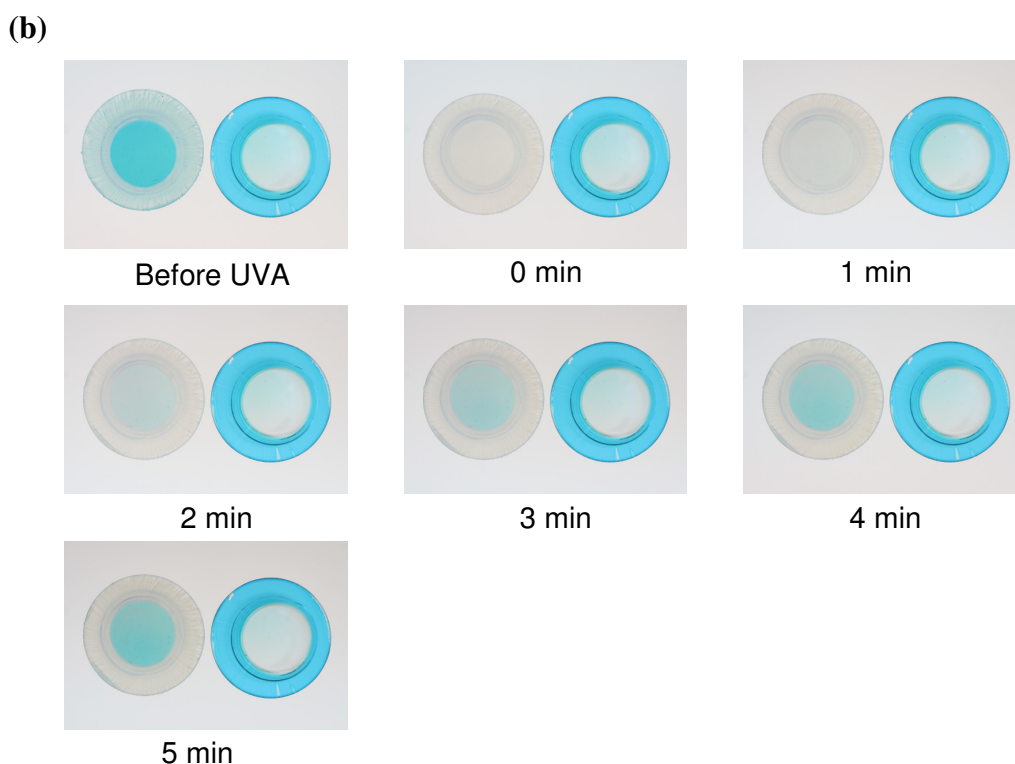


Figure 5.14(b) Shows that the same MB/SPS/TiO₂/glycerol oxygen-indicating ink film (also shown in **Figure 5.14(a)**) can be reactivated with UVA light and re-used, whereas the Lissamine Green film can not.

The above results show the MB-SPS indicator, once activated with UV light, can be used to detect H₂O₂ vapour repeatedly, whereas a LG-PVA film can only be used once.

5.4 CONCLUSION

A novel, solvent-based, water-proof oxygen indicator that coats on hydrophobic polymers, such as polypropylene, was prepared and characterised. The coloured indicator is readily photobleached but has a slow (24 h) recovery. The kinetics of the latter process are independent of [glycerol], [TiO₂] and [MB], but dependent upon RH above a value ca. of 20% at 20°C; the photobleached film does not recover its original colour below this value over a 24 h period. The very slow recovery process makes it possible to use the indicator as a ‘consume-within’ or humidity threshold indicator. This indicator system is currently undergoing trials as a time-temperature indicator for food packaging in the UK by Insignia Ink. This work was done in collaboration with Katherine Lawrie.²²

5.5 REFERENCES

1. A. F. Turbak, *Ind. Eng. Chem. Prod. Res. Dev.*, 1962, **1**, 275.
2. F. Kucera, *Chem. Pap.*, 1996, **50**, 224.
3. R. A. Weiss, S. R. Turner and R. D. Lundberg, *J. Polym. Sci.*, 1985, **23**, 525-533.
4. *IPN 3,870,841 Pat.*, 1975.
5. C. R. Martins, G. Ruggeri and M. D. Paoli, *J. Braz. Chem. Soc.*, 2003, **14**, 797-802.
6. Z. Zhao and E. R. Malonowski, *Appl. Spectrosc.*, 1999, **53**, 1567.
7. A. Mills and D. Hazafy, *Analyst*, 2008, **133**, 213-218.
8. E. Braswell, *J. Phys. Chem.*, 1968, **72**, 2477-2483.
9. G. N. Lewis, O. Goldschmid, T. T. Magel and J. Bigeleisen, *J. Am. Chem. Soc.*, 1943, **65**, 1150.
10. A. Mills, *Chem. Soc. Rev.*, 2005, **34**, 1003-1011.
11. A. Mills and S. Le Hunte, *J. Photochem. Photobiol. A: Chem*, 1997, **108**, 1.
12. J. M. Hermann, *Top. Catal.*, 2005, **34**, 49.
13. F. A. Ozdemir, B. Demirata and R. Apak, *J. Appl. Polym. Sci.*, 2009, **112**, 3442.
14. A. Mills, K. Lawrie and M. McFarlane, *Photochem. Photobiol. Sci.*, 2009, **8**, 421-425.
15. C. S. Turchi and D. F. Ollis, *J. Catal.*, 1990, **122**, 178.
16. D. F. Ollis, *J. Phys. Chem. B*, 2005, **109**, 2439-2444.
17. D. Monllor-Satoca, R. Gómez, M. González-Hidalgo and P. Salvador, *Catal. Today*, 2007, **129**, 247-255.
18. A. V. Emeline, G. V. Kataeva, A. V. Panasuk, V. K. Ryabchuk, N. V. Sheremetyeva and N. Serpone, *J. Phys. Chem. B*, 2005, **109**, 5175-5185.
19. M. Alvaro, *Chem. Phys. Lett.*, 2002, **362**, 435.
20. A. Mills, *J. Chem. Soc., Chem. Commun.*, 1982, 367-368.
21. A. Mills, P. Grosshans and E. Snadden, *Sensor Actuat. B-Chem.*, 2009, **139**, 458-463.
22. A. Mills, D. Hazafy and K. Lawrie, *Catal. Today*, 2011, **161**, 59-63.

CHAPTER 6

**TEMPERATURE ACTIVATED HUMIDITY
SENSORS**

6.1 INTRODUCTION

Humidity sensors are used extensively in industry as well as for environmental monitoring. Their widespread applications cover a broad range of domestic, medical and industrial applications. For example, in food packaging, excess moisture in meat packaging can accelerate food spoilage, and as a consequence desiccants are often included in packaging to extend the shelf life.¹ At low relative humidities (RHs) some dry grain products can undergo rapid free radical oxidation and become rancid.¹ Most fruit and vegetables are composed largely of water, consequently their optimum storage conditions are typically 90–95% RH, $T = 0\text{ }^{\circ}\text{C}$,² whereas products such as sugar and raisins lose their desirable texture if the RH is this high. Thus, most food stuffs require a degree of moisture management and humidity measurement to obtain optimum relative humidity (RH) conditions.¹ Humidity control is also important for the preservation of artefacts such as books and paintings and to prevent bacterial and mould growth in certain manufactured products. Another application is in the packaging and transportation of sensitive electrical appliances/components which are adversely affected by high relative humidity and therefore require accurate monitoring to ensure efficient functionality.³

There are a wide range of commercial products currently available for monitoring relative humidity. These are, more often than not, electronic hygrometers based on capacitive or resistive systems which measure the change in conductivity of a polymer or ceramic film as a function of relative humidity.⁴ Such devices have limitations in their operating conditions and can be expensive and bulky to use.^{5, 6} There have been a number of proposed colorimetric relative humidity indicators, the majority of which are based on the use of inorganic salts⁷⁻¹⁷ such as cobalt(II) chloride, CoCl_2 , which at a defined RH level (typically RH 40%) converts from its anhydrous form to its hydrated form, which is usually marked by a colour change, in the case of CoCl_2 , blue (anhydrous) to pink (hydrated). The sensitivity of this type of indicator can be tailored to the desired application by one of three methods: changing the concentration of the inorganic salt,¹⁸ adding a deliquescent synergic salt¹⁹⁻²¹ or, for systems with a silica support, altering the drying and activation temperatures of the CoCl_2 -doped silica.⁷ Such relative-humidity indicators have been proposed for a

variety of applications including: refrigerated systems,^{12, 13} clothes dryers,¹⁴ shoe storage,¹⁶ desiccant absorbent capacity indicators,^{18, 20, 21} electronic device storage¹⁷ and are often reversed by heating the hydrated salt to regenerate the anhydrous starting material. A typical commercial form, based on CoCl_2 , is the Humitector[®] Humidity Indicator Card (Süd-Chemie Inc., USA).²²

Recently, Matsushima and co-workers have proposed using thiazine and flavylum salts in gels as simple colorimetric humidity and temperature sensors.²³⁻²⁵ These salts exhibit reversible colour changes from blue (dry) to purple (humid), as a result of a change in relative humidity. This has been attributed to the absorption of water vapour by the gel in humid conditions which encourages the dye to form dimers and so leads to a shift in λ_{max} absorbance (ca. $\Delta\lambda = -10-20$ nm) to a lower wavelength (hypsochromic/blue shift). Otsuki *et al.*²⁶ showed that films of PVP containing Rhodamine 6G or Methylene Blue change colour (ca. $\Delta\lambda = -60$ nm) when exposed to air streams of varying relative humidity. An example of this change²⁶ for Methylene Blue can be seen in **Figure 6.1** below.

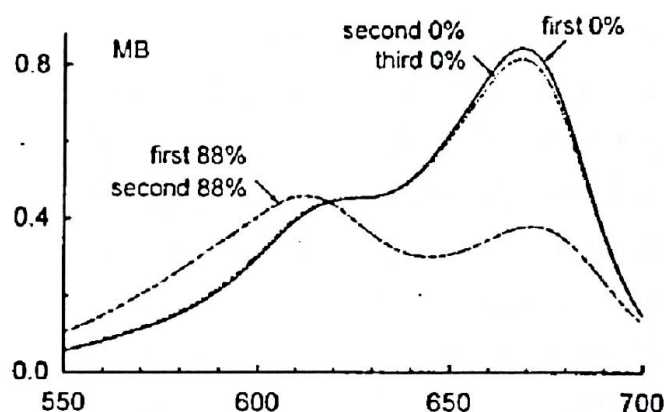


Figure 6.1 - Absorption spectra of MB ($0.0215 \text{ mol kg}^{-1}$) in PVP film at 0 and 88% relative humidity (from Otsuki *et al.*²⁶) spectra indicated 'first' 'second' etc. are from repeat exposures to different humidities.

The authors state that a change in the polarity of the polymer film with humidity is not the only reason for induced dye aggregation but also due to the formation of clusters of water in the film (at high relative humidity) which then attract and accumulate the dye molecules in them causing the formation of the aggregates. Maybe how reasonable this interpretation is given λ_{max} of monomer, dimer and trimer of MB are 665, 605 and 578 nm.²⁷

Recently, we have found two similar dye-encapsulating polymer humidity sensitive systems, both using Methylene Blue (MB) as the dye component and a cellulose derivative as the encapsulating medium. In the first one, the MB was encapsulated within hydroxyethyl cellulose (HEC) and added significant amount of urea, (ca. 20 times w/w more than MB), the product ink is blue, but casts as a thin, opaque pink film, under ambient (RH = 60%, T = 20 °C) or dry conditions, and rapidly and reversibly is rendered blue coloured and clear when exposed to RH values >85%. Note that the observed colour changes for these MB/urea/HEC films are the opposite of those observed by Matsushima *et al.*²³⁻²⁵ for their MB/gel films so the explanation for the effect must necessarily be different. It is also unusual to find a relative-humidity indicator which gives such a sharp, reversible colour change at high relative humidities.

The second humidity responding indicator, which is reported here, used ethanol-soluble, hydroxypropyl cellulose (HPC) as the polymer together with Methylene Blue. Surprisingly, this simple combination formed a reversible colorimetric humidity indicator which casts as a blue film in its dry form and turns purple upon exposure to humid air (RH > 40%). Thus, unlike the above, MB/urea/HEC system, the colour change exhibited by the MB/HPC film followed the observation of Matsushima *et al.* *i.e.* blue dry film to purple/red wet film. Compared to their findings the hypsochromic blue shift ($\Delta\lambda = -100$ nm) was notably higher in our system (as low as 505 nm) suggesting that the observed colour change can not be explained simply by the dye aggregation. Consequently, these novel and promising relative-humidity indicators are the subject of this chapter.

6.2 EXPERIMENTAL

6.2.1 Preparation of Inks

HEC/Urea Inks

A typical relative-humidity sensor was made by spin coating an ink comprising 5 mg MB, 100 mg urea in 2 g of a 5% w/v HEC aqueous solution, for 30 seconds at 3500

rpm on to a 25 mm glass disc (to give a pphr of the dry MB/urea/HEC film to be 5/100/100).

HEC and HPC Inks

A typical ink comprised 5 mg of dye (either Methylene Blue or thionine) in 2 g of a 5% w/v HEC aqueous solution or 1 g of a 10% w/v HPC ethanol solution so that cast films were the same pphr (polymer/dye 100/5 pphr). Inks were cast onto a 25 mm glass disc using a spin-coater (1000 rpm for 15 sec) to make thin transparent coloured films.

6.2.2 Measuring Relative Humidity

The digital hygrometer (HANNA, HI 9564) used in this work was itself calibrated regularly using an analogue horse-hair hygrometer (Fisher) for reference. The set-up of the apparatus is shown in **Figure 6.1**, in which dry nitrogen gas was provided from the gas cylinder (a). The gas stream was split using a simple three-way tap (b), where one way led to humidifiers which ensured the gas has 100% RH (top stream on **Figure 6.2**) and the second was dry nitrogen (bottom stream on **Fig. 6.2**). Gas flowmeters (c, d) (Cole-Parmer, 0-500 ml/min) were used to control the gas flow in each branch. Two Dreschel bottles (e, f) followed the gas flowmeter (c) to saturate the gas with water vapour. The dry-wet gas streams were then recombined at (g) before passing through the gas cell (h) with the sample (i) placed in a spectrophotometer (Varian, Cary 50). Finally, the digital hygrometer probe (j) was connected to the outlet of the gas cell (as close as possible) to measure the relative humidity of the emerging gas. The total flow rate through the apparatus was kept at 300 mL/min by adjusting flows of (c) and (d) and monitoring the flow via a digital flowmeter (l) (Agilent, ADM 1000). In any run, after setting the gasflows, the system was left to equilibrate and adopt the desired humidity for at least 5 minutes (longer times were needed for RH close to 10%) before application to the cell. The humidity was adjusted using the gas flowmeters' valves with upper limit 100% (when the gas flowmeter with dry gas (d) was closed completely) to ca. 0% (when the gas flowmeter providing the 100% RH (c) was completely closed). The outlet pressure on the gas cylinders was adjusted to 1 bar.

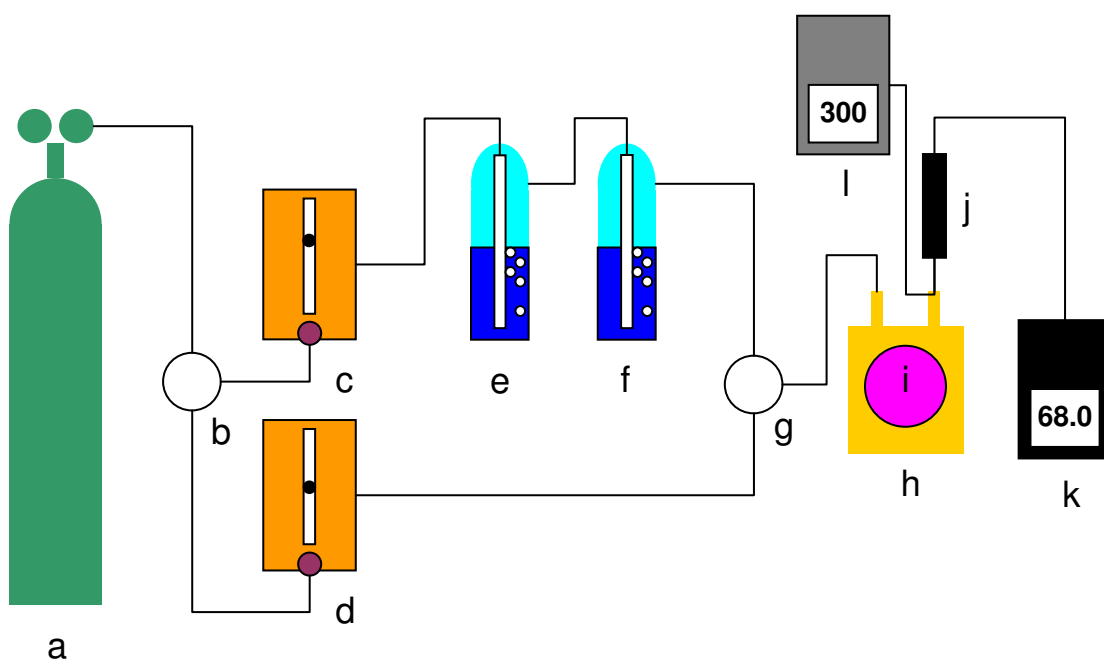


Figure 6.2 (a) Experimental set up for measuring relative humidity (RH). Description is given in the text above.

6.2.3 High Temperature UV/Vis on MB/HPC humidity indicator inks

In this work, all relative humidities were measured at 20 °C unless otherwise stated. A commercial heat gun was used to render the MB/HPC films to be more sensitive towards the humidity. Typically 3 seconds of heating to temperatures of ca. 200°C were enough to change the colour of the film (purple to blue) and remained there indefinitely. Such activated films were kept in dry environment (desiccator under vacuum).

6.2.4 UV/Vis Spectra Recording of the MB/HPC Humidity Indicator Films

All the UV/vis spectra were recorded on a Cary50 (Varian) spectrophotometer except in the temperature activation work in which case a furnace in combination with OceanOptics USB2000 fibre-optic spectrophotometer was used to monitor the

temperature vs. absorbance profile. In this work, the sample was fitted in the furnace as shown on picture in **Figure 6.3**.

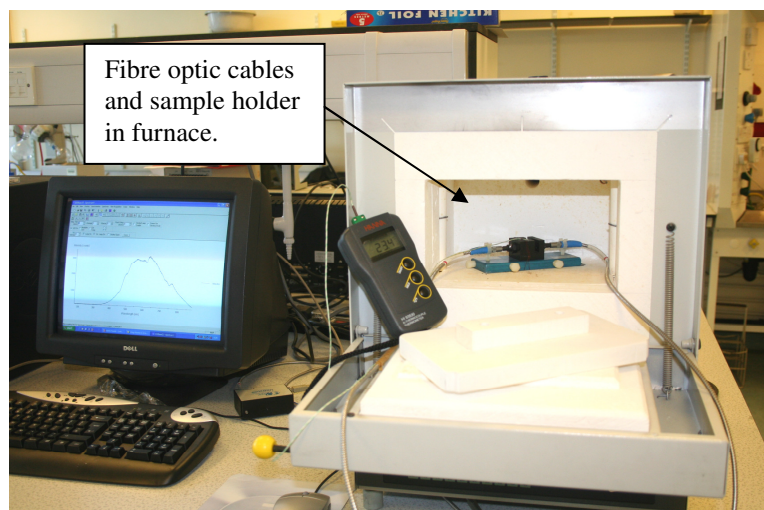


Figure 6.3 The set up used for recording the UV/vis spectra at different temperatures. The sample is fitted in the furnace and connected with the source and detector using optical fibres.

6.3 RESULTS AND DISCUSSION

6.3.1 Methylene Blue/Urea System

When solid Methylene Blue (usually dark green powder) is mixed with an excess of urea (white powder) a pale purple/pink powder is formed. The initial pink colour turns instantly blue if the powder is exposed to highly humid stream of air such as a human breath. These observations led to a formulation for the first humidity indicating system described here, namely: a Methylene Blue and urea encapsulated in hydroxyethyl cellulose (HEC).

A spin coater was used to cast a thin film of the MB/urea/HEC ink. During the spin coating process the initially blue film cast from the blue coloured ink started to turn a pink colour as the aqueous solvent began to evaporate. The final pink colour was further developed by drying the film at 70°C in an oven for a few minutes. The final product was an opaque pink film (ca. 1.7 μm thick) under ambient conditions (40–60% RH) with a λ_{max} at 570 nm, which upon exposure to high relative-humidity

conditions (>85% RH) turns rapidly blue ($\lambda_{\max} = 600$ nm) and clear as illustrated in **Figures 6.4** and **6.5**.

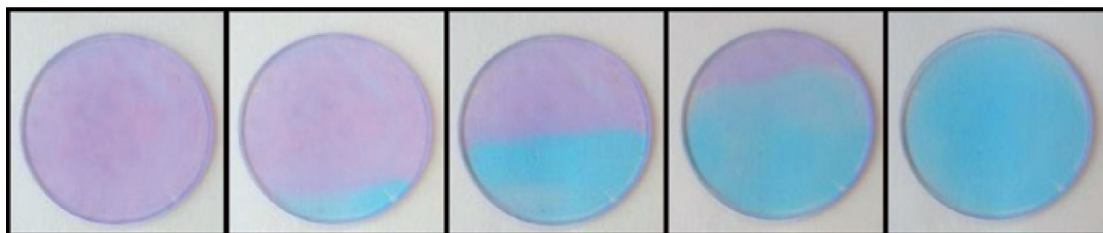


Figure 6.4 - Photographs of a typical MB/urea/HEC relative-humidity indicator changing colour from pink (left) to blue (right) upon exposure to 100% RH air, from the bottom right. The overall time of the colour change was less than 10 seconds.

This colour change process occurs rapidly (response and recovery times: 10 s and 60 s respectively) and is reversible as illustrated by the data in the inset of **Figure 6.5** which show the response and recovery of the absorbance (at λ_{\max} for blue form, 600 nm) for a typical MB/urea/HEC relative-humidity indicator film upon exposure to repeated cycles of humid (100% RH) and dry air.

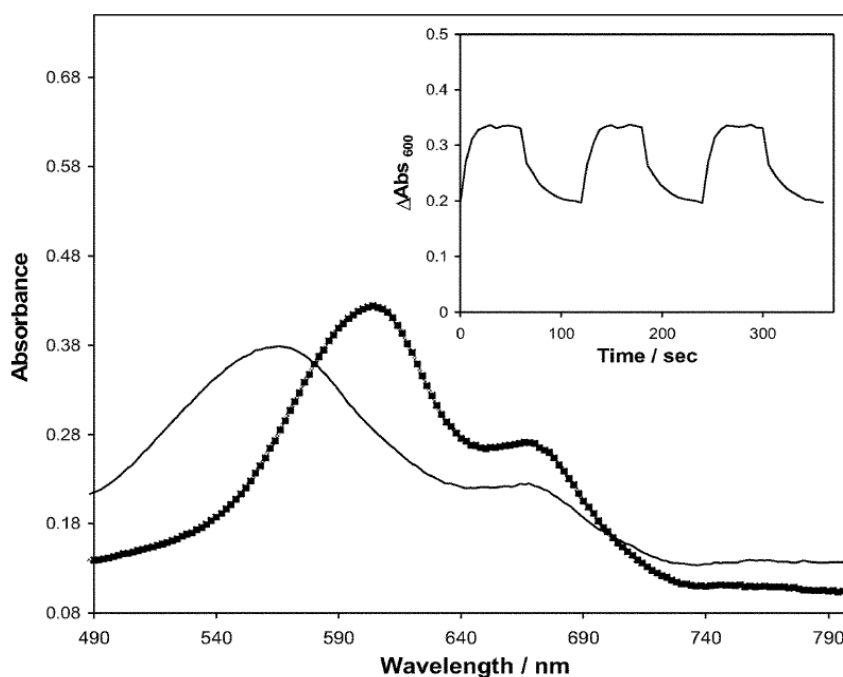


Figure 6.5 Spectral changes of a typical MB/urea/HEC relative-humidity indicator film before (—) and after (■) exposure to 100% RH air. Inset diagram is a plot of the change in absorbance MB λ_{\max} humid (600 nm) for indicator film on exposure to 3 cycles of 1 min 100%RH air and 1 min dry air. Abs_{600} recorded every 6 s. The maximum error was less than 10%.

The initial spectrum of the dry pink film (see **Figure 6.5**) is very different from that observed for the monomer ($\lambda_{\text{max}} = 665 \text{ nm}$) and dimer ($\lambda_{\text{max}} = 600 \text{ nm}$), thus, it is not instantly apparent what the colour change is due to.²⁸⁻³⁰ The absorption spectrum of the pink film ($\lambda_{\text{max}} = 570 \text{ nm}$) is, if anything, like that of the MB trimer ($\lambda_{\text{max}} = 578 \text{ nm}$).²⁷ In contrast, when exposed to high relative humidities the resulting blue film has a spectrum more characteristic of a mixture of the MB monomer and dimer. The monomer is attributed to the smaller peak at 665 nm while the larger peak at 600 nm is attributed to the MB dimer. An inspection of films containing no dye reveals a concomitant change in the optical clarity of the urea/HEC film in the absence (opaque) and presence (clear) of a stream of air containing a high (100%) RH, as illustrated in **Figure 6.6**.

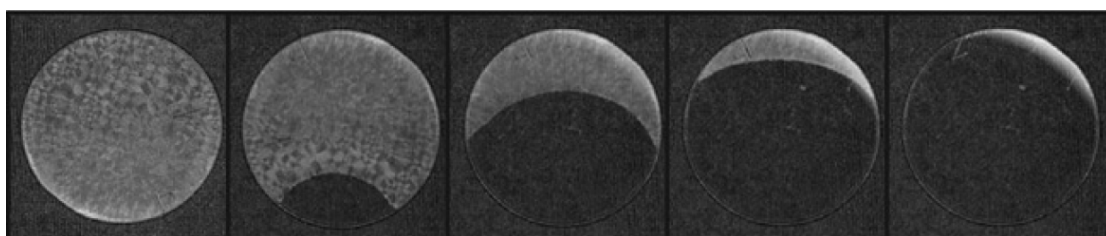


Figure 6.6 - Photographs of a urea/HEC with no dye changing from an opaque film (left) to a clear film (right) upon exposure to 100% RH air.

Further work showed that urea forms highly crystalline, optically opaque films with a characteristic XRD peak at $2\theta = 22.25^\circ$ at moderate and low RH. These crystallites rapidly dissolve when exposed to relative humidities above 85%, rendering a clear film. It is known that some salts, including urea, only begin to absorb water above some critical relative humidity (CRH), *i.e.* the relative humidity of the surrounding atmosphere (at a given temperature) at which the material begins to absorb moisture from the atmosphere and below which it will not absorb atmospheric moisture. For urea this value has been reported as 72.5% RH.³¹ The urea XRD peak reappears when the opacity change is reversed by blowing dry air over the film or placing it in oven (70 °C for few minutes). Thus, it appears that the colour change associated with the MB in the urea film (pink, dry \leftrightarrow blue, humid) is linked to the change in crystallinity of the urea when exposed to high relative humidities. Indeed a dye-free relative-humidity indicator based on optical clarity can be simply created using just

urea in a polymer, such as HEC, since **Figure 6.6** shows that such a film is opaque at medium and low (<85%) RH levels, but clear at RH values >85%; the process is entirely reversible. The polymer used, in this case HEC, does not appear to have any effect on the colour or opacity change, but merely acts as an encapsulation agent. This was confirmed by observing a similar effect in different polymers (such as poly(vinyl alcohol), PVA and poly(ethylene oxide), PEO). Also in a polymer-free environment, achieved by grinding up a sample of urea with MB (100/5 pphr), the resulting pink powder exhibits a similar reversible colour change from pink to blue when exposed to RH >85%.

The simplest explanation of the above findings is that under ambient conditions (RH < 85%) MB is encapsulated in urea crystals as the pink trimer and when exposed to high RHs the urea crystals dissolve, thereby releasing the MB into an environment in which its more stable form is primarily the blue coloured MB dimer and some monomer. In support of this, it is well known that urea is a hygroscopic compound which deliquesces under high RH conditions of >80% RH at 18 °C.³¹⁻³³ The notable features of this type of relative-humidity indicator are not only that it can be used exclusively for monitoring high (>85%) relative humidities, but it is quick to respond, highly reversible and has a good long-term stability. As it stands, such a >85% RH indicator has a potential application in ensuring the correct RH conditions for the storage and ripening of fruit,³⁴ for example. This work was done in collaboration with Pauline Grosshans.

6.3.2 HPC and HEC films of Methylene Blue

During the course of the above work it was noted that in the absence of urea, Methylene Blue in HEC films were, not unexpectedly, blue when exposed to humid air. In contrast, in hydroxypropyl cellulose (HPC), a polymer similar to HEC, but with a more rigid backbone (see **Figure 6.7** for structures), the film was largely pink and became purple/blue upon exposure to humid air. Photos of these indicator films are illustrated in **Figure 6.8**. The MB/HPC inks were therefore studied a little further. These colour changes are not too dissimilar to those observed in the MB/urea indicators, except that the colour change is apparently irreversible.

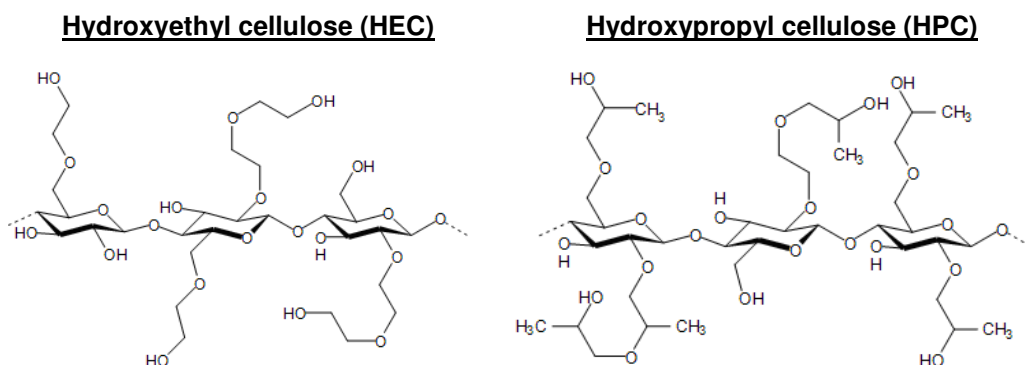


Figure 6.7 Showing the difference in structure between HEC and HPC. HPC is more rigid and therefore prone to form more structured chains than HEC.

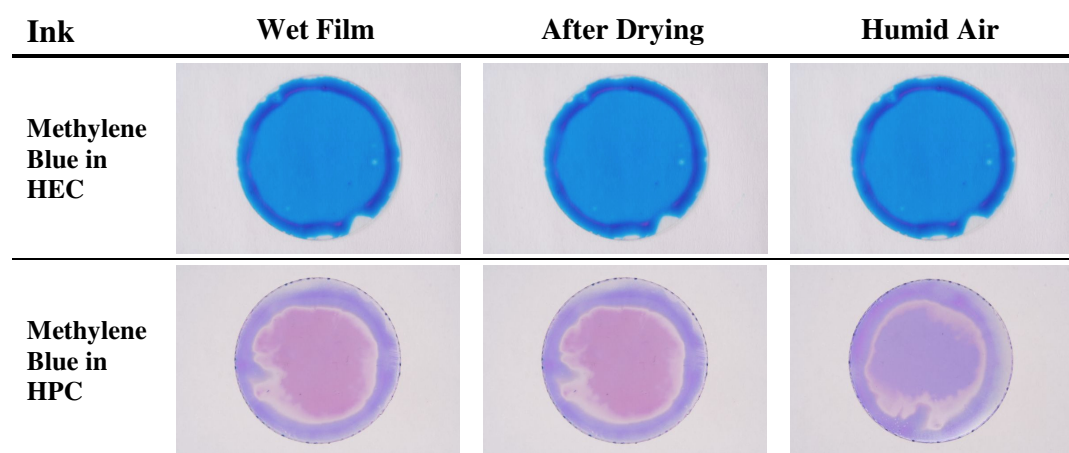


Figure 6.8 Photographs of freshly prepared MB/HEC and MB/HPC films (left); same films left to dry at room temperature (centre); and colour change induced by exposing the dried films to humidity(right).

Using a Heat Gun to Dry the Films: Thermal Activation

It was found that a freshly prepared MB/HPC film changes its colour from the original two-coloured inhomogeneous pattern illustrated in **Fig. 6.8** (bottom photos) to a uniform dark blue colour ($\lambda_{\max} = 605 \text{ nm}$) when it is exposed to high (ca. 200 °C) temperatures. It is worth noting that this temperature is close to the melting temperature of HPC (165°-220°C).^{35, 36} The pictures in **Figure 6.9** show the colour change of Methylene Blue dye HPC in response to a 3 second pulse of heat from a heat gun. No such colour change was observed in case of MB in HEC film. The final blue colour film appears stable indefinitely under ambient conditions.

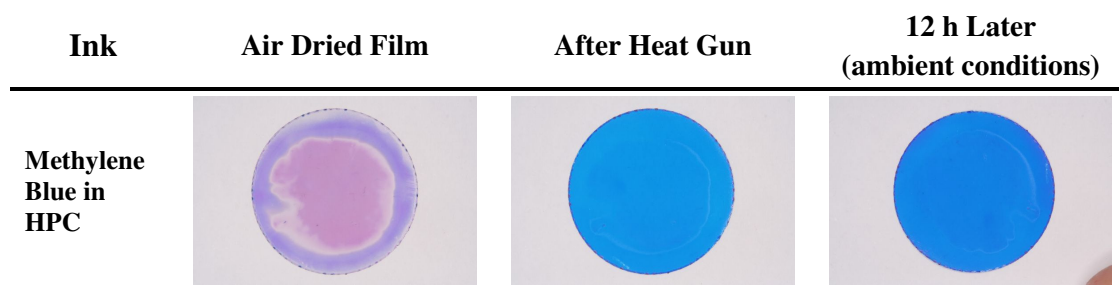


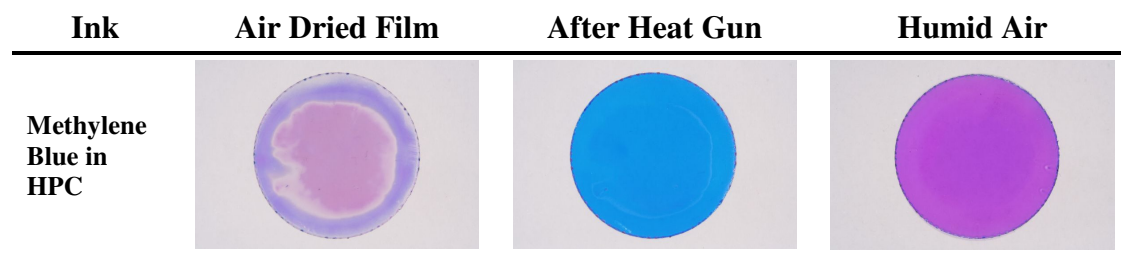
Figure 6.9 Showing the colour change of freshly cast Methylene Blue/HPC exposed to a 3 s heat pulse (ca. 200 °C).

Heat Activated Film Response to Humidity

Interestingly upon exposure of the blue ($\lambda_{\text{max}} = 605 \text{ nm}$) film to 100% humid air the film turns irreversibly to a purple colour ($\lambda_{\text{max}} = 505 \text{ nm}$, $\Delta\lambda = 100 \text{ nm}$). The original blue colour can only be regenerated using a 3 s pulse of a heat gun. These findings are illustrated in **Figure 6.10**. What is immediately clear from these pictures is that the heat activated film's response to humidity is most striking and also opposite to its humidity response shown in **Figure 6.8**. It should also be noted that this response is reversible and repeatable over several cycles in all films (without noticeable further loss in colour).

It is possible that on exposure to humidity the dye-polymer interactions formed under heating are disrupted in favour of water-polymer and water-dye interactions, where the latter favour the formation of dye aggregates. The film has a more intense and uniform colour than before the heat pulse and this would seem to indicate the melted polymer dissolves the dye. This is illustrated by photographs and respective UV/vis absorbance spectra in **Figure 6.10 (a)** and **(b)**.

(a)



(b)

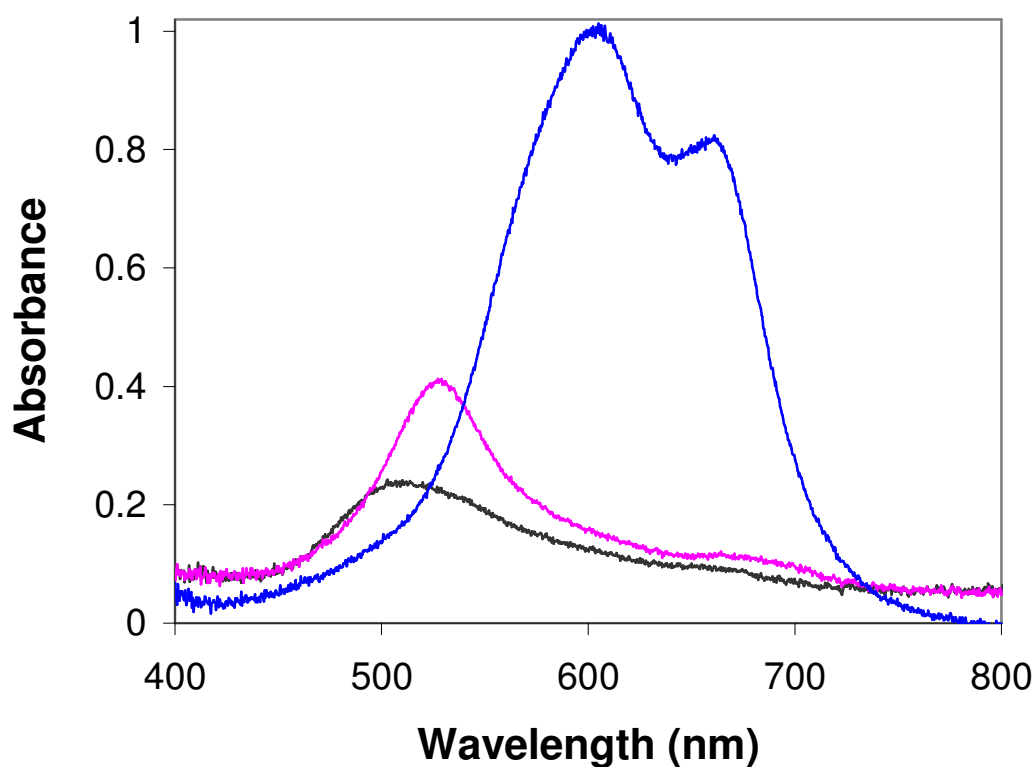
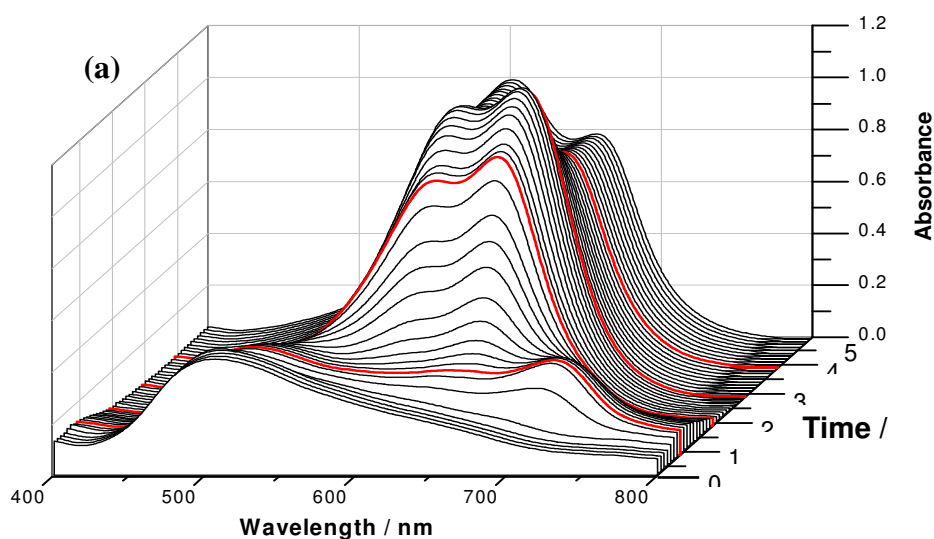


Figure 6.10 (a) Photographs of freshly prepared MB/HPC (left, pink/purple). Same film thermally activated using a heat gun (middle, blue) and then exposed to 100% humid air (right, pink). (b) A UV/vis spectrum of the three colorations of the MB/HPC film from (a). The freshly prepared film shows lower absorbance ($\lambda_{\max} = 505$ nm, black line) and 20 nm blue shift before the heat/humidity activation ($\lambda_{\max} = 530$ nm, red line). Heat gun activated blue film has much higher absorbance ($\lambda_{\max} = 605$ nm, blue line).

6.3.3 Methylene Blue in HPC

The MB/HPC film temperature induced purple to blue colour change was investigated in detail using the Ocean Optics spectrophotometer. Initially the spectrophotometer was placed in a furnace to record the activation *i.e.* the purple to blue transformation. It was observed that the temperature required to achieve the colour change was close to 200°C, although monitoring this process was complicated by the thermal degradation of the dye due to its prolonged exposure to high temperature. Thus, as an alternative, a heat gun was used to raise the temperature of the film in a shorter time (<4 seconds) while the spectra were being acquired. **Figure 6.11 (a)** shows the change in spectrum of a freshly cast MB/HPC ink which starts as the pink-purple colour (see **Figure 6.10 (a)**). The initial λ_{\max} , before the heat is applied (505 nm), is abnormally low and is not readily explained just by formation of the dye aggregates (λ_{\max} of dimer and trimer of MB are 605 and 578 nm, respectively).



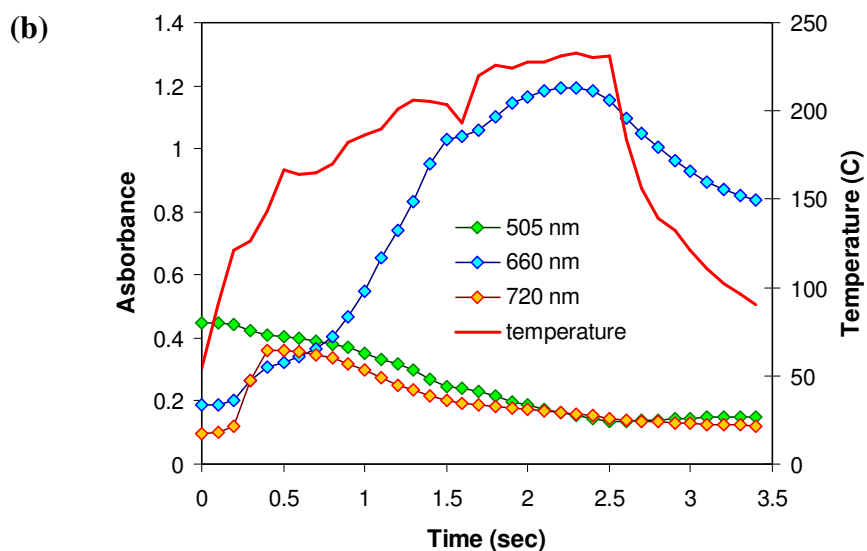


Figure 6.11 (a) A 3D waterfall plot showing the effect of a 3.5 second pulse of heat from a heat gun on the spectrum of a freshly cast MB/HPC film. The spectra marked in red are recorded at 0.9, 1.9, 2.9 and 3.9 seconds. **(b)** A detailed plot of Abs_{λ} vs. time profiles using data from the 3D plot are shown here as well as the temperature vs. time profile (red line). The maximum error was less than 10%.

Surprisingly, this time-resolved spectrum revealed a new transient peak at 720 nm appearing during the first few seconds as the temperature increased to ca. 100°C and then disappearing again. This peak ($\lambda_{max} = 720$ nm) is red shifted from the Methylene Blue monomer/dimer peaks and might be a J-aggregate (head to tail orientation)³⁷ of MB due to the change in arrangement of the dye molecules caused by the increasing temperature. The monomer/dimer peaks at 605 and 660 nm responsible for the blue coloured heat-treated film appear once the temperature exceeds ca. 70°C and reaches a maximum at > 200°C. **Figure 6.11(b)** illustrates the changes in absorbance values at 505, 660 and 720 nm as a function of temperature, using data from **Figure 6.11(a)**. Thermal analyses by differential scanning calorimetry and thermogravimetry have shown that HPC softens at ca. 160°C and melts at 195°C³⁵ and it is suggested that the onset of the colour change of the film is associated with the softening/melting of the polymer. This heat induced activation (505 nm \rightarrow 660 nm) is most interesting as it seems to be unique to the MB/HPC system (HEC shows no such property)³⁸. *Note:* HPC is well known for formation of cholesteric, helical, thermotropic³⁹ and lyotropic^{40, 41} liquid crystals either in concentrated solutions or cast as a film. Experiments that were carried out using

HPC film prepared by the spin-coating showed that UV/vis spectrum of the HPC films (prepared without Methylene Blue) was not affected by temperature. Yet, according to the literature HPC films should exhibit anisotropic liquid crystal phase breakage at around 200°C³⁹ into an isotropic phase in which the film could be ‘frozen’ if rapidly cooled, this phenomena of liquid crystal is well studied.^{42, 43} The involvement of HPC as a liquid crystal polymer in the observed colour change is a subject of further investigation.

A review of the phenomenon of ‘metachromasy’⁴⁴ in Methylene Blue offers a possible explanation of the above observations; it is suggested⁴⁴ that intercalated water molecules in dye aggregates may allow molecules to pack more closely (by reducing repulsion of like charges, due to the high dielectric constant of water) and enhance the blue to red (blue shifted) colour change. Any external factors which remove and/or reduce this effect (such as heating) will reverse the observed colour change. Heat not only removes the water sandwiched in between the stacked planar molecules of the dye, hence increasing the repulsion forces between the Methylene Blue oligomers, but also melts the polymer *i.e.* creating a solvent-like environment. The observed colour change on heats (purple to blue) fits with the knowledge that the association of dyes does not occur in non-aqueous media *i.e.* HPC.⁴⁵ Thus, in the lipophilic, dehydrated environment of a dried film, MB tends to be in its monomer ($\lambda = 665$ nm) form. When the ‘dehydrated’ blue film is then exposed to humid air stream, the hygroscopic HPC absorbs the highly polar water molecules. Which, in accordance with Otsuki *et al.*²⁶ then favours formation of the dye clusters/aggregates and result in a colour change from blue to purple (see **Figure 6.10**).

The heat activated blue MB/HPC film is stable for many days (depending on ambient humidity), but when exposed to a humid stream of air the blue film regains its purple colour. According to Yakimets *et al.*⁴⁶ the hydrogen bond interactions between two highly substituted HPC molecules are quite weak and are easily affected by bound water; the water can displace the well-separated/dispersed monomeric dye molecules and so promote their aggregation.

The Methylene Blue/HPC humidity sensor, once heat activated (blue), remains stable in ambient atmosphere and switches quickly (to purple) only when exposed to high (ca. 100% RH). This behaviour could form the basis of a reliable colour-based

humidity sensor. Thus, in the next section the response of the film is investigated more thoroughly with a view to using it as a humidity sensor.

6.3.4 MB / HPC humidity sensor

The response of a typical MB/HPC film to repeat alternating cycles of exposure to heating and 100% humid air stream is shown in **Figure 6.12**. As can be seen the repeated heating/drying and humidifying cycles do not affect the overall response of the film. Photographs of the film sample during three cycles from the initial thermal activation or “dissolving” step can be seen in **Figure 6.13**.

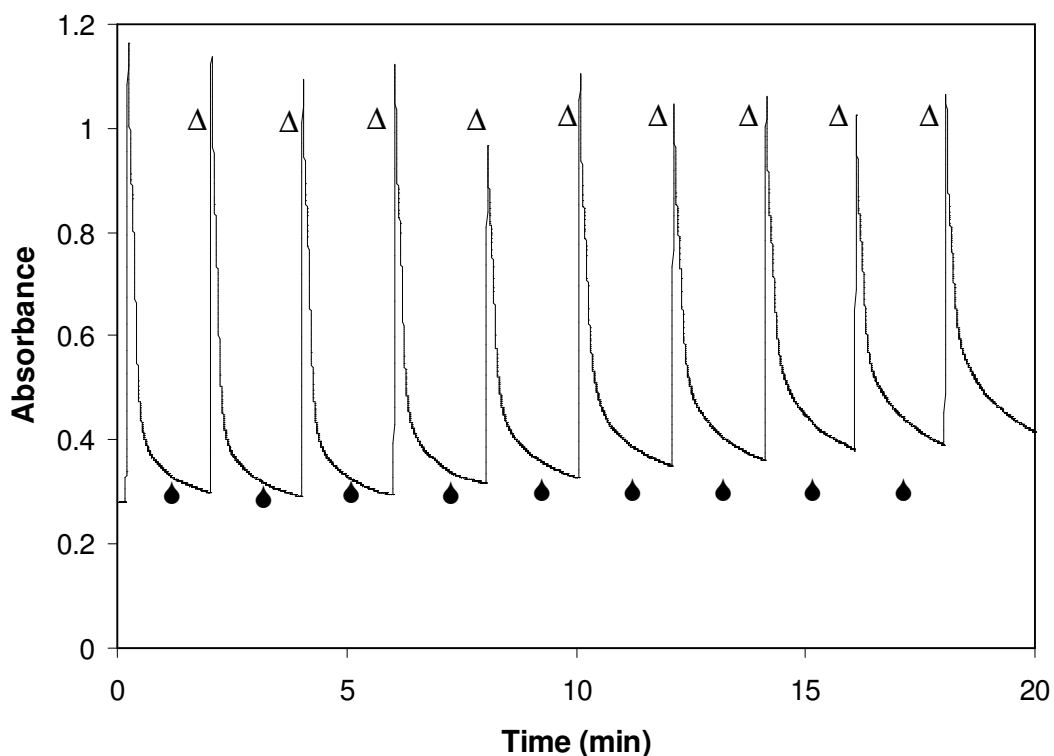


Figure 6.12 MB/HPC disc heat gun pulse (Δ) followed by 100% humid air (\bullet) measured abs at 660 nm.

The as-prepared MB/HPC film is pink in the middle and blue on the edges which is possibly a result of the spin coating technique. The pink centre of the film responds to humidity by going blue, in much the same way as the MB/urea/HEC films do, and

this is also reversible. In a supporting experiment one of these as-prepared films was put under high vacuum (10^{-5} Torr) to see if the water removal by vacuum would be sufficient to achieve the colour change but the film kept the original (pink/blue) colour. This would indicate that the temperature curing step is indeed the key to priming the film for humidity sensitivity.

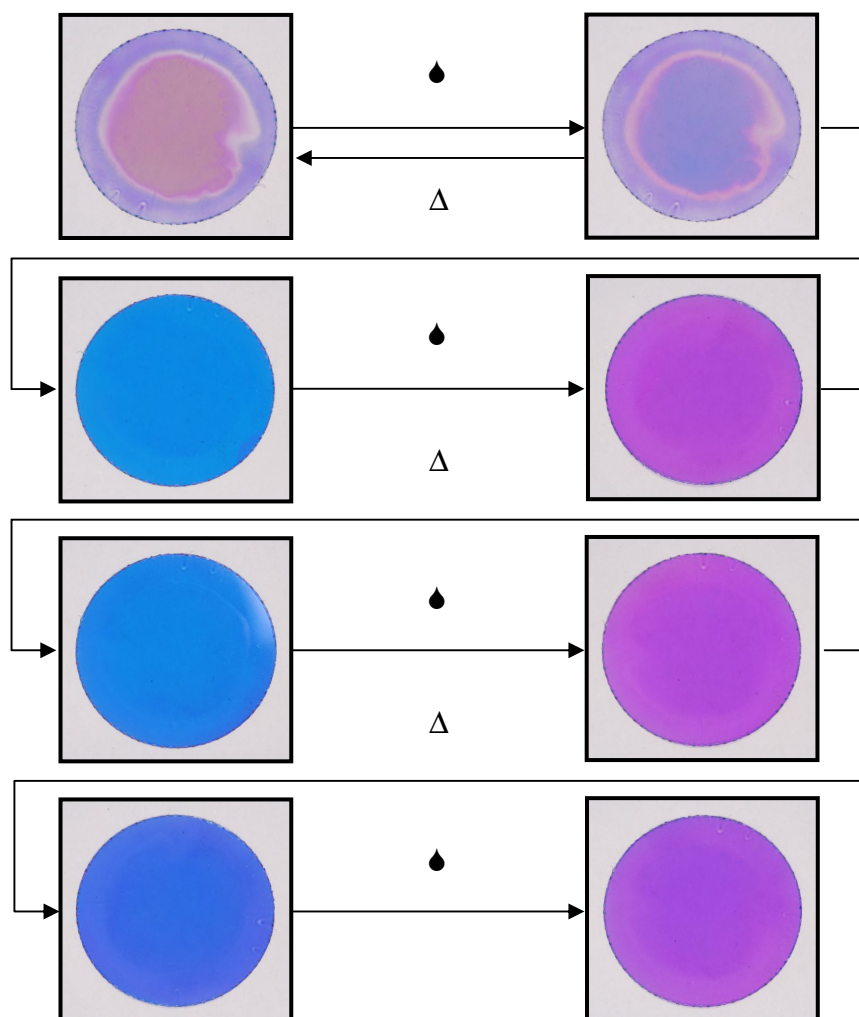


Figure 6.13 Photos of successive humidifying (◆) and heating (Δ) showing the colour of a typical MB/HPC film with dry/heated films on the left and wet films on the right.

A study was carried out of the response of the MB/HPC film to different relative humidity levels ranging from 100% through to 40% in steps of ten. A typical film was activated by heating with a heat gun for 10 seconds and then exposed to an air stream of a given relative humidity and a UV/vis spectrum was recorded every 5

seconds. An example of a typical response is shown in **Figure 6.14** of a film exposed to 70% relative humidity.

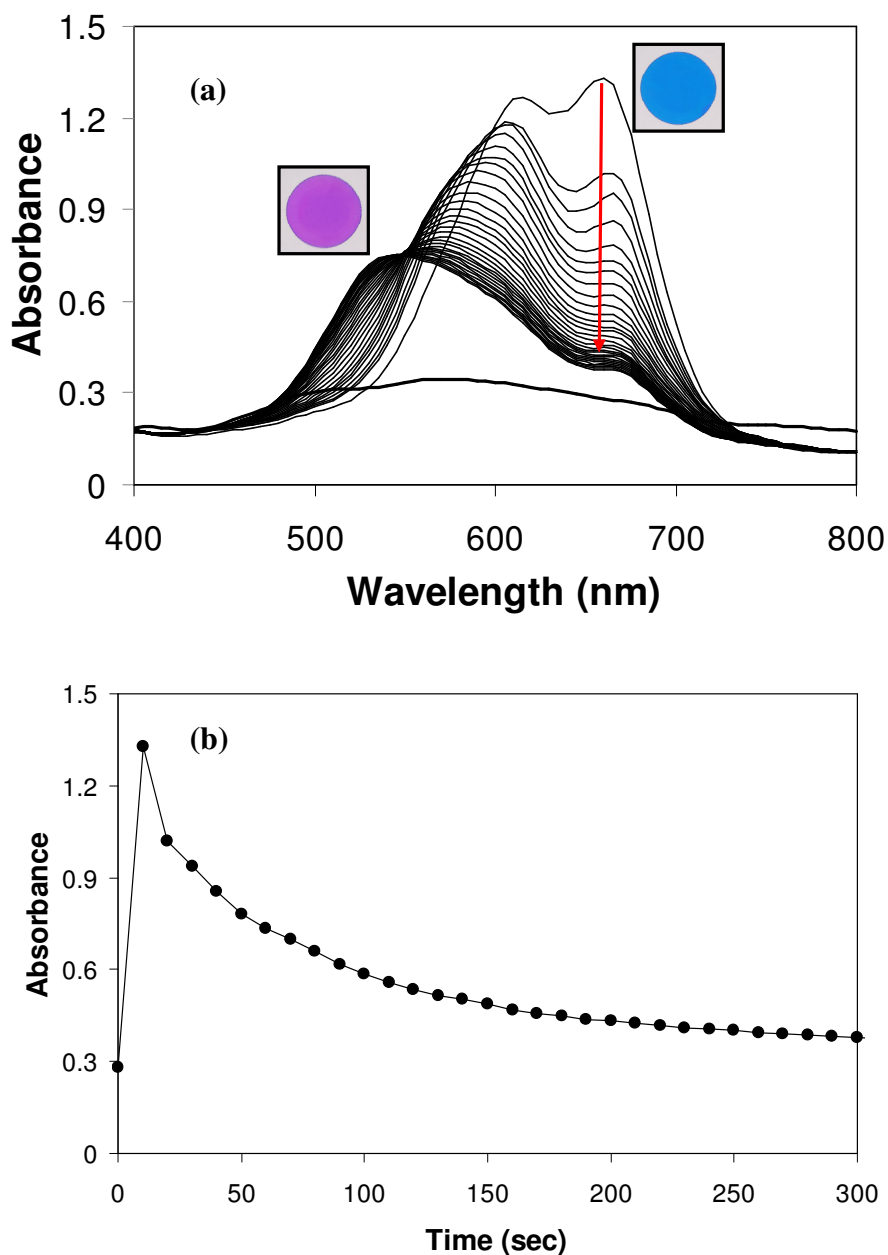


Figure 6.14(a) The response of a typical MB/HPC film under 70% humid air stream ($\lambda_{\text{max}} = 530$ nm for the purple (wet) form and 605/665 nm for the blue (dry) form of the indicating film. **(b)** Absorbance vs time profile shown for the blue (dry) indicator $\lambda_{\text{max}} = 660$ nm. The maximum error was less than 10%.

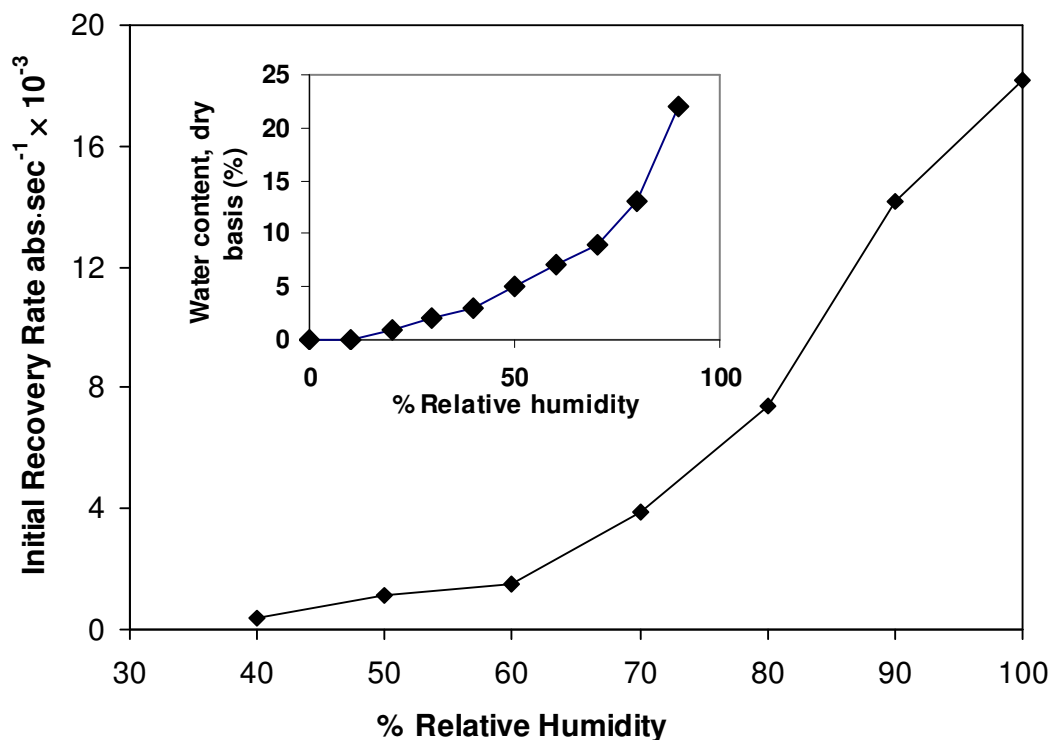


Figure 6.15 Initial rate of recovery vs. % relative humidity of MB/HPC films. The inserted plot shows a sorption isotherm for HPC as a function of RH as measured by Yakimets.⁴⁷ The maximum error was less than 10%.

A plot of the initial rate of recovery vs. % relative humidity for the MB/HPC system is shown in **Figure 6.15**. The data shows an apparent exponential rise in rate with increasing RH and this appears to be very similar to the water sorption isotherm of HPC as measured by Yakimets *et al.*⁴⁷, see inserted graph in **Figure 6.15**. So, the more of the water is absorbed by the HPC film, the faster the colour change of a blue (activated by heat gun) MB film to purple (upon exposure to humid air of different RH). *Note:* the observation of no recovery below humidity of 40% is very similar to that found for MB/urea film. It is not clear why the MB/HPC film shows little response to water vapour at RH values < 40%.

6.4 CONCLUSIONS

A blue ink of Methylene Blue, HEC and urea turns pink on drying and this colour change is reversed on exposure to a humid air stream (relative humidity of over

70%). This colour change is reversible and can be carried out repeatedly. This novel kind of optical humidity indicator appears to work due to the hygroscopic nature of urea and the highly polar environment offered by crystalline urea, which favours MB aggregation. This environment is destroyed by high humidities which dissolves the urea crystals.

A more dramatic and quite opposite colour change can be effected without urea, using a different polymer (HPC), by 'activating' the cast ink film with a short (less than 5 sec) burst of high temperature (200°C) from a heat gun. The bright blue (dry), activated film was stable in ambient conditions but when exposed to a stream of 100% RH air it instantly changes to a bright pink/purple colour (wet). The film could be reactivated using the heat gun and re-used over many cycles.

6.5 REFERENCES

1. R. Esse and A. Saari, *Smart Packaging Technologies*, 1st edn., John Wiley & Sons, West-Sussex, 2008.
2. J. E. Robinson, K. M. Browne and W. G. Burton, *Ann. Appl. Biol.*, 1975, **81**, 339-408.
3. R. H. Feinzig and D. Sullivan, National Conference on Building Commissioning, Chicago, 2007.
4. N. Yamazoe and Y. Shimizu, *Sens. Actuators*, 1986, **10**, 379-398.
5. <http://www.hannainst.com/usa/prods2.cfm?id=012001>,
<http://www.hannainst.com/usa/prods2.cfm?id=012001>, Accessed August, 2011.
6. <http://www.michell.co.uk/products/classification/browse/portables>,
<http://www.michell.co.uk/products/classification/browse/portables>, Accessed August, 2011.
7. P. B. Davis, US Pat. 2460065–2460070, 1949.
8. P. B. Davis, US Pat. 2580737, 1949.
9. D. L. Fuller, US Pat. 4034609, 1977.
10. D. L. Fuller, US Pat. 4150570, 1979.
11. J. S. Haswell, US Pat. 5520041, 1996.
12. W. O. Krause, US Pat. 3533277, 1970.
13. W. O. Krause, US Pat. 3499616, 1970.
14. J. F. McBride, US Pat. 4909179, 1990.
15. S. D. Price, US Pat. 3121615, 1964.
16. E. Wroth and K. Sheraw, US Pat. 5950323, 1999.
17. Y. Yamakawa, US Pat. 7316198 B2, 2008.
18. M. Hamada, US Pat. Appl. 2007/0157702 A1, 2007.

19. P. B. Davis and J. N. Pryor, US Pat. 2526938, 1950.
20. M. Gattiglia, US Pat. 6655315 B1, 2003.
21. M. Gattiglia and E. Gondolfo, WO 02/44712 A1, 2002.
22. http://www.sud-chemie.com/scmcms/web/page_en_6254.htm,
http://www.sud-chemie.com/scmcms/web/page_en_6254.htm, Accessed August, 2011.
23. R. Matsushima, N. Nishimura, K. Goto and Y. Kohno, *Bull. Chem. Soc. Jpn.*, 2003, **76**, 1279-1283.
24. R. Matsushima, A. Ogiue and S. Fujimoto, *Chem. Lett.*, 2000, 590-591.
25. R. Matsushima, A. Ogiue and Y. Kohno, *Chem. Lett.*, 2002, 436-437.
26. S. Otsuki and K. Adachi, *Polym. J.*, 1995, **27**, 655-658.
27. E. Braswell, *J. Phys. Chem.*, 1968, **72**, 2477.
28. E. H. Braswell, *J. Phys. Chem.*, 1972, **76**, 4026-4030.
29. A. Ghanadzadeh, A. Zeini, A. Kashef and M. Moghadam, *J. Mol. Liq.*, 2008, **138**, 100-106.
30. Z. M. Zhao and E. R. Malinowski, *Appl. Spectrosc.*, 1999, **53**, 1567-1574.
31. J. R. Adams and A. R. Merz, *Industrial & Engineering Chemistry*, 1929, **21**, 305-307.
32. A. Clow, *Nature*, 1940, **146**, 26.
33. E. A. Werner, *Nature*, 1937, 512.
34. C. Vazquezsalinas and S. Lakshminarayana, *J. Food Sci.*, 1985, **50**, 1646-1648.
35. T. G. Rials and W. G. Glasser, *J. Appl. Polym. Sci.*, 1988, **36**, 749-758.
36. T. Kararli, J. Hurlbut and T. Needham, *J. Pharm. Sci.*, 1989, **79**, 845-848.
37. A. Czimerova, L. Jankovic and J. Bujdak, *J. Colloid Interf. Sci.*, 2004, **274**, 126-132.
38. C. Demitri, R. Del Sole, F. Scalera and A. Sannino, *J. Appl. Polym. Sci.*, 2008, **110**, 2453-2460.
39. K. Shimamura, J. L. White and J. F. Fellers, *J. Appl. Polym. Sci.*, 1981, **26**, 2165-2180.
40. C. Q. Song, M. H. Litt and I. Manas-Zloczower, *Macromolecules*, 1992, **25**, 2166-2169.
41. R. S. Werbowyj and D. G. Gray, *Mol. Cryst. Liq. Cryst.*, 1976, **34**, 97-103.
42. Y. Nishio and T. Takahashi, *J. Macromol. Sci.-Phys.*, 1984, **B23**.
43. N. Tamaoki, *Adv. Mater.*, 2001, **13**, 1135-1147.
44. J. A. Bergeron and M. Singer, *J. Biophys. Biochem. Cytol.*, 1958, **4**, 433-457.
45. P. Mukerjee and A. Ghosh, *J. Phys. Chem.*, 1963, **67**, 193.
46. I. Yakimets, S. S. Paes, N. Wellner, A. C. Smith, R. H. Wilson and J. R. Mitchell, *Biomacromolecules*, 2007, **8**, 1710-1722.
47. I. Yakimets, N. Wellner, A. C. Smith, R. H. Wilson, I. Farhat and J. Mitchell, *Mech. Mater.*, 2007, **39**, 500-512.

CHAPTER 7

**EFFECT OF ALKALI ON METHYLENE
BLUE AND OTHER THIAZINE DYES**

7.1 INTRODUCTION

As already stated in Chapter 1, there has been a tremendous amount of interest in methylene blue for over a century and, amazingly, this far-reaching and sustained interest shows no evidence of fading with over 4000 MB-related papers being published in the last 5 years. Yet there is still much about this apparently simple dye molecule that can surprise. For example, it was recently reported that MB readily forms a red-coloured ($\lambda_{\text{max}} = 525 \text{ nm}$ in toluene) lipophilic, non-ionic hydroxy-adduct upon treatment with an equimolar amount of sodium hydroxide, to which the *N*-hydroxy structure MB-OH **2** was assigned.¹

Structure **2** is closely related to the reduced leuco-form of MB (**3**) which is of course near colourless². Consequently a molecule of structure **2** would also be anticipated to be colourless, calling into doubt the structural assignment of the red material isolated from base treatment of MB, which is in any case in conflict with the classical literature which reports the main product to be the hydrolysed species Bernthsen's Methylene Violet (MVB; **4**).³ In view of MB's continuing and topical applications the reported chemistry was repeated. A brief overview of the results has been published elsewhere as a comment⁴ on the original paper,¹ accompanied by a reply.⁵

The earlier assignment¹ of structure **2** was based on a proposal by Plater⁶ that the heterocyclic nitrogen of MB is electron-deficient and thus a target for nucleophilic attack. There are three main objectives: to present the full evidence for the characterization of the product from reaction between MB and NaOH; to discuss the nature of MB's heterocyclic N atom, alongside other related dye species; and to summarize the results of investigations into how other thiazine-based dyes behave with base.

Table 7.1 Summary of structural, spectral and physical characteristics of MB and other relevant thiazine dyes and derivatives.

Structure	No.	Abbreviation, name, molecular weight	λ_{\max}/nm		$\text{p}K_{\text{a}}^{\text{c}}$
			Cation ^a	Neutral ^b	
	(1)	MB, Methylene blue, 284.4	665 (746) ^d		
	(2)	MB-OH, 256.32		520 ^f [351]	
	(3)	Leuco-MB, 285.4		256 ^g	
	(4)	MVB, Methylene Violet, 256.32	610 ^e	520 ^h	
	(5)	AB, Azure B, 270.37	645	503 [521]	12.1
	(6)	AA, Azure A, 256.35	628	500 [501]	11.8
	(7)	AC, Azure C, 242.32	615	488 [520]	11.5
	(8)	TH, thionine, 228.29	602	487 [486]	11.0

^a Absorption maxima of cationic species measured in water, ^b Absorption maxima of neutral deprotonated species measured in toluene. Calculated values in square brackets []. See Discussion, section 7.3.3 ^c Data from Bonneau R, Faure J, Jousset-Dubien J. *Talanta*, 1967;14:121. ^d Protonated doubly charged absorption maximum from reference⁷, ^e *O*-protonated MVB, ^f Data from reference¹, assigned to MB-OH but actually for MVB. ^g Data from Obata H. *Bull Chem Soc Jpn* 1961;34:1057; Cohn G. *Ber* 1900;33:1567. ^h Data for neutral unprotonated MVB.

7.2 EXPERIMENTAL

7.2.1 Materials and Chemicals

Methylene blue (96+%, as hydrate, MW. 319.85; MB (**1**)) was purchased from Acros. Azure B (80%+, MW. 305.83; AB (**5**)), Azure A (96%, MW. 291.80; AA (**6**)), Azure C (40%, MW.277.77; AC (**7**)), thionine (85%, MW. 287.34; TH (**8**)) and Methylene Violet (Bernthsen), (80%, MW. 256.33; MVB (**4**)) were purchased from Aldrich; all were chloride salts except thionine acetate. Structures are given in **Table 7.1**. The MB was further purified by continual extraction of red impurities from its buffered aqueous solution by CCl₄ until the latter washings were colourless, followed by crystallization according to a published method⁸. All the other chemicals were used without further purification. Analytical thin layer chromatography was carried out on silica plates using MeOH/CHCl₃/HOAc 90:8:2 as mobile phase.

7.2.2 Spectrophotometric Measurements

All UV/visible spectrophotometric experiments were recorded on a Varian Cary 50 double beam spectrophotometer, using 1 cm quartz cuvettes in dry solvents of highest available purity. A Perkin-Elmer fluorimeter LS-50B was used to record fluorescence spectra.

7.2.3 Mass Spectrum Analysis

Two different mass spectrometers were used in this work. The majority of the experiments were run on an ESI-MS (ThermoFinnigan LCQ DUO MS) using either the direct injection port or via an HPLC system (*i.e.* LC-MS). In the latter, the HPLC column was a Phenomenex Gemini, C18, 5 μm, 50 x 2.0 mm. A graded mobile phase was used comprising initially 0.1% formic acid in water, becoming 0.1% formic acid in acetonitrile, over 15 min at 150 μl/min flow rate. An LDI-MS (Shimadzu, AXIM-CFR) was also used to record the mass spectra of the thiazine dyes as well as the MB base hydrolysis products. Samples of the dyes were prepared and recorded at different pH values (neutral, 10, 12) and the toluene extract prepared by shaking the dye (0.1 mM) in 0.1 M NaOH with an equal volume of toluene (*vide infra*).

7.2.4 Computational Methods

All structures were optimized in the solvent phase using the polarisable continuum model^{9,10} (PCM) at the B3LYP¹¹⁻¹⁶ level of theory with the 6-311++G(d,p) basis set^{17,18}; no symmetry constraints were imposed during the optimization of the dyes. The structures were optimized in two different solvent (dielectric) environments, water ($\epsilon = 78.4$) and toluene ($\epsilon = 2.4$). Time dependent density functional theory¹⁹⁻²¹ (TD-DFT) single-point calculations were performed on the optimized structures to obtain the calculated λ_{\max} values. The PCM approach was employed within the TD-DFT calculations to model the effect of the respective solvents on the absorption spectra. All calculations were done within the Gaussian 03 program.²² The charge distribution of MB was determined using the natural bond orbital (NBO) approach.²³ The calculated values for the absorption λ_{\max} of relevant, different thiazine dye species in toluene are given in **Table 7.1**.

7.2.5 NMR measurements

¹H NMR data were acquired using Bruker AVANCE-III and Avance/DRX NMR spectrometers operating at 600.13 and 500.13 MHz and operating under TopSpin versions 2.0 and 1.3 respectively. Data accumulated for samples solubilized in CCl₄ were acquired in an unlocked mode, with magnetic field homogeneity adjusted manually using lineshape observation-based shimming.

7.3 RESULTS AND DISCUSSION

7.3.1 MB Initial Experiments: Formation of Red MB

The red lipophilic form of MB assigned the MB-OH structure **2**¹, henceforth referred to as ‘red MB’, was reportedly generated by apparently mixing an ‘aliquot’ of aqueous MB (0.1 mM) with NaOH (0.1 mM, *i.e.* pH 10) under toluene.¹ After 1 h standing, the toluene reportedly developed a red colour due to the extraction of the lipophilic red MB from the aqueous solution. However, upon reproducing this simple experimental procedure, no red MB was generated. This was not surprising, given that others have noted MB is ‘indefinitely stable’ in aqueous solution at pH

9.5.^{24,25} Indeed, mixing MB with 0.1 mM alkali and shaking with a water-immiscible solvent (usually dichloromethane) is a published method for purifying MB of the less methylated thiazines, such as Azure B (**5**, usually the most prevalent species), Azure A (**6**) and Azure C (**7**), which are common impurities in most past commercial samples of MB.^{8,26} It is generally accepted that this purification procedure is effective because the latter thiazines are readily deprotonated by the alkali to their neutral, lipophilic orange or red coloured forms²⁶ and MB itself is stable in 0.1 mM alkali. More about this process will be discussed later.

It is *tempting* to explain failure to reproduce the formation of red MB as being due to the earlier¹ use of a source of MB that was contaminated with one or more of the thiazines listed in **Table 7.1**. However, the reported absorption spectrum and λ_{\max} (526 nm) for the red MB is not that of any of the deprotonated thiazines. Interestingly, it is possible to generate a species, with a near identical absorption spectrum to that reported for red MB¹, using the same method, but with 0.1 M, instead of 0.1 mM, NaOH aqueous phase solution shaken with toluene. Thus it would appear a simple mistake had been made over alkali concentration used in the original report.¹ **Figure 7.1(a)** illustrates photographs of equal volumes of an aqueous MB (0.1 mM) solution below toluene at time zero and 5h after the addition of sufficient alkali to render the aqueous solution pH 13 and mixing via thorough shaking. The observed UV/visible spectra of the MB aqueous solution at pH 13 and toluene solution before and 1h and 5h after mixing are also illustrated in **Figure 7.1(b)**.

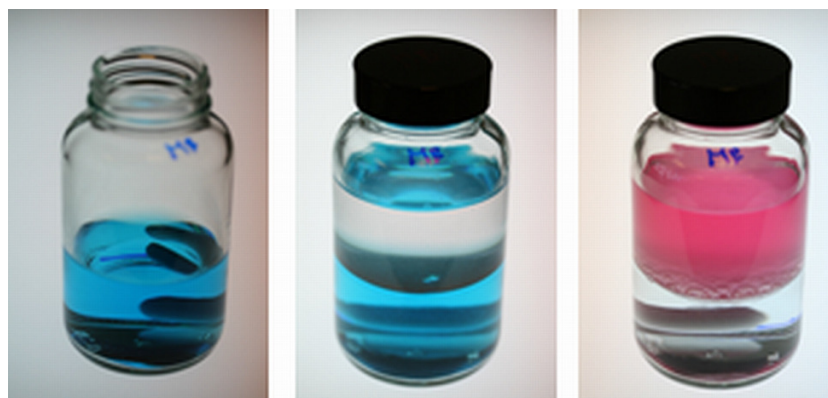


Figure 7.1(a) Top: Photographs of a fresh 10^{-4} M MB, 0.1 M NaOH aqueous solution (from left to right): before, directly after and 5h after mixing and shaking with an equal volume of toluene.

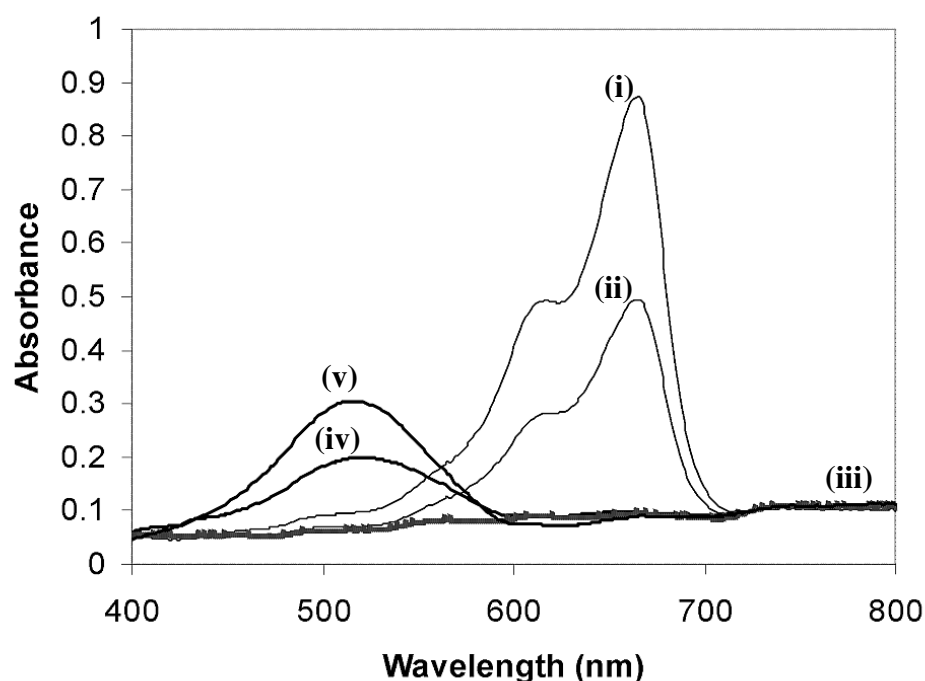


Figure 7.1 (b) - Visible absorption spectrum (measured in 1 cm cuvette) of the *aqueous* MB solution (i) before, (ii) directly following, and (iii) 5h after (grey line) mixing and shaking with an equal volume of toluene. The visible absorption spectra of the toluene solution directly after and 5h following mixing and shaking with the aqueous solution are illustrated by lines (iv) and (v). The maximum error was less than 10%.

These results show that at pH 13 MB is converted to a lipophilic, *i.e.* toluene-soluble, red/pink species which is clearly observable after 1h and for which the reaction is

complete after 5h. It has the same spectral features as the MB-derived species reported¹ but is it really a *N*-hydroxy adduct?

7.3.2 Properties of “Red Methylene Blue”

A number of simple experiments reveal the red MB produced as described above using a pH 13 aqueous solution of MB is not a hydroxy adduct, but rather largely Bernthsen’s Methylene Violet, MVB (**4**).²⁷ The free base form of the latter is not very soluble in water (0.6 mg mL⁻¹, *cf.* MB 50 mg mL⁻¹), but is soluble in most common *organic* solvents, including toluene. Thus, the UV/visible absorption spectrum of a commercial sample of MVB (**4**) dissolved in toluene is identical to that of red MB and both also fluoresce with the maximum of emission at 596 nm (λ (excitation) = 520 nm in toluene), in agreement with the values reported in the literature for MVB fluorescence²⁸. The measured UV/visible spectra of MVB (**4**) in different organic solvents are very similar if not indistinguishable from the spectra reported¹ in the same solvents indicating they are the same. In support of this, the hydrolysis of MB with alkali to produce MVB (**4**) has been suggested previously by others³ usually based on spectral observations.

Further confirmation of the identity of red MB was that when it is re-extracted from toluene by an acidic aqueous layer, the latter turns blue with an absorption spectrum that is not MB ($\lambda_{\text{max}} = 665$ nm) but rather that of protonated MVB ($\lambda_{\text{max}} = 580$ nm). When the red MB in toluene solution is spotted onto an acidic silica TLC plate it also turns blue, as noted earlier^{1,6}, but further work has shown that TLC development caused the original dye spot to separate into two blue spots, neither of which is MB. One – the most striking in depth of colour – has the retention time, R_f , of that of commercial MVB (**4**). The other – which is much weaker in colour – has an R_f value the same as that of Azure B (**5**; see **Table 7.1**).

The NMR spectra recorded for MB (in D₂O; 500.13 MHz), red MB and MVB (in CCl₄; 600.13 MHz) reveals red MB to be identical to MVB and not MB, nor any hydroxy adduct. Thus, the NMR spectra of MB, red MB and MVB depicted in **Figure 7.2** clearly indicate the conversion of a symmetrical molecule (MB, lower NMR spectrum) to an unsymmetrical molecule possessing two unique and clearly distinguishable AMX spin systems entirely consistent with MVB and in contrast to

what would be predicted for the symmetrical MB-OH adduct **2**. Consistent with the above is the mass spectrum of the red MB in toluene solution which revealed the predominant presence of MVB (molecular ion peak at m/z 256) with some Azure B (**5**; m/z peak at 270).

Overall, these experimental findings show that the red MB species introduced by Plater⁶ and subsequently claimed by Pal and co-workers¹ to be the *N*-hydroxy species MB-OH (**2**) is in fact MVB (**4**), possibly containing some Azure B (**5**), generated by adding a high concentration of base (0.1 M NaOH) to an aqueous solution of MB, through a simple, well-established²⁵ hydrolysis reaction.

In the meantime, Plater has indicated that the red material to which he assigned the MB-OH structure **2**⁶ is in fact Azure B (**5**; **Table 7.1**).²⁹ As already stated this is a common MB contaminant, and can be readily formed from MB by base-induced demethylation⁸ at pH 11, a value somewhat lower than that (pH 13) which causes deamination to MVB.

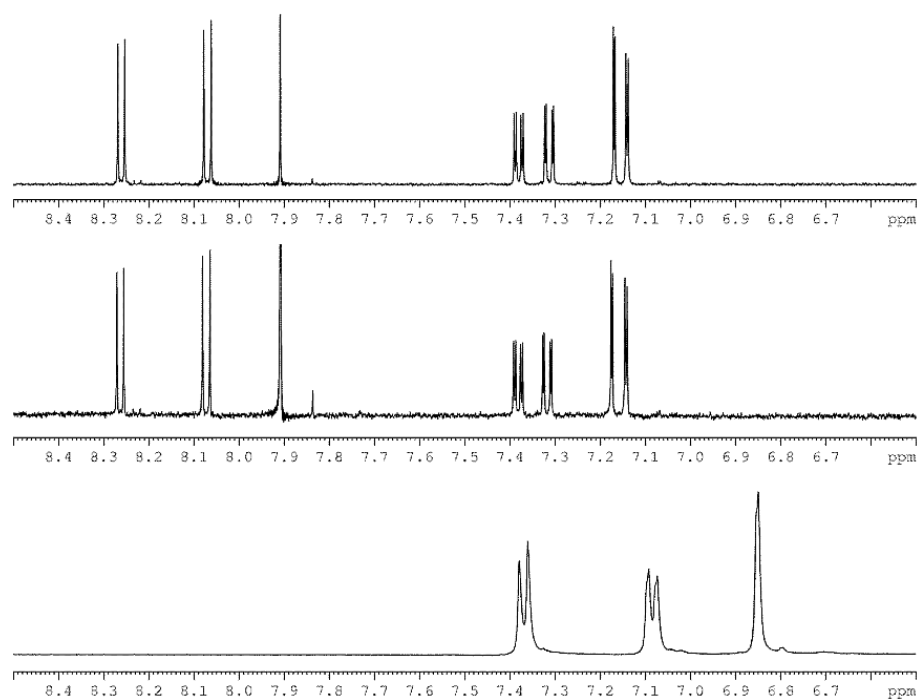


Figure 7.2 ¹H NMR spectra of (top to bottom) purchased MVB (Aldrich), red MB* (both recorded in CCl₄ using Bruker Avance-III 600 NMR spectrometer) and methylene blue (Acros) (recorded in D₂O using Bruker Avance/DRX 500 NMR spectrometer).

7.3.3 The Nature of Heterocyclic Nitrogen in MB and Analogous Dyes

Despite the now evident clarity surrounding the non-formation of any product with a structure MB-OH (**2**), the question of the electronegativity of the heterocyclic nitrogen in MB remained open. **Figure 7.3** shows the main valence bond resonance forms contributing to the structure of MB. A central contention^{1,6} underlying the claimed formation of MB-OH (**2**) was that the central nitrogen in MB is electron deficient. The implication is that the mesomer **N**, characterized by a positive charge localized on the heterocyclic N connecting two fully benzenoid rings, is a significant contributor to the overall structure. However, density functional calculations and application of both the NBO and electrostatic potential (ESP) methods reveal this not to be the case. Rather, it appears the central nitrogen is electron *rich* relative to the remainder of the molecule. Thus, while the magnitude of the charges calculated by each method varies, both methods reveal that the S atom carries a neutral (ESP: +0.04e) to partial positive (NBO: +0.52e) charge, reflecting the importance of mesomer **S**. Importantly, with both methods the heterocyclic N atom of MB has an overall partial *negative* charge (NBO: -0.38e, ESP: -0.79e) as illustrated by the calculated partial charges from the NBO method in **Figure 7.4**. In valence bond terms mesomer **N** is a minor contributor, while mesomers **S** and **D1/D2** more closely resemble the structure of MB.

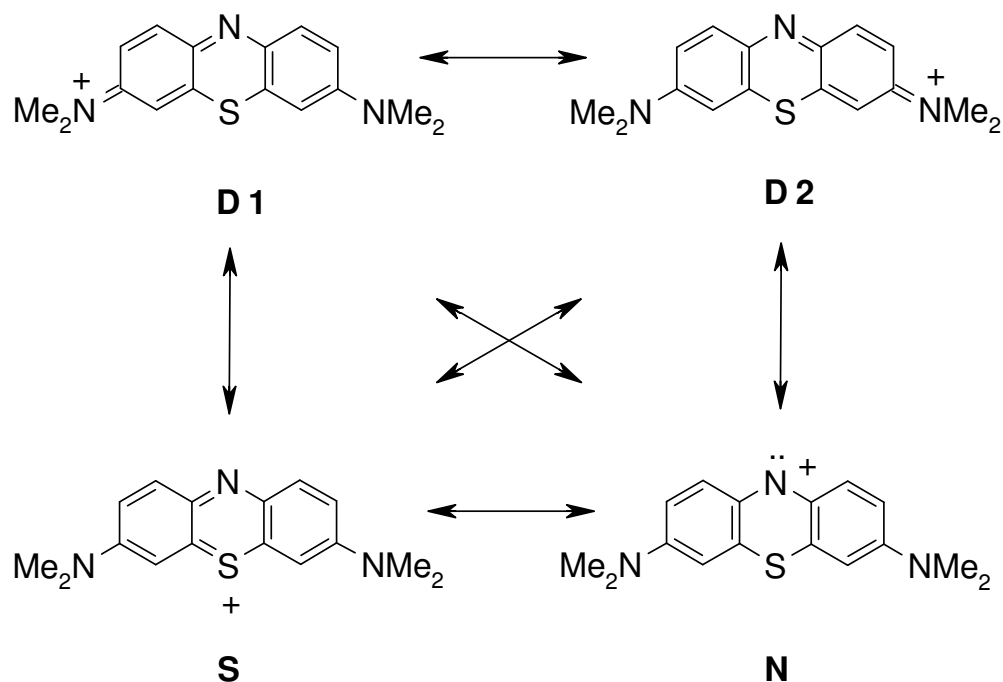


Figure 7.3 Major valence bond resonance structures of MB. Alternative Kekule structures of benzenoid rings and charged-carbon mesomers are not shown.

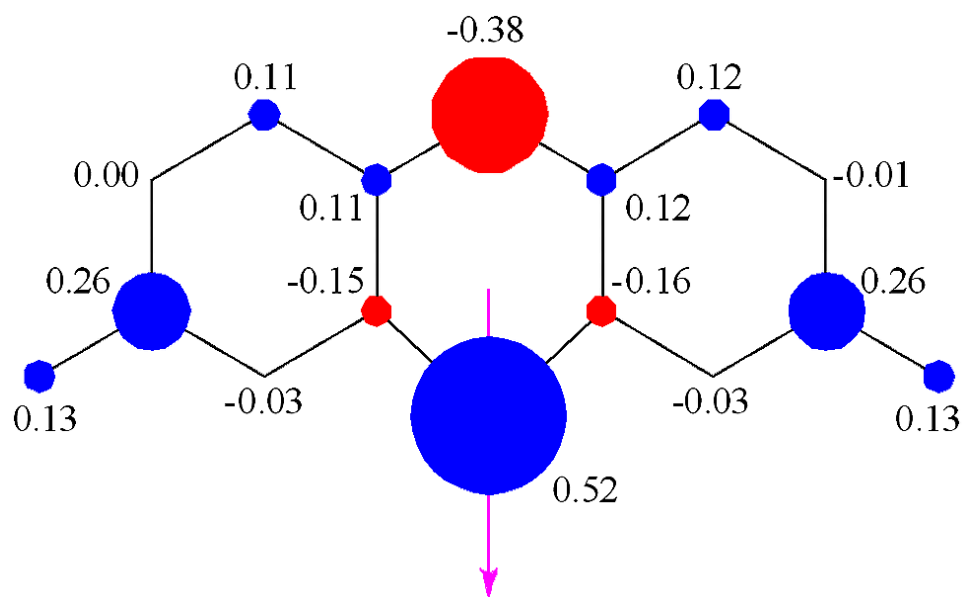


Figure 7.4 NBO charge distribution on the PCM/B3LYP electronic ground state of MB. See Computational Methods for details.

One of the early reasons for questioning the claim for a *N*-hydroxy adduct structure **2** for MB-OH was experience of simple colour-structure relationships. A molecule with the structure **2** of MB-OH would not be expected to be red: the delocalized

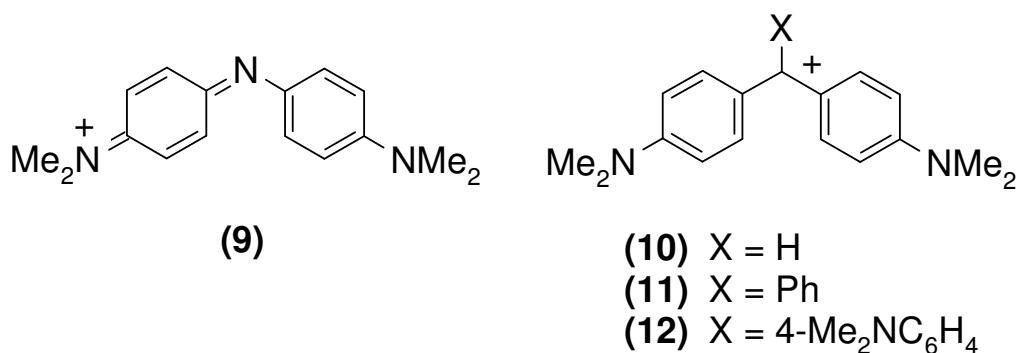
conjugation present in MB is removed in MB-OH, just as it is in (colourless) leuco-MB (**3**), and MB-OH is equally unlikely to be coloured. In much earlier classical dye-structure studies, G.N. Lewis *et al.* had speculated on the formation of a product with structure MB-OH (**2**) by the addition of water to MB as an intermediate in their chemistry, and they also noted it would be colourless.³⁰ Subsequently the absorption maximum for a species with the MB-OH structure **2** has been calculated. After initial geometry optimization, TD-DFT calculations reveal it would have an absorption maximum in the near UV at 351 nm, confirming its essential lack of colour. Similar calculations of the visible spectra of other known thiazine dyes reproduce their experimental absorption maxima with reasonable reliability (**Table 7.1**), demonstrating the suitability of the level of theory used for this work.³¹

Wide-ranging literature search for precedent of hydroxide anion addition at imine-type nitrogen has turned up no example.³² In fairness, Plater⁶ only *speculated* on the electronegative nature of the heterocyclic nitrogen of MB and the formation of MB-OH, and he claimed no direct evidence for its structural characterization. Unfortunately it is clear that this speculation has been over-interpreted by others^{1,5} and has given credence to electron-deficient heterocyclic nitrogen in MB when none is due.

If there is no experimental evidence for electron-*deficient* nitrogen in MB, is there experimental support for this centre being electron-*rich*, as calculated? Protonation of MB in strong acid is well-known to give a bathochromic shift in λ_{\max} , from 664 nm for MB in water to 746 nm in aqueous acidic MB, consistent with protonation at the heterocyclic N atom ($pK_{\text{BH}^+} = -0.26$).^{7,33} Alternative protonation of a pendant Me₂N group would lead to a hypsochromic shift, and is discounted.

All the above evidence suggests that although a valid contributory valence bond MB structure can be written with electron-deficient nitrogen, **N** in **Figure 7.3**, this does not represent the actual structural situation of MB. In fact, the heterocyclic nitrogen atom in **N** is now a formal 6-electron centre, analogous to a diarylnitrenium ion (a known, highly reactive species³⁴). Electron deficiency due to a sub-octet

electron configuration at a relatively electronegative element such as nitrogen is energetically disfavoured, and so even if mesomer **N** appears acceptable on paper, it is in fact unrepresentative of MB. The same conclusion appears to hold across other dye classes which include formally 6-electron positive sp^2 nitrogen centres. There are no reports of *N*-hydroxy derivatives of analogues such as diazines, quinone imines (typified by Bindschedler's Green (**9**), which hydrolyses via successive attack at the two terminal C-NMe₂ groups³⁵), azacyanines, and so on. Furthermore, simple MO calculations of such species always indicate a relatively electronegative nitrogen, bearing a partial negative charge.³⁶ In contrast, when the nitrogen centre of interest is replaced by positively charged sp^2 carbon, hydroxide addition at that centre is well known. Examples include diaryl carbenium ions (e.g. Michler's hydrol, **10**), their triaryl carbenium ion analogues (e.g. Malachite Green, **11**, and Crystal Violet, **12**) and the cyclised acridine, xanthene and thioxanthene series.³⁷ Unlike electronegative nitrogen, the more electropositive carbon is more amenable to supporting a positive charge in an electron deficient 6-electron configuration, and thus can be a site for attack by negative nucleophiles.



7.3.4 Other Thiazines

The purities of the other major thiazines, Azure A, B, C and thionine (**5-8**; see **Table 7.1**), were assessed using LC-MS and the results are summarized in **Table 7.2**. Thus, whereas the commercial sample of thionine (**8**) was very pure (99+%) and Azure B (**5**) of a reasonable purity (*ca.* 86%), the other two thiazines were gross mixtures. Most notably, the sample of Azure A (**6**) was of very low purity (*ca.* 21%) and far from the supplier's claimed value of 96%. However, for the general purpose of

demonstrating the formation of coloured lipophilic species upon treatment with alkali the dyes were used as received. Thus, these four thiazine dyes were treated with an aqueous pH 13 solution, and photographs of the solutions (i) before, (ii) directly after (with shaking), and (iii) 5 h after mixing with an identical volume of toluene, are illustrated in **Figure 7.5**. Given the reports^{1,6} of a coloured, lipophilic hydroxy adduct, some might be tempted to assume that all the thiazine dyes form such species and assign the highly coloured toluene solutions arising from alkaline treatment illustrated in **Figure 7.5** as being due to the *N*-hydroxy adducts of the associated thiazine. However, this work now shows that the reported red MB is, in fact, MVB and that the *N*-hydroxy adduct of any thiazine should be largely colourless. Thus, the alternative, less glamorous, but well established explanation for the results illustrated in **Figure 7.5** still stands, *i.e.* that the other thiazines are simply deprotonated by alkali to form highly coloured lipophilic species. The results in **Figure 7.5** also reveal that the thionine (**8**) and Azure C (**7**) pH 13 *aqueous* solutions (before mixing with toluene) are red, whereas those for Azure A (**6**) and Azure B (**5**) are purple. This feature arises because the pK_a for the thiazine dyes (see **Table 7.1**) decreases with decreasing degree of methylation, so that, for example, at pH 13 most (99%) of the thionine will be in its red, lipophilic deprotonated, free base form, whereas for Azure B at least 11.2% will still be in its purple-blue protonated form.²⁶

Table 7.2 Composition of commercial samples of thiazine dyes used in this study, determined by HPLC.

Commercial Thiazine	%MB (1)	%AB (5)	%AA (6)	%AC (7)	%TH (8)
MB (1)	91	8.7	<1	<1	<1
AB (5)	3	86	10	1	0
AA (6)	36	28	27	8	1
AC (7)	0	7	47	38	7.5
TH (8)	0	0	0	0	99+
MVB (4)	84% MVB, no other thiazines present				

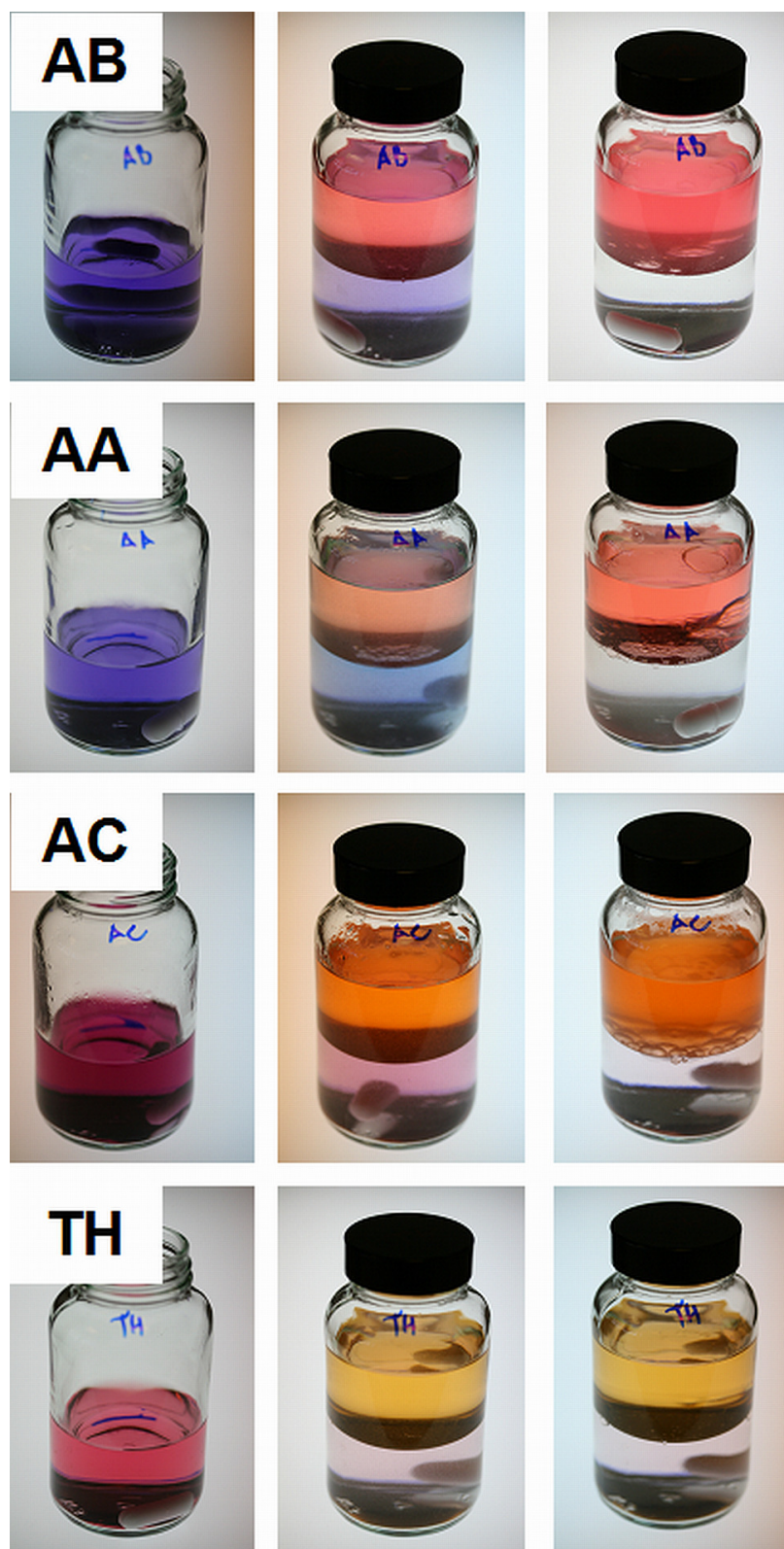


Figure 7.5 Photographs of a range of freshly made 10^{-4} M thiazine dye solutions in 0.1 M NaOH (from left to right): before, directly after, and 5h after mixing and shaking with an equal volume of toluene.

The calculated λ_{max} values in toluene of the deprotonated forms of the thiazine dyes, along with those found experimentally, are listed in **Table 7.1**. The experimental and calculated values compare very well (especially given the impure natures of Azure A and Azure C) and strongly support the deprotonation mechanism. Others³⁸ have used NMR spectroscopy to show that the yellow/orange lipophilic form of thionine, produced by treatment with alkali, is the deprotonated form of the parent dye.

7.4 CONCLUSIONS

The chemistry discussed in this chapter is summarized in **Figure 7.6**. Basic hydrolysis of MB leads mainly to the production of MVB, **4**, and the visible spectral properties of MVB in six solvents and on a TLC plate match very closely the reported properties of what has been claimed¹ to be an *N*-hydroxy adduct of MB, MB-OH (**2**). However, the calculated visible spectrum of MB-OH is reliably predicted to be colourless, not red, and the incorrectly assigned site of hydroxide attack in MB, the heterocyclic N-atom, is not electron deficient as suggested as a reason for MB-OH formation. No literature precedent was found for hydroxide attack at any sp²-hybridised nitrogen atom, and all the experimental evidence points to MVB (**4**) as the main product of alkaline hydrolysis of MB, and not MB-OH (**2**).

It is always difficult to prove a negative. It is not claimed that the nitrogen heterocyclic site in MB or any similar nitrogen can never be electrophilic in appropriate circumstances but rather it has not yet been demonstrated and available evidence, such as the results of calculation and site of protonation, indicate the opposite.

The other major cationic thiazine dyes, which contain one or more amine-attached hydrogen atoms, also do not form hydroxy adducts, but instead are deprotonated in 0.1 M NaOH solution to very differently coloured (λ_{max} hypsochromic shift in aqueous solution typically = 100-150 nm), red or orange lipophilic, free-base forms of the original dye (shown for Azure B, **5**, in **Figure 7.6**) It is also important to note

that similar product formation and spectral changes would be expected for oxazine and phenothiazine dyes.

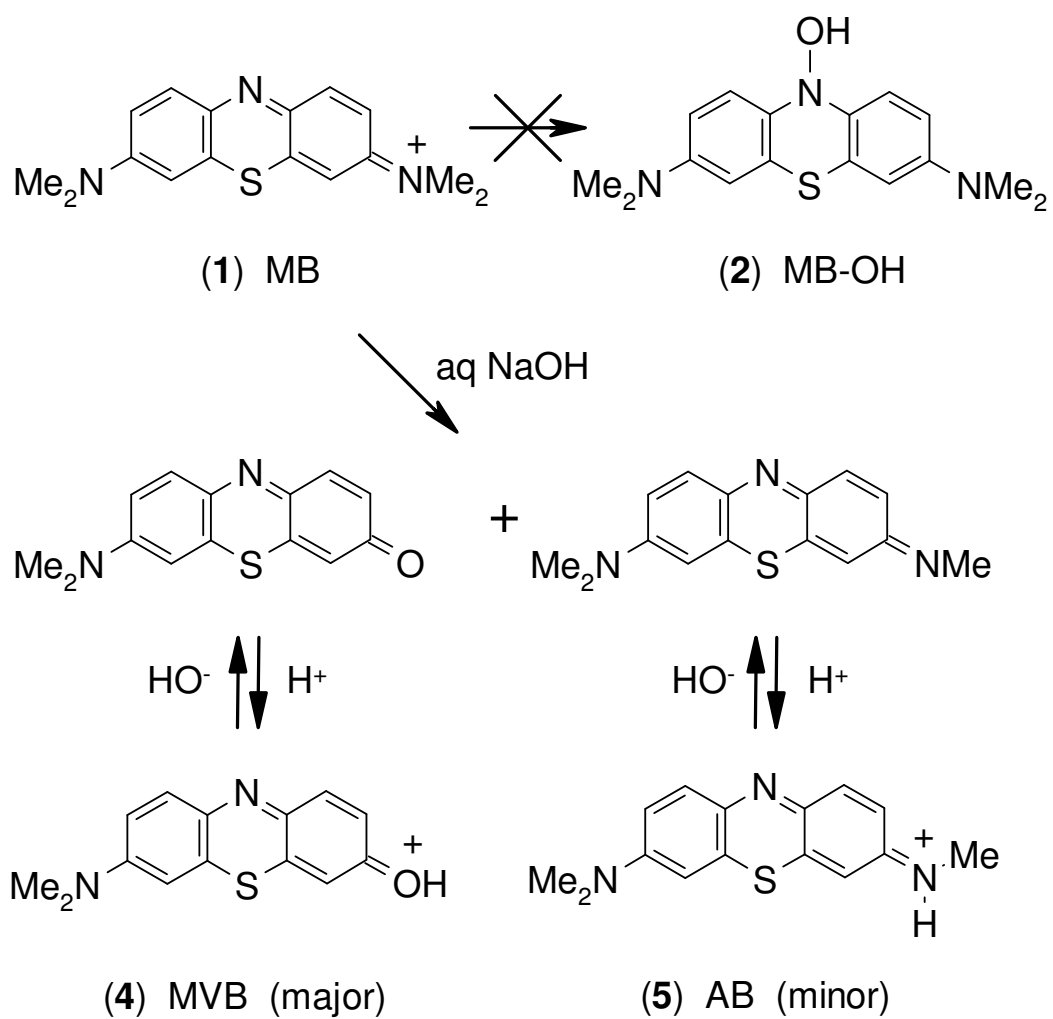


Figure 7.6 Summary of reactions of MB with alkali.

7.5 REFERENCES

1. S. Basu, S. Panigrahi, S. Praharaj, S. K. Ghosh, S. Pande, S. Jana, A. Pal and T. Pal, *J. Phys. Chem. A*, 2007, **111**, 578-583.
2. T. v. Thien (Chapter 3), in *Chemistry and applications of leuco dyes* ed. R. Muthyala, Plenum Press, New York, Editon edn., 1997, p. 67.
3. L. Adamcikova, K. Pavlikova and P. Sevcik, *React. Kinet. Catal. Lett.*, 2000, **69**, 91-94.
4. A. Mills, D. Hazafy, J. A. Parkinson, T. Tuttle and M. G. Hutchings, *J. Phys. Chem. A*, 2009, **113**, 9575-9576.
5. A. Pal, *J. Phys. Chem. A*, 2009, **113**, 9577.
6. M. J. Plater, *ARKIVOC*, 2003, 37-42.
7. H. Nishikiori, S. Nagaya, N. Tanaka, A. Katsuki and T. Fujii, *Bull. Chem. Soc. Jpn.*, 1999, **72**, 915-921.
8. P. N. Marshall and S. M. Lewis, *Stain Technol.*, 1976, **50**, 375-381.
9. V. Barone and M. Cossi, *Journal of Physical Chemistry A*, 1998, **102**, 1995-2001.
10. M. Cossi, N. Rega, G. Scalmani and V. Barone, *J. Comput. Chem.*, 2003, **24**, 669-681.
11. A. D. Becke, *Phys. Rev. A*, 1988, **38**, 3098-3100.
12. A. D. Becke, *J. Chem. Phys.*, 1993, **98**, 5648-5652.
13. R. H. Hertwig and W. Koch, *Chemical Physics Letters*, 1997, **268**, 345-351.
14. C. T. Lee, W. T. Yang and R. G. Parr, *Phys. Rev. B*, 1988, **37**, 785-789.
15. P. J. Stephens, F. J. Devlin, C. F. Chabalowski and M. J. Frisch, *Journal Of Physical Chemistry*, 1994, **98**, 11623-11627.
16. S. H. Vosko, L. Wilk and M. Nusair, *Can. J. Phys.*, 1980, **58**, 1200-1211.
17. P. C. Hariharan and J. A. Pople, *Theor. Chim. Acta*, 1973, **28**, 213-222.
18. R. Krishnan, J. S. Binkley, R. Seeger and J. A. Pople, *J. Chem. Phys.*, 1980, **72**, 650-654.
19. R. Bauernschmitt and R. Ahlrichs, *Chemical Physics Letters*, 1996, **256**, 454-464.
20. M. E. Casida, C. Jamorski, K. C. Casida and D. R. Salahub, *J. Chem. Phys.*, 1998, **108**, 4439-4449.
21. R. E. Stratmann, G. E. Scuseria and M. J. Frisch, *J. Chem. Phys.*, 1998, **109**, 8218-8224.
22. T. G. Frisch MJ, Schlegel HB, Scuseria GE, Robb MA, Cheeseman JR, Montgomery Jr. JA, Vreven T, Kudin KN, Burant JC, Millam JM, Iyengar SS, Tomasi J, Barone V, Mennucci B, Cossi M, Scalmani G, Rega N, Petersson GA, Nakatsuji H, Hada M, Ehara M, Toyota K, Fukuda R, Hasegawa J, Ishida M, Nakajima T, Honda Y, Kitao O, Nakai H, Klene M, Li X, Knox JE, Hratchian HP, Cross JB, Bakken V, Adamo C, Jaramillo J, Gomperts R, Stratmann RE, Yazyev O, Austin AJ, Cammi R, Pomelli C, Ochterski JW, Ayala PY, Morokuma K, Voth GA, Salvador P, Dannenberg JJ, Zakrzewski VG, Dapprich S, Daniels AD, Strain MC, Farkas O, Malick DK, Rabuck AD, Raghavachari K, Foresman JB, Ortiz JV, Cui Q, Baboul AG, Clifford S, Cioslowski J, Stefanov BB, Liu G, Liashenko A, Piskorz P, Komaromi I, Martin RL, Fox DJ, Keith T, Al-Laham MA, Peng CY, Nanayakkara A, Challacombe M, Gill PMW, Johnson B, Chen W, Wong

- MW, Gonzalez C, Pople JA., Gaussian, Inc., Wallingford CT, Editon edn., 2004.
23. A. E. Reed, R. B. Weinstock and F. Weinhold, *J. Chem. Phys.*, 1985, **83**, 735-746.
 24. D. C. Abbott, *Analyst*, 1962, **87**, 286-293.
 25. W. C. Holmes and E. F. Snyder, *Stain Technol.*, 1929, **4**, 7-10.
 26. R. Bonneau, J. Faure and J. Jousot-Dubien, *Talanta*, 1967, **14**, 121-122.
 27. The discoverer's name is frequently appended when naming the thiazine based Methylene Violet, to distinguish it from other species with the same or similar name e.g. Methylene Violet 3RAX, which has an unrelated safranine structure, 3-amino-7-(diethylamino)-5-phenyl phenazinium chloride; see Aldrich Catalogue 307505.,
 28. S. Otsuki and T. Taguchi, *Bull. Chem. Soc. Jpn.*, 1996, **69**, 2525-2531.
 29. M. J. Plater, Private Communication, February 2010.
 30. G. N. Lewis, O. Goldschmid, T. T. Magel and J. Bigeleisen, *J. Am. Chem. Soc.*, 1943, **65**, 1150.
 31. A. Mills, S.-K. Lee and A. Lepre, *J. Photochem. Photobiol. A: Chem*, 2003, **155**, 199.
 32. Beilstein database v.2008/04, via CrossFire Commander v.7.1, © Elsevier Information Systems.
 33. G. N. Lewis and J. Bigeleisen, *J. Am. Chem. Soc.*, 1943, **65**, 1144-1150.
 34. D. E. Falvey, *J. Phys. Org. Chem.*, 1999, **12**, 589-596.
 35. J. Griffiths and R. Cox, *Dyes Pigments*, 1999, **42**, 29-34.
 36. Unpublished Results
 37. H. Zollinger, *Color Chemistry*, third edn., VHCA and Viley-VCH, Zurich, 2003.
 38. V. E. Nicotra, M. F. Mora, R. A. Iglesias and A. M. Baruzzi, *Dyes Pigments*, 2008, **76**, 315-318.

CHAPTER 8

SUMMARY

8.1 DEVELOPMENT OF COLORIMETRIC INDICATORS BASED ON METHYLENE BLUE.

Ion-pairing of Methylene Blue (MB) with dodecyl sulphate (DS), produces a solvent-soluble form of the dye (MB-DS), which can be used to create a solvent-based, UV-activated, oxygen sensitive ink that can be printed on a variety of different hydrophobic polymers, including poly(ethylene terephthalate) (PET). The UV sensitizer in this ink is titania and P25 titania based films are bleached quite rapidly under O₂-free conditions by the relatively small amount of UVA light that is present in white fluorescent lights, such as 'cool white' tubes. After photobleaching these P25 films are also quite slow to recover their original colour when exposed to air in the dark. In contrast, nano-rutile based films are much less sensitive towards the UV light in white fluorescent tubes, even in the absence of O₂, and, in comparison, rapidly recover their original colour when exposed to air. The initial rate of recovery of the original colour of either P25, or nano-rutile MB-DS, photobleached films, in the 'dark' step (2) (see **Figure 1.5**), is proportional to the ambient level of oxygen, allowing these indicators to be used for both qualitative and quantitative analysis of the level of ambient oxygen simply by photobleaching with UVA light and monitoring the initial rate of colour recovery. Finally, these films can be re-used a number of times without exhibiting any evidence of photodegradation, brought on by the UVA activation step.

These solvent-based, colorimetric inks for oxygen appear to offer promise as a possible tamper-evident and/or leakage indicators for MAP packaged products.

The main drawbacks of the MB-DS ink identified in this chapter, the fact that it is susceptible to bleaching under most common visible light fluorescent tubes, is addressed by work carried out in chapter 4. Another drawback, its inability to remain completely insoluble to water, is addressed in chapter 5.

Nanocrystalline SnO₂ can be used as a photocatalyst in a UV-activated colorimetric oxygen indicator comprising: polymer/ SED/ redox dye/ photocatalyst, where polymer = HEC, donor = glycerol, dye = MB and photocatalyst = *n*SnO₂. Previous work had established that P25 TiO₂, although very effective, responds to the UVA component in most fluorescent tubes.

The larger band gap (3.65 eV) of $n\text{SnO}_2$, compared to P25 TiO_2 , renders it UVB, but not UVA, sensitive. In particular, $n\text{SnO}_2$ is unable to absorb photons due to the Hg vapour emission line at 365 nm and as a consequence, a HEC/glycerol/MB/ $n\text{SnO}_2$ film is not activated (*i.e.* photobleached) by the UVA component in white or UVA fluorescent tubes, but is activated by UVB light.

Other work on the $n\text{SnO}_2$ -based O_2 -indicator film reveals a fractional power dependence of the kinetics of UV activation on irradiance, *i.e.* $r_i \propto I^{0.75}$, and that the rate of its response towards oxygen, as measured by t_{50} , could be used to assess the ambient level of oxygen. The use of $n\text{SnO}_2$ as a photocatalyst in the UV activated oxygen-sensitive inks opens up many possible avenues of application as it allows the UV-activation step to be much more controllable. In particular, this modified ink has promise as a quality control and tamper-evident indicator in MAP.

The main drawback of this oxygen indicating system in respect to its potential use in MAP food packaging is its water-based nature and the subsequent disintegration after it is subjected to often very moist environment within such packages. In the next chapter an oxygen indicator that could be printed on plastics and is water stable is introduced.

A novel, solvent-based, water-proof oxygen indicator that coats on hydrophobic polymers, such as polypropylene, was prepared and characterised. The coloured indicator is readily photobleached but has a slow (24 h) recovery. The kinetics of the latter process are independent of [glycerol], [TiO_2] and [MB], but dependent upon RH above a value ca. of 20% at 20°C; the photobleached film does not recover its original colour below this value over a 24 h period. The very slow recovery process makes it possible to use the indicator as a ‘consume-within’ or humidity threshold indicator.

In the search for a solid state sacrificial electron donor it was discovered that a blue film of Methylene Blue, HEC and urea turned pink on drying and that this colour change was reversed on exposure to a humid air stream (relative humidity of over 70%). This colour change is reversible and could be performed repeatedly.

It was also discovered that a more dramatic and quite opposite colour change could be induced without urea, using a different polymer (HPC) and by ‘activating’ the film with a short burst of high heat (200 °C). This bright blue (dry), activated film was stable in ambient conditions but when exposed to a stream of 100% humid air would

almost instantly change to a bright pink/purple colour (wet). The film could be reactivated by heating and re-used over many cycles.

8.2 THE CHEMISTRY OF METHYLENE BLUE AND OTHER THIAZINE DYES

Basic hydrolysis of Methylene Blue leads mainly to the production of Methylene Violet (Bernthsen) (MVB), **4**, and the visible spectral properties of MVB in six solvents and on a TLC plate match very closely the reported properties of what has been claimed to be an *N*-hydroxy adduct of MB, MB-OH (**2**). However, the calculated visible spectrum of MB-OH is reliably predicted to be colourless, not red, and the incorrectly assigned site of hydroxide attack in MB, the heterocyclic N-atom, is not electron deficient as suggested as a reason for MB-OH formation. No literature precedent for hydroxide attack at any sp²-hybridised nitrogen atom has been found, and all the experimental evidence points to MVB (**4**) as the main product of alkaline hydrolysis of MB, and not MB-OH (**2**).

It is not claimed that the nitrogen heterocyclic site in MB or any similar nitrogen can never be electrophilic in appropriate circumstances but rather it has not yet been demonstrated and available evidence, such as the results of calculation and site of protonation, indicates the opposite.

The other major cationic thiazine dyes, which contain one or more amine-attached hydrogen atoms, also do not form hydroxy adducts, but instead are deprotonated in 0.1 M NaOH solution to very differently coloured (λ_{max} hypsochromic shift in aqueous solution typically = 100-150 nm), red or orange lipophilic, free-base forms of the original dye (shown for Azure B, **5**, in **Figure 7.6**) It is also important to note that similar product formation and spectral changes would be expected for oxazine and phenothiazine dyes.

8.3 FURTHER WORK

The first three experimental chapters covered the development and optimisation of the concept of an ideal colorimetric, commercially useful MAP oxygen indicator. Research on this has continued, although none of it is presented in this thesis.

Better control over the rather long recovery times of inks based on sulfonated polystyrene (SPS) would be required to more finely tune the ink to be used with different foods. Initial results have shown that platinised TiO₂ (platinum colloid precipitated onto TiO₂ photocatalyst) is somehow able to speed up the recovery (from 24 to 8 hours, under similar conditions). Further investigation into the mechanism of this phenomenon should result in much finer control of the response of the ink to oxygen.

The demands made of the printing industry to use less volatile organic solvents are increasing all the time so a different solvent system (alcohol or water most probably) may be required in the future. In addition, the ink's viscosity has not been studied in great detail and may have to be altered substantially in order to make printing on a large scale possible. Printing trials have already been carried out with inks using different solvents such as ethyl acetate, ethanol and even a blend of ethanol/water. It was found that the solubility of SPS in some of these systems had to be tuned by varying the degree of sulfonation.

The main application of this indicator, because of its slow recovery (especially at lower temperatures), is now considered to be as a 'consume-within' time-temperature indicator (TTI). In this scenario, a thin film of the indicator is printed on the packaging material and this is covered by a plastic sheet that has low oxygen permeability and can be easily peeled off by a customer. A 'consume within' label is highly sought after by leading supermarkets and a modification of the described ink is currently undergoing production trials for a leading supermarket chain.

Further investigation is needed to fully understand and prove the mechanisms responsible for colour changes observed when Methylene Blue and various polymers are combined and subjected to changes of temperature and humidity. Dyes other than Methylene Blue which have a greater or lesser propensity to form differently coloured H- or J-aggregates could be tested in combination with polymers of varying polarities

and/or melting points. This might shed light on the mechanism and lead to a range of thermally-activated humidity sensors being developed which can be tailored to a specific application.

Regarding the alkaline hydrolysis of Methylene Blue, work is also underway to further investigate the mechanism of this transformation. Interestingly, under visible light illumination, the presence of oxygen can selectively determine whether Methylene Violet (MVB) or Azure B (AB) is the main product. Another experiment revealed a photochemical step in this reaction that leads predominantly to Azure B and not to Methylene Violet. Presumably, oxygen molecules quench the excited states of Methylene Blue, so promoting the formation of Methylene Violet instead of Azure B. Oxazines, dyes similar to phenothiazines, were subjected to this reaction and initial results showed products analogous to that obtained with the phenothiazines.

A solvent-based intelligence ink for oxygen

Andrew Mills* and David Hazafy

Received 31st August 2007, Accepted 7th November 2007

First published as an Advance Article on the web 23rd November 2007

DOI: 10.1039/b713450a

A solvent-based, irreversible oxygen indicator ink is described, comprising semiconductor photocatalyst nanoparticles, a solvent-soluble redox dye, mild reducing agent and polymer. Based on such an ink, a film – made of titanium dioxide, a blue, solvent-soluble, coloured ion-paired methylene blue dye, glycerol and the polymer zein – loses its colour rapidly (<30 s) upon exposure to UVA light and remains colourless in an oxygen-free atmosphere, returning to its original blue colour upon exposure to air. In the latter step the rate of colour recovery is proportional to the level of ambient oxygen and the same film can be UV-activated repeatedly. The mechanism of this novel, UV-activated, solvent-based, colorimetric oxygen indicator is discussed, along with its possible applications.

Introduction

Oxygen is an essential feature of respiration in most organisms and, as such, is a key element in life. Oxygen is also the main reason for food spoilage, not only because it can react chemically with food, but also because its presence is essential for the growth of moulds and other aerobic micro-organisms. It is no surprise, therefore, that a popular method to keep food fresh is to reduce the oxygen content within the package *via* modified atmosphere packaging (MAP), in which the air is flushed out, usually to be replaced with either nothing (as in vacuum packaging), nitrogen or carbon dioxide.^{1,2} The importance of oxygen in many areas and processes is reflected by the large number of analytical methods for making measurements of the percentage of oxygen, %O₂, in the gas phase or saturated in solution.^{3–7} However, many of these oxygen sensors require the use of expensive equipment, and a trained operator and, as a consequence, are not conducive to the measurement of O₂ in a food package.

One solution to this problem is the use of oxygen indicators designed to change colour upon exposure to oxygen, such as Mitsubishi Gas Corporation's commercial, reversible, colorimetric oxygen indicator, Ageless-Eye™; applied either in pellet or label form, it comprises a strong reducing agent and a redox-indicator, such as methylene blue, that is easily re-oxidised by oxygen from its chemically reduced, colourless form.⁸ However such indicators are not cheap, and with their continuous action and high oxygen sensitivity, nor are they easily handled or stored. As a consequence, they are neither appropriate nor promoted as a routine indicator for MAP.

An ideal oxygen indicator should be colorimetric (rendering it detectable by eye), non-toxic and have non-water-soluble components, which preferably have food contact approval, since this addresses the need to place the indicator inside the food package.⁹ It should also have an irreversible response

towards oxygen, since a reversible indicator would give a false-negative reading if a package suffers a very minor break in its integrity and the level of microbe metabolism inside the package rises to such a level that the small rate of oxygen ingress is matched by the rate of microbe respiration; at which point the atmosphere in the package will be largely carbon dioxide.

A new range of oxygen colorimetric indicators have been developed recently,¹⁰ which are irreversible, re-usable, UV-light-activated and use methylene blue as the redox dye indicator. The irreversible nature of the indicator is achieved by using UV-light-activated, nanoparticulate TiO₂, a semi-conducting material with a bandgap of *ca.* 3.2 eV. The use of nano, rather than micro, particulate crystalline titania is preferred since such material has a much higher specific surface area, and as a consequence much less titania is required to make effective inks for oxygen. In addition, nanoparticulate titania can exhibit a much greater photoactivity due to quantisation effects.¹¹

The basic working principles of such an irreversible oxygen indicator are illustrated in Fig. 1. Thus, upon irradiation with UVA light, ultra-bandgap illumination of the TiO₂ semiconductor photo-sensitiser particles create electron-hole pairs [TiO₂* (e⁻, h⁺)]. The photo-generated holes, h⁺, oxidise the

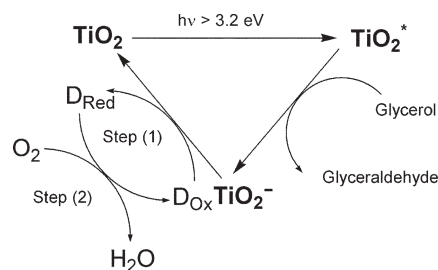


Fig. 1 Schematic illustration of the key processes involved in the UV-activation and subsequent response towards oxygen of a TiO₂/MB/glycerol/HEC visual oxygen indicator. Step (1) refers to photo-induced reduction of the redox-sensitive dye D_{Ox} (MB) to its reduced form, D_{Red}, colourless LMB, whereas step (2) illustrates the 'dark' back re-oxidation of the dye, leading to recovery of its initial colour, by the ambient oxygen.

WestCHEM, Department of Pure & Applied Chemistry, University of Strathclyde, Thomas Graham Building, Glasgow, UK G1 1XL.
E-mail: a.mills@strath.ac.uk; Fax: +44 (0) 141 548 4822;
Tel: +44 (0) 141 548 2458

mild sacrificial electron donor (SED), glycerol to glyceraldehyde. The remaining photo-generated electrons, *i.e.* TiO_2^- in Fig. 1, reduce the redox-sensitive dye, D_{Ox} (in this work D_{Ox} = methylene blue, MB), to a reduced form, D_{Red} (leuco-methylene blue, LMB) that has a different colour to D_{Ox} . The above key components are encapsulated in a polymer, usually hydroxyethyl cellulose (HEC), to create an O_2 -sensitive, UV-activated film, but all are readily dissolved or dispersed in water to create an intelligent, water-based ink for oxygen.¹⁰ The major drawback of this indicator is the hydrophilic, water-soluble nature of the ink, which limits its applications, especially in food packaging, since it is difficult to print such an ink on the mostly hydrophobic plastics used in packaging, such as polypropylene (PP), poly(ethylene terephthalate) (PET) or nylon. In this paper we describe the preparation and characterisation of a colorimetric, UV-activated solvent-based intelligent ink for oxygen, that readily wets and prints onto such plastics.

Experimental

Materials and chemicals

The semiconductor photocatalysts employed to make the inks were: P25 TiO_2 , a mixture of the two TiO_2 crystalline phases, rutile (20%) and anatase (80%) (kindly donated by the Degussa Corporation), and nanopowder rutile TiO_2 from Aldrich. Unless stated otherwise all other chemicals were from Aldrich Chemicals, with the exception of the ethanol-soluble polymer zein, from Fluka. A typical zein polymer solution was prepared by adding 10 g of zein to a solution of 36 g of ethanol and 4 g of water. The supporting substrate, 40 μm PET foil, used to print the final, solvent-based ink, was provided by Crown Holdings Inc. Other hydrophobic polymer substrates, such as nylon, and PP appeared equally effective.

Preparation of solvent-soluble methylene blue (MB)-based films

Methylene blue (MB), a cationic thiazine redox dye, is very water soluble and in order to render it solvent-soluble and water-insoluble, its water-soluble cationic form was ion-paired with a solvent-soluble anion, dodecyl sulfate (DS). The product, MB-DS is water-insoluble, but solvent-soluble. To make MB-DS, 3.74 g (0.01 mol) of MB were dissolved in 200 mL of water and a solution of 2.88 g (0.01 mol) of sodium dodecyl sulfate (SDS) in 150 mL of water added. The mixture was stirred for 12 h, and then chilled to 4 °C for 2 h. The resulting dark blue precipitate was filtered, using a glass frit, washed with water and dried overnight in an oven to give 3.9 g of the desired product, MB-DS. The solvent-based oxygen ink was prepared by combining 3 g of the zein solution with 600 mg of glycerol, 600 mg of titania photocatalyst and 15 mg of the MB-DS dye. The resulting mixture was stirred for 30 min, followed by 30 min sonication to ensure that all of the photocatalyst particles were well dispersed and the MB-DS, glycerol and zein dissolved. The resulting dark blue ink was then cast onto a PET plastic foil using a drawdown technique (RK Print-Coat Instruments Ltd, K-bar No. 2) to produce a film with an average thickness of *ca.* 5 μm . The film was dried in air and stored in the dark.

Irradiation and colour change measurements

In order to make useful absorbance measurements using diffuse reflectance, the MB-DS ink-coated plastic foil, which was highly coloured but also opaque, was cut to fit in a brass gas cell that could be used to maintain the sample in different controlled gaseous atmospheres (*e.g.* N_2 or O_2 or mixtures thereof). In most of the initial work the variation in the diffuse reflectance parameter, FR, was monitored as a function of irradiation time under either aerobic or anaerobic conditions. In a later study of the rate of colour recovery (after photo-bleaching) as a function of % O_2 , the MB-DS film was first irradiated, *i.e.* photo-bleached, outside the gas cell using 2 × 8 W blacklight blue (BLB) UVA tubes (Philips F8/T5/BLB in a Vilber-Lourmat, model no. VL-208 irradiation unit, irradiance = 10 mW cm^{-2}), then placed in the gas cell in a gaseous environment of known % O_2 , produced using a calibrated gas blender, flowing at 300 mL min^{-1} , and its spectrum recorded using a Perkin Elmer Lambda 20 spectrophotometer as a function of time using a diffuse reflectance attachment (Labsphere RSA-PE-20).

In all diffuse reflectance work, the data obtained were reported as the percentage reflectance relative to a white standard reflectance plate, R'_∞ ; the latter was made of non-absorbing material (MgO) that optimally diffuses light. Kubelka and Munk theory for the diffuse reflectance of dyes adsorbed on powdered samples shows that the Kubelka–Munk function (FR), at any wavelength where the dye absorbs, varies linearly with concentration, C ,^{12,13} *i.e.*

$$\text{FR} = \frac{(1 - R'_\infty)^2}{2R'_\infty} = \alpha b C \quad (1)$$

where α is the molar absorptivity of the dye at that wavelength, C is its concentration and b a constant. It follows that in this work the reflectance data can be used to generate the associated FR value at the wavelength of maximum absorption, λ_{max} , which in turn is related to the concentration of the oxidised dye, MB, in the film. The variation in the batch-to-batch reproducibility of these films for both the photo-bleaching, and, more crucially, the dark colour recovery step was better than $\pm 5\%$, which is acceptable for many qualitative or semi-qualitative analyses of oxygen levels.

Results and discussion

MB-DS solvent-based oxygen indicator

Using a typical MB-DS ink to create a film on PET, nanopowder TiO_2 was used as the semiconductor, and the diffuse reflectance spectra of the highly coloured film recorded before and after exposure to 5 s of UVA light ($I = 10 \text{ mW cm}^{-2}$), the results of which are illustrated in Fig. 2. From these results it is clear that the initially highly coloured MB-DS film is photo-bleached rapidly (*i.e.* within 5 s) by the UV light. In the absence of any of the ingredients (*i.e.* TiO_2 or glycerol) this photo-bleaching process does not occur; nor is it effected using visible, rather than UV light.

Fig. 3 contains photographs of a typical ink cast onto a film of PET through a metal template, with the letters 'TiO₂' cut

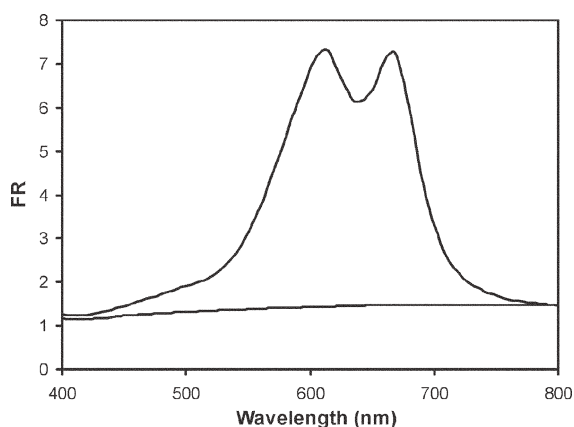


Fig. 2 Typical diffuse reflectance spectrum of $\text{TiO}_2/\text{MB-DS}/\text{glycerol}/\text{zein}$ oxygen indicator, before and after UVA light irradiation (provided by two 8 W blacklight blue tubes), typically for 5 s. The absence of a peak in the latter spectrum indicates that all dye has been reduced to its colourless, LMB form ($I = 10 \text{ mW cm}^{-2}$). FR is the Kubelka–Munk function [see eqn (1)].

through it. The product was a PET film with the image ‘ TiO_2 ’ in blue ink printed on its surface. As illustrated by the results in Fig. 3, this image was photo-bleached upon UV irradiation

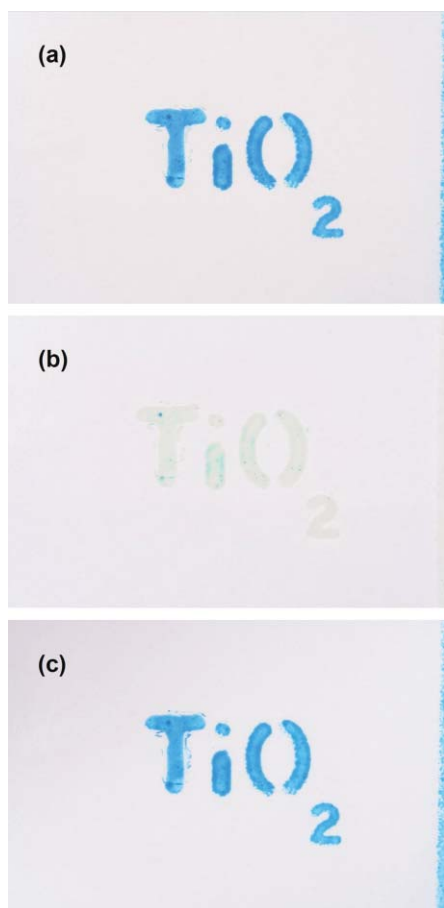


Fig. 3 Photographs of a typical oxygen indicator ink printed as the letters ‘ TiO_2 ’ on plastic. The photographs are for a nano-rutile $\text{TiO}_2/\text{MB-SD}/\text{glycerol}/\text{zein}$ film (a) before, (b) after a 30 s exposure to UVA light ($I = 10 \text{ mW cm}^{-2}$), and (c) 1 h after (b) and storage in the dark in air.

(30 s, $I = 10 \text{ mW cm}^{-2}$) in air [i.e. step (1) in Fig. 1], but subsequently regained its original blue colour in the absence of UV irradiation after 60 min, due to the re-oxidation of LMB [i.e. via step (2) in Fig. 1].

The photo-bleaching process [step (1)]

An important feature of the MB-SD ink is that it is activated, i.e. rendered oxygen-sensitive, by converting MB to LMB using UV light, i.e. light not absorbed by the dye, which has an absorption window in the 330–400 nm region, but rather by the semiconductor photocatalyst particles of titania. Evidence that the titania, and not the dye, is the light-absorbing species responsible for the photo-bleaching process is provided by the observation that visible light (i.e. $\lambda > 400 \text{ nm}$) is not able to photo-bleach the ink. However, most visible fluorescent lights, such as the ‘cool white’ light fluorescent tubes used in food cabinets, have a UVA spike in their emission profiles at 365 nm.

At a normal distance (i.e. $>10 \text{ cm}$) this ‘spike’ is not usually sufficient in intensity ($<0.01 \text{ mW cm}^{-2}$) to photo-bleach a typical MB-SD ink film in air, because the rate of photo-bleaching, i.e. step (1) in Fig. 1, is then very low compared with that of step (2) in Fig. 1, the LMB re-oxidation, colour-recovery step. However, in the absence of oxygen, i.e. in nitrogen, $2 \times 8 \text{ W}$ ‘cool white’ fluorescent tubes (HYBEC F8/T5/CW in a Vilber-Lourmat, model no. VL-208 irradiation unit), when placed close up ($<1 \text{ cm}$) to a MB-SD film, are able to photo-bleach the MB to LMB, albeit very slowly, via step (1), since the colour-recovery step (2), is absent and the UVA irradiance significant, i.e. typically $>0.01 \text{ mW cm}^{-2}$.

This photo-bleaching (activation) by the UVA light component in a white fluorescent tube, in the absence of O_2 , is undesirable if these indicators are to be incorporated in food packages, as such lamps are used in food cabinets and could lead to the reactivation of the O_2 indicator (i.e. photo-bleaching) if the package’s integrity has been compromised (i.e. a false-negative result). However, the UVA absorptivity of titania depends upon many factors, including particle size and morphology, since both can produce a change in the bandgap of the semiconductor and absorptivity. An illustration of this feature was provided by a series of irradiations, using either two 8 W BLB, i.e. UVA ($I = 3 \text{ mW cm}^{-2}$), or two 8 W ‘cool white’ light fluorescent tubes ($I = 0.05 \text{ mW cm}^{-2}$), on two otherwise identical ink films, containing either nanoparticulate rutile, or Degussa P25 titania. The values of the Kubelka–Munk function of these films, i.e. FR, were measured at λ_{max} (665 nm) for MB in the dried ink as a function of irradiation time and the results are illustrated in Fig. 4. These show that whereas both films are photo-bleached at a similar rate using UVA light from a blacklight blue UVA lamp, the rate is slower when a ‘cool white’ lamp placed very close to the films is used as a source of UVA, especially for the nanoparticulate rutile films. Fig. 5 illustrates TEM images of both the P25 titania and nanoparticulate rutile titania and reveal some striking differences, including that P25 titania comprises primary particles of ca. 30 nm diameter, aggregated together to form larger (up to 0.1 μm) particles, whereas the nano-rutile powder comprises thin, needle-like particles (ca. $15 \times 70 \text{ nm}$) that are less

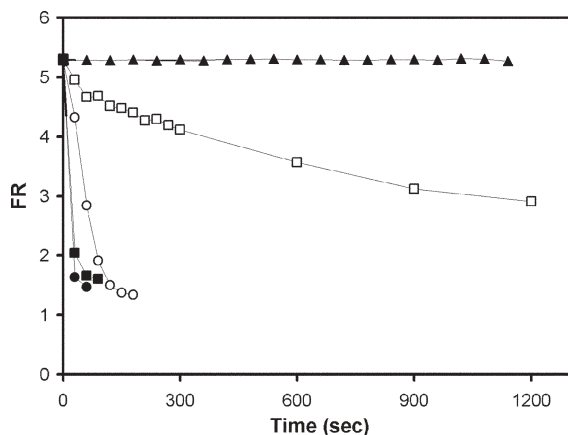


Fig. 4 Plots of FR as a function of irradiation time profiles for the photo-bleaching of P25 and TiO₂ nano-rutile films in N₂ using different light sources conditions. The top straight line refers to P25 and nano-rutile films in the dark (▲). In contrast, the Degussa P25 film irradiated using two 8 W 'cool white' lights (○) is bleached rapidly, whereas the nano-rutile TiO₂ is not (□). When irradiated with two 8 W blacklight blue (BLB) lamps, *i.e.* the usual UVA source used in this work, nano-rutile TiO₂ (■) and P25 (●) were both bleached very rapidly. The irradiance of the incident UVA light was 3 mW cm⁻², when using the 2 × 8 W UVA BLB lamps, and 0.05 mW cm⁻², when using 2 × 8 W 'cool white' fluorescent lights.

aggregated. The latter particles appear to absorb the light associated with the UVA 'spike' in the 'cool white' lamps much less than those in P25 TiO₂, possibly due to a slightly larger bandgap arising from a quantisation effect.¹⁴ Whatever the cause, it is promising to note that these nano-rutile, MB-DS films are not very sensitive to the UVA component in visible fluorescent lamps even when the latter are placed very close (<1 cm).

The kinetics of the photo-reduction of MB to LMB, *i.e.* step (1), is obviously UV irradiance-dependent and an investigation of this feature, using a typical nano-rutile ink, generated the plot of normalised initial rate, R_i [where the initial rate, $r_i = (dFR/dt)_{t=0}$ and $R_i = r_i/FR_{t=0}$] versus the incident UVA irradiance, illustrated in Fig. 6. The plot is typical of many photocatalytic systems,¹⁵ in which, at low irradiances, the initial rate is found to be either proportional to the irradiance, I (indicating that electron-hole recombination is not significant) or proportional to $I^{1/2}$ at high irradiances (indicating that recombination is the predominant fate of photo-generated electron-hole pairs). Often, at intermediate irradiances, the initial rate is found to be proportional to I^θ , where $0.5 < \theta < 1$, and the results of this work are an example of such a case, with $\theta = 0.61$, as indicated by the insert plot of the data in Fig. 6. The low, near 0.5 value, of θ indicates that electron-hole recombination is very significant in these films.

The 'dark' recovery process [step (2)]

Once photo-bleached using UVA light, the solvent-based ink films are very stable in the absence of O₂, remaining colourless for over 12 months, but able to regain their original colour by reacting with ambient oxygen, as illustrated by the photographs in Fig. 3. Fig. 7 illustrates the typical 'dark' recovery in

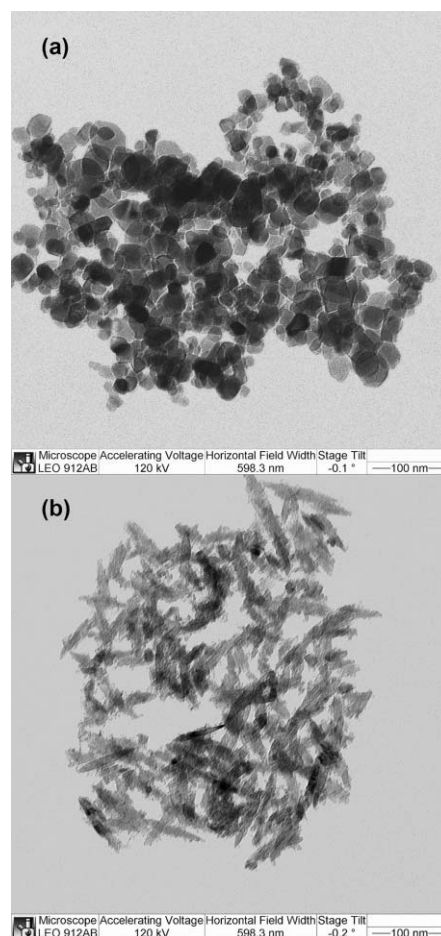


Fig. 5 TEM pictures of Degussa P25 TiO₂ (a) and nano-rutile TiO₂ (b) revealing very different morphologies that may be responsible for the different photoactivities. P25 particles appear aggregated together, forming large clusters; a fact reflected by the smaller surface area for P25 (50 m² g⁻¹) compared to that of nano-rutile TiO₂ (120 m² g⁻¹).

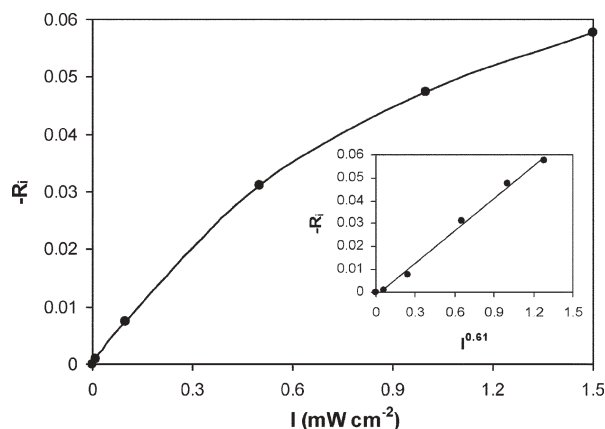


Fig. 6 Plots of normalised initial rate [$R_i = (dFR/dt)_{t=0}/FR_{t=0}$] vs. incident UVA light irradiance, I . The insert diagram shows the initial rate data vs. $I^{0.61}$, where $\theta = 0.61$. This value for θ indicates that electron-hole recombination is significant in these films.

the diffuse reflectance spectrum of a UV-bleached, nano-rutile, MB-DS ink in air and reveals that its final spectral features are very close to its original.

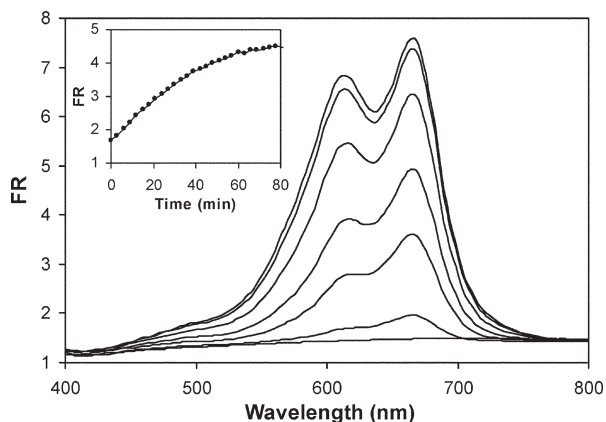


Fig. 7 Dark recovery in the diffuse reflectance spectrum of a nano-rutile TiO₂/MB-DS/glycerol/zein oxygen indicator film after an initial 5 s irradiation with UVA light ($I = 10 \text{ mW cm}^{-2}$). These spectra were recorded in a flow of oxygen (300 mL min^{-1}) for the following times (bottom to top): 0, 3, 6, 9, 15, 30 and 51 min. The inserted plot, recorded in air, shows the variation in FR at λ_{max} for the dark recovery of a photo-bleached nano-rutile TiO₂ (●) film in air (300 mL min^{-1}).

In a separate study, the variation of the initial rate of this recovery, R_i , was studied as a function of the %O₂ in the gas phase, using the nano-rutile ink, and the results are illustrated in Fig. 8. These results show that although, curiously, the 'dark' recovery of colour of a photo-bleached film is slower for a P25/MB-DS film than a nano-rutile film, in both cases the initial rate is directly proportional to %O₂ and so can be used to provide a quantitative measure of the %O₂ in the ambient gas phase. The direct relationship between R_i and %O₂ is not unexpected given the dark reaction responsible is step (2) in Fig. 1, *i.e.* the reaction of photo-generated LMB with O₂. It is not clear why the photo-bleached P25 films react more slowly with O₂ than nano-rutile films, although the latter pigment does have a greater surface area ($120 \text{ m}^2 \text{ g}^{-1}$) than the former ($50 \text{ m}^2 \text{ g}^{-1}$) and the effect may be simply related to a difference in available surface area.

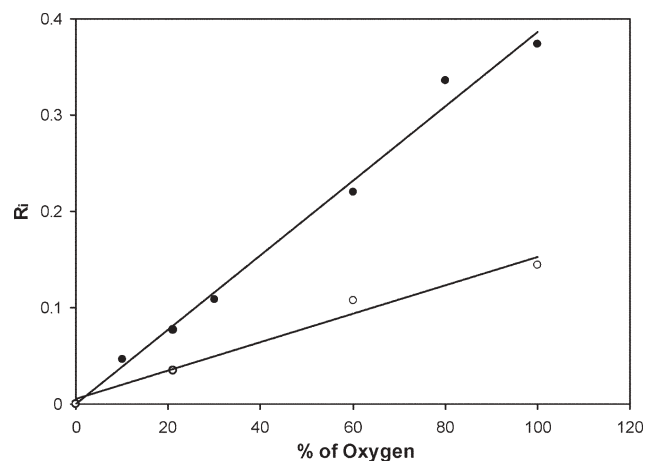


Fig. 8 Initial recovery rates for Degussa P25 (○) and nano-rutile TiO₂ (●) films plotted as a function of the ambient %O₂ in the gas cell. In this work the films were initially photo-reduced with UVA light ($I = 10 \text{ mW cm}^{-2}$ for 5 s).

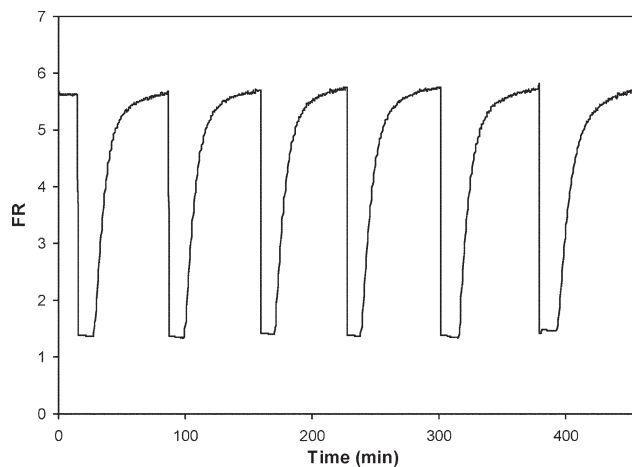


Fig. 9 Variation in FR as a function of time recorded for a typical TiO₂/MB-DS film subjected to repeated UVA irradiation ($I = 10 \text{ mW cm}^{-2}$) and dark recovery in O₂ (six cycles). Irradiation with UVA light was for 5 s (in Ar) and followed by 60 min dark recovery in oxygen at a flow rate of 300 mL min^{-1} .

The above solvent-based, UVA-activated, colorimetric oxygen indicator inks can be re-used a number of times without showing any evidence of deterioration. Thus, a typical nano-rutile titania MB-DS film was subjected to six cycles of a UVA photo-bleaching (in Ar) step followed by a dark recovery step (in O₂), whilst its FR value at λ_{max} (665 nm) was monitored as a function of time. The results of this work are illustrated in Fig. 9 and show that, with each irradiation step, the film is photo-bleached to the same extent in Ar and recovers completely its original colour within *ca.* 40 min in O₂. These results highlight the re-usability of the ink.

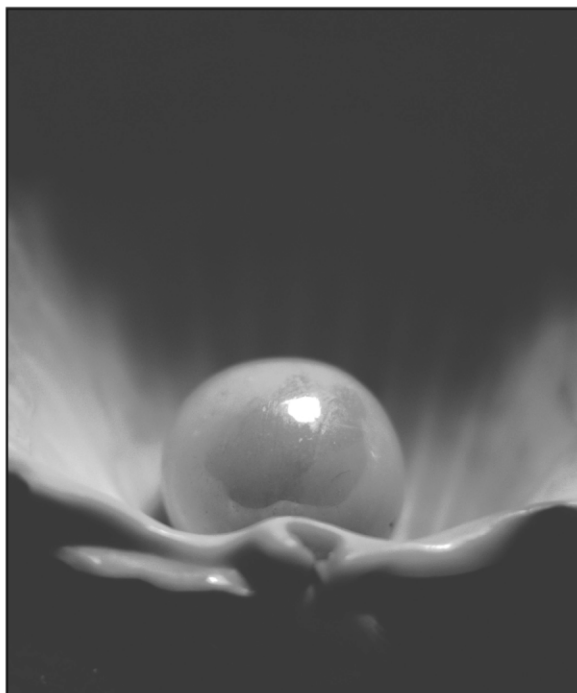
Conclusion

Ion-pairing of MB with dodecyl sulfate (DS), produces a solvent-soluble form of the dye, which can be used to create a solvent-based, UV-activated, oxygen-sensitive ink that can be printed on a variety of different hydrophobic polymers, including poly(ethylene terephthalate) (PET). The UV sensitizer in this ink is titania and P25 titania-based films are bleached quite rapidly under O₂-free conditions by the relatively small amount of UVA light that is present in white fluorescent lights, such as 'cool white' tubes. After photo-bleaching these P25 films are also quite slow to recover their original colour when exposed to air in the dark. In contrast, nano-rutile-based films are much less sensitive towards the UV light in white fluorescent tubes, even in the absence of O₂, and, in comparison, recover their original colour more rapidly when exposed to air. The initial rate of recovery of the original colour of either P25, or nano-rutile MB-DS, photo-bleached films, in the 'dark' step (2) (see Fig. 1), is proportional to the ambient level of oxygen, allowing these indicators to be used for both qualitative and quantitative analysis of the level of ambient oxygen simply by photo-bleaching with UVA light and monitoring the initial rate of colour recovery. Finally, these films can be re-used a number of times without exhibiting any evidence of photo-degradation brought on by the UVA activation step.

These solvent-based, colorimetric inks for oxygen appear to offer promise as possible tamper-evident and/or leakage indicators for MAP packaged products.

References

- 1 A. L. Brody, B. R. Strupinsky and L. R. Kline, *Active Packaging for Food Applications*, Technomic Publishing Co, Lancaster, 2001.
- 2 M. L. Rooney, *Active Food Packaging*, Blackie, London, 1995.
- 3 M. Goto, *JP Pat.*, 62 259059, 1987.
- 4 Y. Yoshikawa, T. Nakazawa, M. Goto and Y. Fujii, *US Pat.*, 4 169 811, 1979.
- 5 E. S. Davis and C. D. Garner, *UK Pat.*, 2 298 273, 1996.
- 6 Y. Yoshikawa, T. Nakazawa, M. Goto and Y. Kondo, *US Pat.*, 4 349 509, 1982.
- 7 H. Nakamura, T. Nakazawa and Y. Kawamura, *JP Pat.*, 62 183834, 1987.
- 8 M. Sumitani, H. Inoue and K. Sugito, *US Pat.*, 6703245, 2004.
- 9 A. Mills, *Chem. Soc. Rev.*, 2005, **34**, 1003–1011.
- 10 S. Lee, A. Mills and A. Lepre, *Chem. Commun.*, 2004, 1912–1913.
- 11 C. Kormann, D. W. Bahnemann and M. R. Hoffmann, *J. Phys. Chem.*, 1988, **92**, 5196–5201.
- 12 M. P. Fuller and P. R. Griffiths, *Anal. Chem.*, 1978, **50**, 1906–1910.
- 13 P. Kortum, W. Braun and G. Herzog, *Angew. Chem., Int. Ed. Engl.*, 1963, **2**, 333–341.
- 14 T. Toyoda and I. Tsuboya, *Rev. Sci. Instrum.*, 2003, **74**, 782–784.
- 15 G. Rothenbergen, J. Moser, M. Graetzel, N. Serpone and D. K. Sharma, *J. Am. Chem. Soc.*, 1985, **107**, 8054–8059.



Looking for that **special** research paper from applied and technological aspects of the chemical sciences?

TRY this free news service:

Chemical Technology

- highlights of newsworthy and significant advances in chemical technology from across RSC journals
- free online access
- updated daily
- free access to the original research paper from every online article
- also available as a free print supplement in selected RSC journals.*

*A separately issued print subscription is also available.

Registered Charity Number: 207890

22030683

RSC Publishing

www.rsc.org/chemicaltechnology



Nanocrystalline SnO₂-based, UVB-activated, colourimetric oxygen indicator

Andrew Mills*, David Hazafy

WestCHEM, Department of Pure & Applied Chemistry, University of Strathclyde, Thomas Graham Building, Glasgow G1 1XL, UK

ARTICLE INFO

Article history:

Received 13 June 2008

Received in revised form 6 December 2008

Accepted 15 December 2008

Available online 31 December 2008

Keywords:

Oxygen

Photocatalyst

Tin(IV) oxide

Indicator

ABSTRACT

Nanocrystalline SnO₂, *nc*SnO₂, is used as a photosensitiser in a colourimetric O₂ indicator that comprises a sacrificial electron donor, glycerol, a redox dye, methylene blue (MB), and an encapsulating polymer, hydroxyethyl cellulose (HEC). Upon exposure to a burst of UVB light the indicator is activated (photo-bleached) as the MB is photoreduced by the *nc*SnO₂ particles. In the absence of oxygen, the film stays bleached, but recovers its original colour upon exposure to oxygen. Unlike its TiO₂-based predecessor, the HEC/glycerol/MB/*nc*SnO₂ O₂ indicator is not activated by UVA light from white fluorescent lamps, but is by UVB light. This feature provides much greater control in the activation of the indicator. Other work shows the rate of activation depends upon $I^{0.75}$, where I is the UVB irradiance, indicating a partial dependence upon the electron–hole recombination process. The half-life of the recovery of the original colour of a UV-activated film, t_{50} , is directly proportional to the ambient level of oxygen. The advantages of using this indicator in modified atmosphere packaging as a possible quality assurance indicator are discussed briefly.

© 2008 Elsevier B.V. All rights reserved.

1. Introduction

Oxygen is an essential feature of respiration in most organisms and is involved in many chemical reactions. As a result, oxygen is one of the most commonly analyzed chemical species and popular techniques include: gas chromatography, voltammetry (Clark cell) and conductivity (metal oxide cells). Most such analytical systems are expensive and require trained personnel to use and maintain the equipment.

One area where the rapid, inexpensive, simple measurement of oxygen is needed is modified atmosphere packaging (MAP), in which the air is flushed out, usually to be replaced with either nothing (as in vacuum packaging) or, nitrogen or carbon dioxide [1,2]. MAP helps ensure that food spoilage microorganisms do not proliferate rapidly and, thus, food stays fresh for longer than if stored in air. Most packaged food is MAP packaged and yet there is, as yet, no simple inexpensive indicator of oxygen ingress that could provide 100% quality assurance [3,4]. Ideally such an indicator should be colourimetric as it would then be assessable by eye and require little or no training before use [5].

Previous work has established that a colourimetric oxygen indicator of promise with respect to MAP can be created using a semiconductor photosensitiser (SC) coupled with a redox dye (D_{ox}) and a sacrificial electron donor (SED) in the form of an intelligent ink [6,7]. In this system, the semiconductor, usually TiO₂, absorbs

UV light in an activation step, creating electron–hole pairs. The photogenerated holes react rapidly with the sacrificial electron donor usually glycerol, leaving the photogenerated electrons to react with the redox dye usually methylene blue (MB), thereby generating a differently coloured (usually bleached) reduced form of the dye, i.e. D_{red}, which is oxygen sensitive; this is step 1 in Fig. 1. The key ingredients, i.e. semiconductor powder particles, redox dye and sacrificial electron donor are chosen so that they are readily dispersed/dissolved in water containing a polymer, such as hydroxyethyl cellulose (HEC) which acts as an encapsulation medium when this intelligent ink is printed and dries to form a UV-activated, O₂-sensitive indicator film.

Activated by a pulse of UV light, the initially highly coloured (due to D_{ox}) polymer/SED/D_{ox}/SC film is rendered a different colour (due to D_{red}), usually colourless, and oxygen sensitive. In the absence of oxygen, the UV-activated film remains colourless indefinitely, but upon exposure to air it rapidly (usually within 10 min) regains its original colour as D_{red} is reoxidised by oxygen to D_{ox} in a dark reaction step, step 2 in Fig. 1.

To date most work has focussed on the creation and characterisation of HEC/glycerol/MB/TiO₂ colourimetric O₂ indicators [6,7]. Obviously a key feature of this type of indicator is the need for photons of energy \geq the bandgap of the semiconductor, E_{bg} , to drive the initial light-activation step—step 1 in Fig. 1. In the case of TiO₂ its bandgap is 3.2 eV, i.e. photons of light of wavelength \leq 388 nm are needed to activate a HEC/glycerol/MB/TiO₂ film. These photons lie in the UVA region of the electromagnetic spectrum (320–400 nm). Unfortunately, most common visible light fluorescent tubes, such as those used in food cabinet display lighting, have an emission peak in

* Corresponding author. Tel.: +44 141 548 2458; fax: +44 141 548 4822.
E-mail address: a.mills@strath.ac.uk (A. Mills).

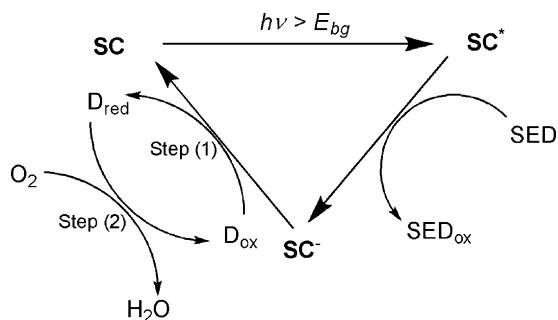


Fig. 1. Schematic illustration of the key processes involved in the UV-activation and subsequent response towards oxygen steps for a polymer/SED/dye/SC visual oxygen indicator. Step (1) refers to the photo-induced reduction of the redox sensitive dye, D_{ox} , to its reduced form, D_{red} , whereas step (2) refers to the 'dark' back re-oxidation of the dye, leading to recovery of initial colour, by the ambient oxygen. E_{bg} is the bandgap energy of the semiconductor photocatalyst, SC, and SED is the sacrificial electron donor.

the UVA region (typically at 365 nm), due to an emission line associated with electronically excited mercury vapour, and so are capable of activating a HEC/glycerol/MB/TiO₂ indicator. This is an undesirable feature, of the otherwise novel UV-activated colourimetric oxygen indicator, since it allows the indicator to be re-activated in an uncontrolled fashion, by, say, the UVA light component in white light fluorescent tubes, or sunlight. If the above semiconductor-sensitised-based indicator technology is to be used in MAP, the ink needs a more controllable route to activation, i.e. not by light commonly present in room or food cabinet lighting, but by, say, UVB light (280–320 nm) which is largely absent from such sources. In this paper, a UVB-activated colourimetric oxygen indicator which uses nano-particulate tin(IV) oxide, $ncSnO_2$, as the semiconductor photosensitiser is described and its response characteristics compared to those of a conventional TiO₂-based, colourimetric oxygen indicator.

2. Experimental

2.1. Materials and chemicals

Nanoparticulate tin(IV) dioxide, $ncSnO_2$, was purchased from Aldrich and nanoparticulate titania, P25 TiO₂, was a gift from Degussa. The use of a nanoparticulate semiconductor sensitiser – like $ncSnO_2$ or P25 TiO₂ – is preferred over the bulk (i.e. microcrystalline) forms of the materials, as the former have much greater specific surface areas than the latter and are less light-scattering, thus ensuring effective photocatalytic reactions and clear films by small amounts of the semiconductor. Whereas TiO₂ is biologically inert, the toxicological properties of SnO₂ have not been thoroughly investigated and so, although stable and largely non-reactive, it may be harmful if swallowed or inhaled and act as an eye and skin irritant. XRD analysis of the $ncSnO_2$ (Siemens D500 powder diffractometer, Cu K α) revealed a crystalline material, displaying the classic pattern of a rutile crystal structure, see Fig. 2(a) [8]. The crystalline and nanoparticulate nature of $ncSnO_2$ was also clear from transmission electron micrographs of the powder, a typical example of which is illustrated in Fig. 2(b). BET analysis of the powder revealed a specific surface area of 15 m² g⁻¹, i.e. about 30% of that of the P25 TiO₂. The polymer, HEC (medium viscosity, cellosize-WP 40) was purchased from Fluka. All the other chemicals were obtained from Aldrich and used without further purification.

2.2. Methods

A typical $ncSnO_2$ O₂-indicator ink was prepared as follows: 2 g of 5 wt.% HEC aqueous solution, 5 mg of redox dye (MB), 100 mg

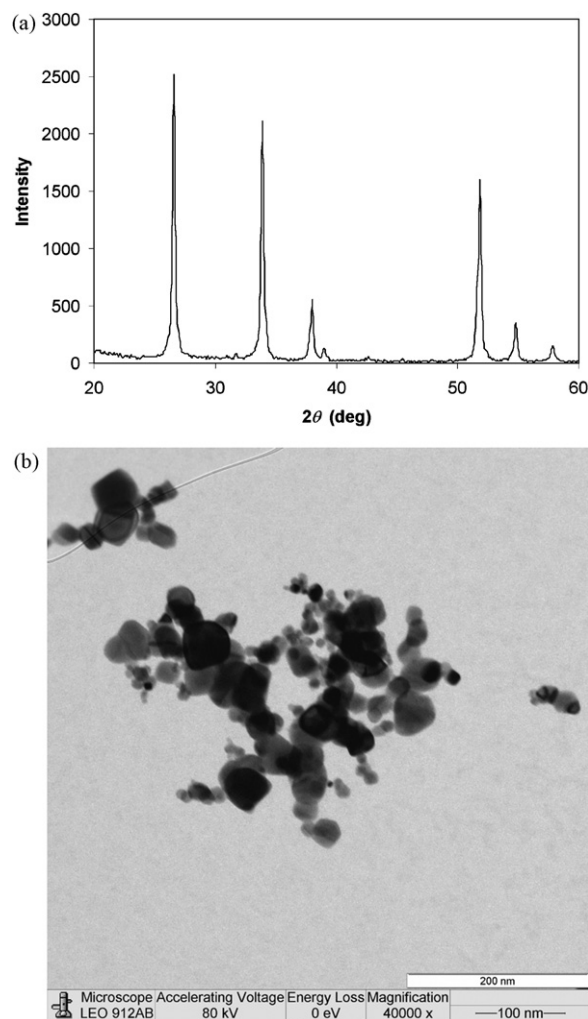


Fig. 2. (a) Powder XRD spectrum of $ncSnO_2$. (b) TEM photographs of $ncSnO_2$ [8].

of sacrificial electron donor SED (glycerol) and 100 mg of $ncSnO_2$ were mixed together and stirred for at least 30 min, followed by 30 min of sonication from an ultrasound bath to ensure thorough mixing and dispersion of the various components. In order to make a typical $ncSnO_2$ film a drop of this blue ink was then placed on the centre of a 25 mm diameter glass cover slip and spun at 3500 rpm for 30 s, to produce a dry film with an average thickness of ca. 5 μ m. The composition of this typical $ncSnO_2$ film with respect to the other component in the HEC/glycerol/MB/ $ncSnO_2$ film can be summarised as follows: 100/100/5/100 pphr where pphr = parts per hundred resin. Otherwise similar, TiO₂-based inks were also prepared with the TiO₂ level at 20 or 100 pphr, to aid comparison.

2.3. Irradiation and colour measurement

UV/visible absorbance measurements were made with a UV/Vis Cary 300 spectrophotometer and diffuse reflectance spectra of the two different semiconductor powders were measured using a Perkin Elmer Lambda 35 spectrophotometer with a diffuse reflectance attachment (Labsphere RSA-PE-20). Unless stated otherwise all irradiations were made in nitrogen, in order to study the UV-activation process, step 1, without any interference from the dark recovery step, step 2 (see Fig. 1). In the study of the dark recovery of oxygen response step, step 2, characterisation of the HEC/glycerol/MB/ $ncSnO_2$ film as a function of %O₂, was carried out using a brass gas cell to maintain the sample in different gas streams

Table 1
UV/visible irradiance levels used in this work with the UVB, UVA and WW lamps.

Lamp	UVA int. (mW cm^{-2})	UVB int. (mW cm^{-2})	Illuminance (lx)	Distance (cm)
UVB 2×20 W TL01	0.18	1	720	15
UVA 2×8 W	1	0.04	120	18
WW 2×8 W	0.04	0.01	7000	10

(e.g. N_2 or O_2 or defined mixtures of these, all with an overall flow rate of 300 mL min^{-1}).

Typically three different fluorescent tubes light sources were used in this work, namely: (i) 2×20 W Philips TL01 UVB lamps with a narrow emission peak at 315 nm, (ii) 2×8 W Philips F8/T5/BLB UVA tubes with a broad emission peak at 365 nm and finally, (iii) 2×8 W GE T5/F8 warm-white (WW) light fluorescent tubes, frequently used in food cabinet lighting. The emission spectra of these three light sources, i.e. UVB (narrow), UVA and WW fluorescent lamps, are illustrated in Fig. 3. The UVA and UVB irradiance levels emitted by these lamps were measured using a UV-meter (UVX digital radiometer, UVP); visible light levels (for the WW lamp) were measured using a LX-101 (Lutron) lux meter. The typical irradiance levels (and required lamp distances) employed in this work are summarized in Table 1. The full emission spectrum of a typical white fluorescent light is reported elsewhere [9].

The intensity measurements reported in Table 1 and the results in Fig. 3 reveal that the amount of UVB (due to the 306 and 310 nm Hg vapour emission lines) emitted by the WW lamps is very small. In contrast, the level of UVA emitted by most white light fluorescent tubes, such as the WW lamps, is significant. The conditions under which the WW lights were used, and their irradiances measured (see Table 1), are similar to those found in the brightest part (top shelf) in most supermarket food cabinets.

3. Results and discussion

3.1. Diffuse reflectance spectra of ncSnO_2 and P25 TiO_2

The diffuse reflectance spectra of the two nanoparticulate semiconductor powders, ncSnO_2 and P25 TiO_2 , were recorded and are illustrated in Fig. 4. An analysis of this spectral data reveals ncSnO_2 to have an absorption edge at ca. 344 nm, corresponding to a bandgap, of 3.65 eV, whereas P25 TiO_2 begins to absorb at ca. 382 nm, corresponding to a bandgap of 3.25 eV [10,11]. Thus, whereas P25 TiO_2 -based indicator will be activated by the UVA and UVB emitted by the WW, UVA and UVB lights used in this work,

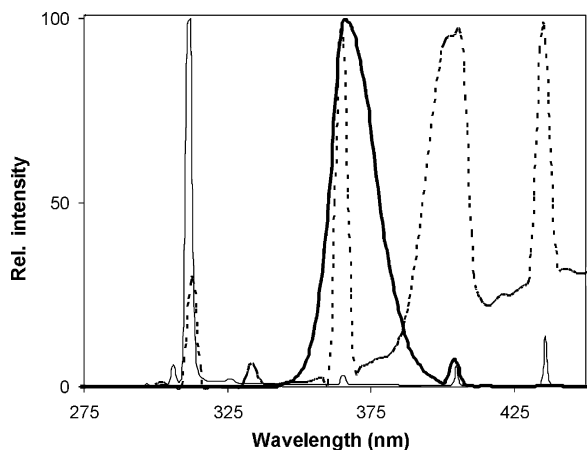


Fig. 3. Normalised relative intensity emission spectra of the lamps used in this work; 20 W UVB narrow band lamp (thin solid line) 8 W BLB UVA (thick solid line) and 8 W warm-white fluorescent tubes (dashed line). Note the prevalence of the Hg-vapour emission lines at 365, 310 and 306 nm.

ncSnO_2 should be activated by only the UVB light source, since there is very little UVB in the WW and UVA sources used here (see Table 1) and the specific surface area of ncSnO_2 is low compared to P25.

3.2. The UVB activation and recovery of a typical ncSnO_2 film

A typical ncSnO_2 film was prepared and irradiated with UVB light (1 mW cm^{-2}) in nitrogen. Photographs of the film before (i), and after (ii) (10 min) irradiation are shown in Fig. 5(a) and reveal the film to be photobleached, i.e. UVB-activated, after this short period of illumination; which corresponds to the activation step, step 1, in Fig. 1. The concomitant change in the UV/visible absorption spectrum of this film is illustrated in Fig. 5(b) and reveals all the MB to be converted to its colourless, reduced form, leuco-methylene blue (LMB), after 10 min of irradiation. In this work the change in the absorbance at the absorption maximum for MB, ca. 605 nm, i.e. ΔAbs_t , was monitored as a function of irradiation time, t , and usually reported as a relative absorbance change, i.e. $\text{rel } \Delta Abs$ where $\text{rel } \Delta Abs = \Delta Abs_t / \Delta Abs_{t=0}$. Whatever the irradiation source, or semiconductor photosensitiser, with this type of ink film, once UV-activated, i.e. photobleached, the indicator dye remains colourless unless, or until, exposed to oxygen, whereupon it regains its original colour as D_{red} is re-oxidised to D_{ox} by O_2 , i.e. as a result of step 2 in Fig. 1. The last photograph in Fig. 5(a), (iii), shows the film regains its original colour when UV activated and then allowed to react with the O_2 in air for 10 min.

3.3. UV sensitivity of ncSnO_2 and P25 TiO_2 -based films (step 1)

Four different HEC/glycerol/MB/semiconductor oxygen-indicator films containing, respectively: (i) no photocatalyst, (ii) 100 pphr ncSnO_2 , (iii) 20 pphr P25 TiO_2 and (iv) 100 pphr P25 TiO_2 were prepared and irradiated under nitrogen using each of the following three different light sources: (a) warm-white (WW) light, (b) UVA and (c) narrow band UVB light at the distances/irradiance levels given in Table 1; the observed variation in $\text{rel } \Delta Abs$ versus irradiation time profiles arising from this work are

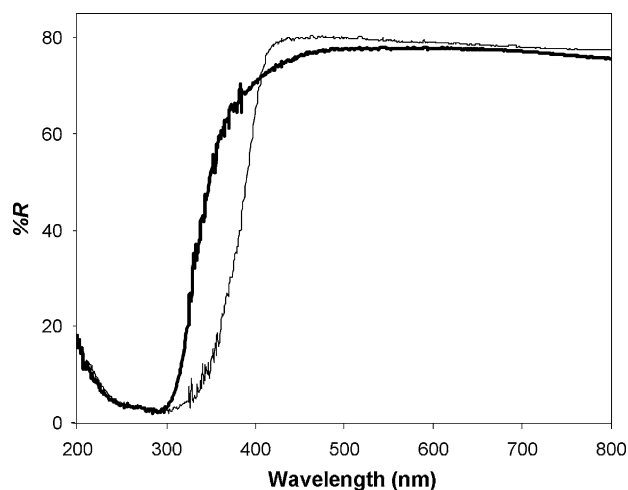


Fig. 4. Reflectance spectra of ncSnO_2 (thick solid line) nanopowder (thin solid line) and P25 titania [9,10].

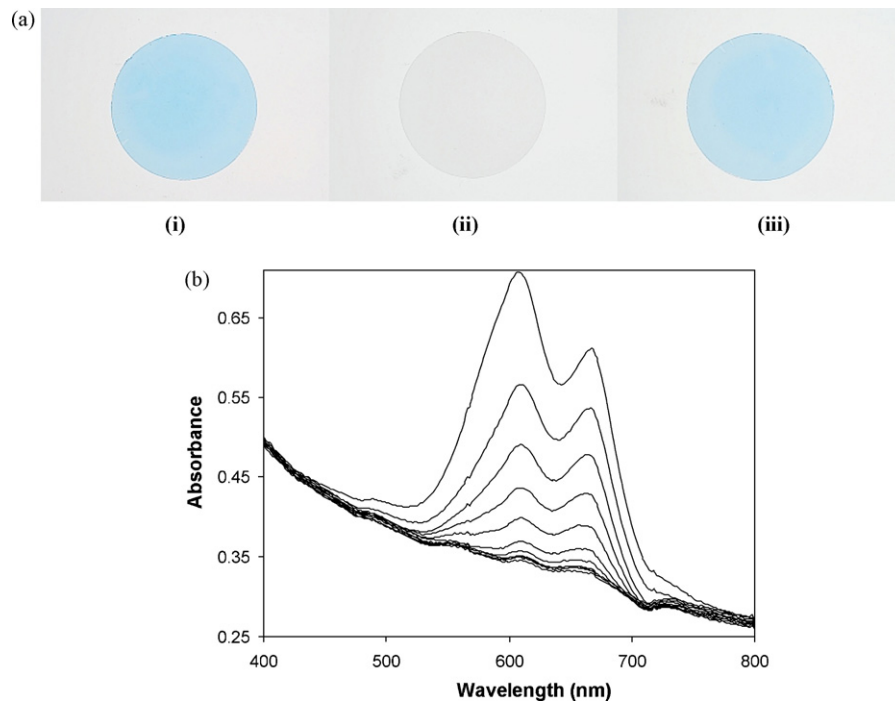


Fig. 5. (a) Photographs of typical $ncSnO_2$ oxygen indicating film on glass cover slip (25 mm diameter) before (i) and after (ii) 10 min of UVB irradiation (in N_2). The last picture, (iii), shows the UV activated film after 15 min in air, by which time it has fully recovered its original colour. (b) UV/vis absorption spectra of a typical $ncSnO_2$ indicator film photobleaching as a function of irradiation time (1 min intervals) in the photobleaching step (spectra taken from top to bottom).

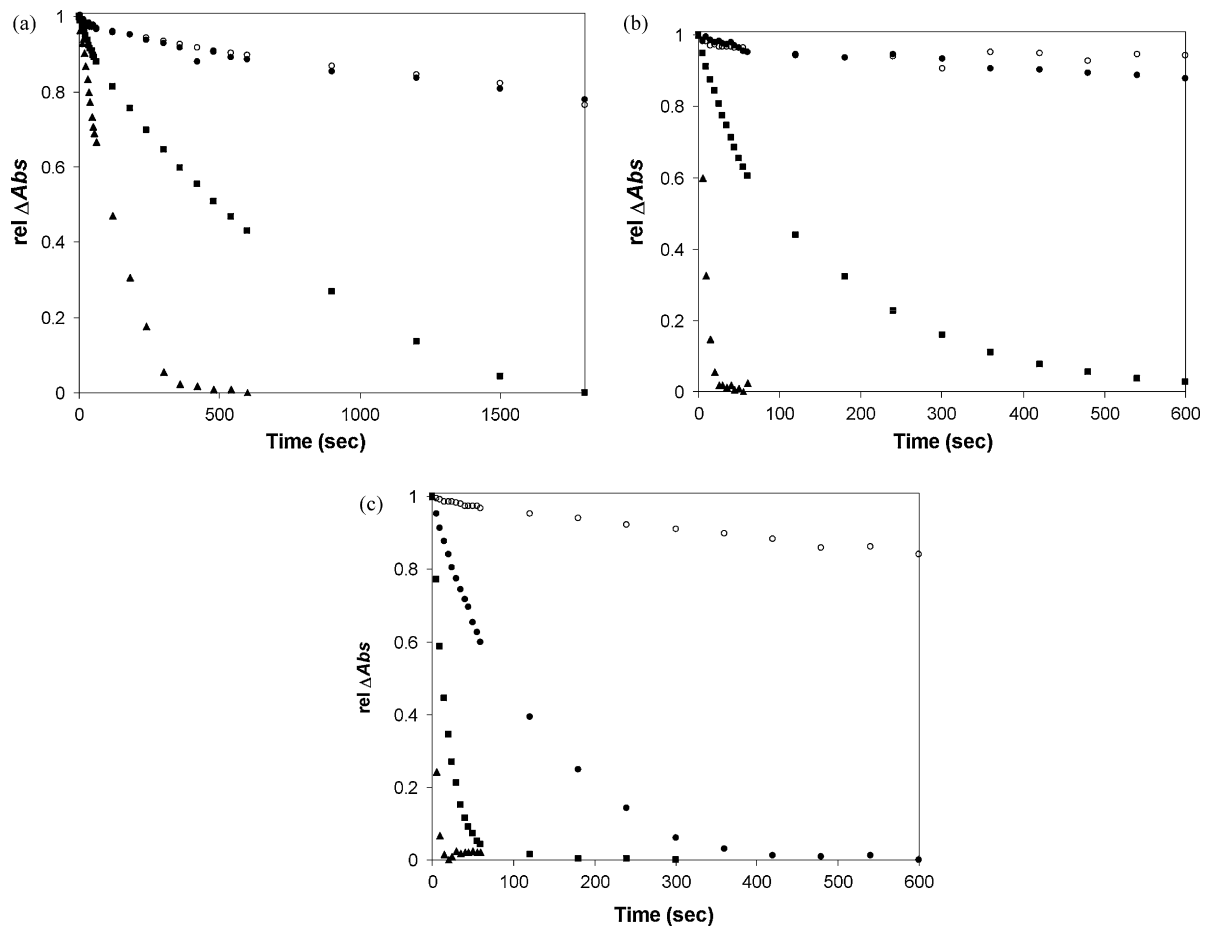


Fig. 6. Photobleaching of typical O_2 indicator films with: (i) $ncSnO_2$, composition: 100/100/5/100 (●), (ii) $P25 TiO_2$, composition: 100/100/5/100 (▲), (iii) $P25 TiO_2$, composition: 100/100/5/20 (■) and (iv) 'no photocatalyst' (○). The films were irradiated approximately for (a) 1 h using 2×8 W warm-white fluorescent tubes ($UVA I = 0.04 \text{ mW cm}^{-2}$, $E_v = 7000 \text{ lx}$), (b) 10 min using 2×8 W BLB UVA tubes ($UVA I = 1.0 \text{ mW cm}^{-2}$) and (c) 10 min using 2×20 W TL01 UVB tubes ($UVB I = 1.0 \text{ mW cm}^{-2}$). All irradiations were carried out under N_2 .

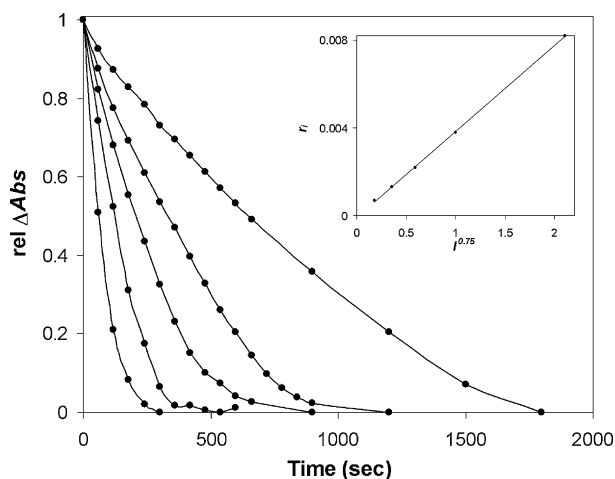


Fig. 7. Plot of the absorbance of a typical $ncSnO_2/MB$ film at λ_{max} 605 nm vs. irradiation time profiles using UVB light (TL01 2×20 W) at different irradiances, I , i.e. from left to right: (0.1, 0.25, 0.5, 1.0 and 2.7 mW cm^{-2}). The insert shows a subsequent plot of the data in the main diagram in the form of initial rate, r_i , of photobleaching as a function of $I^{0.75}$.

illustrated in Fig. 6(a)–(c), respectively. From the results in Fig. 6(a) and (b) it is clear that both the $ncSnO_2$ and ‘no photocatalyst’ films remained largely unbleached when exposed to light from either the WW or UVA light sources. The slight photobleaching of these two films by the WW light source is most likely due to the visible-light driven photolysis of MB. In contrast, P25 TiO_2 loaded films are readily photobleached/activated by both these light sources and not surprisingly, at a rate that increases markedly with the level of photocatalyst present; i.e. the 100 pp/hr P25 TiO_2 is more readily photobleached than the 20 pp/hr P25 TiO_2 film. Both the $ncSnO_2$ and P25 TiO_2 films are bleached by UVB light, with only the ‘no photocatalyst’ indicator film remaining unbleached, i.e. unactivated, when this light source is used, see Fig. 6(c).

From the above results, it is clear that when $ncSnO_2$ is used as the photocatalyst in a HEC/glycerol/MB/semiconductor film, the resultant O_2 indicator is not UVA sensitive and, therefore, not readily photobleached by the UVA component of white light fluorescent tubes, such as a warm-white light. This is not surprising given the bandgap of SnO_2 is 3.65 eV ($\approx 340 \text{ nm}$) whereas the UVA Hg vapour emission line present in the UVA and WW light sources is at 365 nm. In contrast, P25 TiO_2 has a bandgap of 3.25 eV ($\approx 382 \text{ nm}$) and so is able to absorb these UVA photons much more readily than $ncSnO_2$, and so all P25-based films are photobleached by the UVA present in the WW and UVA lamps. The use in this work of $ncSnO_2$, rather than TiO_2 , as the semiconductor photosensitiser, in a UV-activated colourimetric indicator, is a major advance as it is a significant barrier to their uncontrolled activation, given the ambient level of UVB in interior room lighting is very small.

3.4. Photobleaching (step 1) as a function of irradiance

In order to characterise the HEC/glycerol/MB/ $ncSnO_2$ O_2 sensitive film in more detail, the photobleaching of a typical $ncSnO_2$ film was studied as a function of irradiance, I , and the results are illustrated in Fig. 7. The initial rate of photobleaching, r_i , of this film appears to be directly related to the incident irradiance, $I^{0.75}$. Such a dependence on irradiance is not unusual in semiconductor photocatalysis, since it is found that $r_i \propto I$ at low I , due to an efficient photochemical reaction at the surface and $r_i \propto I^{1/2}$ at high I , due to a dominant electron–hole recombination process [12]. Thus, an observed dependence of r_i upon $I^{0.75}$ signifies a mixed dependency that is expected at the moderate irradiance levels (*ca.* 1 mW cm^{-2}) employed here.

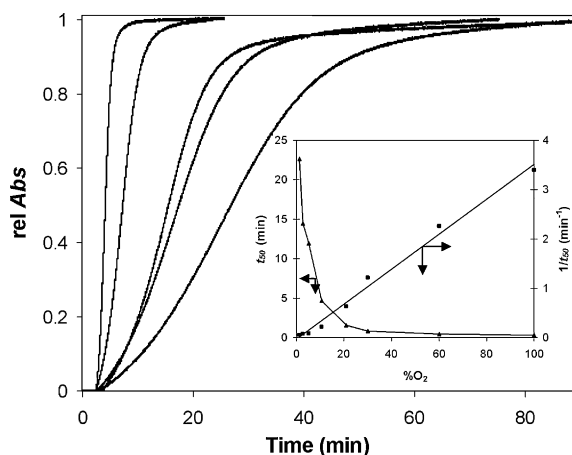


Fig. 8. Recovery of a typical $ncSnO_2$ film when UV activated (in N_2) and then exposed to different O_2 levels (from right to left: 1.3, 2.6, 5.3, 10.5, 21% O_2). The inserted diagram shows a subsequent plot of the data in the form of: t_{50} (\blacktriangle) and $1/t_{50}$ (\blacksquare) (gradient of the slope = 0.35) as a function of % O_2 . The $ncSnO_2$ films were bleached in N_2 prior to the exposure to the O_2 -containing atmosphere using 10 min UVB light from 2×6 W broad band lamps, $I = 2.7 \text{ mW cm}^{-2}$).

3.5. The dark O_2 response (step 2)

Clearly, a key feature of the HEC/glycerol/MB/ $ncSnO_2$ film is its response to oxygen, i.e. step 2 in Fig. 1. The kinetics of this response for a typical UVB-activated (under N_2) $ncSnO_2$ film were recorded as a function of % O_2 and the results are illustrated in Fig. 8. The kinetics due to the diffusion of oxygen into the heterogeneous medium of the polymer film and subsequent reaction with leuco-MB, are not simple, due to the heterogeneous nature of the polymer film and, therefore, distribution of oxygen solubilities and diffusion coefficients [13], although a useful, simple measure is the time taken for a film to recover half its final colour, i.e. t_{50} , when $rel \Delta Abs = 0.5$. Analysis of the recovery data in Fig. 8 allows a plot of $1/t_{50}$ versus % O_2 , shown as an insert plot in the figure, which yields a straight line, suggesting that this type of indicator could be used for the quantitative analysis of the ambient oxygen level simply by initially activating with UVB light, and monitoring the time it takes for the film to recover half its original colour. This time, when compared with the data in a calibration graph, such as illustrated in Fig. 8 (insert), would reveal the ambient level of oxygen present.

4. Conclusion

Nanocrystalline SnO_2 can be used as a photocatalyst in a UV-activated colourimetric oxygen indicator comprising: polymer/SED/redox dye/photocatalyst, where polymer = HEC, donor = glycerol, dye = MB and photocatalyst = $ncSnO_2$. Previous work had established that P25 TiO_2 , although very effective, responds to the UVA component in most fluorescent tubes.

The larger bandgap (3.65 eV) of $ncSnO_2$, compared to P25 TiO_2 , renders it UVB, but not UVA, sensitive. In particular, $ncSnO_2$ is unable to absorb photons due to the Hg vapour emission line at 365 nm and, as a consequence, a HEC/glycerol/MB/ $ncSnO_2$ film is not activated (i.e. photobleached) by the UVA component in white or UVA fluorescent tubes, but is activated by UVB light.

Other work on the $ncSnO_2$ -based O_2 -indicator film reveals a fractional power dependence of the kinetics of UV activation on irradiance, i.e. $r_i \propto I^{0.75}$, and that the rate of its response towards oxygen, as measured by t_{50} , could be used to assess the ambient level of oxygen. The use of $ncSnO_2$ as a photocatalyst in the UV activated oxygen-sensitive inks opens up many possible avenues of application as it allows for a much more controllable UV-activation

step. In particular, this modified ink has promise as a quality control and tamper-evident indicator in MAP.

Acknowledgment

DH wishes to thank the EPSRC for supporting this work via a PhD studentship.

References

- [1] M.L. Rooney, *Active Food Packaging*, Blackie, London, 1995.
- [2] A.L. Brody, B.R. Strupinsky, L.R. Kline, *Active Packaging for Food Applications*, Technomic Publishing Co., Lancaster, 2001.
- [3] M. Sumitani, H. Inoue, K. Sugito, US Patent 6703245, 2004.
- [4] M. Goto, JP Patent 62 259059, 1987.
- [5] A. Mills, Oxygen indicators and intelligent inks for packaging food, *Chem. Soc. Rev.* 34 (2005) 1003–1011.
- [6] S. Lee, A. Mills, A. Lepre, An intelligence ink for oxygen, *Chem. Commun.* (2004) 1912–1913.
- [7] A. Mills, D. Hazafy, A solvent-based intelligence ink for oxygen, *Analyst* 133 (2008) 213–218.
- [8] B. Grzeta, E. Tkalcec, C. Goebbert, M. Takeda, M. Takahashi, K. Nomura, M. Jaksic, Structural studies of nanocrystalline SnO₂ doped with antimony: XRD and Mossbauer spectroscopy, *J. Phys. Chem. Solids* 63 (2002) 765–772.
- [9] G.A. Rechtsteiner, J.A. Ganske, *Chem. Educator* 3 (1998) 1–12.
- [10] T. Sato, Y. Yamamoto, Y. Fujishiro, S. Uchida, Intercalation of iron oxide in layered H₂Ti₄O₉ and H₄Nb₆O₁₇: visible-light induced photocatalytic properties, *J. Chem. Soc., Faraday Trans.* 92 (1996) 5089–5092.
- [11] S. Uchida, Y. Yamamoto, Y. Fujishiro, A. Watanabe, O. Ito, T. Sato, Intercalation of titanium oxide in layered H₂Ti₄O₉ and H₄Nb₆O₁₇ and photocatalytic water cleavage with H₂Ti₄O₉/(TiO₂, Pt) and H₄Nb₆O₁₇/(TiO₂, Pt) nanocomposites, *Chem. Soc., Faraday Trans.* 93 (1997) 3229–3234.
- [12] A. Mills, An overview of semiconductor photocatalysis, *J. Photochem. Photobiol. A* 8 (1997) 1–35.
- [13] A. Mills, Response characteristics of optical sensors for oxygen: models based on a distribution in tau(o) or kappa(q), *Analyst* 124 (1999) 1301–1307.

Biographies

Professor Andrew Mills gained his PhD in 1983 from University of London in Water-Splitting Photosystems. He is currently Professor of Physical Chemistry at University of Strathclyde. His research interests include: semiconductor photochemistry and optical sensors.

David Hazafy gained his degree from Charles University, Prague, in 2004 and is currently engaged in a PhD on novel optical sensors.

COMMENTS

Comment on “Solvent Effect on the Electronic Spectra of Azine Dyes under Alkaline Condition”

Andrew Mills,^{*,†} David Hazafy,[†] John A. Parkinson,[†]
Tell Tuttle,[†] and Michael G. Hutchings[‡]

WestCHEM Department of Pure & Applied Chemistry,
University of Strathclyde, Glasgow G1 1XL, U.K., and
DyStar UK Ltd., Akros Site, Lankro Way, Eccles,
Manchester M30 0BH, U.K.

Received: April 3, 2009

Pal et al.¹ recently proposed that methylene blue (MB) is readily (within 1 h) converted to a nonionic, lipophilic, *N*-hydroxy adduct of MB, referred to as “MB–OH”, when exposed to mild (0.1 mM) alkali (NaOH). MB–OH is readily extracted from the alkaline aqueous solution into toluene to form a red ($\lambda_{\text{max}} = 526$ nm) solution and is solvatochromic, but converted to a blue species, presumed to be MB, when spotted onto a silica-gel-coated TLC plate. The mass spectrum of MB–OH gave a molecular ion, *m/z* 301, appearing to confirm the formation of MB–OH. The structures of MB, MB–OH, and other species relevant to this work are given in Table 1.

The continuing importance of MB in various applications, most notably as a potential new treatment for Alzheimer’s disease,² leads us to submit this Comment on the results of Pal et al.¹ All our attempts to reproduce the observations of Pal et al.¹ have failed. On following their simple experimental procedure we have found no toluene-soluble, red species was formed upon treating MB with 0.1 mM alkali, even after 24 h. Our observation of no reaction is not surprising given others have noted MB is “indefinitely stable” in aqueous solution at pH 9.5,³ and that mixing MB with 0.1 mM alkali and shaking with a water-immiscible solvent (usually dichloromethane) is a published method for purifying MB of the demethylated thiazines, such as azure B (AB; usually the most prevalent species), which are common impurities in some commercial samples of MB.^{4,5} This purification procedure is effective because the latter thiazines are readily deprotonated by alkali to their neutral, lipophilic orange or red forms, the structure of which for AB (i.e., dAB) is illustrated in Table 1.^{5,6} Thus, it would seem that Pal et al.¹ have made an error in reporting the concentration of NaOH used in the production of MB–OH.

Encouragingly, it is possible to generate a species with near identical absorption spectra to those reported by Pal et al. for MB–OH¹ using the same method, but with 0.1 M, instead of 0.1 mM, NaOH aqueous phase solution shaken with toluene. We shall refer to the species generated using the

higher alkali concentration and extracted into toluene as MB-red. If Pal et al.¹ used 0.1 M NaOH, rather than 0.1 mM, then we should expect MB-red to be the hydroxy adduct MB–OH. Promisingly, MB-red shows the same solvatochromic properties as reported by Pal et al.¹ for MB–OH and turns blue when spotted onto a silica-gel-coated TLC plate. These observations would seem to indicate that our red-MB and MB–OH are one and the same.

It is with concern, therefore, to note that subsequent experiments reveal MB-red to be largely methylene violet (Bernthsen), MVB (Table 1). The latter is available commercially and has spectral and physical properties identical to MB-red. For example, MVB is lipophilic and has the same solvatochromic UV/visible absorption characteristics as MB-red (which in turn are near-identical to the species identified as MB–OH). MVB and MB-red also fluoresce with a maximum of emission at 596 nm in toluene ($\lambda_{\text{excit}} = 520$ nm), in agreement with the literature.⁷ As noted above, when MB-red (like MB–OH) in toluene solution is spotted onto a silica TLC plate, the spot turns blue, but on development this spot separates into two, neither of which is MB. The most striking spot in terms of depth of color has the same retention time, *R_f*, as commercial MVB, while the other, which is much weaker in color, has the *R_f* value of AB.

The NMR spectra recorded for MB (in D₂O; 500.13 MHz), MB-red, and MVB (in CCl₄; 600.13 MHz) reveals MB-red to be identical to MVB. (It is not clear why Pal et al.¹ report MB–OH to be too unstable to record NMR spectra, yet stable enough to record visible spectra at room temperature in solvents such as CHCl₃ and CCl₄.)¹ Consistent with the above, the mass spectrum of MB-red in toluene reveals the predominant presence of MVB (molecular ion peak at *m/z* 256) with some AB (*m/z* peak at 270). The latter observations are in contrast to the work of Pal et al.,¹ who observed a molecular ion peak at *m/z* 301,¹ although in the mass spectrum of MB–OH shown in their Supporting Information, there are also substantial peaks at *m/z* 256 (not 257 as Pal et al.¹ state), 270, 320, and 342,¹ and it is difficult to rationalize the latter two fragments in terms of MB–OH.

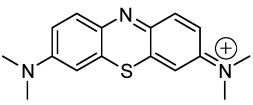
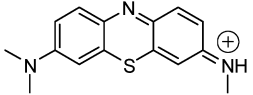
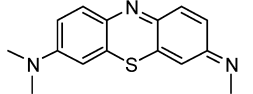
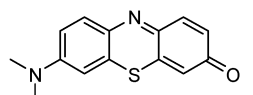
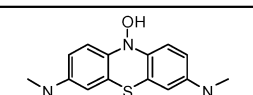
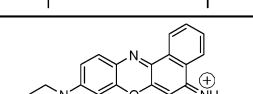
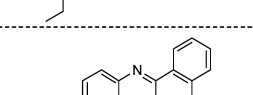
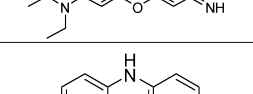
A key justification, used by Pal et al.¹ and earlier by Plater,⁸ for *N*-hydroxylation leading to the formation of MB–OH is the proposal that the central heterocyclic nitrogen in MB is electron deficient. However, this is not supported by the literature cited by Plater,⁸ who also notes in his ref 15 that MB is hydrolyzed to MVB. Contrary to the suggestion of an electropositive central N in MB, our analysis of DFT calculations on MB applying both the NBO and electrostatic potential (ESP) methods to determine the charge distribution of MB reveals that the central heterocyclic N atom in fact has an overall partial *negative* charge (NBO: $-0.38e$, ESP: $-0.79e$; see Figure 1 in the Supporting Information). Such a situation vitiates the basis proposed^{1,8} for nucleophile addition at the heterocyclic N atom and renders formation of the *N*-hydroxy adduct (MB–OH, Table 1) unlikely. In addition, TD-DFT calculations reveal that MB–OH would have an absorption maximum in the near UV at 351 nm, i.e., a species with the structure shown for MB–OH would be colorless,

* Corresponding author. E-mail: a.mills@strath.ac.uk.

[†] WestCHEM Department of Pure & Applied Chemistry, University of Strathclyde.

[‡] DyStar UK Ltd.

TABLE 1: Summary of Structural, Spectral, and Physical Characteristics of MB and Other Relevant Dyes

Cationic dye structure	Abv./name Mol. weight	$\lambda_{\max}(\text{H}_2\text{O})$ /nm	$\lambda_{\max}(\text{toluene})$ ($\lambda_{\max}(\text{calc.}^{**})$)/nm
	MB Methylene blue 284.4	665	n/a
	AB Azure B 270.37	645	n/a
	dAB deprot. AB 269.36	n/a	503 (521)
	MVB Methylene violet 256.32	610	520 (500)
	MB-OH 301.41	662*	526* (351)
	NB Nile blue 318.39	635	n/a
	dNB deprot. Nile blue 317.38	n/a	500 (492)
	LMB <i>leuco-</i> Methylene blue 285.41	256***	n/a

* Reference 1. ** Calculated using TD-DFT. *** Reference 9.

as expected. (MB–OH is simply the *N*–OH analogue of the well-known colorless reduced form of MB, leuco methylene blue (LMB); see Table 1.⁹) Interestingly, G. N. Lewis et al. in related chemistry more than 60 years ago had speculated on the formation of MB–OH by the addition of water to MB and noted that if formed it would be colorless.¹⁰

In conclusion, our findings indicate that the red-MB species observed by Pal and co-workers,¹ and claimed to be the *N*-hydroxy adduct MB–OH, is in fact MVB, possibly containing some AB, both of which are formed by hydrolysis. The observation here and by others that AB is also rendered lipophilic by deprotonation brings into question the reported¹ formation of a colored hydroxy adduct of nile blue (NB; an oxazine dye; Table 1), when deprotonation of the amine group (just as in AB) to form dNB appears much more likely (see Table 1).

Supporting Information Available: Description of computational methods and a figure illustrating calculated charge

distribution for MB using the NBO and ESP charge models. This material is available free of charge via the Internet at <http://pubs.acs.org>.

References and Notes

- (1) Basu, S.; Panigrahi, S.; Praharaj, S.; Ghosh, S. K.; Pande, S.; Jana, S.; Pal, A.; Pal, T. *J. Phys. Chem. A* **2007**, *111*, 578–583.
- (2) Murray, A. D.; Stuff, R. T.; Ahearn, T. S.; Bentham, P.; Seng, K. M.; Wischik, C. *Alzheimer's Dementia* **2008**, *4*, T786–T787.
- (3) Abbott, D. C. *Analyst* **1962**, *87*, 286–293.
- (4) Marshall, P. N.; Lewis, S. M. *Stain. Technol.* **1976**, *50*, 375.
- (5) Bonneau, R.; Faure, J.; Joussot-Dubien, J. *Talanta* **1967**, *14*, 121–122.
- (6) Davis, M. M.; Hetzer, H. B. *Anal. Chem.* **1966**, *38*, 451–461.
- (7) Otsuki, S.; Taguchi, T. *Bull. Chem. Soc. Jpn.* **1996**, *69*, 2525–2531.
- (8) Plater, M. J. *ARKIVOC* **2003**, 37–42.
- (9) Lee, S.-K.; Mills, A. *Chem. Comm.* **2003**, 2366–2367.
- (10) Lewis, G. N.; Bigeleisen, J. *J. Am. Chem. Soc.* **1943**, *65*, 1144–1150.

JP9030927

A novel reversible relative-humidity indicator ink based on methylene blue and urea

Andrew Mills,* Pauline Grosshans and David Hazafy

Received 15th September 2009, Accepted 11th November 2009

First published as an Advance Article on the web 19th November 2009

DOI: 10.1039/b918985h

A new relative-humidity sensitive ink based on methylene blue and urea is described which can utilise the deliquescent nature of urea.

Humidity sensors are used extensively in industry as well as for environmental monitoring. Their widespread applications cover a broad range of domestic, medical and industrial applications. For example, in food packaging, excess moisture in meat packaging can accelerate food spoilage, and as a consequence desiccants are often included in packaging to extend the shelf life.¹ At low relative humidities (RHs) some dry grain products can undergo rapid free-radical oxidation and become rancid.¹ Most fruit and vegetables are composed largely of water, consequently their optimum storage conditions are typically 90–95% RH, $T = 0\text{ }^{\circ}\text{C}$,² whereas products such as sugar and raisins lose their desirable texture if the RH is this high. Thus, most food stuffs require a degree of moisture management and humidity measurement to obtain optimum relative-humidity (RH) conditions.¹ Humidity control is also important for the preservation of artefacts such as books and paintings and to prevent bacterial and mould growth in certain manufactured products. Another application is in the packaging and transportation of sensitive electrical appliances/components which are adversely affected by high relative humidity and therefore require accurate monitoring to ensure efficient functionality.³

There are a wide range of commercial products currently available for monitoring relative humidity. These are, more often than not, electronic hygrometers based on capacitive or resistive systems which measure the change in conductivity of a polymer or ceramic film as a function of relative humidity.⁴ Such devices have limitations in their operating conditions and can be expensive and bulky to use.^{5,6}

There have been a number of proposed colorimetric relative-humidity indicators, the majority of which are based on the use of inorganic salts^{7–17} such as cobalt(II) chloride, CoCl_2 , which at a defined RH level (typically RH 40%) convert from their anhydrous form to their hydrated form, which is usually marked by a colour change, in the case of CoCl_2 , blue (anhydrous) to pink (hydrated). The sensitivity of this type of indicator can be tailored to the desired application by one of three methods: changing the concentration of the inorganic salt,¹⁸ adding a deliquescent synergic salt^{19–21} or, for systems with a silica support, altering the drying and activation temperatures of the CoCl_2 -doped silica.⁷ Such relative-humidity indicators have been proposed for a variety of applications including: refrigerated systems,^{12,13} clothes dryers,¹⁴ shoe storage,¹⁶ desiccant absorbent capacity indicators,^{18,20,21} electronic device storage¹⁷ and

are often reversed by heating the hydrated salt to regenerate the anhydrous starting material. A typical commercial form, based on CoCl_2 , is the Humitector[®] Humidity Indicator Card (Süd-Chemie Inc., USA).²²

Recently, Matsushima *et al.* have proposed using thiazine and flavylium salts in gels as simple colorimetric humidity and temperature sensors.^{23–25} These salts exhibit reversible colour changes from blue (dry) to purple (humid), as a result of a change in relative humidity. This has been attributed to the absorption of water vapour by the gel in humid conditions which encourages the dye to form dimers and so leads to a shift in λ_{max} absorbance (*ca.* 10–20 nm) to a lower wavelength.

Whilst looking at this system, we have found that when the thiazine dye, methylene blue (MB), is encapsulated within a polymer, such as hydroxy ethyl cellulose (HEC), with a notable excess of urea, (20 times w/w more than MB), the product ink is blue, but casts as a thin, opaque pink film, under ambient (RH = 60%, $T = 20\text{ }^{\circ}\text{C}$) or dry conditions, and rapidly and reversibly is rendered blue coloured and clear when exposed to RH values >85%. Note that the observed colour changes for MB/urea/HEC films are the *opposite* of those observed by Matsushima *et al.*^{23–25} for their MB/gel films so the explanation for the effect is very different. It is also unusual to find a relative-humidity indicator which gives such a sharp, reversible colour change at high relative humidities. Consequently, this novel and promising relative-humidity indicator is the subject of this communication.

In this work, all relative humidities were measured at $20\text{ }^{\circ}\text{C}$ unless otherwise stated. A typical relative-humidity sensor was made by spin coating an ink comprising 5 mg MB, 100 mg urea in 2 g of a 5% w/v HEC aqueous solution, for 30 seconds at 3500 rpm on to a 25 mm glass disc. Following the drying of the film at $70\text{ }^{\circ}\text{C}$ for a few minutes, the final product is an opaque pink film (*ca.* 1.7 μm thick) under ambient conditions (40–60% RH) with a λ_{max} at 570 nm, which upon exposure to high relative-humidity conditions (>85% RH) turns rapidly blue ($\lambda_{\text{max}} = 600\text{ nm}$) and clear as illustrated in Fig. 1 and Fig. 2.

This colour change process occurs rapidly (response and recovery times: 10 s and 60 s respectively) and is reversible as illustrated by the

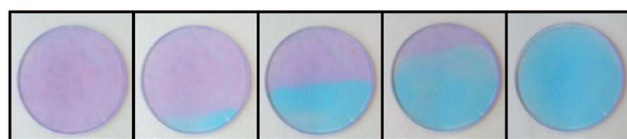


Fig. 1 Photographs of a typical MB/urea/HEC relative-humidity indicator changing colour from pink (left) to blue (right) upon exposure to 100% RH air, from the bottom right.

Department of Pure & Applied Chemistry, University of Strathclyde, Glasgow, UK G1 1XL. E-mail: a.mills@strath.ac.uk; Fax: +44 (0) 141 548 4822; Tel: +44 (0) 141 548 2458

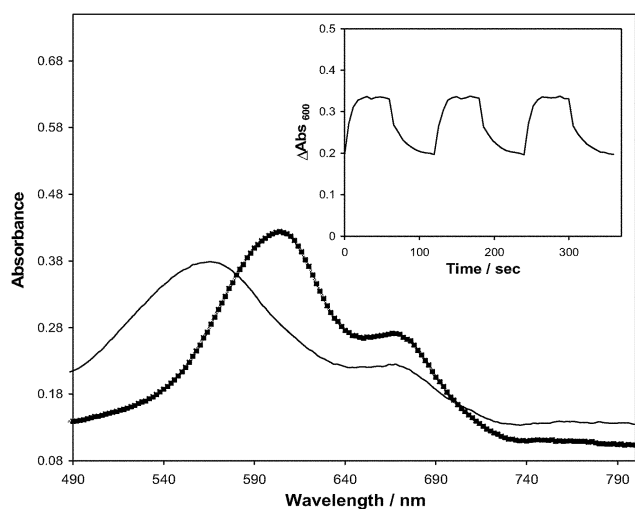


Fig. 2 Spectral changes of a typical MB/urea/HEC relative-humidity indicator film before (—) and after (■) exposure to 100% RH air. Inset diagram is a plot of the change in absorbance MB λ_{\max} humid (600 nm) for indicator film on exposure to 3 cycles of 1 min 100% RH air and 1 min dry air. Abs₆₀₀ recorded every 6 s.

data in the inset of Fig. 2 which show the response and recovery of the absorbance (at λ_{\max} for blue form, 600 nm) for a typical MB/urea/HEC relative-humidity indicator film upon exposure to repeated cycles of humid (100% RH) and dry air.

The initial spectrum of the dry film (see Fig. 2) is very different from that observed for the monomer and dimer, thus, it is not instantly apparent what the colour change is due to.^{26–28} Under ambient conditions the film is pink and the absorption spectrum of the film ($\lambda_{\max} = 570$ nm) is, if anything, like that of the MB trimer ($\lambda_{\max} = 578$ nm).^{26,28}

When exposed to high relative humidities the resulting blue film has a spectrum more characteristic of a mixture of the MB monomer and dimer.^{26–28} The monomer is attributed to the smaller peak at 665 nm while the larger peak at 600 nm is attributed to the MB dimer. An inspection of films containing no dye reveals a concomitant change in the optical clarity of the urea/HEC film in the absence (opaque) and presence (clear) of a stream of air containing a high (100%) RH, as illustrated in Fig. 3.

Further work shows that urea forms highly crystalline, optically opaque films with a characteristic XRD peak at $2\theta = 22.25^\circ$ at moderate and low RH. These crystallites rapidly dissolve when exposed to relative humidities above 85%, rendering a clear film. The urea XRD peak reappears when the opacity change is reversed by blowing dry air over the film or placing it in oven (70 °C for few minutes). Thus, it appears that the colour change associated with the MB in the urea film (pink (dry) \leftrightarrow humid (blue)) is linked to the change in crystallinity of the urea when exposed to high relative

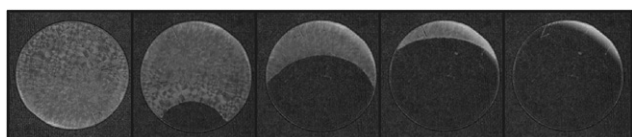


Fig. 3 Photographs of a urea/HEC with no dye changing from an opaque film (left) to a clear film (right) upon exposure to 100% RH air.

humidities. Indeed a dye-free relative-humidity indicator based on optical clarity can be simply created using just urea in a polymer, such as HEC, since Fig. 3 shows that such a film is opaque at medium and low (<85%) RH levels, but clear at RH values >85%; the process is entirely reversible. The polymer used, in this case HEC, does not appear to have any effect on the colour or opacity change, but merely acts as an encapsulation agent. This was confirmed by observing a similar effect in different polymers (such as polyvinyl alcohol, PVA and polyethylene oxide, PEO). Also in a polymer-free environment, achieved by grinding up a sample of urea with MB, the resulting pink powder exhibits a similar reversible colour change to blue when exposed to RH >85%.

The simplest explanation is that under ambient conditions (RH < 85%) MB is encapsulated in urea crystals as the pink trimer and when exposed to high RHs the urea crystals dissolve, thereby releasing the MB into an environment in which its more stable form is the blue coloured MB dimer and monomer. In support of this, it is well known that urea is a hygroscopic compound which deliquesces under high RH conditions of >80% RH at 18 °C.^{29–31}

The notable features of this type of relative-humidity indicator are not only that it can be used exclusively for monitoring high (>85%) relative humidities, but it is quick to respond, highly reversible and has a good long-term stability. As it stands, such a >85% RH indicator has a potential application ensuring the correct RH conditions for the storage and ripening of fruit,³² for example. Further work is in progress developing this system using a series of hygroscopic, urea and non-urea-related, compounds which undergo deliquescence at different relative humidities (e.g. *N,N*-dimethylurea deliquesces at RH >63% at 18 °C) to generate a set of relative-humidity indicators for providing a sharp register at different, defined relative-humidity levels that span the RH scale.

Notes and references

- R. Esse and A. Saari, in *Smart Packaging Technologies*, ed. J. Kerry and P. Butler, John Wiley & Sons, West-Sussex, 2008, pp. 130–149.
- J. E. Robinson, K. M. Browne and W. G. Burton, *Ann. Appl. Biol.*, 1975, **81**, 399–408.
- R. H. Feinzig and D. Sullivan, Commissioning Humidity Control Systems in Critical Environments, in *National Conference on Building Commissioning*, held at Chicago, IL, 2–4 May 2007.
- N. Yamazoe and Y. Shimizu, *Sens. Actuators*, 1986, **10**, 379–398.
- <http://www.hannainst.com/usa/prods2.cfm?id=012001>, last accessed November 2009.
- <http://www.michell.co.uk/products/classification/browse/portables>, last accessed November 2009.
- P. B. Davis, *US Pat.* 2460065–2460070, 1949.
- P. B. Davis, *US Pat.* 2580737, 1949.
- D. L. Fuller, *US Pat.* 4034609, 1977.
- D. L. Fuller, *US Pat.* 4150570, 1979.
- J. S. Haswell, *US Pat.* 5520041, 1996.
- W. O. Krause, *US Pat.* 3533277, 1970.
- W. O. Krause, *US Pat.* 3499616, 1970.
- J. F. McBride, *US Pat.* 4909179, 1990.
- S. D. Price, *US Pat.* 3121615, 1964.
- E. Wroth and K. Sheraw, *US Pat.* 5950323, 1999.
- Y. Yamakawa, *US Pat.* 7316198 B2, 2008.
- M. Hamada, *US Pat. Appl.* 2007/0157702 A1, 2007.
- P. B. Davis and J. N. Pryor, *US Pat.* 2526938, 1950.
- M. Gattiglia, *US Pat.* 6655315 B1, 2003.
- M. Gattiglia and E. Gandolfo, WO 02/44712 A1, 2002.
- http://www.sud-chemie.com/scmcms/web/page_en_6254.htm, last accessed November 2009.
- R. Matsushima, N. Nishimura, K. Goto and Y. Kohno, *Bull. Chem. Soc. Jpn.*, 2003, **76**, 1279–1283.

- 24 R. Matsushima, A. Ogiue and S. Fujimoto, *Chem. Lett.*, 2000, 590–591.
- 25 R. Matsushima, A. Ogiue and Y. Kohno, *Chem. Lett.*, 2002, 436–437.
- 26 E. Braswell, *J. Phys. Chem.*, 1968, **72**, 2477–2483.
- 27 A. Ghanadzadeh, A. Zeini, A. Kashef and M. Moghadam, *J. Mol. Liq.*, 2008, **138**, 100–106.
- 28 Z. Zhao and E. R. Malinawski, *Appl. Spectrosc.*, 1999, **53**, 1567–1574.
- 29 J. R. Adams and A. R. Merz, *Ind. Eng. Chem.*, 1929, **21**, 305–307.
- 30 A. Clow, *Nature*, 1940, **146**, 26.
- 31 E. A. Werner, *Nature*, 1937, **139**, 512.
- 32 C. Vazquez-Salinas and S. Lakshminarayana, *J. Food Sci.*, 1985, **50**, 1646–1648.



Effect of alkali on methylene blue (C.I. Basic Blue 9) and other thiazine dyes

Andrew Mills^a, David Hazafy^a, John Parkinson^a, Tell Tuttle^a, Michael G. Hutchings^{b,*}

^a Department of Pure & Applied Chemistry, University of Strathclyde, Glasgow G1 1XL, UK

^b School of Chemistry, University of Manchester, Manchester M13 9PL, UK

ARTICLE INFO

Article history:

Received 1 March 2010

Received in revised form

12 May 2010

Accepted 25 May 2010

Available online 11 June 2010

Keywords:

Methylene blue

Methylene violet

C.I. Basic Blue 9

Thiazine

Hydrolysis

DFT

ABSTRACT

A detailed study of the action of alkali on methylene blue (C.I. Basic Blue 9) and other thiazine dyes was carried out through a combination of UV/visible spectroscopy, thin layer chromatography, mass and NMR spectrometry and computational methods. In 0.1 M aq alkali solution, methylene blue forms a highly coloured, lipophilic species that is mainly Bernthsen's methylene violet *i.e.* a hydrolysis decomposition product, this being contrary to the report of a red *N*-hydroxy methylene blue adduct. The nature of the heterocyclic nitrogen atom in C.I. Basic Blue 9 is discussed and it is concluded there is no basis for the proposal of nucleophile addition at this site of the dye. In contrast, other thiazine dyes are deprotonated by alkali to form their neutral, highly coloured, lipophilic conjugate base forms.

© 2010 Elsevier Ltd. All rights reserved.

1. Introduction

C.I. Basic Blue 9 (Methylene Blue (MB; **1**; Table 1)) is a classical, basic dye, originally synthesized by Heinrich Caro, that has been commercially available since its first production by BASF in 1876 [1]. It enjoys manifold, widespread uses such as a dye for hair, leather and cellulosic fibres, redox indicator, ISO test pollutant in semiconductor photocatalysis, photosensitizer for singlet oxygen generation, antioxidant and antiseptic, stain for fixed and living tissues, diagnostic agent in renal function tests, antidote to cyanide and nitrate poisoning and as a treatment for malaria [2,3]. It has recently been reported to be effective in arresting the progress of Alzheimer's and other neurodegenerative diseases [4–6].

Amazingly, this far-reaching and sustained interest shows no evidence of fading insofar as >4000 MB-related papers were published in the last 5 years. However, there is still much about this apparently simple dye molecule that can surprise. For example, it was recently reported that MB readily forms a red-coloured ($\lambda_{\max} = 525$ nm in toluene) lipophilic, non-ionic hydroxy adduct upon treatment with an equimolar amount of sodium hydroxide, to which the *N*-hydroxy structure MB-OH **2** was assigned [7].

Structure **2** is closely related to the leuco form of MB (**3**) which is almost colourless [8]. Consequently a molecule of structure **2** would

also be anticipated to be colourless, thereby calling into doubt the structural assignment of the red material isolated from alkali treatment of MB, which, in any case, is in conflict with the classical literature which reports the main product to be the hydrolysed species, Bernthsen's methylene violet (MVB; C.I. 52041; **4**) [9]. In view of MB's continuing and topical applications, the chemistry of MB and related examples was reviewed; a brief overview of the results has been published elsewhere as a comment [10] on the original paper [7], accompanied by a reply [11].

The earlier assignment [7] of structure **2** was based on a proposal by Plater [12] that the heterocyclic nitrogen of MB is electron deficient and thus a target for nucleophilic attack. Although the current authors considered this proposal unlikely, comments from referees and others induced us to address this point in more detail in this paper. The objectives of this work were to present the full evidence for the characterization of the product obtained from reaction between MB and NaOH, to discuss the nature of MB's heterocyclic N atom alongside other related dye species and to summarize the results of investigations into how other thiazine-based dyes behave towards alkali.

2. Experimental

2.1. Materials and chemicals

Methylene blue (96+%, as hydrate, MW. 319.85; MB (**1**)) was purchased from Acros. Azure B (80%+, M_r 305.83; C.I. 52010; AB (**5**)),

* Corresponding author.

E-mail address: mike.hutchings@manchester.ac.uk (M.G. Hutchings).

Table 1
Summary of structural, spectral and physical characteristics of MB and other relevant thiazine dyes and derivatives.

Structure	No.	Abbreviation, name, molecular weight	λ_{\max}/nm		pK_a^c
			Cation ^a	Neutral ^b	
	(1)	MB Methylene blue 284.4	665 (746) ^d		
	(2)	MB-OH 256.32		520 ^f [351]	
	(3)	Leuco-MB 285.4		256 ^g	
	(4)	MVB Methylene violet 256.32	610 ^e	520 ^h	
	(5)	AB Azure B 270.37	645	503 [521]	12.1
	(6)	AA Azure A 256.35	628	500 [501]	11.8
	(7)	AC Azure C 242.32	615	488 [520]	11.5
	(8)	TH Thionine 228.29	602	487 [486]	11.0

^a Absorption maxima of cationic species measured in water.

^b Absorption maxima of neutral deprotonated species measured in toluene. Calculated values in square brackets []. See Discussion, Section 3.3.

^c Data from Bonneau R, Faure J, Jousot-Dubien J. *Talanta*, 1967; 14:121.

^d Protonated doubly charged absorption maximum from reference [40].

^e O-protonated MVB.

^f Data from reference [7], assigned to MB-OH but actually for MVB.

^g Data from Obata H. *Bull Chem Soc Jpn* 1961; 34:1057; Cohn G. *Ber* 1900; 33:1567.

^h Data for neutral unprotonated MVB.

Azure A (96%, M_r 291.80; C.I. 52005; AA (6)), Azure C (40%, M_r 277.77; C.I. 52002; AC (7)), thionine (85%, M_r 287.34; C.I. 52000; TH (8)) and methylene violet (Bernthsen), (80%, M_r 256.33; C.I. 52041; MVB (4)) were purchased from Aldrich; all were chloride salts except thionine acetate. Structures are given in Table 1. MB was further purified by continual extraction of red impurities from its buffered aqueous solution by CCl_4 until the latter washings were colourless, followed by crystallization according to a published method [13]. All other chemicals were used without further purification. Analytical thin layer chromatography was carried out using silica plates employing $\text{MeOH}/\text{CHCl}_3/\text{HOAc}$ 90:8:2 as mobile phase.

2.2. Spectrophotometric measurements

All UV/visible spectrophotometric experiments were recorded on a Varian Cary 50 double beam spectrophotometer, using 1 cm

quartz cuvettes in dry solvents of highest available purity. A Perkin–Elmer fluorimeter LS 50 B was used to record fluorescence spectra.

2.3. Mass spectrum analysis

Two different mass spectrometers were used in this work. The majority of the experiments were run on an ESI-MS (Thermo-Finnigan LCQ DUO MS) using either the direct injection port or via an HPLC system (*i.e.* LC-MS). In the latter, the HPLC column was a Phenomenex Gemini, C18, 5 μm , 50 \times 2.0 mm. A graded mobile phase was used comprising initially 0.1% formic acid in water, becoming 0.1% formic acid in acetonitrile, over 15 min at 150 $\mu\text{l}/\text{min}$ flow rate. An LDI-MS (Shimadzu, AXIM-CFR) was also used to record the mass spectra of the thiazine dyes as well as the MB base hydrolysis products. Samples of the dyes were prepared and

recorded at different pH values (neutral, 10, 12) and the toluene extract prepared by shaking the dye (0.1 mM) in 0.1 M NaOH with an equal volume of toluene (*vide infra*).

2.4. Computational methods

All structures were optimized in the solvent phase using the polarisable continuum model [14,15] (PCM) at the B3LYP [16–21] level of theory with the 6–311++G(d,p) basis set [22,23]; no symmetry constraints were imposed during the optimization of the dyes. The structures were optimized in two different solvent (dielectric) environments, water ($\epsilon = 78.4$) and toluene ($\epsilon = 2.4$). Time dependent density functional theory [24–26] (TD-DFT) single-point calculations were performed on the optimized structures to obtain the calculated λ_{max} values. The PCM approach was employed within the TD-DFT calculations to model the effect of the respective solvents on the absorption spectra. All calculations were done within the Gaussian 03 program [27]. The charge distribution of MB was determined using the natural bond orbital (NBO) approach [28]. The calculated values for the absorption λ_{max} of relevant, different thiazine dye species in toluene are given in Table 1.

2.5. NMR measurements

^1H NMR data were acquired using Bruker AVANCE-III and Avance/DRX NMR spectrometers operating at 600.13 and 500.13 MHz and operating under TopSpin versions 2.0 and 1.3 respectively. Data accumulated for samples solubilized in CCl_4 were acquired in an unlocked mode, with magnetic field homogeneity adjusted manually using lineshape observation-based shimming.

3. Results and discussion

3.1. MB initial experiments: formation of Red MB

The red lipophilic form of MB assigned the MB-OH structure 2 [7], henceforth referred to as ‘red MB’, was reportedly generated by mixing an ‘aliquot’ of aqueous MB (0.1 mM) with NaOH (0.1 mM, *i.e.* pH 10) under toluene [7]. After 1 h standing, the toluene reportedly developed a red colour due to the extraction of the lipophilic red MB from the aqueous solution. However, in our hands, upon reproducing this simple experimental procedure, no red MB was generated. This was not surprising, given others have noted MB is ‘indefinitely stable’ in aqueous solution at pH 9.5 [29,30]. Indeed, mixing MB with 0.1 mM alkali and shaking with a water-immiscible solvent (usually dichloromethane) is a published method for purifying MB of the less methylated thiazines, such as azure B (5; usually the most prevalent species), azure A (6) and azure C (7), which are common impurities in most past commercial samples of MB [13,31]. It is generally accepted that this purification procedure is effective because the latter thiazines are readily deprotonated by the alkali to their neutral, lipophilic orange or red-coloured forms [31] and MB itself is stable in 0.1 mM alkali. More about this process will be discussed later.

It is tempting to explain our failure to reproduce the formation of red MB as being due to the earlier [7] use of a source of MB that was contaminated with one or more of the thiazines listed in Table 1. However, the reported absorption spectrum and λ_{max} (526 nm) for red MB is not that of any of the deprotonated thiazines. Interestingly, it is possible to generate a species, with a near identical absorption spectrum to that reported for red MB [7], using the same method, but with 0.1 M, instead of 0.1 mM, NaOH aqueous phase solution shaken with toluene. The simplest explanation for the formation of the red dye in the original account would appear to be the use of a more concentrated alkaline solution than reported [7].

Fig. 1 shows photographs of equal volumes of an aqueous MB (0.1 mM) solution below toluene at time zero and 5 h after the addition of sufficient alkali to render the aqueous solution pH 13 and mixing via thorough shaking. The observed UV/visible spectra of the MB aqueous solution at pH 13 and toluene solution before and 1 h and 5 h after mixing are also shown in Fig. 1. These findings show that at pH 13 MB is converted to a lipophilic, *i.e.* toluene-soluble, red/pink species which is clearly observable after 1 h and for which the reaction is complete after 5 h. It has the same spectral features as the MB-derived species reported [7] but is it really a *N*-hydroxy adduct?

3.2. Properties of ‘red methylene blue’

A number of simple experiments reveal the red MB produced as described above using a pH 13 aqueous solution of MB is not a hydroxy adduct, but rather largely Bernthsen’s methylene violet, MVB (4) [32]. The free base form of the latter is not very soluble in water (0.6 mg mL^{-1} , *cf.* MB 50 mg mL^{-1}), but is soluble in most common organic solvents, including toluene. Thus, the UV/visible absorption spectrum of a commercial sample of MVB (4) dissolved in toluene is identical to that of red MB and both also fluoresce with the maximum of emission at 596 nm (λ (excitation) = 520 nm in toluene), in agreement with the values reported in the literature for MVB fluorescence [33]. The measured UV/visible spectra of MVB (4) in different organic solvents are very similar if not indistinguishable from the spectra reported [7] in the same solvents indicating they are the same. In support of this, the hydrolysis of MB with alkali to

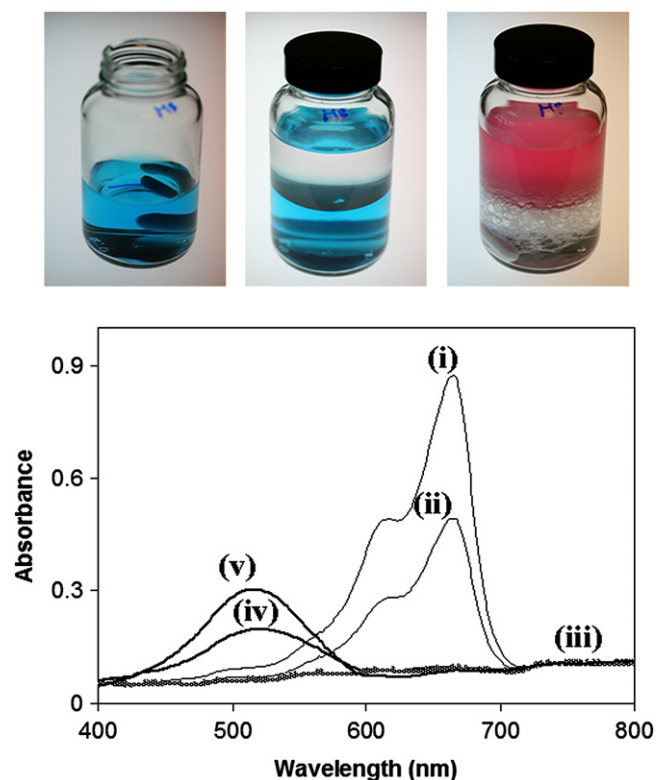


Fig. 1. Top: Photographs of a fresh 10^{-4} M MB, 0.1 M NaOH aqueous solution (from left to right): before, directly after and 5 h after mixing and shaking with an equal volume of toluene. Bottom: Visible absorption spectrum (measured in 1 cm cuvette) of the aqueous MB solution (i) before, (ii) directly following, and (iii) 5 h after mixing and shaking with an equal volume of toluene. The visible absorption spectra of the toluene solution directly after and 5 h following mixing and shaking with the aqueous solution are illustrated by lines (iv) and (v).

produce MVB (**4**) has been suggested previously by others [9] usually based on spectral observations.

Further confirmation of the identity of red MB was afforded by the observation that when it is re-extracted from toluene by an acidic aqueous layer, the latter turns blue with an absorption spectrum that is not MB ($\lambda_{\max} = 665$ nm) but rather that of protonated MVB ($\lambda_{\max} = 580$ nm). When the red MB in toluene solution is spotted onto an acidic silica TLC plate it also turns blue, as noted earlier [7,12], but TLC development causes the original dye spot to separate into two blue spots, neither of which is MB namely, one (the most striking in terms of depth of colour) has the retention time, R_f , of that of commercial MVB (**4**) and the other, which is much weaker in colour, has an R_f value the same as that of azure B (**5**; see Table 1).

The NMR spectra recorded for MB (in D_2O ; 500.13 MHz), red MB and MVB (in CCl_4 ; 600.13 MHz) reveals red MB to be identical to MVB and not MB, nor any hydroxy adduct. Thus, the NMR spectra of MB, red MB and MVB depicted in Fig. 2 clearly indicate the conversion of a symmetrical molecule (MB, lower NMR spectrum) to an unsymmetrical molecule possessing two unique and clearly distinguishable AMX spin systems entirely consistent with MVB and in contrast to what would be predicted for the symmetrical MB-OH adduct **2**. Consistent with the above is the mass spectrum of the red MB in toluene solution which revealed the predominant presence of MVB (molecular ion peak at m/z 256) with some azure B (**5**; m/z peak at 270).

Overall, these experimental findings show that the red MB species introduced by Plater [12] and subsequently claimed by Pal and co-workers [7] to be the *N*-hydroxy species MB-OH (**2**) is in fact MVB (**4**), possibly containing some azure B (**5**), generated by adding a high concentration of base (0.1 M NaOH) to an aqueous solution of MB, through a simple, well-established [30] hydrolysis reaction.

In the meantime, Plater has indicated that the red material to which he assigned the MB-OH structure **2** [12] is in fact Azure B

(**5**; Table 1) [34]. As already stated this is a common MB contaminant, and can be readily formed from MB by alkali-induced demethylation [35,36] at pH 11, a value somewhat lower than that (pH 13) which causes deamination to MVB.

3.3. The nature of heterocyclic nitrogen in MB and analogous dyes

Based on our foregoing investigations with MB and the lack of information of any product with a structure MB-OH (**2**), we remained interested in the question of the electronegativity of the heterocyclic nitrogen in MB. Fig. 3 shows the main valence bond resonance forms contributing to the structure of MB. A central contention [7,12] underlying the claimed formation of MB-OH (**2**) was that the central nitrogen in MB is electron deficient. The implication is that the mesomer **N**, characterized by a positive charge localized on the heterocyclic N connecting two fully benzenoid rings, is a significant contributor to the overall structure. However, density functional calculations and application of both the NBO and electrostatic potential (ESP) methods reveal this not to be the case. Rather, it appears the central nitrogen is electron rich relative to the remainder of the molecule. Thus, while the magnitude of the charges calculated by each method varies, both methods reveal that the S atom carries a neutral (ESP: +0.04e) to partial positive (NBO: +0.52e) charge, reflecting the importance of mesomer **S**. Importantly, with both methods the heterocyclic N atom of MB has an overall partial negative charge (NBO: -0.38e, ESP: -0.79e) as illustrated by the calculated partial charges from the NBO method in Fig. 4. In valence bond terms mesomer **N** is a minor contributor, while mesomers **S** and **D1/D2** more closely resemble the structure of MB.

One of our early reasons for questioning the claim for a *N*-hydroxy adduct structure **2** for MB-OH was experience of simple colour–structure relationships. A molecule with the structure **2** of

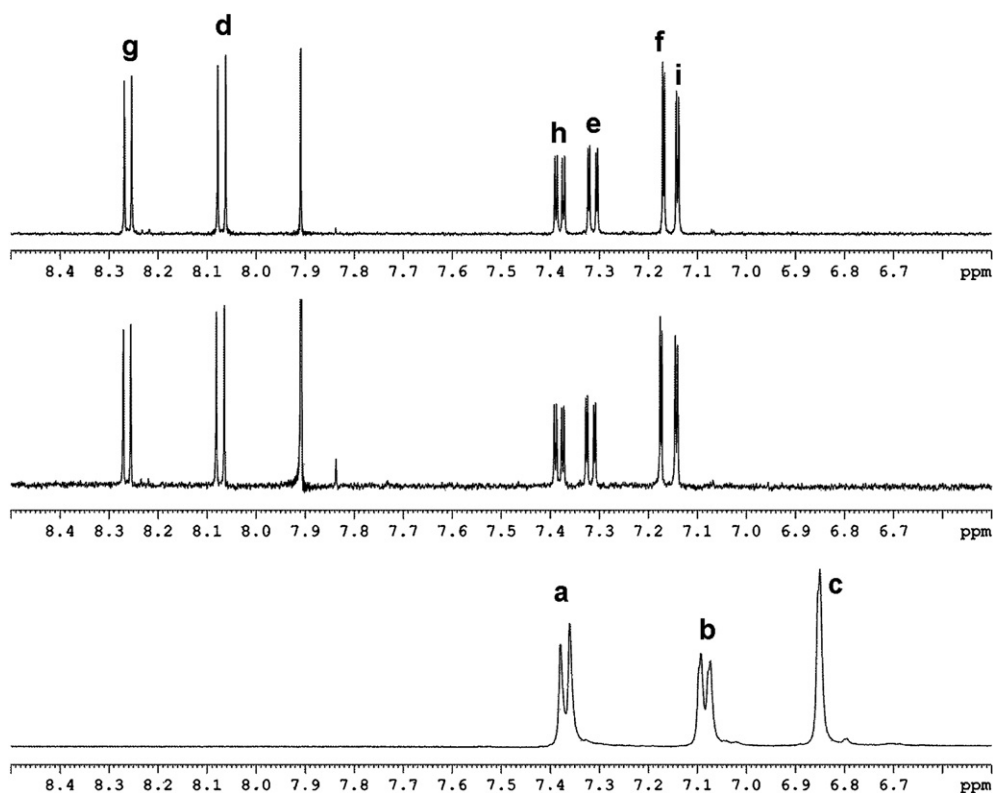


Fig. 2. 1H NMR spectra of (top to bottom) purchased MVB (Aldrich), red MB (both recorded in CCl_4 using Bruker Avance-III 600 NMR spectrometer) and methylene blue (Acros) (recorded in D_2O using Bruker Avance/DRX 500 NMR spectrometer).

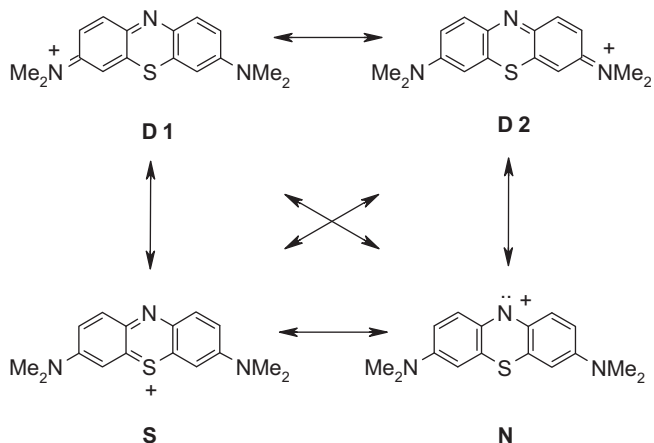


Fig. 3. Major valence bond resonance structures of MB. Alternative Kekulé structures of benzenoid rings and charged-carbon mesomers are not shown.

MB-OH would not be expected to be red: the delocalized conjugation present in MB is removed in MB-OH, just as it is in (colourless) leuco-MB (**3**), and MB-OH is equally unlikely to be coloured. In much earlier classical dye–structure studies, Lewis et al. speculated on the formation of a product with structure MB-OH (**2**) by the addition of water to MB as an intermediate in their chemistry, and they also noted it would be colourless [37]. Subsequently we have calculated the absorption maximum for a species with the MB-OH structure **2**. After initial geometry optimization, TD-DFT calculations reveal it would have an absorption maximum in the near UV at 351 nm, confirming its essential lack of colour. Similar calculations of the visible spectra of other known thiazine dyes reproduce their experimental absorption maxima with reasonable reliability (Table 1), demonstrating the suitability of the level of theory used for this work [38].

Our own wide-ranging literature search for precedent of hydroxide anion addition at imine-type nitrogen has turned up no example [39]. Whilst Plater [12] only speculated on the electronegative nature of the heterocyclic nitrogen of MB and the subsequent formation of MB-OH, albeit without any direct structural characterization, it is apparent that this speculation has been over-interpreted by others [7,11] and has given credence to electron-deficient heterocyclic nitrogen in MB when none is due.

If there is no experimental evidence for electron-deficient nitrogen in MB, is there experimental support for this centre being electron rich, as calculated? Protonation of MB in strong acid is well known to give a bathochromic shift in λ_{\max} , from 664 nm for MB in water to 746 nm in aqueous acidic MB, consistent with protonation at the

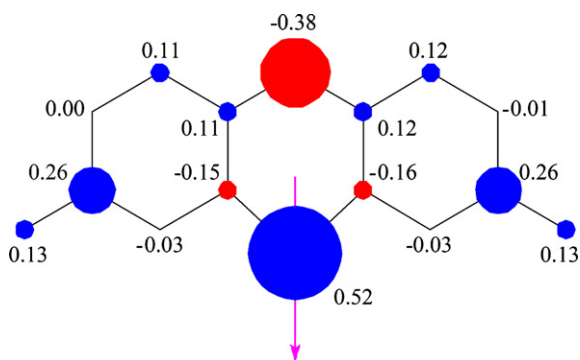
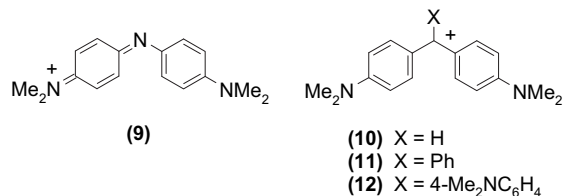


Fig. 4. NBO charge distribution on the PCM/B3LYP electronic ground state of MB. See Computational Methods for details.

heterocyclic N atom ($pK_{\text{BH}^+} = -0.26$) [40,41]. Alternative protonation of a pendant Me_2N group would lead to a hypsochromic shift, and is discounted.

All the above evidence suggests that although a valid contributory valence bond MB structure can be written with electron-deficient nitrogen, **N** in Fig. 3, this does not represent the actual structural situation of MB. In fact, the heterocyclic nitrogen atom in **N** is now a formal 6-electron centre, analogous to a diarylnitrenium ion (a known, highly reactive species [42]). Electron deficiency due to a sub-octet electron configuration at a relatively electronegative element such as nitrogen is energetically disfavoured, and so even if mesomer **N** appears acceptable on paper, it is in fact unrepresentative of MB. The same conclusion appears to hold across other dye classes which include formally 6-electron positive sp^2 nitrogen centres. As far as we are aware, there are no reports of *N*-hydroxy derivatives of analogues such as diazines, quinone imines (typified by Bindschedler's Green (C.I. 76125; **9**), which hydrolyses via successive attack at the two terminal C-NMe₂ groups [43]), azacyanines, and so on. Furthermore, simple MO calculations of such species always indicate a relatively electronegative nitrogen, bearing a partial negative charge [44]. In contrast, when the nitrogen centre of interest is replaced by positively charged sp^2 carbon, hydroxide addition at that centre is well known. Examples include diaryl carbenium ions (e.g. Michler's hydrol, **10**), their triaryl carbenium ion analogues (e.g. Malachite Green (C.I. Basic Green 4; **11**), and Crystal Violet (C.I. Basic Violet 3; **12**)) and the cyclised acridine, xanthene and thioxanthene series [45]. Unlike electronegative nitrogen, the more electropositive carbon is more amenable to supporting a positive charge in an electron-deficient 6-electron configuration, and thus can be a site for attack by negative nucleophiles.



3.4. Other thiazines

The purities of the other major thiazines, namely Azures A, B, C and thionine (**5–8**; see Table 1), were assessed using LC-MS and the results are summarized in Table 2. Thus, whereas the commercial sample of thionine (**8**) was very pure (99+%) and azure B (**5**) of a reasonable purity (ca. 86%), the other two thiazines were gross mixtures. Most notably, the sample of azure A (**6**) was of very low purity (ca. 21%) and far from the supplier's claimed value of 96%. However, for the general purpose of demonstrating the formation of coloured lipophilic species upon treatment with alkali the dyes

Table 2
Composition of commercial samples of thiazine dyes used in this study, determined by hplc.

Commercial thiazine	%MB (1)	%AB (5)	%AA (6)	%AC (7)	%TH (8)
MB (1)	91	8.7	<1	<1	<1
AB (5)	3	86	10	1	0
AA (6)	36	28	27	8	1
AC (7)	0	7	47	38	7.5
TH (8)	0	0	0	0	99+
MVB (4)	84% MVB, no other thiazines present				

were used as received. Thus, these four thiazine dyes were treated with an aqueous pH 13 solution, and photographs of the solutions (i) before, (ii) directly after (with shaking), and (iii) 5 h after mixing with an identical volume of toluene, are shown in Fig. 5. Given the reports [7,12] of a coloured, lipophilic hydroxy adduct, some might be tempted to assume that all the thiazine dyes form such species and assign the highly coloured toluene solutions arising from alkaline treatment illustrated in Fig. 5 as being due to the *N*-hydroxy adducts of the associated thiazine. However, this work now shows that the reported red MB is, in fact, MVB and that the *N*-hydroxy adduct of any thiazine should be largely colourless. Thus, the alternative, less glamorous, but well-established explanation for the results illustrated in Fig. 5 still stands, *i.e.* that the other thiazines are simply deprotonated by alkali to form highly coloured lipophilic

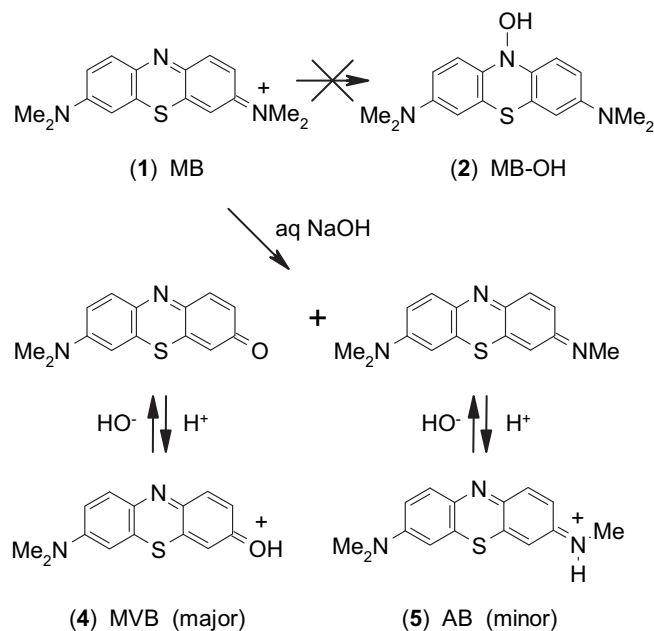


Fig. 6. Summary of reactions of MB with alkali.

species. The results in Fig. 5 also reveal that the thionine (8) and azure C (7) pH 13 aqueous solutions (before mixing with toluene) are red, whereas those for azure A (6) and azure B (5) are purple. This feature arises because the pK_a for the thiazine dyes (see Table 1) decreases with decreasing degree of methylation, so that, for example, at pH 13 most (99%) of the thionine will be in its red, lipophilic deprotonated, free base form, whereas for Azure B at least 11.2% will still be in its purple–blue protonated form [31].

The calculated λ_{max} values in toluene of the deprotonated forms of the thiazine dyes, along with those found experimentally, are listed in Table 1. The experimental and calculated values compare very well (especially given the impure natures of azure A and azure C) and strongly support the deprotonation mechanism. Others [46] have used NMR spectroscopy to show that the yellow/orange lipophilic form of thionine, produced by treatment with alkali, is the deprotonated form of the parent dye.

4. Conclusions

The chemistry discussed in this paper is summarized in Fig. 6. Basic hydrolysis of MB leads mainly to the production of MVB, 4, and the visible spectral properties of MVB in six solvents and on a tlc plate match very closely the reported properties of what has been claimed [7] to be an *N*-hydroxy adduct of MB, MB-OH (2). However, the calculated visible spectrum of MB-OH is reliably predicted to be colourless, not red, and the incorrectly assigned site of hydroxide attack in MB, the heterocyclic N atom, is not electron deficient as suggested as a reason for MB-OH formation. We have been unable to find any literature precedent for hydroxide attack at any sp^2 -hybridised nitrogen atom, and all the experimental evidence points to MVB (4) as the main product of alkaline hydrolysis of MB, and not MB-OH (2).

It is always difficult to prove a negative. We are not claiming that the nitrogen heterocyclic site in MB or any similar nitrogen can never be electrophilic in appropriate circumstances. But as far as we can determine this has not yet been demonstrated, and available evidence such as the results of calculation and site of protonation indicates the opposite.

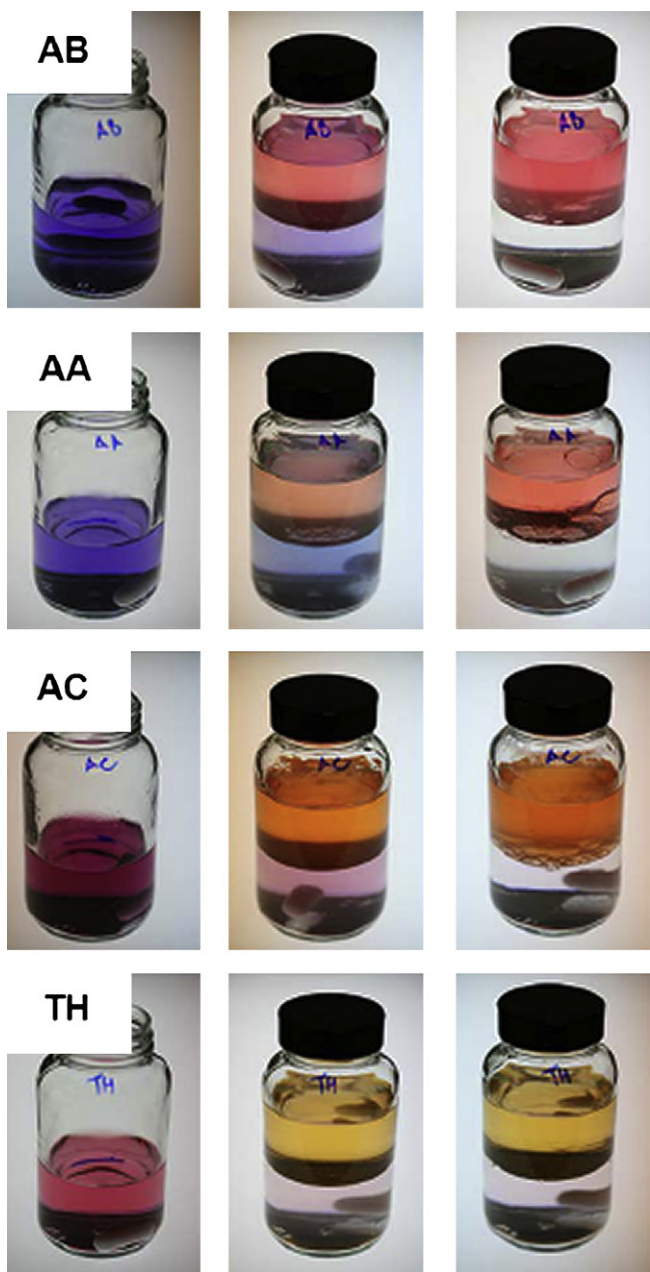


Fig. 5. Photographs of a range of freshly made 10^{-4} M thiazine dye solutions in 0.1 M NaOH (from left to right): before, directly after, and 5 h after mixing and shaking with an equal volume of toluene.

The other major cationic thiazine dyes, which contain one or more amine-attached hydrogen atoms, also do not form hydroxy adducts, but instead are deprotonated in 0.1 M NaOH solution to very differently coloured (λ_{\max} hypsochromic shift in aqueous solution typically = 100–150 nm), red or orange lipophilic, free base forms of the original dye (shown for azure B, **5**, in Fig. 6) It is also important to note that similar product formation and spectral changes would be expected for oxazine and phenothiazine dyes. Thus the claim [7] that Nile Blue (C.I. Basic Blue 12) forms a coloured, lipophilic *N*-hydroxy adduct, rather than a deprotonated lipophilic species (like its near thiazine equivalent, Azure A, **6**), appears as unlikely as that of a coloured, *N*-hydroxy adduct of MB.

Acknowledgement

We thank Dr M.J. Plater of Aberdeen University for helpful discussions about his own studies on methylene blue and its interaction with hydroxide, especially clarification of the red material he obtained from MB at pH 11.

References

- [1] Travis AS. The rainbow makers. London: Associated University Presses; 1993.
- [2] The merck index. Rahway: Merck & Co., Inc.; 1989.
- [3] http://en.wikipedia.org/wiki/Methylene_blue accessed 01 2010.
- [4] Murray AD, Stuff RT, Ahearn TS, Bentham P, Seng KM, Wischik C. Alzheimer's Demen 2008;4:T786.
- [5] Wischik CM, Rickard JE, Harrington CR, Horsley D, Storey JMD, Marshall C, Sinclair JP, Tan HW. Methods of chemical synthesis and purification of diaminothiazinium compounds including methylthioninium chloride, U.S. patent 2006/0287523 A1 published Dec 21st 2006.
- [6] <http://www.examiner.com/x-11432-Pittsburgh-Medical-Technology-Examiner~y2010m1d9-Methylene-blue-may-hold-the-cure-for-neurodegenerative-diseases-such-as-Alzheimers-disease?cid=edition-rss-Pittsburgh>; January 09 2010.
- [7] Basu S, Panigrahi S, Prahara S, Ghosh SK, Pande S, Jana S, et al. J Phys Chem A 2007;111:578.
- [8] Thien TV [chapter 3]. In: Muthyala R, editor. Chemistry and applications of leuco dyes. New York: Plenum Press; 1997. p. 67.
- [9] Adamcikova L, Pavlikova K, Sevcik P. React Kinet Catal Lett 2000;69:91; Holmes WC, French RW. Stain Technol 1926;1:17; MacNeal WJ, Killian JA. J Am Chem Soc 1926;48:740.
- [10] Mills A, Hazafy D, Parkinson JA, Tuttle T, Hutchings MG. J Phys Chem A 2009;113:9575–6.
- [11] Pal T. J Phys Chem A 2009;113:9577.
- [12] Plater MJ. ARKIVOC; 2003:37–42.
- [13] Marshall PN, Lewis SM. Stain Technol 1976;50:375.
- [14] Barone V, Cossi M. J Phys Chem A 1998;102:1995.
- [15] Cossi M, Rega N, Scalmani G, Barone V. J Comput Chem 2003;24:669.
- [16] Becke AD. Phys Rev A 1988;38:3098.
- [17] Becke AD. J Chem Phys 1993;98:5648.
- [18] Hertwig RH, Koch W. Chem Phys Lett 1997;268:345.
- [19] Lee CT, Yang WT, Parr RG. Phys Rev B 1988;37:785.
- [20] Stephens PJ, Devlin FJ, Chabalowski CF, Frisch MJ. J Phys Chem 1994;98:11623.
- [21] Vosko SH, Wilk L, Nusair M. Can J Phys 1980;58:1200.
- [22] Hariharan PC, Pople JA. Theor Chim Acta 1973;28:213.
- [23] Krishnan R, Binkley JS, Seeger R, Pople JA. J Chem Phys 1980;72:650.
- [24] Bauernschmitt R, Ahlrichs R. Chem Phys Lett 1996;256:454.
- [25] Casida ME, Jamorski C, Casida KC, Salahub DR. J Chem Phys 1998;108:4439.
- [26] Stratmann RE, Scuseria GE, Frisch MJ. J Chem Phys 1998;109:8218.
- [27] Frisch MJ, Trucks GW, Schlegel HB, Scuseria GE, Robb MA, Cheeseman JR, et al. Gaussian 03, revision E.04. Wallingford CT: Gaussian, Inc.; 2004.
- [28] Reed A, Weinstock RB, Weinhold F. J Chem Phys 1985;83:735.
- [29] Abbott DC. Analyst 1962;87:286.
- [30] Holmes WC, Snyder EF. Stain Technol 1929;4:7.
- [31] Bonneau R, Faure J, Jousot-Dubien J. Talanta 1967;14:121.
- [32] The discoverer's name is frequently appended when naming the thiazine-based Methylene Violet, to distinguish it from other species with the same or similar name e.g. Methylene Violet 3RAX, which has an unrelated safranin structure, 3-amino-7-(diethylamino)-5-phenyl phenazinium chloride; see Aldrich Catalogue 307505.
- [33] Otsuki S, Taguchi T. Bull Chem Soc Jpn 1996;69:2525.
- [34] Plater MJ. Private communication, February 2010.
- [35] Mills A, Hazafy D. unpublished results.
- [36] Marshall PN, Lewis SM. Biotech Histochem 1975;50:375–81.
- [37] Lewis GN, Goldschmid O, Magel TT, Bigeleisen J. J Am Chem Soc 1953;65:1150.
- [38] A recent paper examines the use TD DFT calculations of excitation energies of dyes, including MB. Fabian J Dyes Pigm 2010;84:36–53.
- [39] Beilstein database v.2008/04, via CrossFire Commander v.7.1, © Elsevier Information Systems.
- [40] Nishikiori H, Nagaya S, Tanaka N, Katsuki A, Fujii T. Bull Chem Soc Jpn 1999;72:915–21.
- [41] Lewis GN, Bigeleisen J. J Am Chem Soc 1943;65:1144–50.
- [42] Falvey DE. J Phys Org Chem 1999;12:589–96.
- [43] Griffiths J, Cox R. Dyes Pigm 1999;42:29–34; Möhlau R. Ber Deutschen Chem Ges 1884;18:2915.
- [44] Unpublished results.
- [45] Zollinger H. Color chemistry [chapter 4]. 3rd ed. Zürich: Vhca and Wiley-VCH; 2003.
- [46] Nicotra VE, Mora MF, Iglesias RA, Baruzzi AM. Dyes Pigm 2008;76:315.



Novel photocatalyst-based colourimetric indicator for oxygen

Andrew Mills*, David Hazafy, Katherine Lawrie

WestCHEM, Department of Pure & Applied Chemistry, University of Strathclyde, 295 Cathedral Street, Thomas Graham Building, Glasgow G1 1XL, UK

ARTICLE INFO

Article history:

Received 7 May 2010

Received in revised form

10 September 2010

Accepted 20 October 2010

Available online 26 November 2010

Keywords:

Oxygen

Photocatalyst

Indicator

Methylene blue

Titania

ABSTRACT

The preparation and characterisation of a novel, UV-activated solvent-based, colourimetric indicator for O₂ is described, comprising a redox dye (methylene blue, MB), semiconductor photocatalyst (TiO₂), and a sacrificial electron donor (SED), all dispersed/dissolved in a polymer medium (sulfonated polystyrene, SPS). Upon exposure, the indicator is readily photobleached as the MB is converted into its oxygen-sensitive, leuco form, LMB. Unlike its water-based counterpart, the recovery of the original colour is very slow (ca. 5 days cf. 6 min), probably due to the largely hydrophobic nature of the polymer encapsulation medium. The kinetics of film photobleaching appear to fit very well, in terms of: irradiance, [TiO₂] and [MB], to the usual Langmuir-Hinshelwood type equation associated with a photocatalytic process. The glycerol appears not only to function as a SED, but also a plasticizer and medium for dye dissolution. The kinetics of colour recovery of the photobleached film appear directly dependent upon the ambient level of O₂ but shows a more complex dependence upon the relative humidity, RH. The photobleached film does not recover any of its colour over a 24 h period if the RH < 20% at 21 °C but does recover at an increasing rate with increasing RH above 20%. The dye appears to form a very stable, water-insoluble ion-pair moiety with the SPS, so much so that the dye cannot be leached out by immersing the indicator in water. Potential uses of this UV light activated indicator are discussed briefly.

© 2010 Elsevier B.V. All rights reserved.

1. Introduction

Oxygen is an essential element for all living organisms; it also plays an important role in many chemical industrial processes, especially where a fine control of oxygen concentration, or the absence of oxygen, is required. Detection of oxygen is therefore important in many technologies, although many of the preferred methods (such as: gas chromatography (GC), mass spectrometry (MS) and electrochemical techniques) require rather expensive equipment and trained operators. Optical oxygen indicators [1], on the other hand, are fast-responding, inexpensive and easy to use. As a result, significant research has been conducted in their development, especially with regards to their use in modified atmosphere packaging (MAP). MAP is a common food-packaging technique in which the oxygen inside the package is either removed, or replaced by an inert gas, such as N₂ or CO₂, to help maintain the freshness of food for longer [2,3]. Research into optical O₂ indicators in MAP has been dominated by luminescence-based indicators, and although several commercial products have emerged [4,5], all are presently still too expensive, both in terms of the indicators and the associated supporting analytical equipment, for

routine incorporation in MAPed packages. As a consequence, they remain a useful R&D food-packaging tool. As an alternative, an easy to read, inexpensive, colour-based O₂ indicator would appear a potential ideal quality control device in MAP, as it would provide the necessary assurance that the integrity of the package remained uncompromised during the journey from package to consumer. Some commercial colourimetric oxygen indicators are already on the market, for example Ageless Eye™, but their retail costs are currently too high (typically 1 Euro ea for Ageless Eye™) to realistically provide 100% QA for MAP. None of the oxygen colour-based indicators reported to date are irreversible in response and printable as inks [6,7], both of which are additional, desirable features of a quality control optical O₂ indicator for MAP.

Recently this group reported [8] a novel, water-based colourimetric O₂ indicator that is UV light activated and comprises: a redox dye, methylene blue (MB), a sacrificial electron donor (SED), glycerol, and a nanoparticulate semiconducting photocatalyst (SC), TiO₂. Unfortunately, because of its water-based nature, this indicator is not suitable for direct printing on most polymer packaging material, which is largely hydrophobic. This paper describes a solvent-based, O₂ indicator which is sufficiently water-proof to allow direct contact with water, without loss of dye, and suitably hydrophobic to allow direct printing on polymer materials commonly used in food packaging such as polypropylene.

* Corresponding author. Tel.: +44 0141 548 2458; fax: +44 0141 548 4822.
E-mail address: a.mills@strath.ac.uk (A. Mills).

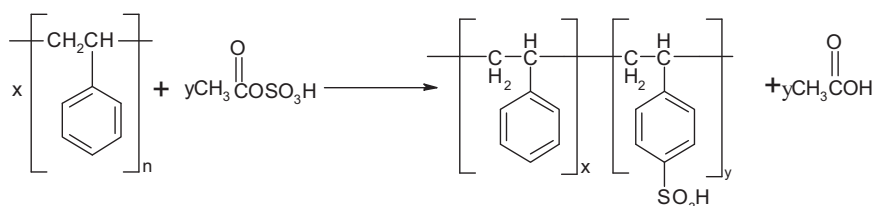


Fig. 1. The reaction scheme of the sulfonation of polystyrene.

2. Experimental

Unless stated otherwise all chemicals were obtained from Aldrich Chemicals and the water used to make up solutions was double-distilled and de-ionised.

2.1. Sulfonation of polystyrene

Previous work by others [9–11] have shown that hydrophobic polystyrene (PS), can be rendered increasingly soluble in polar solvents, by increasing the degree of sulfonation (see Fig. 1). Thus, in this work an acetone-soluble sample of 10% sulfonated PS was prepared according to an establish literature method [12,13], in which 52 g of polystyrene (average molecular weight 250,000, supplied by Acros Organics) were placed in a 3-necked, round-bottomed flask and dissolved in 245 mL of dichloromethane (DCM) through vigorous stirring.

In a separate experiment, a sulfonating agent, acetyl sulfate, was prepared by adding 9.5 mL of acetic anhydride to 50 mL of DCM and the resulting solution then placed under an inert atmosphere of argon and cooled to 0 °C. 3.5 mL of 95% sulfuric acid were added to the DCM/acetic anhydride solution dropwise and then 35 mL of this sulfonation reagent mixture were added to the original polystyrene solution, and the mixture refluxed for 4 h. 50 mL of ethanol were added to the solution after the reflux and the mixture then poured slowly into 1.75 L of boiling water. As the solution was added, the sulfonated polystyrene precipitates rapidly as a white solid. After filtering in air, the precipitate was washed with water several times and dried in an oven at 40 °C overnight. Typically the synthesis, as outlined above, yields ca. 50 g of 10% sulfonated PS (SPS) from 52 g of polystyrene (89% isolated yield).

2.2. Ink preparation

0.25 g of the SPS were weighed into a sample vial and dissolved in 2 g of acetone. To this solution were then added 0.25 g glycerol and, for a standard ink, 0.1 g nanorutile TiO₂ (titanium (IV) oxide, rutile nanopowder, <100 nm particle size, 99.5% trace metals basis). The photocatalyst was dispersed throughout the ink, typically by stirring for 15 min, followed by 30 min sonication. Once complete, 2.5 mg of methylene blue was added and the ink, placed in a stoppered bottle, was stirred for 3 h to ensure all the methylene blue had dissolved. The composition of this typical, acetone-based, oxygen indicating MB/SPS/TiO₂/glycerol film can be summarised as follows: 1/100/40/100 pphr where pphr = parts per hundred resin (where the resin is the SPS). The resulting blue ink is very stable and can be used for at least 6 months without showing any signs of deterioration.

2.3. Ink film preparation

A doctor-blade technique was used to cast the MB/SPS/TiO₂/glycerol ink onto a plastic film, typically polypropylene (Goodfellow, 75 μm) using a K-bar no. 4 to produce an ink film which was ca. 4–5 μm thick when dry. The resulting blue, dry

ink film on the plastic substrate showed good adherence and was stable for more than 6 months under ambient, dark conditions.

2.4. Methods

All UV/vis spectra and absorbance data were recorded using a Varian Cary 50 Bio UV–visible spectrophotometer. Unless otherwise stated, films were monitored in a static system under ambient conditions (21 °C, 58% RH). However, when gas was blown over the system, the gases were blended using a Cole Parmer gas-blender, and a constant flow rate of 100 mL/min was maintained.

3. Results and discussion

3.1. Photo-activation step (step 1)

The MB/SPS/TiO₂/glycerol type of colourimetric oxygen indicator relies on UV activation to initiate the detection process by generating electron–hole pairs in the semiconductor photocatalyst (TiO₂ in this case). The sacrificial electron donor (SED = glycerol in this work) then reacts rapidly and irreversibly with the photo-generated holes, leaving the photogenerated electrons to reduce the redox dye, D_{ox} (=methylene blue) to its differently coloured, usually bleached, reduced form, D_{red} (=leuco-methylene blue). Upon reacting with the photogenerated holes, glycerol is itself oxidised; oxidation products could include [14]: glyceraldehyde, 1,3-dihydroxyacetone, formic acid and carbon dioxide. The leuco-methylene blue is O₂-sensitive, so that after UV activation (*i.e.* step 1) the UV activated ink film will remain in its bleached, reduced form in the absence of oxygen, but will have its original colour restored upon exposure to air (*via* step 2). These processes are summarised in Fig. 2.

Thus a typical MB/SPS/TiO₂/glycerol film is first activated, *i.e.* photobleached, by exposing it to ultraviolet light, which takes less than 60 s when using a 2 × 8 W UVA lamp (irradiance 4.5 mW cm⁻²). The change in the UV/vis absorption spectrum of the film as a function of irradiation time was monitored by UV/vis spectrophotometry and Fig. 3(a) shows the results of this work. Interestingly, the UV/vis spectrum of the original, unbleached film resembles that of the monomer of MB, with a maximum absorbance

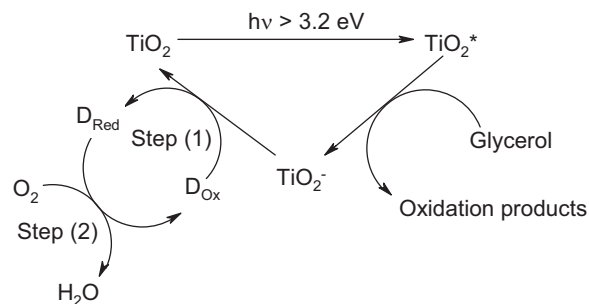


Fig. 2. Mechanism of UV light driven reduction of methylene blue (photoactivation step (1)) and its subsequent re-oxidation by ambient air (if present) (dark step (2)).

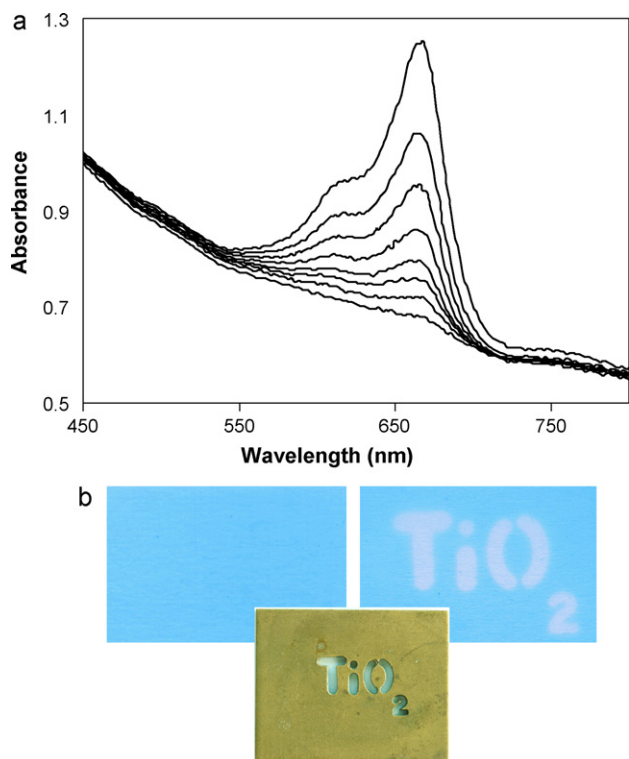


Fig. 3. (a) Plot of UV/vis spectra of a typical MB/SPS/TiO₂/glycerol oxygen-indicating film before and during the UVA light activation (60 s of UVA/4.5 mW cm⁻²) step (step (1), Fig. 2). The irradiation times are (from top to bottom): 0, 2, 4, 6, 8, 10, 15 and 60 s respectively. (b) Photographs of this film before (left) and after (right) the pulse of UVA light shone through the brass 'TiO₂' mask (middle).

at 665 nm [15], whereas, in contrast, water-based inks generate films in which the MB appears largely to be in the form of its dimer ($\lambda_{\max} = 605$ nm) [16,17]. These observations are consistent with the fact that MB shows little sign of aggregate formation in non-aqueous solvents [18]. The photographs in Fig. 3(b) show a typical film before and after UVA light activation through a brass 'TiO₂' mask. In the absence of UV light, the photobleached areas regained their original blue colouration within 5 days upon exposure to air. *Note:* this very slow recovery is in striking contrast to that exhibited by its water-based counterpart (where the dark recovery step is complete within 6 min). It is not clear why LMB reacts so slowly with O₂ in a hydrophobic polymeric film; although, such a delay is useful as the indicator could then be used to indicate how long a package has been open, i.e. as a 'consume-within' indicator. Such an indicator has some potential in the food packaging industry, as greater attention is given to finding ways to minimise food wastage. A particular problem with regard to the latter is the throwing away of food in opened packages that is still good to eat because of not necessarily warranted concerns regarding freshness. A consume-within indicator would go some way to alleviate these concerns [1] and reduce consumer food waste.

The time needed to fully photobleach a typical MB/SPS/TiO₂/glycerol film was <1 min, which is ca. 3 times faster than that for a similar, water-based indicator, most likely due to the latter's much reduced kinetics for step 2 in Fig. 2; i.e. a much reduced rate of response towards O₂.

The initial rate of photobleaching for a typical film was studied as a function of the incident light irradiance and Fig. 4 shows the absorbance at λ_{\max} of MB (665 nm) vs. irradiation time profiles for different UVA light irradiances. For most photocatalytic systems, at low irradiances, the initial rate is found to be proportional to the irradiance, I (indicating that electron-hole recombination

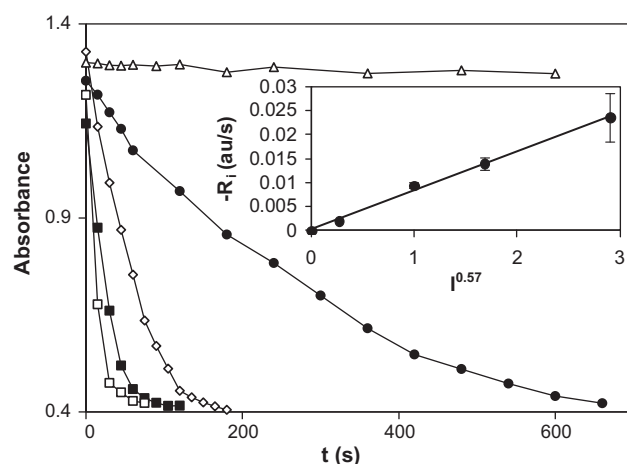


Fig. 4. Absorbance vs. time profiles for a typical O₂ indicator film photobleaching as a function of different UVA irradiances. The irradiances used were: 0 (Δ), 0.1 (\bullet), 1.0 (\diamond), 2.5 (\blacksquare) and 6.5 (\square) mW cm⁻². The insert shows the initial rate (absorbance units (au)/s) dependence on the irradiance, along with associated error bars.

is not significant) and, at high irradiancies, proportional to $I^{1/2}$ (indicating that recombination is the predominant fate of photo-generated electron-hole pairs) [19]. Often [20], at intermediate irradiancies, the initial rate is found to be proportional to I^θ , where $0.5 < \theta < 1$, and the results of this work is an example of such a case, with $\theta = 0.57$, as indicated by the insert plot of the data in Fig. 4. For a modest irradiance ($I = 6.5$ mW cm⁻²) the quantum efficiency of the photobleaching process was calculated to be 2.9%, based on an initial rate of photobleaching at 665 nm of 4.8 absorbance units (au)/min, an assumed molar absorptivity for MB of 84,300 M⁻¹ cm⁻¹ [21] and a film thickness of ca. 5.0 μ m.

A study was carried out on the effect of semiconductor photocatalyst concentration in the MB/SPS/TiO₂/glycerol indicator on the rate of film photobleaching, using a series of inks prepared with the following different TiO₂ contents: 0, 4, 7, 10, 20 and 40 pp/hr. The results of this work are illustrated in Fig. 5 and revealed the initial photobleaching rate to be directly proportional to the amount of TiO₂, which is quite typical of many photocatalytic systems [22]. Further addition of TiO₂ above 40 pp/hr caused a marked increase in scattering, preventing accurate absorbance measurements.

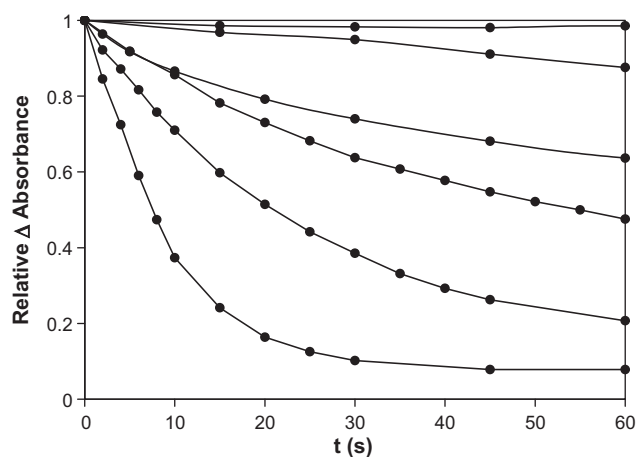


Fig. 5. Relative change in absorbance, Δ Abs, vs. time of UVA photobleaching of a MB/SPS/TiO₂/glycerol film as a function of TiO₂ concentration in the film. The data lines refer to 0, 4, 7, 10, 20 and 40 pp/hr (top to bottom) of TiO₂ used in the O₂ indicator formulation. The relative Δ Absorbance was calculated using: $\text{rel}\Delta\text{Abs} = (\text{Abs}_{\lambda_{\max}} - \text{Abs}_{\lambda_{800\text{nm}}})_t / (\text{Abs}_{\lambda_{\max}} - \text{Abs}_{\lambda_{800\text{nm}}})_{t=0}$.

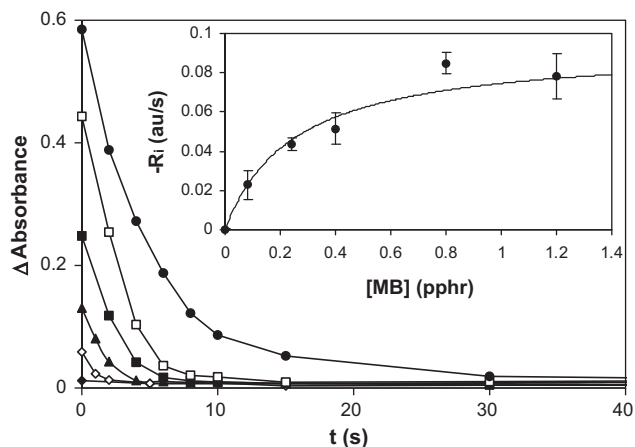


Fig. 6. Plot of ΔAbs vs. the time of irradiation for a typical O_2 indicator film containing different pphr of MB. The covering range: 0 (\blacklozenge), 0.08 (\diamond), 0.24 (\blacktriangle), 0.4 (\blacksquare), 0.8 (\square) and 1.2 (\bullet) pphr of MB. The insert diagram is a subsequent plot of the data in the form of initial rate, r_1 vs. $[\text{MB}]$, along with associated error bars.

The effect of the variation of the concentration of the sacrificial electron donor, glycerol, used in the MB/SPS/ TiO_2 /glycerol was also investigated. From the results of this work it was apparent (from the film's initial absorbance, ΔAbs , at $\lambda_{\text{max}}(\text{MB}) = 665 \text{ nm}$) that the function of glycerol was not just as a source of electrons but also as an aid to dye dissolution. Thus, $\Delta\text{Abs}_{t=0}$ decreased with decreasing $[\text{glycerol}]$ even though the amount of dye used to formulate the ink was the same each time. Indeed, if no glycerol was used, the film was barely blue and no dye-photobleaching (*i.e.* step 1 in Fig. 2) could be observed! At the high glycerol level (100 pphr) used in this work for a typical MB/SPS/ TiO_2 /glycerol indicator, most of the MB appeared to be dissolved, since further additions of glycerol had no effect on the initial absorbance of the film.

Finally, the effect of MB concentration used in the film formulation on the kinetics of the photobleaching step was also studied and results of this work are illustrated in Fig. 6. The insert shows that the kinetics are described by a simplified Langmuir-Hinshelwood type equation which is common [23] in semiconductor photocatalysis:

$$r(\text{MB}) = k \frac{K[\text{MB}]}{1 + K[\text{MB}]} \quad (1)$$

where $r(\text{MB})$ is the rate of photobleaching and k and K are apparent constants.

The shape of the plot illustrated in Fig. 6 is typical of semiconductor photocatalytic reactions carried out in solution and implies Langmuir-Hinshelwood type kinetics also apply in the polymer ink films under study here. An analysis of the data illustrated in the insert diagram in Fig. 6 revealed values of 0.09 absorbance units (au)/s and 4.02 pphr^{-1} for k and K , respectively, for the line of best fit to the data according to Eq. (1).

3.2. Dark recovery step (step 2)

As noted earlier, what is most striking about the MB/SPS/ TiO_2 /glycerol colourimetric O_2 indicator reported here, is the very slow (*ca.* 5 days) dark recovery step (step 2 in Fig. 2), which, in contrast, takes only 6 min in a water-based version of the ink, as illustrated by the recovery data for the two different films in Fig. 7. In order to gain a better understanding of the cause of this slow recovery step (step 2), two 10^{-5} M methylene blue solutions were prepared using, respectively, water and acetonitrile as a solvent. Both solutions were purged with nitrogen for 10 min and zinc amalgam (0.5 g into 100 mL of the MB solution) added to reduce the MB to LMB. After the solutions were bleached and the amalgam was filtered off,

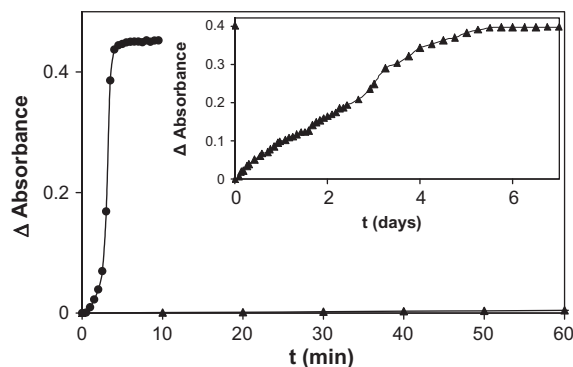


Fig. 7. A comparison of the recovery (step 2, Fig. 2) kinetics exhibited by two different MB-based oxygen indicators, namely, an aqueous-based P25 indicator (\bullet) and the novel acetone-based nanorutile indicator; which recovers in *ca.* 5 days (\blacktriangle) as shown in the insert plot.

the recoveries, due to reaction (2), of the original colours of these two solutions were monitored in a spectrophotometer in an open, well-stirred, UV/vis spectrophotometer cell. The rate of recovery in water was found to be 15 times faster than that for acetonitrile. This slower recovery in acetonitrile is even more remarkable given that the molar solubility of oxygen is *ca.* 9 times higher in acetonitrile than in water [24]! The key reaction associated with this dark, colour recovery, reaction is as follows:



Thus, the neutral leuco-methylene blue is oxidised by oxygen to form the original cationic, oxidised form of the dye, MB^+ and OH^- , both of which are charged species. The results of the above work in films and solutions indicates that the kinetics of reaction (2) are much slower in a less hydrophilic medium (such as that of an ink film or in acetonitrile), rather than in an aqueous solution or a water-based ink film, presumably because the reaction products are much less stable, and so more difficult to form, in such a hydrophobic environment. It is not surprising that charge separation is inhibited in a solvent with such a low dielectric constant.

This slow recovery feature opens up new potential uses for this indicator, such as the 'consume-within' indicator, mentioned earlier. It also enhances their potential utilisation in MAP, since there would be less need for maintaining an O_2 free atmosphere during the UV-activation step.

The kinetics of the dark, recovery step (2) appear insensitive to variations in $[\text{glycerol}]$ and $[\text{TiO}_2]$ as expected given the nature of reaction (2). However, unlike water-based O_2 inks, the recovery of the original blue colour was found to be significantly dependent upon the relative humidity in the ambient gas phase, as illustrated by the results in Fig. 8. As well as acting as the SED in the film, and helping solubilise the dye, it is believed that glycerol acts as a plasticizer by improving gas-diffusion within the film. Thus, the observed increase in dark step recovery time with decreasing RH is possibly due, in part at least, to the improved plasticizing action of the glycerol due to the latter's hygroscopic nature and tendency to become less viscous, and so, more permeable, with increasing RH. However, the increased level of water in the film, due to an increase in RH, could also contribute to the improved kinetics of reaction (2), by stabilising the ionic products. Interestingly, further work showed that the film exhibited no or little recovery at $\text{RH} < 20\%$ (over 24 h) at 21°C and this feature opens up the possibility of using the solvent-based indicator as an indirect detector of water vapour for RH values $> 20\%$ (at 21°C).

Additional work showed that the rate of the dark film recovery step (step 2, in Fig. 2) is proportional to the $\%\text{O}_2$ in the ambient gas phase. Thus, in a series of experiments, nitrogen and oxygen

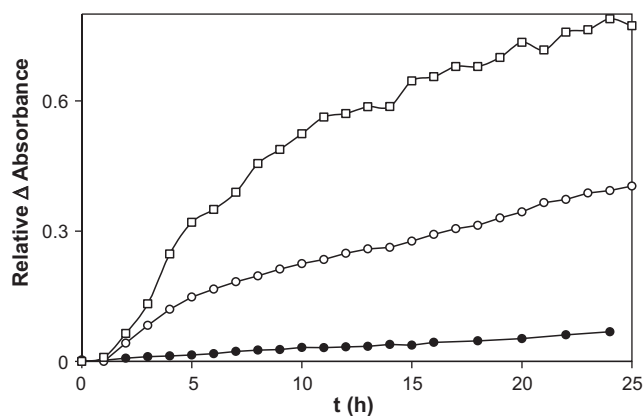


Fig. 8. Plot of the relative absorbance of a typical, photobleached indicator vs. time of recovery, in air at 21 °C, as a function of relative humidity (RH). In this work the humidity was maintained at: 18%, 57% and 96% RH, respectively (bottom to top).

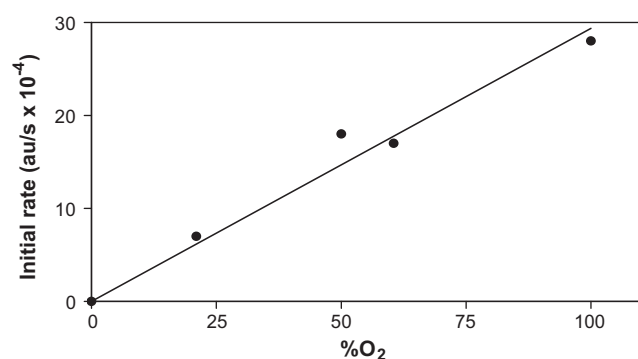


Fig. 9. Plot of initial rate of recovery of a typical photobleached film vs. concentration of oxygen in 100% RH blends of oxygen and nitrogen gas. Associated errors were found to be <2%.

gas were blended to produce O₂/N₂ mixtures of defined %O₂, and then, saturated with water vapour. These were then flowed over a typical, photobleached O₂ indicator and their recoveries monitored spectrophotometrically. A plot of the initial rate of recovery against oxygen concentration revealed a linear dependence as indicated by the results in Fig. 9 and suggested by reaction (2).

A final, significant advantage of the solvent-based O₂ indicator is its striking stability in water. For example, when a *solvent-based* and an *aqueous-based* oxygen indicating film were immersed in water, the dye in the *aqueous-based* indicator was leached out very rapidly (<1 min), whereas the ion-paired MB in the MB/SPS/TiO₂/glycerol

film remained contained in the film indefinitely. The water-proof nature of the *solvent-based* oxygen indicator was further tested under water. In this experiment, the film was first bleached and then put in a cell filled with water, purged with a N₂/O₂ mixture with a defined oxygen content, and the recovery monitored with UV/vis spectrophotometer. When this was repeated using different O₂/N₂ mixtures (0%, 21% and 100% O₂) it was found that the recovery in water was about 5 times faster than in 100% RH (at 21 °C) ($t_{1/2} = 1.5$ h compared to ca. 8 h at 21% O₂) and dependent directly upon the dissolved oxygen concentration. Thus, a final further potential application of this solvent-based O₂ indicator is in the measurement of dissolved levels of oxygen in water.

4. Conclusion

A novel, solvent-based, water-proof oxygen indicator that coats on hydrophobic polymers, such as polypropylene, was prepared and characterised. The coloured indicator is readily photobleached but has a slow (5 days) recovery. The kinetics of the latter process are independent of [glycerol] and [TiO₂], but dependent upon RH above a value ca. of 20% at 21 °C; the photobleached film does not recover any of its original colour below this value over a 24 h period. The very slow recovery process makes it possible to use the indicator as a 'consume-within' or humidity threshold indicator.

References

- [1] A. Mills, Chem. Soc. Rev. 34 (2005) 1003.
- [2] M.L. Rooney, Active Food Packaging, Blackie, London, 1995.
- [3] A.L. Brody, B.R. Strupinsky, L.R. Kline, Active Packaging for Food Applications, Technomic Publishing Co., Lancaster, 2001.
- [4] OxySense® Inc., <http://www.oxySense.com/> (accessed 2010).
- [5] MOCON Inc., <http://www.mocon.com/> (accessed 2010).
- [6] M. Sumitani, H. Inoue, K. Sugito, US Patent 6,703,245 (2004).
- [7] M. Goto, JP 62,259,059 (1987).
- [8] S.K. Lee, M. Sheridan, A. Mills, Chem. Mater. 17 (2005) 2744.
- [9] A.F. Turbak, Ind. Eng. Chem. Prod. Res. Dev. 1 (1962) 275.
- [10] F. Kucera, J. Jancar, Chem. Pap. 50 (1996) 224.
- [11] R.A. Weiss, S.R. Turner, R.D. Lundberg, J. Polym. Sci. 23 (1985) 525.
- [12] C.R. Martins, G. Ruggeri, M.D. Paoli, J. Braz. Chem. Soc. 14 (2003) 797.
- [13] H.S. Makowski, R.D. Lundberg, G.H. Singhal, IPN 3,870,841 (1975).
- [14] V. Augugliaro, H.A. Hamed El Nazer, V. Loddo, A. Mele, G. Palmisano, L. Palmisano, S. Yurdakal, Catal. Today 151 (2010) 21.
- [15] Z. Zhao, E.R. Malonowski, Appl. Spectrosc. 53 (1999) 1567.
- [16] A. Mills, D. Hazafy, Analyst 133 (2008) 213.
- [17] E. Braswell, J. Phys. Chem. 72 (1968) 2477.
- [18] G.N. Lewis, O. Goldschmid, T.T. Magel, J. Bigeleisen, J. Am. Chem. Soc. 65 (1943) 1150.
- [19] A. Mills, J. Photochem. Photobiol. A 108 (1997) 1.
- [20] J.M. Hermann, Top. Catal. 34 (2005) 49.
- [21] F.A. Ozdemir, B. Demirata, R. Apak, J. Appl. Polym. Sci. 112 (2009) 3442.
- [22] A. Mills, K. Lawrie, M. McFarlane, Photochem. Photobiol. Sci. 8 (2009) 421.
- [23] C.S. Turchi, D.F. Ollis, J. Catal. 122 (1990) 178.
- [24] M. Alvaro, Chem. Phys. Lett. 362 (2002) 435.